A DISCRETE VORTEX MODEL FOR THE CALCULATION OF AERODYNAMIC LOADS ON A BLADE OF A N-BLADED HELICOPTER ROTOR IN RECTILINEAR FLIGHT

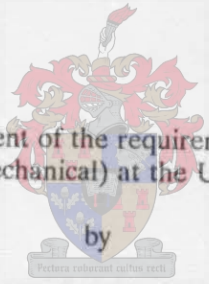

Thesis presented in partial fulfilment of the requirements for the degree of Master of Engineering Sciences (Mechanical) at the University of Stellenbosch

by

JACOB ARNOLD

December 1992

Study Leader: DR. G.D. THIART

DECLARATION

I, the undersigned, declare that the work contained in this thesis is my own original work which has previously not been submitted to any other university, partially or fully, in order to obtain a degree.

DATE: 5/12/91

ABSTRACT

A model for the calculation of aerodynamic loads on a blade of a n-bladed helicopter rotor in rectilinear flight was developed and computerized. The model is based on a lifting line blade representation and a vortex lattice wake representation. Both a rigid and a semi-rigid wake geometry are available as options, while lifting line options include a classical and an extended lifting line representation. Viscous, unsteady and compressibility effects are also included as modelling options. Blade dynamics is restricted to rigid body flapping motion.

A literature survey is presented, fundamental theoretical concepts are discussed, a mathematical model is derived and a discretized model is presented, including empirical modelling of blade profile aerodynamic characteristics. Calculated results are presented and compared with published experimental and calculated data, using different types of configurations and modelling options.

OPSOMMING

'n Model vir die berekening van die lugdinamiese belading op die lem van 'n n-lem helikopterrotor is ontwikkel en gerekenariseer. Die model is gebaseer op 'n heflyn lemvoorsteiling en 'n werwelrooster naloopvoorstelling. Beide 'n starre en 'n semi-starre naloopgeometrie is beskikbaar as opsies, terwyl heflyn modelleringsopsies 'n klassieke en 'n verlengde heflynvoorstelling behels. Die effekte van viskositeit, onbestendige vloei en samedrukbaarheid is ook as modelleringsopsies ingesluit. Lemdinamika is beperk tot starliggaam flapbeweging.

'n Literatuuroorsig word gelewer, fundamentele teoretiese konsepte word bespreek, en 'n wiskundige model word afgelei, gediskretiseer en geprogrammeer, insluitend empiriese modellering van die lugdinamiese karakteristieke van die lemprofiel. Berekende resultate word aangebied en vergelyk met gepubliseerde eksperimentele en berekende data, deur verskillende rotorkonfigurasies en modelleringsopsies te beskou.

ACKNOWLEDGEMENTS

Dr G D Thiart, for his support as thesis supervisor.

The Foundation for Research Development (CSIR) and the Bureau for Mechanical Engineering (US) for their material support.

Mrs S Beer, for her excellent typesetting.

My wife and children for their moral support and privation during the period of study.

The Lord, for the abundance of undeserved blessings.

NOMENCLATURE

Roman

a	Lift curve slope
A	Rotor disc area (πR^2)
b	Blade semi-chord (c/2)
	Bound vortex cell influence coefficient
c	Blade chord
	Coefficient (if subscripted)
C	Lift deficiency function
d	2-Dimensional (local) drag
e	Hinge offset
f	Local force
	Free vortex cell influence coefficient
F	Force
g	Biot-Savart function
H	Rotor side force
I	Moment of inertia
k	Spring constant
	Reduced frequency
ℓ	2-Dimensional (local) lift
m	2-Dimensional (local) moment
M	Moment
	Mach number
na	Number of azimuthal stations
nb	Number of blades
nr	Number of radial stations
nz	Number of wake layers
r	Blade radial coordinate
R	Rotor radius

s	Semi-span (of wing)
t	Time
T	Rotor thrust
u	Velocity component (x-direction)
U	Velocity seen by blade element
v	Velocity component (y-direction)
V	Velocity seen by rotor hub
w	Velocity component (z-direction)
X	Rotor side force

Greek

α	Angle of attack
β	Angle of sideslip
	Blade flapping angle
γ	Vorticity/unit length
	Lock number ($\rho a\, c\, R^4/I_\beta$)
	Gas ratio
Γ	Circulation
δ	Distance along chord
	Prandtl-Glauert correction factor
Δ	Effective sweep angle
θ	Blade local pitch angle
λ	Inflow ratio ($(w + w_i)/\Omega R$)
μ	Rotor advance ratio ($u/\Omega R$)
	Absolute viscosity
ν	Blade flapping frequency
ρ	Air density
	Blade radial coordinate
σ	Rotor solidity ($Nc/\pi R$)
ϕ	Blade section inflow angle

Φ	Wagner function
χ	Wake angle
ψ	Blade azimuthal angle
ω	Frequency
Ω	Rotor rotational speed

Subscripts

a	Aerodynamic centre
b	Bound vortex
	Blade
c	Cosine coefficient of Fourier series
cg	Centre of gravity
cp	Control plane
d	drag
ds	Dynamic stall
f	Free vortex
fp	Flapping plane
h	Rotor hub
hp	Hub plane
i	Induced
	Index over radial control points
j	Index over azimuthal control points
k	Index over blades
ℓ	Index over wake layers
	Lift
m	Moment
n	Non-circulatory
o	Static, Steady
	Reference blade
	Collective pitch

	inner radius
p	Index over radial nodes
P	Perpendicular component
q	Index over azimuthal nodes
	Quasi-static
R	Radial component
s	Sine coefficient of Fourier series
ss	Static stall
t	Twist/unit length
	Unsteady
te	Trailing edge
T	Tangential component
β	Flapping hinge
∞	2-Dimensional
	Free stream

Superscripts

-	Vector
-	Average, approximate
•	Time derivative
'	Derivative
b	Blade
c	Control point
	Control angle
o	Steady, static
t	Unsteady
w	Wake

LIST OF CONTENTS

CHAPTER 1
INTRODUCTION

The capability to accurately model the aerodynamic and hence, the dynamic behaviour of helicopter rotors in rectilinear flight, is necessary to be able to predict helicopter loads, performance, flight dynamics, aeroelastic stability, vibration and noise characteristics. Such a capability is also required to serve as a basis for further development in rotary wing theory and modelling.

The aerodynamic flow field of a rotor disc is very complex and is highly coupled with blade motion. It involves three dimensional, unsteady, viscous, compressible flow with flow phenomena such as transonic flow with shock waves on the advancing blade tip, flow reversal and stalled flows on the retreating side and radial flow at the fore and aft position of a rotor in rectilinear flight. A useful aerodynamic theory must account for the effects due to viscosity, such as wake formation and dynamic stall, which are important even at moderate operating conditions.

Navier Stokes solutions of the entire rotor flow field are, however, well beyond present capabilities. In most of the advanced methods for rotor analysis, inviscid (potential) aerodynamics is used as basis. Flow phenomena involving viscosity are analysed and modelled separately for inclusion in potential flow models of rotors, depending on the level of sophistication required for such a model.

This thesis involves the development of a potential flow model of a rotor in rectilinear flight, including vertical flight and hover. In this chapter a historical overview, a description of the classical model and a literature survey of some of the important contemporary contributions will be presented, after which the scope of the thesis, outlining objectives, restrictions and typical applications of the rotor model will be defined. In subsequent chapters the theoretical building blocks of such a model will be discussed, after which details of the model will be presented. Finally, the model will be evaluated against published experimental data and analysed to illustrate the effect of some typical simplifications.

Conclusions will be drawn and recommendations for further development or refinements will be made.

1.1 Historical Overview

The development of a theoretical model representing the flow through a rotor is closely related to developments in airscrew and wing theory. Accounts of the most important contributions to the development of a theoretical rotor model as obtained from Von Kármán [1954], Bisplinghoff et al [1955], Baskin et al [1976] and Johnson [1980a] is presented below.

1.1.1 Momentum and blade element theory

The momentum theory for propellers and windmills was developed by Rankine in 1865 and Froude in 1885. This theory relates thrust and power of a propeller to the increase in velocity of the wake and the size of the rotor disc. In order to relate all the geometric design parameters (number of blades, rotor radius, blade geometry, etc) to the performance (thrust and power) of a rotor, blade element theory was developed by Drzewiecki between 1892 and 1920. This theory forms the foundation of almost all analysis of helicopter aerodynamics, because it deals with the detailed flow and loading of a blade element and, when integrated over the radius and azimuth of a rotor, yields the rotor forces and moments. Initial attempts to calculate blade loads using this theory yielded inaccurate results because the effect of the increased velocity through the disc (free stream velocity plus an induced velocity) was not included in the analysis. The phenomenon of induced velocity was not clearly understood until the development of lifting line theory.

1.1.2 Theory of lift

Kutta in 1902 and Joukovski in 1907 independently developed a vortex theory of lift, modelling the lift developed by a two-dimensional airfoil (infinite wing) by a potential vortex placed in a uniform stream. The strength of the vortex is related to the airfoil

geometry and flow kinematics by imposing the so called Kutta boundary condition, requiring finite velocity at the sharp trailing edge. The lift of the airfoil was found to be proportional to the circulation and directed perpendicular to the free stream. This model was extended to finite wings, qualitatively by Lancaster in 1908 and quantitavely by Prandtl in 1919, using vortex theroms for potential flow postulated in 1858 by Helmholz. The model consists of a bound vortex representing circulation and hence lift on the wing and a system of trailing vortices leaving the bound vortex such that the boundary condition of zero lift at the wing tips is satisfied. The trailing vortices, giving rise to induced velocities or a wake at the bound vortex and further downstream according to the Biot-Savart law, changes the velocity vector seen by a wing section, hence influencing the magnitude of the circulation distribution, giving rise to a so called induced drag (drag due to a tilt of the lift vector).

1.1.3 Combined blade element and momentum theory

The concept of a wake and its effect on the load distribution was introduced into blade element theory by Glauert and Lock in 1928, using the induced velocity obtained from momentum theory, thereby developing the first successful rotor model for the analysis and synthesis of helicopter rotors. Because induced velocity obtained from momentum theory is uniform over the actuator disc, this model actually represents a rotor with an infinite number of blades. Furthermore, the blade of a rotor in forward flight sees a higher velocity when advancing than when retreating, giving rise to asymmetric loading and hence induced flow, requiring more detailed analysis, as is obtained from vortex theory.

1.1.4 Combined blade element and vortex theory

Joukovski laid the foundations for vortex theory from 1912 to 1929. He investigated the induced velocity due to the helical wake geometry of a propeller, but had to solve an infinite blade representation due to the mathematical complexities involved. The results of momentum theory were confirmed with this model. In 1918, Joukovski proposed the use of two-dimensional airfoil characteristics with induced velocity taken from vortex theory. This approach laid the theoretical foundation of modern blade element theory, which is

essentially lifting line theory for a rotary wing. In 1929, Goldstein was the first to derive an exact solution, taking into account a finite number of blades. Since the aerodynamic environment of a rotor blade in forward flight is asymmetric and hence unsteady, an appropriate unsteady model of a two dimensional airfoil must be incorporated. The unsteady environment implies a continuous change in bound circulation with associated shed vorticity parallel to the blade according to Helmholz theorems. This problem was first solved by Theodorson in 1935 for an infinite wing and extended in 1957 by Loewy to include the effect of a returning shed wake, as is the case for helicopter rotor blades.

1.1.5 Refinements to classical theory

More recent refinements of the model developed thus far involve corrections to the lifting line model for yawed (radial) flow, or alternatively replacing the lifting line model with a lifting surface model of the rotor blade. Efforts in contempory rotary wing aerodynamics are directed primarily towards the solution of the classical rotor model by including empirical corrections obtained from experimental studies. Solution techniques are essentially numerical in nature, and require extensive computations.

1.2 Discussion of the classical model

1.2.1 Description of the model

The classical rotor model consists of an inner problem and an outer problem. The inner problem concerns the aerodynamics of a blade section. The flow over the blade section acts as if it is two-dimensional, with the influence of the wake and the rest of the blade represented entirely by a chordwise induced velocity distribution, or a constant chordwise distribution in the case of a lifting line representation, giving rise to an induced change in angle of attack. Two-dimensional airfoil theory, computational fluid dynamics, or experimental results are used to represent airfoil characteristics to obtain blade loads (lift, drag and pitching moment). The outer problem involves the calculation of induced velocity using the wake model, which consists of helical vortex sheets trailed behind each blade.

Because the rotary wing encounters its own wake and the wake from preceding blades, a detailed and accurate model of the blade is required to obtain an estimate of the induced velocity at the blade. The inner and outer problems are coupled typically by the kinematic condition of no flow through the surface of the blade, as well as the fluid mechanical condition of pressure equalization and hence zero circulation at the trailing edge and the blade tip.

1.2.2 Solution of the model

An entirely analytical solution, analogous to the fixed wing model, is not possible due to the helical geometry of the wake, except in the case of the infinite blade representation, as already mentioned. To obtain a tractable mathematical formulation for calculating induced velocity, the vorticity in the wake is usually modelled by a series of discrete line vortex elements. This is equivalent to considering a stepped bound circulation distribution, both radially and azimuthally. A vortex line representation of the inboard trailed and shed vorticity, forming a vortex grid, introduces singularities in the induced velocity near each line element, but this can be avoided if a finite vortex core is assumed.

1.2.3 Wake geometry

Modelling the kinematics (geometry) of the wake poses another physical uncertainty, although various experiments have verified the general helical, though distorted, geometry of the wake. Generally, however, these models are inconsistent because continuity is violated.

Wake geometries used in solving the wake model are the rigid, semi-rigid and free wake models. The rigid wake model assumes an undisturbed helical geometry, in which all the wake elements are convected with the same mean velocity. According to this method the geometry is known a priori, and one has only to find the circulation distribution along the blade. The semi-rigid wake model assumes that each vortex element is convected downward with the induced velocity of the point on the rotor disc where it was created. The semi-

rigid wake geometry does not require additional computation compared to the rigid wake since it uses only the non-uniform inflow at the rotor disc. The free wake, or non-rigid model, includes the distortion from the basic helix, as each vortex element is convected with the local flow, including the velocity induced by the wake itself. Calculating the distorted wake requires evaluating the induced velocity throughout the wake, rather than just at the rotor disc and therefore it involves a very large computational effort.

The choice of the wake model is usually a balance between accuracy and economy. For many problems an economical free wake calculation is not presently possible, so a rigid wake model is used. Moreover, the increased accuracy possible with a distorted wake model will be wasted unless consistent advances are also made in the other parts of the model, as will be shown in the discussion of the literature survey.

1.3 Literature survey

1.3.1 Classical wing theory

Classical airfoil and wing theory are described in detail by amongst others Belotserkovskii [1967], Bisplinghoff et al. [1955] and Schlichting & Truckenbrodt [1979] for steady flow.

1.3.2 Unsteady wing theory

Unsteady airfoil theory is described by Bisplinghoff et al [1955], Johnson [1980a] and van Holten [1975, 1976], the latter of which discusses the validity of lifting line concepts in rotor analysis. Enlightening notes on unsteady aerodynamics is also found in Piziali [1966] and Friedman [1983, 1987]. Extensions to three-dimensional modelling are presented in Bisplinghoff [1955]. A practical computation of unsteady lift to helicopter rotor blades is presented by Beddoes [1984].

1.3.3 Classical rotor theory

A detailed account of classical rotor theory is given by Baskin et al. [1976], including experimental verification of visual flow illustrations. Stepniewski [1984] is also a useful reference for various classical models.

1.3.4 Contemporary rotor modelling

Discussions on discrete modelling and numerical methods developed to solve the classical rotor aerodynamic model are found in Bramwell [1976] and Johnson [1980a]. Examples of rigid and semi-rigid wake modelling are presented by Miller [1964], Piziak [1965] and Rand & Rosen [1982], while Landgrebe [1969], Clark & Leiper [1970], Sadler [1971], Scully [1975] and Favier et al. [1987] describe the implementation of free wake models. A comprehensive analysis of rotorcraft aerodynamics and dynamics based on the free wake model of Scully [1975] is presented in Johnson [1980b], and represents the current state of the art. A simplified approach giving reasonable accuracy is presented by Miller [1987]. According to Johnson [1986], [1990], lifting line theory is still the only practical viscous method for rotors. In a study, evaluating lifting line and lifting surface theory using a rigid and a free wake, Johnson [1980a] concludes that a free wake model should only be used with a lifting surface representation of the blade. Unrealistic results for the lifting line model using a free wake model were obtained in the case of close blade and (returning) vortex interactions. Although using a lifting surface model yields good results for vortex blade interaction, viscous phenomena, like separation and dynamic stall, are difficult to simulate with this model, and are still the subject of research (Johnson [1986]). It is suggested in this reference that a hybrid lifting surface (or Navier Stokes), lifting line and free wake analysis should be used.

1.3.5 Computational fluid dynamics (CFD)

Recent literature reported on the successful implementation of full potential, Euler and Navier-Stokes codes (CFD codes) to calculate rotor blade loading in compressible flow. A

general discussion is presented in Davis & Chang [1987] while a comparative study of lifting line and CFD methods is reported on by Bousman et al. [1989], verifying the present superiority of lifting line methods. An application of the full potential method, which is an approximation to the invicid Euler equations, is given by Arieli et al. [1986]. The Euler solvers, discussed by Wake et al [1989], allows vorticity as well as entropy gradients (compressibility effects), providing an advantage over full potential solvers, with the additional advantage of being easily upgradeable to a Navier-Stokes solver. Only recently, Navier-Stokes solvers have been used to calculate the flow about the rotor blade. A report of such an application for a non-lifting rotor is given by Wake & Sankar [1989]. The results in the report were found encouraging, but a tremendous amount of computational power is required, thus making it impracticle for most applications.

1.3.6 Separated unsteady flow

The phenomena of blade stall, and more specifically dynamic stall, is discussed in detail by Johnson [1980a] and Friedman [1987]. Recent dynamic stall models are presented by Johnson [1980a], Tran & Falchero [1982] and Beddoes [1983]. All current dynamic stall models are empirical, fitting models to experimental airfoil data. An extensive survey in the progress in analysis and prediction of dynamic stall, was performed by Carr [1988]. The latter reference also includes illustrations of flow studies.

1.3.7 Blade Dynamics

Representation of blade dynamics is treated theoretically in detail by Bisplinghof [1955], Bramwell [1976] and Johnson [1980a]. A solution technique of such a model is presented in detail by Scully [1975], which is based on a finite difference scheme. More recent approaches use finite element descriptions of the blade dynamics, as discussed by Friedman [1983] and Rosen & Rand [1987]. Bramwell [1976] treats various methods of solution for uncoupled blade motion in detail.

1.3.8 Prescribed inflow models

Such models are extensively used in performance and simulation modelling of helicopters, using integrated (explicit) rotor equations. An excellent account of such linear models, obtained by fitting experimental data to empirical models, is presented by Chen [1989]. These models are also relevant in numerical aerodynamic analysis, because they serve as initial estimates of the induced velocities.

1.3.9 Experimental Studies

A theoretical and experimental investigation of the induced velocities near a lifting rotor, often used as a reference for verification of numerical models, is described in Heyson & Katzhoff [1957]. A more recent publication of experimental results in forward flight is that of Cheeseman & Haddow [1989]. Scheiman and Ludi [1963] represent data on loads measured on a model rotor. A survey of major wind tunnel tests and full scale flight tests conducted, was done by Hooper [1984], comparing airload distributions for rotors of various configurations.

1.4 Scope of Thesis

The objective of this thesis as stated in the title, is a general statement, requiring some further qualification with respect to application and intent. Application of vortex rotor models typically varies from global rotor performance estimation to aeroelastic and acoustic analysis, requiring different levels of sophistication of aerodynamic and structural modelling.

The primary objective is to establish a platform for research and development in rotor dynamics and aerodynamics. The model is therefore generically structured to lend itself to parametric analysis and to accommodate more advanced developments in aerodynamic and structural dynamic modelling. The applications of the model envisaged, which is a secondary objective, include performance and dynamic analysis and preliminary design synthesis, but exclude specialized analysis of aeroelastic stability and acoustic characteristics.

The emphasis is placed on aerodynamic modelling, although, due to the aerodynamic and structural dynamic coupling effects, basic structural dynamic modelling is included.

The activities involved in support of these objectives are:

a. Development of a model based on the most fundamental concepts, but accounting for all aerodynamic flow phenomena.

b. Discretization and computerization of the model developed.

c. Verification of the computerized model against experimental data published by Scheiman & Ludi [1963] for blade aerodynamic loads, and computational data presented by Johnson [1980a] for aerodynamic loads and flow kinematics.

d. Parametric analysis to investigate the sensitivity of the calculated data to further approximations in modelling, eg. uniform inflow modelling and neglecting compressibility, stall and unsteady effects.

The complexity of the model is limited due to the doubtful advantages in terms of accuracy obtained, as well as the computational expense in using advanced concepts such as vortex panel and free wake modelling. The following features and restrictions therefore apply to the model developed:

a. A semi-rigid discrete vortex wake model is assumed, with provision for the variation in the prescribed kinematics of the wake and vortex core radii.

b. Unsteady lifting line theory is used to represent the blade loading. The effect of the shed wake can either be included as an integral part of the model, or can be accounted for separately by means of a shed vortex model.

c. Radial and reverse flow, dynamic stall and the effect of compressibility are represented by simplified models.

d. Only rigid body flapping is included in the blade motion solution. No lag or torsional motion of the blade, nor any kinematic coupling is included. Flapping hinge offset is included and a spring restraint about the flapping hinge can be used to represent non-articulated blades.

e. Motion of the rotor hub is restricted to steady rectilinear motion.

The model is evaluated as if mounted in a wind tunnel, that is, the flow kinematics are given as inputs, while the control input is adjusted until a specified thrust is obtained. Both hover and forward flight are considered. The model is structured to accommodate advanced structural modelling, including coupling effects.

CHAPTER 2

THEORETICAL BACKGROUND

In this chapter, the fundamentals underlying rotor theory will be discussed in more detail. Expressions or models derived from these fundamentals will act as building blocks or will serve as initial approximations in the solution of a vortex model of a rotor, subject to the assumptions as discussed in the scope of the thesis.

2.1 Momentum theory

The basic laws of fluid mechanics (continuity, momentum and energy conservation), leads to a simple model relating the thrust developed by a device, called an actuator disc, to the velocity induced in the plane of the disc. Such a relation was developed by Rankine and Froude for axial flow and extended by Glauert to non-axial translation, see Stepniewski [1984]. With reference to fig. (2.1), the relationship between induced velocity and thrust is

$$w_i = \frac{\frac{T}{2\rho A}}{\left[(V\cos\alpha)^2 + (V\sin\alpha + w_i)^2\right]^{1/2}} \qquad (2.1)$$

for $V \sin \alpha \geq 0$. The case of autorotation or descent $(V\sin \alpha < 0)$ should be treated separately, as outlined in Johnson [1980a]. Eqn. (2.1), can be solved for a given V and α and for a known thrust T, disc area A and density, using for example the Newton-Raphson method.

2.2 Vortex theory of lift

The vortex theorem of lift relates the lift created by a two-dimensional body to the amount of circulation generated by the body. A mathematical expression for this relation, known as the Kutta-Joukovski theorem, is

$$\ell = \rho V \Gamma \tag{2.2}$$

Eqn. (2.2) plays an essential role in subsonic aerodynamic analysis. Mechanisms for creating the circulation are all of viscous nature. Some of the most important are a sharp trailing edge (Kutta effect), rotation of axi-symmetric bodies (Magnus effect) and boundary layer control (Coanda effect).

2.3 Kelvin's theorem

In an inviscid homogeneous flow with conservative body forces (potential flow) Kelvin's theorem, also known as Thomson's theorem, states that the circulation Γ around a closed fluid line remains constant with respect to time, expressed mathematically as

$$\frac{d\Gamma}{dt} = 0 \tag{2.3}$$

A closed fluid line is a line enclosing the same particles, eg the fluid inside and leaving a reservoir, or the atmosphere containing a body of revolution. The implication of this theorem is that a change in circulation and hence, lift on a airfoil is always accompanied by an equal and opposite change in circulation in the form of a vortex being shed from the airfoil, an important phenomenon when unsteady airfoil behaviour is considered.

2.4 Helmholz vortex theorems

In extending two-dimensional vortex theory of lift to three dimensions, the Helmholz vortex theorems for vortex lines (or filaments) must be observed. Those are

a. The circulation around a given vortex line (i.e. the strength of the vortex filament) is constant along its length.

b. A vortex filament cannot end in a fluid. It must form a closed path, end at a boundary or extend to infinity.

c. A vortex filament consists of the same particles of fluid i.e. no interchange between a filament and its surrounding occurs. Combining this with Kelvin's theorem implies that vortices are preserved as time passes.

These theorems are proved for inviscid flow, see Keuthe & Chow [1976], but are also valid to a good approximation in viscous flow regions where viscosity may be neglected.

2.5 Biot-Savart law

The velocity induced by a vortex filament of strength Γ and length ds at a point P, as illustrated in fig. (2.2), is analogous to the law of Biot-Savart for an electro-magnetic field given by

$$d\bar{V}_i = \frac{\Gamma\, d\bar{s} \times \bar{r}}{4\pi r^3} \tag{2.4}$$

This expression known as the Biot-Savart law and discussed amongst others by Chia-Shun Yih [1977], forms the basis for the mathematical representation of the flow field of vortex models.

With reference to fig. (2.2), the velocity induced at the point P by a straight line segment is given by

$$\bar{V}_i = \frac{\Gamma}{4\pi} \bar{r}_1 \times \bar{r}_2 \left(\frac{1}{r_1} + \frac{1}{r_2}\right)\left[r_1 r_2 + \bar{r}_1 \bullet \bar{r}_2\right]^{-1} \tag{2.5}$$

as presented in Johnson [1980a]. The vectors $\bar{r}_1$ and $\bar{r}_2$ can be in any convenient reference frame.

A special form used in airfoil and wing theory is obtained when the line vortex is placed on the x-axis between 0 and x of the chosen reference system and the angles β_1 and β_2 are used as parameters, see fig. (2.2). The result is

$$\bar{V}_i = \bar{k}\frac{\Gamma}{4\pi h}\left(\cos\beta_1 + \cos\beta_2\right) \tag{2.6}$$

where h is defined in the same figure. This form easily renders expressions for the velocity induced by vortices of semi-infinite and infinite lengths, by letting (β_1, β_2) assume the appropriate values.

The finite strength line vortex is however an idealization in which a finite amount of vorticity is concentrated into a line of infinitesimal cross-section. There is a singularity at such a vortex line, with the induced velocity increasing as the inverse of the distance from the line. In a real fluid, viscosity eliminates this singularity by diffusing the vorticity into a tube of small but finite radius, called the vortex core, within which the vorticity is approximately constant. The maximum induced velocity occurs at some distance from the centre of the line vortex, defined as the core radius. Inside the core radius empirical models, of which solid body rotation is typical, are employed to calculate the induced velocity.

Prandtl showed, see Kuethe & Chow [1976], that the important dimensionless parameter representing decay of a vortex filament is $\rho r^2/\mu t$. The vortex core is roughly represented by solid body rotation with radii proportional to $\sqrt{\rho t/\mu}$, increasing with time.

An empirical vortex core model has been introduced by Scully [1975], for specific application to rotor wake modelling, and will be discussed in more detail later. In this type of application, the vortex core radius is typically expressed as a fraction of some geometric characteristic of the flow, typically a fraction of the rotor radius in the case of helicopter rotor models.

2.6 Thin airfoil theory

Thin airfoil theory relates the geometry and incidence (angle of attack) of a two-dimensional airfoil to the amount of circulation, hence yielding an expression for lift according the Kutta-Joukovski theorem in terms of geometric and kinematic parameters. In this theory or model, the airfoil is replaced by its camber line, which in turn is replaced by a line of variable vorticity of strength $\gamma(x)$ per unit length of chord, as illustrated in fig. (2.3). The total circulation, assuming small camber, is

$$\Gamma = \int_0^c \gamma(x)\, dx \tag{2.7}$$

Because the camber line must represent a streamline, the kinematic condition, assuming small angles,

$$V\left[\frac{dz}{dx} - \alpha\right] = w_i \tag{2.8}$$

must be satisfied everywhere on the camber line. According to the Biot-Savart law, the circulation $d\Gamma = \gamma(x)\, dx$ at x induces a velocity at the point x^*, given by

$$dw_i = \frac{1}{2\pi} \frac{\gamma(x)\, dx}{x - x^*} \tag{2.9}$$

Integrating this expression to obtain w_i and substitution in eqn. (2.8), yields the thin airfoil equation

$$V\left[\frac{dz}{dx} - \alpha\right] = \frac{1}{2\pi}\int_o^c \frac{\gamma(x)\,dx}{x - x^*} \tag{2.10}$$

Any solution of eqn. (2.10) must however satisfy the Kutta condition, which requires finite velocities and pressures at the trailing edge of the profile. This implies that $\gamma(c) = 0$ at the trailing edge.

The solution for $\gamma(x)$ which satisfies the thin airfoil equation and the Kutta condition for a given shape of camber line $z(x)$ and angle of attack α can be introduced in eqn. (2.7) to obtain the circulation and in eqn. (2.2) to obtain the lift. An expression for the moment about the leading edge is given by

$$m_{le} = -\int_o^c x\,\gamma(x)\,dx \tag{2.11}$$

The above results are restricted to thin airfoils in incompressible steady inviscid flow.

In linearized potential theory, the effect of thickness can be treated separately, after which the result can be superimposed (summed) to the thin airfoil result, as discussed in Kuethe & Chow [1976].

2.6.1 Exact Solution

An exact series solution developed by Glauert in 1929 is described in Schlichting & Truckenbrodt [1979], expressing the various aerodynamic coefficients in terms of a finite number of the coefficients of an infinite series representing the vorticity distribution. For a symmetrical airfoil, the lift coefficient $c_\ell = \ell / \frac{1}{2}\rho V^2 c$, is given by

$$c_\ell = 2\pi\alpha \tag{2.12}$$

and hence $dc_\ell/d\alpha = 2\pi$, while the moment coefficient $c_m = m/\frac{1}{2}\rho V^2 c^2$ about the leading edge is

$$c_{m_{le}} = -\frac{\pi}{2}\alpha \tag{2.13}$$

The centre of pressure is shown to be at the quarter-chord point at all angles of attack for a symmetrical airfoil and is hence referred to as the aerodynamic centre. The effect of camber and thickness on these parameters is discussed in detail in Schlichting & Truckenbrodt [1979] and others.

2.6.2 Approximate solution

An approximate solution of particular importance in the application of lifting line theory (discussed later), is that of Weissinger [1963], described in McCormick [1967] and illustrated in fig. (2.4). In this approximation, the vorticity distribution $\gamma(x)$ is replaced by a single vortex of unknown strength, Γ, placed at the quarter-chord of the assumed flat plate section. The reason for placing the vortex at the quarter-chord point is tied to the fact that

the centre of pressure (lift) is at that position for a flat plate airfoil, and approximately for a cambered airfoil, see Schlichting & Truckenbrodt [1979]. The kinematic boundary condition and the Kutta condition will then be satisfied only at one point, the three-quarter-chord point. For this approximation eqn. (2.10) becomes $V\alpha = \Gamma/\pi c$ or

$$\Gamma = V\, c\, \pi\, \alpha = \tfrac{1}{2} V\, c\, c_\ell \tag{2.14}$$

from which follows, using eqn. (2.2)

$$\ell = \tfrac{1}{2} \rho\, V^2 c \left(\frac{dc_\ell}{d\alpha}\right) \alpha \tag{2.15}$$

where $dc_\ell/d\alpha = 2\pi$, the same result as obtained with the exact approach. Experiment gives a slightly lower value, typically 5.8 per radian.

The validity of this representation is verified by the theorem of Pistolesi (see Schlichting & Truckenbrodt [1979]) who showed that the induced downwash velocities at the three-quarter-chord point for the exact theory and the approximation for a flat plate airfoil are equal, as illustrated in fig. (2.4). Hence this is the correct station to evaluate induced velocities for the lifting line approximation of a three dimensional lifting surface model where a single vortex is placed at the quarter chord.

To be able to predict the correct value for the pitching moment [illegible] cambered sections, more panels with discrete vortex strengths are required, [illegible] in McCormick [1979].

2.7 Lifting line theory

For a finite wing, the concept of thin airfoil theory was extended by representing the wing by a vortex line, called a bound vortex. The existence and behaviour of this vortex line is however subject to physical laws expressed by Helmholz theorems. These constraints, together with experimental observation, led to the Lancaster-Prandtl lifting line theory.

The lifting line model, presented in fig. (2.5), consists of a system of bound, trailed and shed vorticities, which induces a velocity w_i at the bound vortex and gives rise to a tilt in the airflow seen by the airfoil section. Because lift is defined perpendicular to the far upstream velocity, the tilt in the relative airflow and hence tilt of the circulatory force produces a component tangentially to the upstream velocity, known as induced drag d_i, as illustrated in fig. (2.6).

As was discussed previously, the correct position of the bound vortex is at the quarter-chord point, while the induced velocity (downwash) w_i should be calculated at the three-quarter-chord point, in order to satisfy two-dimensional boundary conditions. Classical lifting line theory, however, used the quarter-chord point, while what is known as extended lifting line theory uses the Weissinger (or three-quarter-chord) approximation.

The mechanism for the development of trailing vortices is the equalization of the pressure difference on the upper and lower surfaces at the (finite) wing tips. This leads to a spanwise flow, inward on the upper and outward on the lower surfaces. At the trailing edges, due to viscous effects, a vortex sheet is formed as a result of the velocity differences.

The existence of the starting vortex, which has been extensively verified experimentally, is in accordance with Kelvin's theorem. In an unsteady kinematic environment and resulting continuous change in bound circulation, vortices are continuously shed parallel to the bound

vortex, a phenomenon that will be treated in later sections.

A lifting line model of a finite wing, linking kinematic, geometric and aerodynamic parameters of a wing section to the bound circulation distribution $\Gamma(y)$, is developed with reference to figs. (2.5) and (2.6). Assuming small angles the kinematic flow condition characterizing (postulating) lifting line theory is, see fig. (2.6)

$$V_\infty \alpha_\infty(y) = V_\infty \alpha(y) - w_i(y) \tag{2.16}$$

where w_i is assumed positive downward.

An expression for the induced velocity at y is obtained by applying the Biot-Savart law to the semi-infinite trailing vortex system of fig. (2.7), yielding

$$w_i(y) = -\frac{1}{4\pi} \int_{-s}^{s} \frac{d\Gamma}{dy^*} \frac{dy^*}{y-y^*} \tag{2.17}$$

The effective angle of attack $\alpha_\infty(y)$ is related to the circulation $\Gamma(y)$ at station y by the approximate thin airfoil theory relation as expressed by eqn. (2.14)

$$\Gamma(y) = \tfrac{1}{2}\, c(y) \frac{dc_\ell}{d\alpha}(y)\, V_\infty(y)\, \alpha_\infty(y) \tag{2.18}$$

Where $dc_\ell/d\alpha$ replaces its theoretical value of 2π. Combining eqns. (2.16), (2.17) and (2.18) yields

$$\Gamma(y) = \tfrac{1}{2}c(y)\,\frac{dc_\ell}{d\alpha}\,(y)\left[\alpha(y) + \frac{1}{4\pi}\int_{-s}^{s}\frac{d\Gamma}{dy^*}\,\frac{dy^*}{y-y^*}\right] \qquad (2.19)$$

which is known as the Prandtl integrodifferential equation for the circulation distribution of a finite wing. Derivation of this equation can be found in any fundamental text on aerodynamics treating classical lifting line theory.

The basic assumption underlying steady lifting line theory is that the circulation representing the wing is concentrated on one line (quarter-chord) and the local flow is two-dimensional. This approximation is fairly good for a real wing of large aspect ratio ($b > 5c$), except where strong spanwise pressure gradients and hence spanwise flow occurs, such as at the wing tips. Furthermore, the model can not be used for swept back wings or yawed flow (radial flow in the case of a rotor blade), although sometimes an empirical cosine sweep correction is employed as discussed by Van Holten [1976] and described in Johnson [1980b]. To overcome this problem, one has to revert to extended lifting line theory (three-quarter-chord method) or more complex lifting surface methods (eg vortex lattice methods). Such methods are described amongst others in Schlichting & Truckenbrodt [1979], Bertin & Smith [1979], Moran [1984] and Bisplinghoff et al [1955], the latter of which gives an extensive mathematical treatment of these theories.

2.8 Unsteady airfoil theory

Unsteady airfoil theory treats the effect of the variations in the kinematics of an airfoil on the aerodynamic loads. Kinematic variations typically involve variations in pitch, vertical translation and horizontal translations. The effect of such variations is a change in the bound circulation and hence vorticity distribution, accompanied by vorticity being shed in the wake in accordance with Kelvin's theorem. This in turn influences the bound circulation by inducing a velocity along the airfoil chord. Furthermore, aerodynamic forces, known as added or virtual mass effects, also arise due to acceleration of an airfoil section in a fluid. An airfoil operating in an unsteady environment, typically in the case of a rotor blade in forward translation, should therefore be represented by an unsteady model accounting for the abovementioned effects. A detailed treatment of this subject is presented by Bisplinghoff et al [1955] and Johnson [1980a], and only the results are presented here. First an exact solution to the two-dimensional problem will be given, followed by an approximation, after which the form of a generalized model, suitable for applications in rotating and translating wings such as a rotor blade, will be discussed. Finally unsteady separated flow will be discussed and the outlines of a semi-empirical dynamic stall model introduced for two-dimensional airfoils.

2.8.1 Exact solution

The flow geometry and the airfoil kinematics for this problem are presented in figs. (2.7) and (2.8) respectively. An exact solution for the lift and moment of an oscillating airfoil was first obtained by Theodorson (see Bisplinghoff et al [1955]) for V(t) = constant and sinusoidal variations of pitching and heaving i.e. $\alpha(t) = |\alpha(t)| \exp(i\omega t)$ and $h(t) = |h(t)| \exp(i\omega t)$. The expression for lift as derived in Johnson [1980a] is

$$\ell = C(k)\ell_q + \ell_n \tag{2.20}$$

where ℓ_q is the quasi-static lift, the only term present for the steady case, given by

$$\ell_q = 2\pi\rho V b\left[V\alpha + \dot{h} + b\dot{\alpha}\left(\tfrac{1}{2} - \eta\right)\right] \tag{2.21}$$

and ℓ_n is the non-circulatory lift representing the forces due to acceleration, given by

$$\ell_n = \rho\pi b^2\left[V\dot{\alpha} + \ddot{h} - \eta b\ddot{\alpha}\right] \tag{2.22}$$

The function C(k) is known as the Theodorson lift deficiency function, defined by

$$C(k) = \frac{\int_1^\infty \frac{\zeta}{\sqrt{\zeta^2 - 1}}\, e^{-ik\zeta}\, d\zeta}{\int_1^\infty \sqrt{\frac{\zeta + 1}{\zeta - 1}}\, e^{-ik\zeta}\, d\zeta} \tag{2.23}$$

where the parameter k is the reduced frequency, defined by

$$k = \omega b/V \tag{2.24}$$

If $k \to 0, |C(k)| \to 1,$ the steady state case, while if $k \to \infty, |C(k)| \to 0.5.$ The phase shift has a maximum of approximately -15° at $k = 0.3$, but approaches zero when $k \to \infty.$ For small frequencies, an approximation for the lift deficiency function is given by Johnson [1980a] as

$$C(k) \approx \left(1 - \frac{\pi}{2} k\right) + i k \left(\ln \frac{k}{2} + \gamma\right) \tag{2.25}$$

where $\gamma \approx 0.5772$, the Euler constant.

An expression for the unsteady moment about an axis at $x = \eta b$ (positive nose upward) is

$$m = b\left(\frac{1}{2} + \eta\right) C(k)\, \ell_q + \rho \pi b^3 \left[\eta \ddot{h} - \left(\frac{1}{2} - \eta\right) V\dot{\alpha} - b\left(\frac{1}{8} + \eta^2\right)\ddot{\alpha}\right] \tag{2.26}$$

With the pitch axis at the quarter-chord ($\eta = -\frac{1}{2}$), there is no moment due to lift.

In the preceding expressions, the effect of a time varying free-stream V(t) was ignored i.e. V(t) was assumed constant. Accounting for this effect, according to Johnson [1980a], requires only a few modifications to the above analysis, leading to a new deficiency function. In the same reference, it is also shown that, for small variations in free-stream velocity, this function is approximately the same as the Theodorson function. Specific approximations for applications in rotors are also presented in the same reference.

Another restriction of the preceding analysis is that of sinusoidal (periodic) variations in the kinematics. Wagner considered a step variation in angle of attack, as described by

Bisplinghoff et al [1955]. The result for the change in the circulatory part of lift is

$$\ell = 2\pi\rho V^2 b\ \Delta\alpha\ \Phi(s) \tag{2.27}$$

where $\Delta\alpha$ represents the step change in angle of attack, measured at the three-quarter-chord point. The function $\Phi(s)$ is known as the Wagner function, with parameter $s = Vt/b$. Applications of this method, using approximate expressions for $\Phi(s)$, are described in Beddoes [1984] and Torok & Chopra [1989], the latter of which considers the more general case developed by Küssner, see Bisplinghoff [1955].

As a further development, Loewy [1957] developed a two-dimensional model for the unsteady aerodynamics of the blade section of a hovering rotor, including the effect of the returning shed wake. The analysis, also described in Johnson [1980a], yielded a modified lift deficiency function, known as Loewy's function, in which the wake spacing and phasing were introduced as parameters. Although of theoretical importance, the restriction to vertical flight, which is essentially a symmetrical flight condition, limits its practical use, except maybe to investigate the rotor stability and control in hover.

2.8.2 Approximate solutions

In the exact solutions, the effect of the wake was completely absorbed in a deficiency function. Furthermore these functions are complex integral expressions for simplified prescribed shed wake geometry, and kinematics at a priori known frequencies. Such is not the case in rotor dynamics and aerodynamics and there is a need (a) to obtain expressions for unsteady lift and moment where the induced velocity caused by the shed wake is an explicit parameter for use in discrete three-dimensional vortex models and (b) to obtain simplified expressions for deficiency functions to efficiently calculate near shed wake effects

using two-dimensional models. These objectives are achieved simultaneously, as is shown below.

It is shown in Bramwell [1976] that the part of the lift arising from bound circulation is proportional to the downwash at the three-quarter-chord point. For this reason, this point is frequently referred to as the rear aerodynamic centre. This is the appropriate chordwise position, consistent with the steady state case, to consider for application of the kinematic boundary condition in unsteady airfoil analysis used in lifting line theory. Such an approach was followed by Miller [1964] and also adopted by Piziali [1966] to represent unsteady airfoil behaviour. For this approximation, the effect of the shed wake is treated separately, using the lifting line model of the airfoil. The unsteady lift is presented by

$$\ell = \ell_q - \rho V 2\pi b \lambda + \ell_n \tag{2.28}$$

where ℓ_q and ℓ_n are as defined before. The non-dimensional induced velocity λ is obtained from the shed wake vorticity. In the classical lifting line approximation, the induced velocity is evaluated at a single point, namely the quarter-chord point, which is also the location of the bound vortex ($x = -b/2$). For the wake extended up to this point

$$\lambda = \frac{1}{2\pi} \int_{-b/2}^{\infty} \frac{\gamma_w}{\left(\frac{b}{2} - \zeta\right)} d\zeta \tag{2.29}$$

Using the same approach as Theodorson, an approximate lift deficiency function is obtained, given by

$$C(k) \approx \frac{1}{1 + \frac{\pi}{2} k} \tag{2.30}$$

where k is defined in eqn. (2.24). The result is the same as the approximation for small reduced frequency k, given by eqn. (2.25). This can be explained by the fact that the lifting line assumption of high aspect ratio also implies low reduced frequency.

In deriving C(k) for this approximation, the imaginary part was ignored because it was presented by an infinite integral. This was explained by the fact that the shed vorticity sheet extended up to the bound vortex, giving rise to infinite induced velocities according to the Biot-Savart law. A parametric study, fitting the form of the approximate model to the Theodorson function, showed that the correct starting position for the (continuous) shed wake is at a quarter-chord behind the point where the induced velocity is calculated. Therefore, for the classical lifting line model it should start at the mid-chord, while for the extended lifting line model, it should start at the trailing edge.

Piziali [1966] evaluated a discrete representation of the shed wake from an airfoil represented by a chordwise vorticity distribution, and found that the discrete shed wake for this special case should start at a distance d/3 from the trailing edge, where $d = 2\pi V/Nb\omega$ and N is the vortices per cycle of oscillation at frequency ω. No physical explanation was, however, given for this observation.

Miller [1964] also derived an approximate solution for the Loewy deficiency function, valid for reduced frequencies k = 0.5 or less. Because of its restrictive application, results will not be represented here.

An approximation to the Wagner function frequently used in unsteady airfoil models is presented in Bisplinghoff et al [1955] and is given by

$$\Phi(s) = 1 - A_1 e^{-a_1 s} - A_2 e^{-a_2 s} \tag{2.31}$$

where $A_1 = 0.1650$, $A_2 = 0.3350$, $a_1 = 0.0455$ and $a_2 = 0.3000$. An application of this approximation, corrected for compressibility effects, is discussed by Beddoes [1982].

2.8.3 Generalised model

In order to incorporate an unsteady airfoil model into a rotor aerodynamic model, several effects should be accounted for, not considered up till now, to be able to accurately predict rotor aerodynamic loads or dynamic behaviour. Such effects are spanwise (radial) and reverse flow. The effect of the shed wake, the wake induced velocity λ, should also be kept as a parameter in order to be able to account for the returning shed wake in forward flight. Also, the possibility to include corrections for real flow effects on profile aerodynamic characteristics of the blade should be allowed for. Such a model, which was specifically developed for application to rotors and which represents the most advanced development in this field, is described in Johnson [1980a, 1980b]. The basis for this model, and all such models, is two-dimensional airfoil theory, or approximations thereof, with separate treatment for the near shed wake and the returning wake.

With reference to fig. (2.9), the unsteady aerodynamic lift and moment about the pitch axis for the rotary wing is given by Johnson [1980a] as

$$\ell = c \frac{dc_\ell}{d\alpha} \left\{ \frac{1}{2} | U_T | w + \frac{c}{4} U_T \frac{dw}{dx} \left[1 \pm \frac{2}{c} \left(x_a + \frac{c}{4} \mp \frac{c}{4} \right) \right] + \frac{c}{8} \left(\frac{dw}{dt} + U_R \frac{dw}{dr} \right) \right\} \tag{2.32}$$

$$m = c \frac{dc_\ell}{dx} \left\{ -\frac{1}{2} \left(x_a + \frac{c}{4} \mp \frac{c}{4} \right) | U_T | W \mp \frac{c^2}{32} U_T \frac{dw}{dx} \left[1 \pm \frac{4}{c} \left(x_a + \frac{c}{4} \mp \frac{c}{4} \right) \right]^2 \mp \frac{c^2}{32} \left(\frac{dw}{dt} + U_R \frac{dw}{dr} \right) \left[1 \pm \frac{4}{c} \left(x_a + \frac{c}{4} \mp \frac{c}{4} \right) \right] \right\} \tag{2.33}$$

where dw/dr and dw/dx are the spanwise and chordwise gradient of the upwash, approximated by $w = U_T \sin\theta - U_P \cos\theta$. The upper part of the double sign is for normal flow and the lower part for reverse flow, i.e. $\pm$ = sign (V) where $V = U_T \cos\theta + U_P \sin\theta$.

An extension to the above model, including the effect of an unsteady wake geometry, is presented by Johnson [1988]. Such refinement however, will only be required in advanced aeroelastic analysis, and will not be considered here.

2.8.4 Dynamic stall

The stall of an airfoil in unsteady flow, called dynamic stall, is very different from that in steady flow. A finite rate of increase in angle of attack ($\dot{\alpha}>0$) has the effect of delaying the occurrence of stall, so that the dynamic stall angle of attack and hence lift, is larger than the angle for static stall. With dynamic stall much greater transient lift and pitching moments are associated than in the static case, giving rise to excessive vibration and control

system loads.

Theoretical and experimental analysis established a basis from which empirical models were developed, which correlated well with experimental data, as described by Friedman [1982]. The essence of the phenomena is described below, following the discussion in Johnson [1980b].

As the angle of attack increases, there is a delay in the occurrence of stall due to the unsteady flow. The linear lift and low pitching moment are maintained to an angle of attack α_{ds} greater than the static stall angle α_{ss}. When the dynamic stall angle α_{ds} is reached, which is dependent on $\dot{\alpha}$, there is a loss of leading edge suction, accompanied by the shedding of a strong vortex from the vicinity of the leading edge of the airfoil. This vortex moves aft over the upper surface of the airfoil, at a velocity much lower than the free stream value. The vortex induces a pressure disturbance on the airfoil upper surface, an area of high suction, moving aft. This pressure disturbance produces the high transient lift, moment and drag forces on the airfoil, that characterize dynamic stall. There is a large peak lift, followed by a large peak nose-down moment. After passage of the leading edge vortex over the upper surface, the flow progresses to the fully separated state, and hence to static stall loads. The flow at this points depends greatly on the transient blade motion, including the magnitude of the mean and oscillatory angles of attack (secondary vortices may be shed from the leading edge) and torsional coupling effects. If the angle of attack decreases, the flow eventually reattaches to an angle below the static stall angle of attac

To develop a model for the separated flow regime, recourse is made to static airfoil windtunnel data, such as presented in Abbott & van Doenhoff [1949] for several NACA profiles. For each Mach number, the angle of attack α_1, which delimits attached flow is determined by the break in pitching moment and a further angle α_2 is used to represent the condition where flow separation and hence centre of pressure has stabilized. In typical

dynamic stall models, with reference to fig. (2.10), when the local value of angle of attack exceeds α_1, the onset of separation is assumed to be delayed for a finite period of time τ_1 to point a, during which the lift and moment behave as appropriate for attached flow. When the time delay is exceeded, flow separation is assumed to be initiated by the shedding of a vortex from the surface of the airfoil, and after a further period of time τ_2 to point b, during which the vortex traverses the chord, and passes free of the surface. In this interval, lift is generated by the vortex and the overall level is higher or is maintained equivalent to that for fully attached flow, but the centre of pressure moves aft as a function of both angle of attack and time. When the vortex passes free of the surface, the lift decays rapidly to a value appropriate to fully separated flow assuming that the angle of attack is still sufficiently high (point c). If and when the angle of attack reduces below the value α_1, reattachment of the flow is represented by the attached flow model.

Several dynamic stall models of varying complexity are used in rotor aerodynamic modelling. A general discussion on such models is presented by Friedman [1982], while specific models are described in Scully [1975], Johnson [1981], Beddoes [1983] and Gangwani [1984]. The model described and developed by Johnson [1980b] was implemented with some minor changes, of which details will be presented later.

2.9 Vortex theory of rotating wings

In the vortex theory, the rotating wing is replaced by a system of bound and free vortices. Associated with the lift of a rotating wing is a bound circulation, while conservation of vorticity requires that the bound circulation be trailed in the so called wake from the tip and the root. Vorticity is also left in the wake as a consequence of radial and azimuthal changes in the bound circulation giving rise to spiral (or trailing) vorticity and radial (or shed) vorticity. This basic flow geometry is illustrated in fig. (2.11).

2.9.1 Structure of the wake

Turning now to the detail of the geometry of the wake of an advancing helicopter rotor blade, it was found by flow studies such as reported in Baskin et al. [1976] that the vortices are distributed over a surface that may be practically considered as a cylinder with an elliptical cross-section, while vortices themselves form a helix with constant pitch. From these observations it was concluded that (a) vortex elements move in space together with particles of a uniform rectilinear flow with velocity $\bar{V}$ and (b) the axis of the elliptical cylinder did not coincide with the direction of the undisturbed flow $\bar{V}_\infty$ due to the influence of induced velocities on the movement of the vortices. Results from such experiments can, according to Baskin et al. [1976], be sufficiently accurately described by the hypothesis of the constancy of velocity of the movement of the vortices, expressed by the vectorial relationship

$$\bar{V} = \bar{V}_\infty + \bar{w}_i \qquad (2.35)$$

The structure of the helical wake is presented in fig. (2.12). For a rigid wake, $\bar{w}_i$ is the induced velocity averaged over the disc, represented normally by the momentum theory result as expressed by eqn. (2.1). At sufficiently high forward speeds, $V \approx V_\infty$, giving rise to the so called flat wake approximation. For a semi-rigid wake, the vorticity trailed and shed at a point (r,ψ) is transported down at the local induced velocity $w_i(r,\psi)$, while Miller [1964] used an induced velocity averaged only over the radius, using a series representation over the azimuth. Due to the mutual interference of the vortices, the wake is continuously being deformed, resulting in a rather complex wake structure, specifically at low forward speed. It is however difficult to account for these deformations of the system of trailing and shed vorticity. Therefore, in theoretical models, no attempts have been made to take these deformations into account.

2.9.2 Velocity induced by the wake

If the form of the wake is known, the Biot-Savart law as expressed by eqn. (2.4) can be used to determine the velocity induced at a point P(x,y,z) by a vortex filament $d\bar{l}$ of strength Γ located at a point $Q(\xi,\eta,\zeta)$ a distance $\bar{l}$ from P(x,y,z), as illustrated in fig. (2.12). The circulation Γ is assumed positive if the vorticity per unit length is in the same (vectorial) direction as $d\bar{l}$, while $\bar{l}$ is the position vector from P to Q. The equation of the curve S in parametric form is

$$\xi = \xi(p),\ \eta = \eta(p),\ \zeta = \zeta(p) \tag{2.36}$$

where p is usually selected as either some angle or length of a segment on curve S. As the parameter p varies from its initial value P_i to its final value P_f, point $Q(\xi,\eta,\zeta)$ describes curve S. The vector $\bar{l}$ can be expressed as

$$\bar{l} = (\xi - x)\bar{i} + (\eta - y)\bar{j} + (\xi - z)\bar{k} \tag{2.37}$$

while its derivative $d\bar{l}$, which is always tangent to curve S, is obtained from eqns. (2.36) and (2.37) as

$$d\bar{l} = \left(\frac{\partial \xi}{\partial p}dp\right)\bar{i} + \left(\frac{\partial \eta}{\partial p}dp\right)\bar{k} + \left(\frac{\partial \zeta}{\partial p}dp\right)\bar{k} \tag{2.38}$$

Using eqn. (2.4), with $\bar{l} = -\bar{r}$ yields

$$d\bar{V} = \frac{d\Gamma}{4\pi}\frac{\bar{l}xd\bar{l}}{l^3} \tag{2.39}$$

Introducing eqn. (2.37) and (2.38) in (2.39) and integrating between P_i and P_f the projections of the induced velocity at point P is given by

$$u_i = \frac{1}{4\pi}\int_{P_i}^{P_f} \Gamma\left[\frac{\partial \eta}{\partial p}(z-\zeta) - \frac{\partial \zeta}{\partial p}(y-\eta)\right]\frac{dp}{l^3} \tag{2.40a}$$

$$v_i = \frac{1}{4\pi} \int_{P_i}^{P_f} \Gamma \left[\frac{\partial \zeta}{\partial p} (x-\xi) - \frac{\partial \xi}{\partial p} (z-\zeta) \right] \frac{dp}{l^3} \tag{2.40b}$$

$$w_i = \frac{1}{4\pi} \int_{P_i}^{P_f} \Gamma \left[\frac{\partial \xi}{\partial p} (y-\eta) - \frac{\partial \eta}{\partial p} (x-\xi) \right] \frac{dp}{l^3} \tag{2.40c}$$

where

$$l = \left[(x-\xi)^2 + (y-\eta)^2 + (z-\zeta)^2 \right]^{1/2} \tag{2.41}$$

The above relations are presented in Baskin et al. [1975], including a correction for the effect of compressibility, not considered here.

To obtain parametic equations of the vortex surface, the movement of an arbitrary vortex element, which has separated from the lifting line, has to be considered. With reference to fig. (2.13), representing a N-bladed rotor with angular velocity Ω submerged in a rectilinear air stream flowing with velocity V, element C was generated at the instant when segment OB = ρ of the lifting line was in the position OA. After its separation at point A, the element began to move with speed V and reached point C at the moment when segment OA moved to position OB.

The coordinates at point A are

$$\xi_A = \rho \cos \left(\psi_n - \phi \right) \tag{2.42a}$$

$$\eta_A = \rho \sin\left(\psi_n - \phi\right) \tag{2.42b}$$

$$\zeta_A = 0 \tag{2.42c}$$

neglecting deviation of the blade from the plane of rotation. The time of rotation of the lifting line (blade n) from its position OA to position OB is ϕ/Ω, where ψ_n is the azimuth of blade n at the instant of time in question and ϕ is the azimuth at the instant of time the vortex was shed. During this time the vortex element is displaced with respect to A by the increments

$$\Delta\xi_A = V_\infty \left(\phi/\Omega\right) \cos\alpha \tag{2.43a}$$

$$\Delta\eta_A = 0 \tag{2.43b}$$

$$\Delta\zeta_A = -\left(\phi/\Omega\right)\left[V_\infty \sin\alpha + w_i\left(\rho, \psi_n - \phi\right)\right] + z\left(\rho, \psi_n - \phi\right) \tag{2.43c}$$

Therefore, combining eqns. (2.42) and (2.43), the coordinates of an arbitrary point Q is given by

$$\xi = \rho\cos\left(\psi_n - \phi\right) + V_\infty \left(\phi/\Omega\right) \cos\alpha \tag{2.44a}$$

$$\eta = \rho \sin\left(\psi_n - \phi\right) \tag{2.44b}$$

$$\zeta = -\left(\phi/\Omega\right)\left[V_\infty \sin\alpha + w_i\left(p, \psi_n - \phi\right)\right] + z\left(\rho, \psi_n - \phi\right) \tag{2.44c}$$

where

$$\epsilon\, R \le \rho \le R, \quad 0 \le \psi_n \le 2\pi, \quad 0 \le \phi \le \infty \tag{2.45}$$

It is assumed that the xz-plane is orientated parallel to $\bar{V}_\infty$ and the xy-plane is perpendicular to the rotor shaft.

Eqn. (2.44) represent the parametric equations of the vortex wake. If, in these equations, ρ, ψ_n and w_i are constant, then for given values of V_∞ and α and with ϕ as parameter, an equation of a skewed helical curve is obtained. If the radius ρ varies within the limits expressed by eqn. (2.45), a family of such lines is obtained, completely covering the vortex wake surface. Along those lines extend the elementary spiral (trailing) vortices with circulation

$$\Gamma_t = -\frac{\partial}{\partial\rho}\,\Gamma\left(\rho, \psi_n - \phi\right) d\rho \tag{2.46}$$

The negative sign is in accordance with the first theorem of Helmholz, requiring a positive (negative) vorticity being shed if the bound vorticity decreases (increases).

If, in eqn. (2.44), ψ_n, ϕ and w_i are assumed constant for given values of V_∞ and α, a trace of the lifting line with parameter ρ is obtained, while varying ϕ within the limits expressed by eqn. (2.45) yields a family of those segments, covering the vortex wake surface. On those lines, the elementary radial (shed) vortices are located, with circulation given by

$$\Gamma_s = - \frac{\partial}{\partial \psi} \Gamma \left(\rho, \psi_n - \phi\right) d\psi \tag{2.47}$$

where the negative sign is in accordance with Kelvin's theorem, which requires constancy of circulation within a closed contour.

The equations presented in this section form the basis of rotor vortex theory. An expression for the induced velocity in the plane of the rotor can be obtained and taken into consideration when the true (effective) angles of attack of the blade sections at various r and ψ are determined. Then the loads on the blades can be determined by expressions such as eqn. (2.15). Usually the induced velocities are expressed by the sum of three components

$$w_i = w_b + w_t + w_s \tag{2.48}$$

representing velocities induced by the bound, trailing and shed vorticity respectively. The effect of velocities induced in the xy-plane are neglected. Expressions for each term in eqn. (2.48) will be obtained in the following sections for an arbitrary blade n (say n=0) of a N-bladed rotor.

2.9.3 Induced velocity from bound vortices

Bound vortices have a circulation equal to $\Gamma_n\left(r,\psi_n\right)$ and are located along the rotor blades. The subscript n = 0, 1, ..., N - 1 denotes the numeral of the rotor blade, while N is the number of blades. Parametric equations of the lifting line follow from the eqn. (2.44) with $\phi = 0$, giving

$$\xi_b = \rho \cos\psi_n \tag{2.49a}$$

$$\eta_b = \rho \sin\psi_n \tag{2.49b}$$

$$\zeta_b = z\left(\rho,\psi_n\right) \tag{2.49c}$$

The induced velocity is calculated at points along the blade n = 0 at azimuth ψ_o. For this blade

$$x_b = r \cos\psi_o \tag{2.50a}$$

$$y_b = r \sin\psi_o \tag{2.50b}$$

$$z_b = z_o\left(r,\psi_o\right) \tag{2.50c}$$

while an expression for the velocity induced by the bound vortex follows from eqn. (2.40c) with $p = \rho$, yielding

$$w_b = \sum_{n=o}^{N-1} \frac{1}{4\pi}\int_{eR}^{R} \Gamma\left(\rho,\psi_n\right)\left[\frac{\partial\xi_b}{\partial\rho}\left(y_b - \eta_b\right) - \frac{\partial\eta_b}{\partial\rho}\left(x_b - \xi_b\right)\right]\frac{d\rho}{l^3} \tag{2.51}$$

where

$$\frac{\partial\zeta_b}{\partial\rho} = \cos\psi_n \tag{2.52a}$$

$$\frac{\partial\eta_b}{\partial p} = \sin\psi_n \tag{2.52b}$$

and

$$\psi_n = \psi_o + 2\pi n/N \tag{2.53}$$

Note that $w_{z_{on}} = 0$ for $n = 0$, because the bound vortex at ψ_o does not induce velocities along the radius at ψ_o.

2.9.4 Induced velocity from spiral vortices

To determine the induced velocities from spiral (trailing) vortices, the velocities induced by vortices trailing from different radii of the blade, as well as from different blades, must be summed. Parametric equations for the spiral vortices are given by eqn. (2.44). The induced velocity is calculated along azimuth ψ_o at points defined by eqn. (2.49), while an expression for the velocity induced by the spiral vortices follows from eqn. (2.40c) with $p = \phi$. The circulation of a spiral vortex element is given by eqn. (2.46). Integrating this result radially yields

$$w_{z_t} = -\sum_{n=o}^{N-1} \frac{1}{4\pi} \int_{eR}^{R} \int_{o}^{\infty} \left[\frac{\partial}{\partial \rho} \Gamma \left(\rho, \psi_n - \phi \right) \right] \left[\frac{\partial \xi_t}{\partial \phi} \left(y_t - \eta_t \right) - \frac{\partial \eta_t}{\partial \phi} \left(x_t - \xi_t \right) \right] \frac{d\phi d\rho}{l^3} \quad (2.54)$$

where, from eqn. (2.44)

$$\frac{\partial \xi_t}{\partial \phi} = \rho \sin \left(\psi_n - \phi \right) + \frac{V_\infty}{\Omega} \cos\alpha \quad (2.55a)$$

$$\frac{\partial \eta_t}{\partial \phi} = -\rho \cos \left(\psi_n - \phi \right) \quad (2.55b)$$

and ψ_n is as defined in eqn. (2.53).

2.9.5 Induced velocity from radial vortices

An expression for the velocity induced by radial vortices is obtained, as before, from eqn. (2.40c) with p = ρ, while the circulation for this case is given by eqn. (2.47).

Integrating this result with respect to ϕ between 0 and ∞ yields

$$w_s = -\sum_{n=0}^{N-1} \int_0^{\infty} \int_R^R \left[\frac{\partial}{\partial \phi} \Gamma(\rho, \psi_n - \phi)\right] \left[\frac{\partial \xi_s}{\partial \rho}(y_s - \eta_s) - \frac{\partial \eta_s}{\partial \rho}(x_s - \xi_s)\right] \frac{d\rho d\phi}{\ell^3} \qquad (2.56)$$

where

$$\frac{\partial \xi_s}{\partial \rho} = \cos(\psi_n - \phi) \qquad (2.57a)$$

$$\frac{\partial \eta_s}{\partial \rho} = \sin(\psi_n - \phi) \qquad (2.57b)$$

and ψ_n as defined in eqn. (2.53). Parametric expressions for the radial vortices are given by eqn. (2.44) while the location for calculating the induced velocities is at points defined by eqn. (2.49).

2.9.6 Integrodifferential equation of rotor vortex theory

To determine the aerodynamic load on the blade profile, the induced downwash must be determined from all free and bound vortices of all the blades, with the exception of the bound vortex of the blade in question (n = 0). Similarly to lifting line theory, the kinematic flow condition postulated by eqn. (2.16) must be satisfied at the blade section, which, for small angles becomes

$$U_T \alpha_\infty = U_T\theta - U_T \alpha_a \tag{2.58}$$

where

$$U_T = \Omega r + V_\infty \cos\alpha \sin\psi_o \tag{2.59}$$

as illustrated in fig. (2.9). With reference to the same figure, the angle α_a can be approximated as

$$\alpha_a = \frac{U_P}{U_T} + \frac{w_i}{U_T} \tag{2.60}$$

where

$$U_P = V_\infty \sin\alpha + z + \frac{\partial z}{\partial t} V_\infty \cos\alpha \cos\psi_o \tag{2.61}$$

and θ is measured to the zero-lift line of the blade section. Similar to eqn. (2.18), the effective (two-dimensional) angle of attack and the circulation is related by

$$\Gamma_o = \tfrac{1}{2} c \frac{dc_\ell}{d\alpha} U_T \alpha_e \tag{2.62}$$

based on the assumption of linear variation of c_l and α_e. Hence, substituting eqns. (2.51), (2.54) and (2.56) in eqn. (2.48) and subsequently substituting the expression for w_i, together with equation (2.58) and (2.60) into eqn. (2.62) yields the integrodifferential equation for the circulation distribution of a N-bladed rotor in rectilinear flight, represented by a lifting line semi-rigid wake model. The result is

$$\Gamma\left(r,\psi_o\right) = \tfrac{1}{2} c \frac{dc_\ell}{d\alpha}\left(\theta - \frac{U_P}{U_T}\right) - w_b - w_i - w_s \tag{2.63}$$

Expressions for w_b, w_t and w_s as well as all the geometric parameters x_i, y_i, ψ_i and η_i and their derivatives are given in the previous sections. The subscript of ψ_o may be neglected and the summations involved in calculating the induced velocity of the bound vortices may start from $n=1$, because for $n=0$ the integral reduces to zero. The blade aerodynamics is coupled with the dynamics primarily through the U_P and U_T terms, while the dynamics is in turn dependent on $\Gamma(r,\psi)$. The above derivation was based on discussions and derivations presented by Mil' et al. [1966], Bramwell [1976] and Baskin [1976].

No general method exists for solving eqn. (2.63), even with a rigid wake assumption and neglecting blade dynamics. One possible way is to use the method of successive approximations, which involves assuming a simple induced velocity distribution, eg. from

eqn. (2.1), after which $\Gamma(r,\psi_o)$ is calculated. In subsequent approximations, the previous value of $\Gamma(r,\psi_o)$ is used to calculate the induced velocity (integrals) and hence a new value for $\Gamma(r,\psi_o)$, until convergence is achieved. According to Mil' [1966] and Bramwell [1976], convergence is obtained only in particular cases. A specific problem involved in numerical integration is the fact that the induced velocities become infinite on the lifting line, the reason being (a) vortices being formed close and parallel to the lifting line in the case of unsteady flow and (b) spiral vortices shed from the blade makes an angle differing from $\pi/2$ with the blade axis in the case of oblique flow through the rotor. Consequently, infinite velocities will be induced at the lifting line, except in the case of axial steady flow. These difficulties can be overcome by neglecting unsteady effects and by assuming trailing vortices normal to the rotor blades, rendering, however, only approximate solutions. If a lifting surface rather than a lifting line model is assumed, this problem is avoided, but a penalty is paid in terms of increased complexity and restricted applications, eg attached flow conditions.

In this thesis, a discretized model such as described by Piziali [1966] and Baskin et al. [1976] will be derived from the theoretical model and solved for rectilinear flight. Details of this model, which will also incorporate non-linear effects, such as stall and compressibility, and also blade dynamic modelling, are discussed in subsequent chapters.

CHAPTER 3

ROTOR AERODYNAMIC MODEL

In the previous chapter, an analytical rotor vortex model was developed from basic theory, subject to linear, steady section characteristics and small angles approximations. In this chapter, these restrictions will be lifted and a discrete vortex rotor model, accounting for the most important flow phenomena, will be developed.

3.1 Rotor flow description

All forces and velocities are resolved in the hub plane, which is perpendicular to the rotor shaft, as illustrated in fig. (3.1). The rotor is rotating at speed Ω and the velocity V of the air as seen by the rotor disc has components u, v and w. The angles of attack and sideslip of the rotor disc are defined by

$$\alpha_h = \sin^{-1}\left(\frac{w}{V}\right) \tag{3.1a}$$

$$\beta_h = \tan^{-1}\left(\frac{v}{u}\right) \tag{3.1b}$$

The air velocity U as seen by the rotor blade section has components U_T, U_R and U_P as illustrated in fig. (2.9) and is due to the rotor rotation, the helicopter forward speed, the induced velocity w_i and the out of plane motion (flapping, pitching, bending and twisting) of the blades. These components, which are functions of both radius r and azimuth ψ and include induced velocities, are given by

$$U_T(r,\psi) = \Omega R + \left[u + u_i(r,\psi)\right]\sin\psi + \left[v + v_i(r,\psi)\right]\cos\psi + \dot{y}_o(r,\psi) \tag{3.2a}$$

$$U_R(r,\psi) = \left[u + u_i(r,\psi)\right]\cos\psi - \left[v + v_i(r,\psi)\right]\sin\psi \tag{3.2b}$$

$$U_P(r,\psi) = \left[w + w_i(r,\psi)\right] + \dot{z}_o(r,\psi) + U_R \frac{d}{dr}\left[\dot{z}_o(r,\psi)\right] \tag{3.2c}$$

The induced velocities and blade motion in the plane of rotation will be henceforth neglected. More elaborate expressions, including shaft motion, are presented by Johnson [1980b].

The effective (two-dimensional) angle of attack seen by a blade section is given by

$$\alpha(r,\psi) = \theta(r,\psi) - \tan^{-1}\left(U_P/U_T\right) \tag{3.3}$$

where, assuming no torsional motion, control system flexibility or kinematic coupling effects, the pitch angle is expressed as

$$\theta(r,\psi) = \theta_o + \theta_t(r) + \sum_n \theta_{nc}\cos n\psi + \sum_n \theta_{ns}\sin n\psi \tag{3.4}$$

The coefficients in the summation represents harmonics of the lateral and longitudinal cyclic pitch variation respectively.

The local Mach number seen by a blade section is given by

$$M(r,\psi) = \left[\left(U_T^2 + U_P^2\right)/(\gamma RT)\right]^{1/2} \tag{3.5}$$

where, for air, γ can be taken as 1.4 and R, (the gas constant) as 287 Nm/kgK, under normal operating conditions.

3.2 Geometry of the vortex model

Blade k at azimuth ψ_k of an nb-bladed rotor is divided into nr radial segments as illustrated in fig. (3.2). The centre point on each segment is designated by i = 1,2,...,nr, while the points of division (nodes) are p = 1,2,...,nr+1. Distance of i and p from the rotor axis are given by

$$r_i = \frac{R-R_o}{nr}\left(i - \frac{1}{2}\right) + R_o \qquad i = 1,2,...,nr \tag{3.6a}$$

$$\rho_p = \frac{R-R_o}{nr}(p-1) + R_o \qquad p = 1,2,...,nr+1 \tag{3.6b}$$

The azimuth of the rotor disc and each of the nz revolutions of the helical wake below each blade is divided into na segments, where na is a multiple of the number of blades. The revolutions of layers of the wake are designated by $\ell = 1,2,...,nz$, while the points of division (nodes) are at $q = 1,2,...,na+1$. The azimuth or wake angle ϕ of node q of layer ℓ of the wake, measured from an arbitrary blade, is given by

$$\phi_{q\ell} = \frac{2\pi}{na}(q-1) + 2\pi(\ell-1) \tag{3.7}$$

The location of each blade $k = 1,2,...,nb$ is denoted by ψ_k, while the location of blade k is related to that of the first (reference) blade, expressed by

$$\psi_k = \psi + \frac{2\pi}{nb}(k-1) \tag{3.8}$$

Nodes $j = 1,2,...,na$ are located at a fixed distance δ_c in front of and perpendicular to the dividing lines between the azimuthal segments representing successive locations of a rotor blade. The azimuth or disc angles ψ associated with these lines are defined as

$$\psi_j = \frac{2\pi}{na}(j-1) \qquad j = 1,2,...,na \tag{3.9a}$$

$$\psi_q = \frac{2\pi}{na}(q-1) \qquad q = 1,2,\ldots,na+1 \tag{3.9b}$$

A node (ij) is denoted a control point and the network of these nodes, representing the rotor disc, are designated by N^c_{ij}. Nodes of the network representing the rotor wake are designated by N^w_{pqkl}. The bound circulation or lifting line is considered to be concentrated at a fixed distance $(\delta_b - \delta_c)$ in front of the control point, with nodes designated by N^b_{pqk}. This ordering scheme is illustrated in fig. (3.2).

The coordinates of the control points N^c_{ij} are, from eqn (2.42), including blade motion

$$x^c_{ij} = r_i \cos\psi_j - \delta_c \sin\psi_j \tag{3.10a}$$

$$y^c_{ij} = r_i \sin\psi_j + \delta_c \cos\psi_j \tag{3.10b}$$

$$z^c_{ij} = z(r_i,\psi_j) \tag{3.10c}$$

The coordinates of the nodes representing the helical wake are

$$x^w_{pqkl} = r_p \cos(\psi_k - \phi_{qkl}) + \left(\frac{\phi_{qkl}}{\Omega}\right) U_T(r_p,\psi_k - \phi_{qkl}) \tag{3.11a}$$

$$y^{w}_{pqkl} = r_p \sin\left(\psi_k - \phi_{qkl}\right) \tag{3.11b}$$

$$z^{w}_{pqkl} = -\left(\frac{\phi_{pl}}{\Omega}\right) U_P\left(r_p, \psi_k - \phi_{qkl}\right) + z\left(r_j, \psi_j\right) \tag{3.11c}$$

Finally, the coordinates of the nodes representing the lifting line are

$$x^{b}_{pk} = r_p \cos\psi_k - \left(\delta_b\right) \sin\psi_k \tag{3.12a}$$

$$y^{b}_{pk} = r_p \sin\psi_k + \left(\delta_b\right) \cos\psi_k \tag{3.12b}$$

$$z^{b}_{pk} = z\left(r_p, \psi_k\right) \tag{3.12c}$$

The above equations define the basic wake geometry. A correction to account for wake contraction can be introduced here, but was not considered.

3.3 Induced Velocities

The bound and free vorticity associated with the circulation of the lifting surface (line) and wake respectively, induces velocities according to the Biot-Savart law at any arbitrary point in the flow, which changes the circulation of the lifting surface as well as the geometry of the wake. Neglecting the deformation of the wake and assuming that the lifting surface is represented by a lifting line, the induced velocities need only be calculated at (na) azimuthal and (nr) radial locations, after which its effect must be accounted for in calculating the bound circulation.

3.3.1 Free vortices

Free vortices involve trailing and shed vorticity associated with radial and azimuthal changes of blade circulation respectively. Using the ordering scheme introduced, let a cell S_{pqkl} be formed by intersection of a pair of lines p and p+1 with a pair of lines q and q+1. A closed discrete vortex with constant circulation Γ_{pqkl} extends along the boundaries of the cell S_{pqkl}, as illustrated in fig. (3.3).

The circulation Γ_{pqkl} of a cell is equal to the lifting line circulation on the line segment (p,p+1) of blade k at the instant the blade was at azimuth

$$\psi_q = \psi_k - \left(\phi_q + 2\pi\ell\right) \tag{3.13}$$

Therefore, because circulation is a periodic function of azimuth, it follows that

$$\Gamma_{pqk\ell} = \Gamma_{pqk(\ell+1)} \tag{3.14}$$

Furthermore, when each blade passes an azimuth ψ_k within the range $[0,2\pi]$, a cell with circulation Γ_{pq} is shed which, in the case of a semi-rigid wake, translates downward and rearward with the same local vertical and horizontal velocity component respectively. It then follows that

$$\Gamma_{pqk} = \Gamma_{pq(k+1)} \tag{3.15}$$

and therefore, there are only (na*nr) unknown values of discrete circulation Γ_{pq} to be determined. Therefore, at radius r_p and wake azimuth angle expressed as

$$\begin{aligned} \phi_{qkl} &= \psi_k - \psi_q + 2\pi(\ell-1) && 0 \le \psi_q \le \psi_k \\ &= \psi_k + (2\pi - \psi_q) + 2\pi(\ell-1) && \psi_k < \psi_q < 2\pi \end{aligned} \tag{3.16}$$

relative to blade k, a layer of (nb*nz) cells with the same geometry and circulation Γ_{pq} are shed, as illustrated in fig. (3.3). The velocity induced by such a layer of cells S_{pqkl} at control point N_{ij}^{c} in the z-direction is expressed as

$$w_{ijpq}^{f} = \Gamma_{pq}\, f_{ijpq} \tag{3.17}$$

where

$$f_{ijpq} = \sum_{k}^{nb} \sum_{\ell}^{nz} g\left[\left(x_{ij}^{c}, y_{ij}^{c}, z_{ij}^{c}\right), \left(x_{pqkl}^{w}, y_{pqkl}^{w}, z_{pqkl}^{w}\right)\right] \tag{3.18}$$

is denoted the influence coefficient of a layer of similar cells, calculated by applying the Biot-Savart law, presented by the function g, to a cell of the layer assuming unit circulation. The velocity induced by all the layers representing the wake, or free vorticity, at node (ij), is given by

$$w_{ij}^{f} = \sum_{p}^{nr} \sum_{q}^{na} \Gamma(r_p, \psi_q)\, f_{ijpq} \tag{3.19}$$

Calculation of the influence coefficients will be detailed later.

3.3.2 Bound vortices

The blade (lifting line) is represented by (nr) rectangular vortex cells with circulation equal to the adjacent free vortex cells. The bound and its adjacent free vortex cell geometry are illustrated in fig. (3.4a) for the classical lifting line model and in fig. (3.4b) for the extended lifting line model. These representations are in accordance with the requirements that the lifting line should be positioned at the quarter chord, the spiral (trailing) vortices should start at the quarter chord and the radial (shed) vortices should start at a quarter chord behind the position where the induced velocity is calculated (control point). A rectangular geometry is prescribed to avoid infinite velocities induced at the control point by the trailing vortices for the classical lifting line blade representation, as discussed in §2.9.5. To avoid this singularity, a more elementary scheme is described by Baskin et al [1976].

The velocity induced by a bound vortex cell S_{pq} with circulation Γ_{pq} at control point N_{ij}^{c} is given by

$$w_{ijpq}^{b} = \Gamma_{pq}\, b_{ijpq} \tag{3.20}$$

where

$$b_{ijpk} = g\left[\left(x_{ij}^{c}, y_{ij}^{c}, z_{ij}^{c}\right), \left(x_{pk}^{b}, y_{pk}^{b}, z_{pk}^{b}\right)\right] \tag{3.21}$$

is the bound vorticity influence coefficient, calculated similarly to the free vorticity influence coefficient. The velocity induced by all the bound vortex cells is given by

$$w_{ij}^{b} = \sum_{k}^{nb} \sum_{p}^{nr} \Gamma(r_p, \psi_q) b_{ijpk} \tag{3.22}$$

where

$$\begin{aligned} q &= j + \frac{na}{nb}(k-1) && q \le na \\ &= \left[j + \frac{na}{nb}(k-1) \right] - na && q > na \end{aligned} \tag{3.23}$$

to facilitate indical calculation of the circulation Γ. In the above expressions, the blade azimuth angle ψ of the reference (first) blade is replaced by ψ_{ij}.

3.4 Blade circulation

3.4.1 Lifting Line Model

The bound circulation of a blade section at arbitrary radius r_i and azimuth ψ_j is, according to Johnson [1980b], given by

$$\Gamma_{ij} = \Gamma_{ij}^{o} + \Gamma_{ij}^{t} \tag{3.24}$$

where

$$\Gamma^{o}_{ij} = \left[\frac{1}{2}\, U_T\, c\, c_\ell(\alpha,M)\right]_{ij} \tag{3.25}$$

is the steady circulation, while

$$\Gamma^{t}_{ij} = \left[\left(\frac{dc_\ell}{d\alpha}\right)\frac{c^2}{4}\left(\dot{\theta} + \Omega\,\frac{dz}{dr} + U\,\frac{d\theta}{dr}\sin\psi\right)\left(1 + 2\,\frac{\delta_a}{c}\right)\right] \tag{3.26}$$

represents the unsteady circulation below stall, obtained from thin airfoil theory as described by Johnson [1980a]. Above stall, the unsteady effects are accounted for in a dynamic stall model for c_ℓ, as will be presented later. The section aerodynamic characteristics for attached (unstalled) flow can be obtained from a suitable model, or tables, with the angle of attack and Mach number, given by eqns. (3.3) and (3.5), as inputs. Details of this procedure will also be discussed in a later section.

The blade circulation distribution $\Gamma(r_i,\psi_j)$ is obtained by solving eqn. (3.24) for all i and j. The right hand side of this equation is however dependent on the induced velocities and hence circulation distribution, therefore an iterative procedure is required. (Assuming steady, linearized aerodynamic characteristics yields a system of (nr⋆na) linear equations for the unknown Γ_{ij} as described by Piziali [1966]). The procedure adopted is as follows: (a) Calculate initial values for induced velocities and blade motion assuming uniform inflow as obtained from momentum theory (to expedite the process), (b) Calculate the influence coefficients, (c) Calculate the angle of attack and Mach number distribution and hence the sectional aerodynamic characteristics for the r_i, ψ_j on the rotor disc. (d) Solve eqn. (3.24)

to obtain a new circulation distribution $\Gamma(r_i,\psi_j)$. Use these new values to calculate the induced velocities, using the previous values of influence coefficients. (e) Recalculate the sectional properties and bound circulation or every i and j using eqn. (3.24). (f) Repeat the procedure until $\Gamma(r_i,\psi_j)$ converges. Calculate the blade motion by solving the blade dynamic equations (presented later) and repeat this procedure for every converged $\Gamma(r_i,\psi_j)$ until the blade motion $\beta(r_i,\psi_j)$ has converged. (g) Calculate the blade load distribution and rotor forces. If the control position $\theta(r_i,\psi_j)$ is given, the process terminates. If a rotor force (thrust) is specified, the process is repeated for a new value of $\theta(r_i,\psi_j)$ until the calculated value converges within a certain tolerance to the specified value.

This procedure is outlined in fig. (3.5). Subsequent sections will treat detailed modelling involved in the procedure.

3.4.2 Approximate lifting surface model

An approximate lifting surface model can be constructed by representing the rotor blade by a series of single vortex panels along the radius. The kinematic flow condition used in lifting surface theory is that there be no flow through the surface. If the rotor blade section is assumed to have no camber, this condition reduces to

$$w_{ij} \approx U_{T_{ij}}\, \alpha_{ij} \tag{3.27}$$

where α in this case excludes the induced angle of attack. A system of (nr$\star$na) algebraic equations is obtained, expressed in matrix form as

$$\left\{U_{T_{ij}}\, \alpha_{ij}\right\} = \left[f_{ijpq}\right] \left\{\Gamma_{ij}\right\} \tag{3.28}$$

with Γ_{ij} the unknown circulation distribution (the subscripts of the rows of the vectors and the matrix are taken as i = 1,2,...,nr, j = 1,2,...,na, while the subscripts of the columns of the matrix are taken as p = 1,2,...,nr, q = 1,2,...,na). This system can be solved directly using Gauss-Jordan elimenation or iteratively using the Gauss-Seidel procedure. The model described by eqn. (3.28) is a linear model, restricted to attached flow conditions, which is, however, not generally the case in rotor applications.

3.5 Influence coefficients

The influence coefficients are determined by using eqn. (2.5), but with a correction accounting for a finite core radius, as introduced by Scully [1975]. Only the z-component is considered, and with induced velocity defined positive downward, an expression for this component is given by

$$w_i = -\frac{\Gamma}{4\pi}\left[\frac{\left(r_{1_x} r_{2_y} - r_{2_x} r_{1_y}\right)\left(r_{11} + r_{22}\right)\left(1 - r_{12}^2/r_{11}\, r_{22}\right)}{r_{11}^2\, r_{22}^2 - r_{12}^4 + r_c^2\left(r_{11}^2 + r_{22}^2 - 2r_{12}^2\right)}\right] \tag{3.29}$$

where

$$r_{mn} = \left[r_{m_x} r_{n_x} + r_{m_y} r_{n_y} + r_{m_z} r_{n_z}\right]^{1/2} \tag{3.30}$$

and r_c is the vortex core radius. Inside the vortex core, the velocity induced decreases linearly to zero. Assuming unit circulation Γ and substituting the radius vector from the nodes pq of a cell to the control point ij on the disc, yields the influence coefficients.

3.5.1 Free vortex cells

Consider the four sides of an arbitrary cell S_{pqkl} in the wake, assuming they can be approximated as straight line segments. The position vector of the control point (i,j) is given by eqn. (3.10), while that of the node (p,q,k,l) by eqn. (3.11), for the chosen reference system. It then follows that for the vortex line connecting (p,q,k,l) and (p+1,q,k,l) with positive circulation

$$\begin{aligned} r_{1_{(\ )}} &= (\ )^{w}_{pqkl} - (\ )^{c}_{ij} \\ r_{2_{(\ )}} &= (\ )^{w}_{(p+1)qkl} - (\ )_{ij} \end{aligned} \qquad (3.31a)$$

where ( ) denotes x, y or z. A function value g_1, is obtained if these values are substituted in eqn. (3.31a) with $\Gamma = 1$. Continuing in the positive direction of circulation expressions for the radius vectors and hence functions g_n for the remaining three line segments of the cell can be obtained. For the line segment connecting (p+1,q,k,l) and (p+1,q+1,k,l)

$$\begin{aligned} r_{1_{(\ )}} &= (\ )^{w}_{(p+1)qkl} - (\ )^{c}_{ij} \\ r_{2_{(\ )}} &= (\ )^{w}_{(p+1)(q+1)kl} - (\ )^{c}_{ij} \end{aligned} \qquad (3.31b)$$

The line segment connecting (p+1,q+1,k,l) and (p,q+1,k,l) has radius vector components

$$r_{1_{(\ )}} = (\ )^{w}_{(p+1)(q+1)k\ell} - (\ )^{c}_{ij}$$
$$r_{2_{(\ )}} = (\ )^{w}_{p(q+1)k\ell} - (\ )^{c}_{ij} \qquad (3.31c)$$

while, for the last segment, connecting (p,q+1,k,l) and (p,q,k,l), these components are

$$r_{1_{(\ )}} = (\ )^{w}_{p(q+1)k\ell} - (\ )^{c}_{ij}$$
$$r_{2_{(\ )}} = (\ )^{w}_{pqk\ell} - (\ )^{c}_{ij} \qquad (3.31d)$$

The influence coefficient of this cell is then

$$f_{ijpqk\ell} = \sum_{n}^{4} g_n \qquad (3.32)$$

while a layer of geometrically similar cells, with the same Γ, shed from all the blades and coupled by the wake angle given by eqn. (3.16) has an influence coefficient

$$f_{ijpq} = \sum_{k}^{nb} \sum_{\ell}^{nz} \sum_{n}^{4} g_n \qquad (3.33)$$

The procedure to calculate the (nr*na) influence coefficients associated with an arbitrary control point (i,j) is as follows: For each (p,q) with upper limits (nr,na) and for each (k,ℓ) with upper limits (nb,nz), the position vectors and hence g_n for the four line segments n are calculated using eqn. (3.31) with $\Gamma = 1$. These functions are then summed over n, ℓ and k respectively, as expressed by eqn. (3.33) and stored in a (nr*na) matrix. For every control point (i,j) such a matrix should be constructed. In the case of a rigid wake and known (given) blade motion, these matrices have only to be determined during initialization of the program.

3.5.2 Bound vortex cells

The influence coefficients of the bound vortex cells at an arbitrary control point (i,j) are determined along similar lines as described above. The coordinates are obtained from eqn. (3.12) but are depended on the geometry of the cell adopted. For the classical lifting line scheme, $\delta_c = 1/4$ and $\delta_b = 1/4$ for the segment on the leading edge side, while $\delta_b = \delta_c = 0$ for the segment on the trailing edge side. For the extended lifting line scheme $\delta_c = 1/4$ and $\delta_b = 3/4$ for the segment closest to the leading edge, while $\delta_c = \delta_b = 0$ for the segment closest to the trailing edge. Starting with the segment closest to the leading edge, connecting (p,k) and (p+1,k) in the direction for positive Γ, yields

$$r_{1_{(\ )}} = \left[(\ )^b_{pk} - (\ )^c_{ij}\right]_{\delta_b,\,\delta_c}$$

$$r_{2_{(\ )}} = \left[(\ )^b_{(p+1)k} - (\ )^c_{ij}\right]_{\delta_b,\,\delta_c} \qquad (3.34a)$$

The subsequent line segment in the radial direction has coordinates

$$r_{1_{(\ )}} = \left[(\ )^b_{(p+1)k} - (\ )^c_{ij}\right]_{\delta_b,\,\delta_c}$$
$$r_{2_{(\ )}} = \left[(\ )^b_{(p+1)k} - (\ )^c_{ij}\right]_{0,0} \qquad (3.34b)$$

For the line segment on the trailing edge side connecting (p+1,k) and (p,k) with $\delta_q = \delta_b = 0$

$$r_{1_{(\ )}} = \left[(\ )^b_{(p+1)k} - (\ )^c_{ij}\right]_{0,0}$$
$$r_{2_{(\ )}} = \left[(\ )^b_{pk} - (\ )^c_{ij}\right]_{0,0} \qquad (3.34c)$$

while the components for the remaining segment are

$$r_{1_{(\ )}} = \left[(\ )^b_{pk} - (\ )^c_{ij}\right]_{0,0}$$
$$r_{2_{(\ )}} = \left[(\ )^b_{pk} - (\ )^c_{ij}\right]_{\delta_b,\,\delta_c} \qquad (3.34d)$$

The Biot-Savart function g_n is then calculated for each segment using eqn. (3.29) with $\Gamma = 1$, after which the influence coefficient of a cell S_{pqk} at control point (i,j) is obtained as

$$b_{ijpk} = \sum_{n}^{4} g_n \qquad (3.35)$$

There are (nb*nr) such coefficients associated for each (i,j) and these coefficients, calculated by a similar procedure as described in the previous section, need only be calculated once, if the blade motion is a priori known for both a rigid and semi-rigid wake.

3.6 Aerodynamic loads

3.6.1 Blade section forces and moments

The aerodynamic forces are lift ℓ and drag d, normal and parallel to the resultant velocity U respectively and an aerodynamic moment m_a about the elastic (or pitch) axis, positive nose up. The section lift is expressed as

$$\ell = \ell_o + \ell_t \qquad (3.36)$$

where

$$\ell_o = \pm \frac{1}{2}\rho U^2 c C^*(k) c_\ell \qquad (3.37)$$

is the steady lift and

$$\ell_t = \rho c \frac{dc_\ell}{d\alpha} \left\{ \frac{c}{4} C^*(k) U_T \frac{dw}{dx} \left[1 \pm \frac{2}{c} \left(\delta_a + \frac{c}{4} \mp \frac{c}{4} \right) \right] + \frac{c}{8} \left(\Omega \frac{dw}{d\psi} + U_R \frac{dw}{dr} \right) \right\} \quad (3.38)$$

is the unsteady lift for attached flow, as discussed in sec. (3.8.3). The double sign represents normal and reverse flow ie $\pm$ = sign $(U_T \cos\theta + U_P \sin\theta)$. The derivative of w with respect to the chord x is given by

$$\frac{dw}{dx} = \dot{\theta} + \Omega \frac{dz}{dr} + \frac{d\theta}{dr} U \cos\psi \quad (3.39)$$

while expressions for derivatives with respect to time and radius are presented by Johnson [1980b]. These derivatives can however be evaluated numerically from the expression

$$w = U_T \sin\theta - U_P \cos\theta \quad (3.40)$$

if sufficient radial and azimuthal stations are chosen. The lift deficiency function C*(k) has been asterixed to indicate optional inclusion, ie in the case where the shed vorticity is not included (or only partially included) in the wake model.

The sectional drag is defined as

$$d = \frac{1}{2} \rho U^2 c c_d \quad (3.41)$$

and is always in the opposite direction of U. Unsteady (primarily added mass) effects are small compared to viscous effects, and are therefore neglected.

The sectional moment about the elastic axis, or pitch axis in the case of an assumed rigid blade, is expressed as

$$m_a = m_o + m_t \pm \frac{1}{2}\rho U^2 \delta_a c c_\ell \tag{3.42}$$

where

$$m_o = \pm \frac{1}{2}\rho U^2 c^2 c_{m_{ac}} \tag{3.43}$$

is the steady moment about the section aerodynamic centre, and

$$m_t = \rho c \frac{dc_\ell}{d\alpha} \frac{c^2}{32} \left\{ \mp U_T \frac{dw}{dx} \left[1 \pm \frac{4}{c}\left(\delta_a + \frac{c}{4} \mp \frac{c}{4}\right)\right]^2 \mp \left(\frac{dw}{dt} + U_R \frac{dw}{dr}\right)\left[1 \pm \frac{4}{c}\left(\delta_a + \frac{c}{4} \mp \frac{c}{4}\right)\right]\right\} \tag{3.44}$$

is the unsteady moment, with parameters defined and calculated as for unsteady lift.

The unsteady effects modelled in this section are only applicable to attached flow. For separated (stalled) flow, these unsteady forces and moments are set equal to zero, while the unsteady effects are accounted for in a dynamic stall model, presented later, for the aerodynamic coefficients c_ℓ, c_d and c_m, presented later.

The components of the section aerodynamic forces and moments relative to the hub plane axis in a rotating frame are

$$\begin{aligned} f_x &= \ell \sin\phi_P + d\cos\phi_P \\ f_y &= d\sin\phi_R \\ f_z &= \ell \cos\phi_P - d\sin\phi_P \\ m_y &= m_a \end{aligned} \tag{3.45}$$

where f_y is in the radial direction along the elastic axis of a blade. The radial drag force is based on the assumption that the viscous drag force is in the direction of the local flow. The flow angles are defined by

$$\begin{aligned} \phi_P &= \tan^{-1} \frac{U_P}{U_T} \\ \phi_R &= \tan^{-1} \frac{U_R}{U_T} \end{aligned} \tag{3.46}$$

The angle ϕ_P is generally known as the inflow angle.

3.6.2 Rotor forces and moments

The rotor forces are obtained by integrating the blade section forces along the span of a arbitrary blade. This is done numerically, using the same ordering scheme as before, by summating the forces at the centre of the nr segments of length Δr. Using a rotating hub plane reference system, numerical expressions for the rotor forces and moments at the hinges are

$$
\begin{aligned}
F_x(\psi) &= \sum_{p=p_0}^{nr} f_x\left(\psi, r_p\right)\Delta r \\
F_y(\psi) &= \sum_{p=p_0}^{nr} \left[f_y\left(\psi, r_p\right) - f_z\left(\psi, r_p\right)\frac{dz}{dr}\right]\Delta r \\
F_z(\psi) &= \sum_{p=p_0}^{nr} \left[f_z\left(\psi, r_p\right) + f_y\left(\psi, r_p\right)\frac{dz}{dr}\right]\Delta r \\
M_y(\psi) &= \sum_{p=p_0}^{nr} m_y\left(\psi, r_p\right)\Delta r
\end{aligned}
\tag{3.47}
$$

where

$$
\begin{aligned}
\Delta r &= r_{p+1} - r_p \\
\frac{dz}{dr} &= \frac{z_{p+1} - z_p}{r_{p+1} - r_p}
\end{aligned}
\tag{3.48}
$$

Steady rotor forces are denoted by thrust T, normal to the rotor disc, rotor drag force H in the plane of the disc, positive aft, and the rotor side force Y in the plane of the disc positive toward the advancing side. These forces are calculated by averaging eqns. (3.47) over the azimuth for a rotor blade and multiplying by the number of blades. Expressions for these forces are

$$T = \frac{nb}{2\pi} \sum_{q=1}^{na} F_z(\psi_q)\Delta\psi$$

$$H = \frac{nb}{2\pi} \sum_{q=1}^{na} \left[F_x(\psi_q) \sin\psi_q + F_y(\psi_q)\cos\psi_q\right]\Delta\psi \qquad (3.49)$$

$$Y = \frac{nb}{2\pi} \sum_{q=1}^{na} \left[F_y(\psi_q) \sin\psi_q - F_x(\psi_q) \cos\psi_q\right]\Delta\psi$$

where

$$\Delta\psi = \psi_{q+1} - \psi_q \qquad (3.50)$$

The average torque Q of the rotor is calculated using the expression

$$Q = \frac{nb}{2\pi} \sum_{q=1}^{na} \sum_{p=p_o}^{nr} r_p\, f_x\left(r_p, \psi_q\right) \Delta r\, \Delta\psi \qquad (3.51)$$

where Δr and $\Delta \psi$ are as defined before.

3.7 Airfoil steady aerodynamic characteristics

The lift, drag and moment coefficients, as well as the lift curve slope and location of the aerodynamic centre (centre of pressure) of an airfoil representing the blade section of a rotor, is required to calculate the blade loads. These characteristics are in general a function of the flow geometry (angle of attack) airfoil geometry, Reynolds number and Mach number, and no simple model exists expressing the airfoil characteristics as a function of these parameters. In an accurate aerodynamic analysis, experimental data in the form of tables, representing aerodynamic characteristics as a function of angle of attack and Mach number, should be used, while frequently only an approximate dependence on angle of attack is assumed with corrections for compressibility effects. Both cases are considered for inclusion, while in both cases a correction for radial flow must also be introduced.

For separated (stalled) flow the steady aerodynamic characteristics should be replaced by unsteady characteristics obtained from a dynamic stall model.

3.7.1 Experimental data

Two-dimensional experimental data, such as presented by Piziali [1966] and Mil' et as [1966] for discrete values of angle of attack and Mach number are arranged in tabular form and interpolated using a linear scheme, outlined below.

Associated with each angle of attack α_i and Mach number M_j is a parameter c(i,j), where i = 1,2,...,m and j = 1,2,...,n, with $\alpha_i < \alpha_{i+1}$ and $M_j < M_{j+1}$. Such a representation is illustrated in fig. (3.6). For an arbitrary α and M, the parameter c is obtained from the

interpolation formula

$$c(\alpha,M) = \sum_{g=o}^{1} \sum_{h=o}^{1} a_{i+g}\, b_{j+h}\, c(i+g,\, j+h) \tag{3.52}$$

where

$$\begin{aligned} i &= \text{int}\left[\frac{\alpha - \alpha_1}{\Delta\alpha} + 1\right] \\ j &= \text{int}\left[\frac{M - M_1}{\Delta M} + 1\right] \end{aligned} \tag{3.53}$$

$$\begin{aligned} a_i &= \frac{\alpha_{i+1} - \alpha}{\Delta\alpha} \\ a_{i+1} &= \frac{\alpha - \alpha_i}{\Delta\alpha} \\ b_j &= \frac{M_{j+1} - M}{\Delta M} \\ b_{j+1} &= \frac{M - M_j}{\Delta M} \end{aligned} \tag{3.54}$$

and

$$\Delta\alpha = \frac{\alpha_m - \alpha_1}{m-1}$$
$$\alpha M = \frac{M_n - M_1}{n-1} \qquad (3.55)$$

Data should be available for $-0.20 \leq \alpha \leq 0.20$ and $0 \leq M \leq 0.9$, else extrapolation or approximate modelling should be used.

3.7.2 Approximate modelling

An approximate model of the static lift and drag coefficients valid in the range $[-\pi,\pi]$ and based on two-dimensional airfoil theory and experimental data is presented here. It is assumed that the airfoil stalls at an absolute angle of attack of 0.21 rad, and that the lift curve slope below and above the stall angle is 5.8 per rad and -0.9 respectively.

3.7.2.1 Lift coefficient

The two-dimensional lift coefficient is approximated by

$$\begin{aligned}
c_\ell &= a_\infty(\alpha + \pi) && -\pi < a \leq -\pi - \alpha_{ss} \\
&= a_\infty a_s(\alpha + \pi/2) && -\pi + \alpha_{ss} < \alpha - \alpha_{ss} \\
&= a_\infty \alpha && -\alpha_{ss} < \alpha \leq \alpha_{ss} \\
&= a_\infty a_s(\alpha - \pi/2) && \alpha_{ss} < \alpha \leq \pi - \alpha_{ss} \\
&= a_\infty(\alpha - \pi) && \pi - \alpha_{ss} < \alpha \leq \pi
\end{aligned} \qquad (3.56)$$

where

$$a_\infty = \frac{dc_\ell}{d\alpha}$$
$$a_{ss} = \frac{\alpha_{ss}}{\alpha_s - \pi/2} \qquad (3.57)$$

and $\alpha_{ss} = 0.21$ rad is the static stall angle of attack. The form of the dependence of lift coefficient on α is illustrated in fig. (3.7a).

3.7.2.2 Drag coefficient

The two-dimensional drag coefficient is given by

$$\begin{aligned}
C_d &= \delta_1 + \delta_2(\pi + \alpha) + \delta_3(\pi + \alpha)^2 && -\pi < \alpha \le -\pi + \alpha_{ss} \\
&= \delta_4 + \delta_5 \sin(\pi + \alpha) && -\pi + \alpha_{ss} < \alpha \le -\alpha_{ss} \\
&= \delta_1 + \delta_2\alpha + \delta_3\alpha^2 && -\alpha_{ss} < \alpha \le \alpha_{ss} \\
&= \delta_4 + \delta_5 \sin\alpha && \alpha_{ss} < \alpha \le -\alpha_{ss} \\
&= \delta_1 + \delta_2(\pi - \alpha) + \delta_3(\pi - \alpha)^2 && \pi - \alpha_{ss} < \alpha \le \pi
\end{aligned} \qquad (3.58)$$

where

$$\delta_1 = c_{d_0}$$

$$\delta_2 = 0.0216$$

$$\delta_3 = 0.4000$$

$$\delta_4 = \left(c_d(\alpha_s) - \sin\alpha_{ss}\right)/\left(1 - \sin\alpha_{ss}\right)$$

$$\delta_5 = \left(c_d(\alpha_s) - 1\right)/\left(1 - \sin\alpha_{ss}\right)$$

The coefficients δ_i where determined empirically from airfoil experimental data, see eg Johnson [1980a]. The form of the dependence of drag coefficient on α is illustrated in fig. (3.7a).

3.7.3 Corrections for compressibility

The only practical means of accounting for the effect of compressibility in detail is to use data for the airfoil aerodynamic characteristics expressed as a function of Mach number and angle of attack. The effects of the increased lift curve slope on the rotor loads and blade motion due to compressibility can however be estimated using the Prandtl-Glauert similarity rule, expressed by the factor

$$\delta = \left[1 - M^2\right] \qquad (3.59)$$

and discussed eg in Abott & van Doenhoff [1959]. The lift curve slope corrected for compressibility is

$$\frac{dc_\ell}{d\alpha} = \frac{1}{\delta}\left[\frac{dc_\ell}{d\alpha}\right]_{inc} \tag{3.60}$$

Alternatively, the lift coefficient can be corrected by the same multiplying factor $1/\delta$.

3.7.2.3 Moment coefficient

The two-dimensional moment coefficient about the aerodynamic centre is

$$\begin{aligned}
c_m &= c_{m_o} && --\pi < \alpha \leq -\pi + \alpha_{ss} \\
&= c_{m_o} - \left(c_{m_s} - c_{m_o}\right) && -\pi + \alpha_{ss} < \alpha \leq -\alpha_{ss} \\
&= c_{m_o} && -\alpha_{ss} < \alpha \leq \alpha_{ss} \\
&= c_{m_o} + \left(c_{m_s} - c_{m_s}\right) && \alpha_{ss} < \alpha \leq \pi - \alpha_{ss} \\
&= c_{m_o} && \pi - \alpha_{ss} < \alpha \leq \pi
\end{aligned} \tag{3.61}$$

where the gradient between attached and separated flow, as illustrated in fig. (3.7a), has been neglected.

3.7.4 Correction for yawed flow

The effect of yawed flow, or radial flow in the case of a rotor blade, is discussed in detail by Johnson [1980a]. The lift and drag coefficients for yawed flow are

$$c_\ell(\alpha) = c_{\ell_{2d}}\left(\alpha\cos^2\Delta\right)/\cos^2\Delta \tag{3.62}$$

and

$$c_d(\alpha) = c_{d_{2d}}\left(\alpha\cos\Delta\right)/\cos\Delta \tag{3.63}$$

where

$$\cos\Delta = U_T/\left(U_T^2 + U_R^2\right)^{1/2} \tag{3.64}$$

These results are based on the assumption that the resultant drag force is in the yawed free stream direction and on the equivalence assumption for swept wings. The correction must be applied to both experimental data and approximate relations for these coefficients.

3.8 Dynamic stall model

The features associated with dynamic stall, as discussed in § 2.8.4, are modelled based on a procedure introduced by Johnson [1980b], but modified to incorporate refinements as presented by Beddoes [1983].

Dynamic stall is characterized by a delay in the occurrence of separated flow due to blade motion and high transients loads induced by a vortex shed from the leading edge at the onset of stall. The first phenomenon is accounted for by defining a dynamic stall angle of attack

$$\alpha_{ds} = \alpha_{ss} + \Delta\alpha \tag{3.65}$$

where, according to Johnson [1980b], $\Delta\alpha = 0.05$ rad gives good results. In general $\Delta\alpha$ is a function of U_T, $d\alpha/dt$, Mach number and blade and profile geometry. A typical value for the static stall angle of attack $\alpha_{ss} = 0.21$ rad. The lift and moment coefficient up to dynamic stall is

$$c_\ell = \frac{c_\ell(\alpha_{ss}) - c_\ell(o)}{\alpha_{ss}}\,\alpha + c_\ell(o) \tag{3.66}$$

and

$$c_m = c_{m_o} \tag{3.67}$$

Alternatively, a delayed angle of attack, as introduced by Johnson, can be used to evaluate these properties up to the dynamic stall angle of attack.

The second phenomenon is modelled by defining a transient lift and moment coefficient movement. The section properties during dynamic stall are then expressed as

$$c_\ell = \frac{c_\ell(\alpha_{ss}) - c_\ell(o)}{\alpha_{ss}} \alpha_{d_s} + c_\ell(o) + f\,\Delta c_\ell \tag{3.68}$$

and

$$c_m = c_{m_o} + f\,\Delta c_m \tag{3.69}$$

where

$$f = \min\left[\frac{\delta_d\,\Delta\psi}{\Delta\psi_s}, 2 - \frac{\delta_d \Delta\psi}{\Delta\psi_s}\right] \tag{3.70}$$

The parameter δ_d is incremented for every successive azimuth position during dynamic stall, which terminates when the separated flow lift coefficient, approximated by

$$c_\ell = 1.1 \sin(2\alpha) \tag{3.71}$$

is reached, after which eqn. (3.71), based on a similar expression used by Beddoes [1976] is used to calculate the lift coefficient. The moment coefficient for fully separated flow is

$$c_m = c_{m_{ss}} \tag{3.72}$$

where the constant on the right hand side is obtained from experimental data. The azimuth angle $\Delta\psi_s$ at which the transient loads are at their maximum is typically 0.20 rad, as discussed by Johnson [1980b]. Therefore the peak load increases linearly to a maximum value and then falls linearly to its static separated flow values. Attached flow is assumed to be established again only when the angle of attack falls below the static stall angle of attack. Typical values for the movements in lift and moment coefficients are $\Delta c_\ell \approx 2$ and $\Delta c_m \approx -0.65$, as presented by Johnson [1980b].

The above relations hold for angles of attack in the range $[0, \pi/2]$. To extend its validity to all angles of attack (including the reverse flow region) and to ensure consistency with the static model properties as presented in fig. (3.7a), appropriate transformations must be made. Furthermore, corrections for radial flow and compressibility, as discussed in sec. (3.7) should also be incorporated. The typical behaviour of a dynamic stall model of an airfoil oscillating at an angle of attack in the range $[-\pi, \pi]$ is presented in fig. (3.7b). Corrections to the drag characteristics due to dynamic effects have been neglected, as insufficient information was available to account for its effect.

3.9 Approximate induced velocity and blade motion

In this section, simplified computational models will be presented for the calculation of induced velocities and blade motion. These models are required to determine initial

conditions and will also be used for purposes of comparison with more advanced representations.

3.9.1 Uniform induced velocity

Application of momentum theory to a rotor in forward flight yields an expression for a uniform or average induced velocity as given by eqn. (2.1). Applying the Newton-Raphson method, expressed in general for a function $f(w_i) = 0$ as

$$\left[w_i\right]_{n+1} = \left[w_i\right]_n - \left[\frac{f(w_i)}{f'(w_i)}\right]_n \tag{3.73}$$

to eqn. (2.1) yields

$$\left[\tilde{w}_i\right]_{n+1} = \left[\frac{u^2 + (w + \tilde{w}_i)\,\tilde{w}_i + (w + \tilde{w}_i)^2}{(w + \tilde{w}_i) + (2\rho A/T)\left[u^2 + (w + \tilde{w}_i)^2\right]^{3/2}}\right]_n \tag{3.74}$$

To initiate this iterative procedure a starting value

$$\left[\tilde{w}_i\right]_o = T/2\rho A$$

can be used, which corresponds to the average induced velocity of a rotor in hover.

3.9.2 Linearly distributed induced velocity

Due to the asymmetric flow field in forward flight, the induced velocity will also be distributed asymmetrically. A linearly distributed induced velocity is usually expressed as

$$w_i(r,\psi) = \bar{w}_i \left[1 + \frac{r}{R}\left(k_c \cos\psi + k_s \sin\psi\right)\right] \tag{3.75}$$

where the uniform induced velocity is calculated from eqn. (3.74). Over the years, several authors have developed formulas for the constants appearing with the harmonic components in eqn. (3.75), and a summary is presented by Chen [1989]. The most widely used expressions for these coefficients are

$$\begin{aligned} k_c &= \frac{4}{3}\left(1 - 1.8\mu^2\right)\tan\frac{\chi}{2}\right) \\ k_s &= -2 \end{aligned} \tag{3.76}$$

where χ is the wake angle, defined by

$$\chi = \operatorname{atan}(\mu/\lambda) \tag{3.77}$$

The empirical expressions used, however, depend on the intended application, as well as the flight state of the rotor.

3.9.3 Blade motion

The blade motion is required to calculate the induced velocities and hence blade aerodynamic loading. This motion in general involves rigid body motion about hinges, and elastic deformations in planes tangential and normal to blade motion, as well as about the blade pitch axis, denoted by lead-lag, flap and pitch motion respectively. Due to the importance of flap motion, specifically the first natural mode, only this type of motion will be considered in this section. A spring restrained articulated rigid blade will be considered, but application of the results to hingeless and glimballed (teetering) rotors will also be discussed. A detailed model of blade dynamics can be found in various references, as already discussed.

The equation of motion of a spring restrained rigid blade with hinge offset, as illustrated in fig. (3.8) is

$$I_\beta \frac{d^2\beta}{dt^2} + \left(I_\beta \Omega^2 + eRr_{cg} m_b \Omega^2 + \frac{k_\beta}{1-e} \right) \beta = \int_{eR}^{R} r F_z \, dr \qquad (3.78)$$

Derivation of this equation, based on taking moments about the flap hinge, is derived in detail in eg Bramwell [1976]. The natural frequency of the flap motion is

$$\nu = \left[\left(1 + \frac{eRr_{cg}m_b}{I_\beta}\right)\Omega^2 + \frac{k_\beta}{I_\beta(1-e)}\right]^{1/2} \tag{3.79}$$

A solution of eqn. (3.78) is obtained by converting to non-dimensional time $\psi = \Omega t$ and assuming a periodic solution of the form

$$\beta = \beta_o + \sum_n \beta_{nc} \cos n\psi + \sum_n \beta_{ns} \sin n\psi \tag{3.80}$$

Substitutions of eqn. (3.80) into eqn. (3.78) and equating coefficients, yields expressions for the coefficients of eqn. (3.80) as presented by Arnold & De Waard [1990] using symbolic manipulation software. Simplified expressions, retaining only the first harmonic of flap and pitch and neglecting the effect of offset, e, as well as radial, reversed and separated flow in the aerodynamic terms, are

$$\begin{aligned}
\tilde{\beta}_o &= \frac{\gamma}{\nu^2}\left[\frac{\theta_o}{8}\left(1+\mu^2\right) + \frac{\theta_t}{10}\left(1 + \frac{5}{6}\mu^2\right) + \frac{\mu}{6}\theta_{1s} - \frac{\lambda}{6}\right] \\
\tilde{\beta}_{1c} &= \left[\delta_{22}\left(\delta_{13} + \delta_{14}\right) - \delta_{11}\left(\delta_{23} + \delta_{24}\right)\right] / \left[\delta_{12}\,\delta_{22} - \delta_{11}\,\delta_{12}\right] \\
\tilde{\beta}_{1s} &= \left[\delta_{21}\left(\delta_{13} + \delta_{14}\right) - \delta_{12}\left(\delta_{23} + \delta_{24}\right)\right] / \left[\delta_{12}\,\delta_{22} - \delta_{11}\,\delta_{21}\right]
\end{aligned} \tag{3.81}$$

where

$$\delta_{11} = 1 - \frac{1}{2}\mu^2$$

$$\delta_{12} = 8\left(\gamma^2 - 1\right)/\gamma$$

$$\delta_{13} = -\delta_{11}\theta_{1c}$$

$$\delta_{14} = \frac{4}{3}\mu\beta_o$$

$$\delta_{21} = -\left(-\left(\frac{1}{2}\right)\mu^2\right)$$

$$\delta_{22} = 8\left(\gamma^2 - 1\right)/\gamma$$

$$\delta_{23} = \delta_{21}\,\theta_{1s}$$

$$\delta_{24} = -\frac{8}{3}\mu\left[\theta_o + \frac{3}{4}\theta_t - \frac{3}{4}\left(\lambda - \mu\theta_{1s}\right)\right]$$

The cyclic coefficients represent the tip path plane tilt relative to the chosen reference plane (the hub plane).

Justification for neglecting the effect of offset on aerodynamic terms is based on the observation that the effect of hinge offset on thrust is small, as shown in the same reference.

3.9.3.1 Hingeless rotor

According to Johnson [1980a], a hingeless rotor can be modelled by using the correct flap frequency, but with a simple approximate mode shape. The flap frequency must be obtained from numerical or experimental analysis, while an appropriate mode shape is that

of rigid rotation about a virtual or equivalent offset hinge. The offset can be chosen by matching the slope of the actual mode shape at an appropriate station, such as 75% radius. A virtual offset around e = 0.10R is typical of hingeless rotors.

3.9.3.2 Gimballed or Teetering rotor

This type of rotor is described by two degrees of freedom, corresponding to the cyclic degrees of freedom of the articulated rotor. The coning degree of freedom is replaced by a fixed pre-cone angle. It is shown by Johnson [1980a], that the form of the differential equation for tip path plane tilt (cyclic flapping) is the same as that for an articulated rotor, but with natural frequency

$$\nu = \left[\Omega^2 + \frac{k_\beta}{QI_\beta}\right]^{1/2} \tag{3.82}$$

Therefore, eqn. (3.81) can be used with β_o = constant and ν described by eqn. (3.82), with Q = N/2 for a gimballed rotor (N ≥ 3) and Q = 2 for a teetering rotor (N=2).

3.10 Model input requirements

The rotor behaviour (loads and motion) in rectilinear flight is completely determined if the kinematic state of the hub (or shaft) given by the velocities (u, v, w) and the control position, expressed as

$$\theta^c = \theta_o^c + \sum_n \theta_{nc} \cos n\psi + \sum_n \theta_{ns} \sin n\psi \tag{3.83}$$

is known, together with the rotor and blade geometry. The rotor thrust T and in-plane forces in the hub plane axis system are obtained and can be transformed to an axis system in the flapping or tip path plane by the relations, assuming small angles

$$\begin{aligned} T &\approx T_{fp} \\ H &\approx H_{fp} - \beta_{1c}\, T_{fp} \\ Y &\approx Y_{fp} - \beta_{1s}\, T_{fp} \end{aligned} \tag{3.84}$$

where β is the blade flapping angle, expressed by the harmonic series given by eqn. (3.80). If the flapping motion is known, no blade dynamic calculations are required. The various planes and angles are illustrated in fig. (3.9).

Frequently, however, only a thrust (coefficient) and the kinematic state of the hub is known (specified), while the control position required to attain this thrust must be determined. This will also be the case when the control position is known but the rotor thrust does not equal the specified value, requiring an adjustment to the control setting. This procedure must be performed iteratively (representing the outer loop in fig. (3.5)), as there does not exist an explicit expression relating thrust and control position. To initiate this procedure an approximate expression given by

$$\hat{T} = \pi \sigma \rho A (\Omega R)^2 \left[\frac{\theta_o^c}{3}\left(1 + \frac{3}{2}\mu^2\right) + \frac{\theta_t}{4}\left(1 + \mu^2\right) - \frac{\lambda}{2} \right] \tag{3.85a}$$

or its inverse

$$\tilde{\theta}_o^c = \left[\frac{T}{\pi\sigma\rho A\,(\Omega R)^2} - \frac{\theta_t}{4}\left(1+\mu^2\right) + \frac{\lambda}{2}\right] \Big/ \left[\frac{1}{3} + \frac{1}{2}\mu^2\right] \tag{3.85b}$$

may be used. The above expression is derived from more extensive expressions as presented amongst others by Johnson [1980a].

Experimental data, obtained from either wind tunnel tests or actual flight tests, must be used to validate the model. If such data is obtained from a rotor mounted in a wind tunnel, the velocity V, the thrust T and the angle of attack relative to the tip path plane is normally specified. If the rotor model has only collective control, the angle of attack of the hub required to calculate the hub kinematics, is given by

$$\alpha = \alpha_{fp} - \beta_{1c} \tag{3.86}$$

as indicated in fig. (3.9). This value must be determined iteratively, as the longitudinal flapping angle depends on α. If the shaft angle is given, this value becomes

$$\alpha = \phi_y \tag{3.87}$$

If the rotor model is fitted with cyclic pitch control as well, its values will be assumed specified. Then the same equations are used, as for the cases above, to calculate the angle of attack of the hub. The hub kinematics are given by

$$\begin{aligned} u &= V\cos\alpha \\ v &= 0 \\ w &= V\sin\alpha \end{aligned} \tag{3.88}$$

while the collective pitch angle is determined iteratively, until the required thrust is attained.

If experimental data obtained from flight tests are used, the collective and cyclic control angles and normally also the rigid flapping harmonic coefficients, will be known, as well as the kinematic state of the rotor hub. With these parameters known, the rotor forces relative to the hub plane reference system can be calculated. If the calculated forces deviate much from the measured values, the collective pitch can be adjusted until thrust equality is achieved, as discussed previously.

3.11 Extensions to the rotor model

The model developed in this chapter was based on a lifting line blade representation, semi-rigid wake modelling and rigid blade flapping dynamics. These features will remain the basis of aerodynamic modelling. A next level of advancement will accommodate a lifting surface blade representation, a free wake model and modelling of elastic blade deformations. The model structure will allow such advanced representations, if required.

Details of extensions of this model to incorporate lifting surface and free wake modelling are discussed by Sadler [1971], while references are given in the first chapter for more advanced blade dynamic modelling.

CHAPTER 4

STRUCTURE OF THE PROGRAMMED MODEL

This chapter describes the structure of the programmed model with respect to input requirements, modelling options, initialization and iteration procedures, relaxation requirements and limitations. Computer and software requirements are also outlined.

4.1 General description

The model described in the previous chapter was programmed in standard FORTRAN. It consists of a main program ROTCAL and various subroutines. The bulk of the calculations are performed in the main program, including blade and flow kinematics, blade circulation, blade loads and rotor forces and moments. Initial estimates for (uniform) induced velocity are obtained from subroutine INFLOW, while approximate (rigid) blade motion is calculated by subroutine BLDAPP. Approximate values for rotor thrust or collective pitch are determined by subroutines ROTTHR or ROTCON, requiring collective pitch or rotor thrust as inputs, respectively. The wake influence coefficients are calculated by INFCFF for the free vortex cells and by INFCFB for the bound vortex cells, both subroutines using BIOSAV to calculate the velocity induced by a finite vortex line with unit circulation. Static aerodynamic data are calculated by either subroutine STATIC, or SECTAB if supplied in tabular form, while dynamic stall calculations are performed by subroutine DYNMIC. Unsteady aerodynamic calculations, as well as various corrections to aerodynamic data, are performed in the main program. Rotor geometric and kinematic input data, as well as numerical parameters and modelling options, are contained in a blockdata subroutine ROTDAT. The program source code is presented in appendix A.

4.2 Modelling options

Various modelling options, representing levels of approximation (or sophistication) are available. Wake options include no wake (nonwke=true), rigid wake (rigwke=true) or

semi-rigid wake (semwke=true) modelling. A rigid wake implies a prescribed inflow distribution which can either be uniform or linear. Induced flow or inflow modelling has options of uniform inflow (uniind=true), linear inflow distribution (linind=true), or nonuniform inflow (nonind=true). If nonuniform inflow is selected, either a uniform or linear inflow should also be selected to obtain a first approximation of the induced velocity, or to dictate the geometry of a prescribed (rigid) wake. The rotor blade is represented by a lifting line model of which two options, the classical lifting line model (cllmod=true) or the extended lifting line model (ellmod=true) are available. However, a single panel vortex lattice blade representation was also modelled and included as an option (vlmmod-true). Flow phenomena associated with viscuous compressible flow can also be optionally included. These are unsteady aerodynamic modelling using lift deficiency functions (unsmod=true), dynamic stall modelling (dynmod=true), radial flow modelling (radmod=true) and inclusion of the effect of compressibility (cmpmod=true). Except for the first option, the effect of shed vorticity should be included (shdmod=true). Input options, which will overrule approximations used in the program, are cases when control input is given (ctlinp=true) and/or blade kinematics is known (bldinp=true). A final input option is for the case when blade section aerodynamic characteristics are given (secinp=true) in the form of tables. All these options are set in the blockdata subroutine.

4.3 Data input

Apart from the modelling options discussed above, the following data relating to the physical state and configuration of the rotor are also required in the blockdata subroutine.

4.3.1 Rotor environment

The environment is characterized by the local density, temperature, gas ratio and gas constant. The later two values are assumed that of air.

4.3.2 Kinematic rotor state

The rotor state is defined by three velocity components of the rotor relative to the atmosphere. These components are described in an axis system parallel to the hub or shaft of the rotor. Frequently, only the angle of attack and the total flow velocity relative to a different axis system (typically one parallel to the blade tip path plane) are given. In this case appropriate transformations should be made to obtain the velocity components as required.

4.3.3 Rotor parameters

The rotor parameters required are the radius, the number of blades and the configuration. The configuration relates to the type of blade attachment, ie articulated, hingeless, gimballed or teetering. Related to the configuration is a hinge offset, or in the case of a rigid hub, an equivalent hinge offset.

4.3.4 Blade parameters

Aerodynamic, geometric and inertia characteristics are assumed to vary linearly from root to tip, therefore the value at the root and a constant, representing the linear gradient, are required as inputs. The aerodynamic parameters are lift curve slope, zero lift angle of attack, stall angle, zero lift drag coefficient, drag coefficient at stall and moment coefficient at zero lift and stall. Geometric parameters required are the chord and twist. Inertia characteristics, used to calculate blade kinematics, if not supplied as input, are blade mass, centre of mass and moment of inertia. A hinge (or equivalent hinge) spring constant is also required as input. Blade kinematics is represented (optionally) by a Fourier series, up to five coefficients.

4.3.5 Control parameters

Collective and cyclic control are also represented optionally by the coefficients of a Fourier

series. Usually only the first three coefficients are required, representing collective, lateral and longitudinal cyclic respectively.

4.3.6 Rotor forces

Frequently, from experimental data, a thrust coefficient is specified for a rotor to be evaluated computationally. In such cases the thrust coefficient and other force coefficients (if known) must be converted to dimensional forces in the hub axis system.

4.3.7 [illegible]er

Other input data required are numerical modelling parameters, logical variables for program control and numerical constants. These parameters are all fixed, except for those defining the size and resolution of the grid. They are, however, prompted for verification or change in the main program.

4.4 Initialization procedure

This procedure involves calculation of control or force, blade motion and uniform induced velocity. The calculation process is, however, iterative because rotor control or force, blade motion and induced velocity are all interdependent. This procedure therefore constitutes the first secondary iteration loop of the program, revisited each time an adjustment in control or force to meet the specified value, is required, representing the second secondary iterative process or loop.

4.5 Iteration process

The primary iteration process involves the calculation of the induced velocity. This requires calculation of the ($nr^2 \star na^2$) free vortex cell and the ($nr^2 \star nb \star na$) bound vortex cell influence coefficients, once for the case of a rigid wake model, and repeatedly for the case of a semi-rigid or free wake model. This procedure is the most time consuming calculation process.

For an initial estimate of the circulation and induced velocity, the induced velocity distribution is calculated, using relaxation, constituting the first primary loop. Then new values for the circulation distribution, the second primary loop, are calculated, also using relaxation. This process is repeated until convergence is obtained, after which the blade loading and rotor forces are calculated. If the specified rotor force (coefficient) is obtained, the process terminates, else the second secondary loop is re-entered.

An alternative option to select is the vortex lattice blade representation, in which the induced velocity is explicitly determined and the resulting ($nr^2 \star na^2$) matrix equation is solved using an iterative Gauss-Siedel algorithm. This option implies only one primary loop or iterative process.

For both the lifting line and the vortex lattice model, convergence was only achieved if the program was initiated with a large (finite) vortex core, decreased successively to a realistic value. This required a third iterative process, denoted the convergence loop. Introduction of this loop, however, implies that the influence coefficients have to be recalculated for each iteration, hence slowing down the calculation process substantially.

4.6 Model output

Standard model output include the induced velocity, angle of attack, lift coefficient, blade section circulation and normal force for each of the ($nr \star na$) control points. These are written to files for further processing. All major variables are however available (common) in the main program.

4.7 Computer requirements

The program was developed in MS-FORTRAN V5.1 on a PC-386 machine. The memory requirements are 640 KB RAM and at least 1 MB on (hard) disc for a fairly coarse grid ($nr = 15$, $na = 18$) and should be increased to 4 MB for a finer grid ($nr = 24$, $na = 36$). To expedite the program enough RAM should be available to create a virtual disc, as was done

during development of the program. The program is also VAX compatible, and if compiled on a VAX system should be defined for the influence coefficients to be saved in dynamic memory instead of being written to and read from files.

CHAPTER 5

RESULTS AND CONCLUSIONS

The program described in the previous chapter was evaluated against published experimental and calculated data. Some modelling options were also varied to show their effect on the resultant flow and load distribution. The results are presented and discussed in this chapter, after which conclusions are drawn and recommendations for applications and further development are made.

5.1 Published Data

Data on experimentally measured airloads were obtained from Scheiman and Ludi [1963], which is a widely used source for these purposes. Only one kinematic state and rotor configuration was considered, as presented in the source code (block data), appendix A. The kinematic flow state involves high speed forward flight (μ = 0.23) at low angle of attack. The rotor configuration is a four bladed articulated rotor, with pitch and flapping angles (including higher harmonics) given. The normal force coefficient at three different radial stations as a function of azimuth is presented in fig. (5.1.0.0). Also presented in the same reference are calculated results for the normal force coefficients.

Published data on calculated results for both airload and induced velocity distribution were obtained from Johnson [1980a], who was responsible for the development of CAMRAD, a widely used program for dynamic and aerodynamic analysis, see Johnson [1980b]. These data, presented in fig. (5.2.0.0) for uniform inflow and in fig. (5.3.0.0) for non-uniform inflow distributions, were used for both qualitative and quantitative verification of the model. For the case of uniform inflow only the angle of attack and lift distribution were considered, while for the case of non-uniform inflow, the inflow distribution was included for purposes of verification. The rotor configuration and kinematic flow state involved a three bladed rotor at high forward speed (μ = 0.25), with only the first harmonic components of blade pitching and flapping known. Although experimental data on induced

velocity distribution is presented in Heyson and Katzhoff [1957], values in the plane of the disc were only obtained by means of interpolation and hence were considered inaccurate for a detailed investigation.

5.2 Calculated results

Calculations were performed for several cases, involving different modelling options, for both types of rotors and their associated kinematic states. The results for the two configurations considered are presented in fig. (5.1.1.1) to fig. (5.1.2.5) and fig. (5.2.1.1) to fig. (5.3.4.1) for the published experimental and calculated results respectively. The corresponding modelling options selected for the calculation of the flow and load distributions are presented in table (5.1) to table (5.3). A description of these various options was presented in the previous chapter. For all the calculations a grid size of [nr,na] = [15,18] was used, which is considered as sufficient in the literature (see e.g. Johnson [1980a]).

Initially, difficulty was experienced in attaining convergence of the interdependent inflow and circulation distribution, except for the cases of hovering and vertical flight. At that stage no vortex core modelling was used. Attempts to attain convergence by using small relaxation factors were unsuccessful. Eventually it was decided to use a finite vortex core radius, decreasing its value for successive convergence of inflow and circulation distribution. This technique, although time consuming, due to the introduction of another (outer) iterative process, yielded excellent results. However, to expedite the calculations, a vortex core radius slightly larger than half the distance between two adjacent control points was used. This ensured convergence, but calculated results can therefore be considered only approximate, although fairly accurate. A further problem with convergence was experienced when dynamic stall modelling, due to its highly non-linear nature, is introduced. This problem was successfully solved by initializing the process using static aerodynamic characteristics, after which dynamic stall with relaxation is introduced. No convergence could be obtained using single panel vortex lattice blade modelling and a Gauss-Siedel iterative solution scheme, even using extremely small relaxation. This option, which

requires further attention, was however only introduced to attempt to solve the initial problems experienced in achieving convergence.

A general discussion on inflow and load distribution is presented by Johnson [1980a]. In the next section the specific cases are considered in more detail, but it can be stated that qualitatively, the model developed gave realistic results for all flight states and rotor configurations considered, which include hovering and forward flight states and multibladed configurations.

It should also be noted that in all test cases, no adjustments to control angles and uniform induced velocity, used to calculate the wake geometry, were made to achieve equal rotor thrust (coefficients). This would have obscured the effect of modelling options on the blade load distribution and the total rotor thrust, an effect that need also to be taken cognizance of.

5.3 Evaluation of results

Calculated normal force coefficients as a function of azimuth angle, agreed well with experimental results, compare fig. (5.1.1.1) to fig. (5.1.2.5) with fig. (5.1.0.0). The best agreement was obtained when radial flow and dynamic stall modelling was incorporated. Parametric analyses showed that increasing the transient lift increment (see § 3.8) increases the normal force coefficient on the retreating blade considerably. Therefore, adjusting its value yielded improvement in the match between experimental and calculated data. It should be noted that the value suggested in Johnson [1980b] seems to be too high, resulting in excessive load peaks, therefore a smaller value was used in the calculations. This aspect however, is a specialized one, needing further attention. With respect to lifting line modelling, both the classical and the extended lifting line model yielded approximately the same results, the latter being slightly lower. This observation could be ascribed to the fact that a finite (too large) vortex core was used, therefore no accurate conclusions can be drawn from this comparison.

The next evaluation involved comparing published data using a uniform inflow distribution, obtained from Johnson [1980a], with that obtained from calculations, using the model with appropriate options selected. Published data are presented in fig. (5.2.0.0) (a) and (b), while calculated data are presented in fig. (5.2.1.1) to fig. (5.2.1.5) for different modelling options outlined in tab. (5.2). From these results it is evident that radial flow modelling should be included in any rotor aerodynamic model to accurately predict rotor loads. No conclusions with respect to inclusion of unsteady and dynamic stall modelling could be derived due to low angles of attack (disc loading) attained for this case. The angles of attack are generally lower due to lower rotor thrust, explaining the dissimilarity in the distribution, if compared to the published results.

The final evaluation involved cases where the inflow distribution was nonlinear due to the effect of the wake. Published data, obtained from Johnson [1980a] and presented in fig. (5.3.0.0) (a) - (d) are compared with calculated results, presented in fig. (5.3.1.1) - (5.3.2.5) for a rigid wake with symmetrical helical geometry (uniform downward translation), fig. (5.3.3.1) for a rigid wake with skewed symmetrical geometry (linearly distributed downward translation) and fig. (5.3.4.1) for a semi-rigid wake (nonlinear downward translation). Again different modelling options were selected for each wake representation, as presented in tab. (5.3). In general, the qualitative agreement between calculated and published results is good, although different modelling options show large quantative variations. The higher harmonic content of the flow and load distribution, leading to vibration and noise, is evident from inspection of these graphs. Using the observations made during the previous two evaluations, the results including radial flow modelling should be the most accurate. This is true for the flow distribution (inflow and angle of attack), although higher values were obtained, but this was not the case for the load distribution. The latter discrepancy could be ascribed to inaccurate compressibility modelling and the former to thrust inequality between the reference and actual cases. The detail of the modelling used in this reference case was, however, not presented in the reference used, therefore no accurate (quantative) conclusions can be drawn from the available data. A more detailed study has to be made systematically and fundamentally, evaluating the effects of each modelling option. This was however considered beyond the scope of this thesis.

5.4 Conclusions and Recommendations

The primary objective of this thesis, namely to develop and computerize a rotor aerodynamic model to serve as a platform for research and development in rotor dynamics and aerodynamics, has been achieved. Evaluation of calculated results against published data, as well as exposition of some of the modelling options (constituting the secondary objective) showed favourable agreement, both quantitatively and qualitatively. Due to the higher harmonic content of the flow and load distribution for non-uniform inflow, as observed from the results, it is evident that wake modelling is essential in advanced applications such as vibration analysis. It can therefore be concluded that the objectives of this thesis have been achieved, and a model has been developed that can be used in various practical applications.

However, it is evident from the results that more attention should be given to detail involved in the modelling to accurately predict the loads, specifically the higher harmonic content thereof. Furthermore, the model developed is based on a multiple of assumptions, approximations and restrictions. These should be thoroughly investigated in order to accurately predict aerodynamic loads on rotor blades, especially at extreme operating conditions. Finally, determining the rotor forces and moments using this model requires an extensive amount of computational effort and storage, and no emphasis was placed on efficiency. Hence, to incorporate the model in eg a simulation program, more emphasis should be placed on computational efficiency.

FIGURES

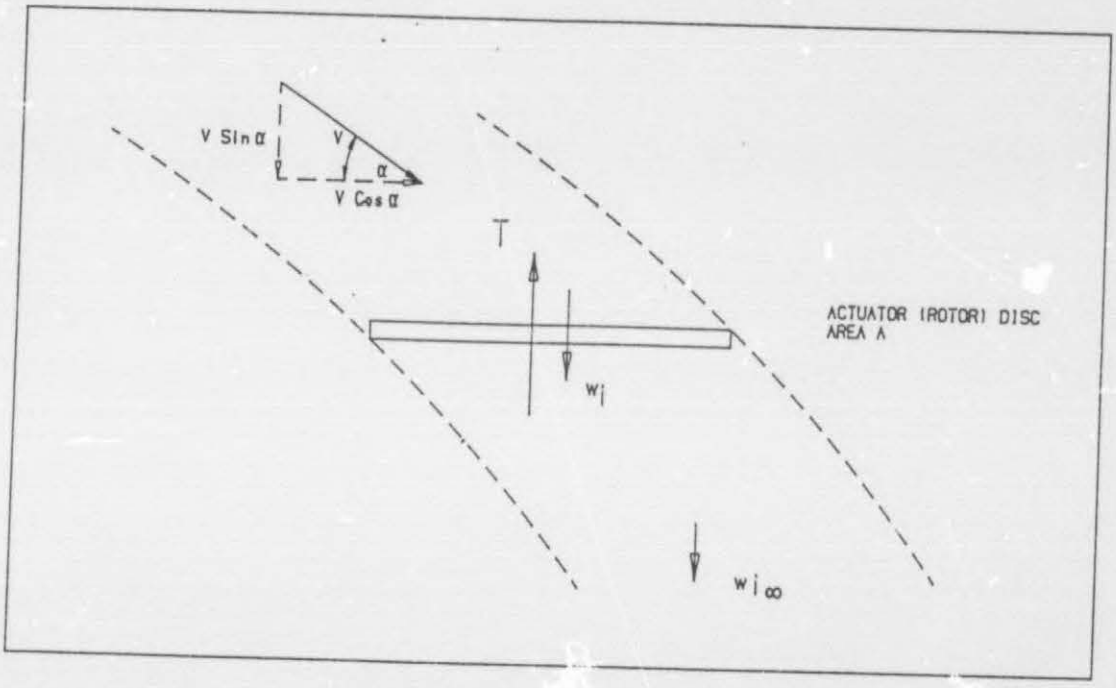

Fig 2.1 Momentum theory

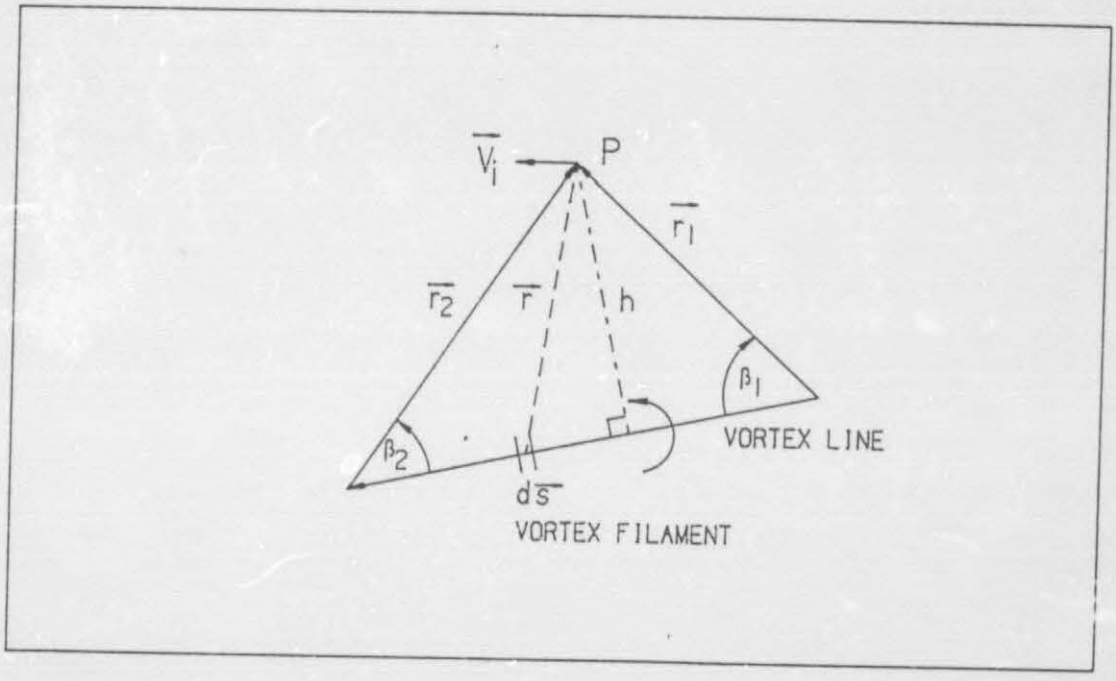

Fig 2.2 Biot-Savart law for induced velocity

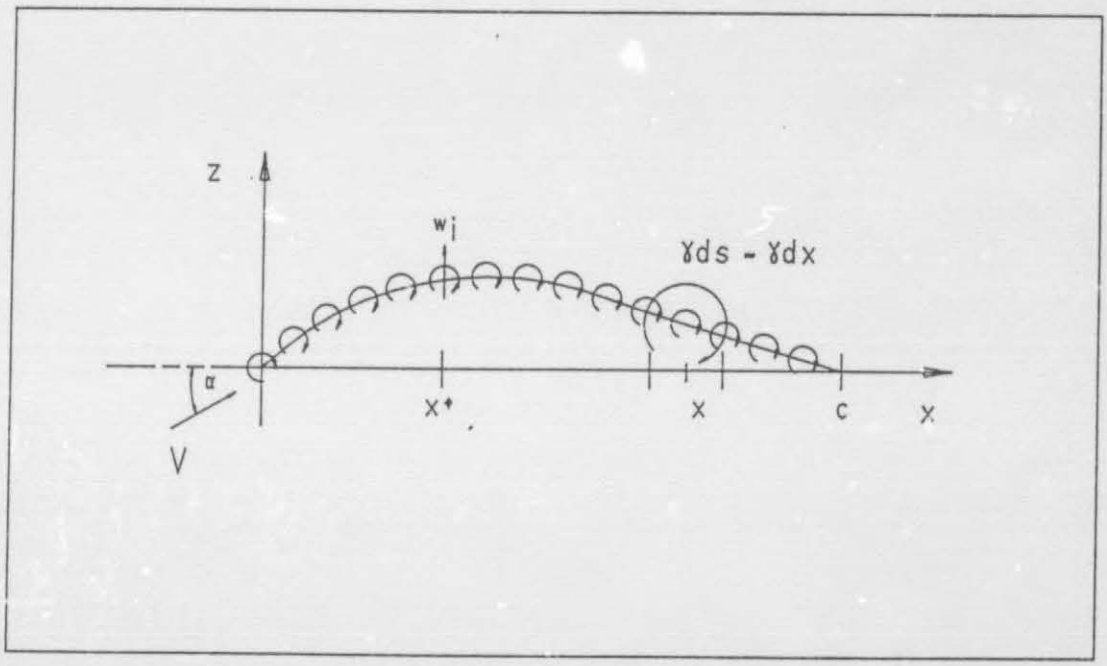

Fig 2.3 Thin airfoil theory continuous model

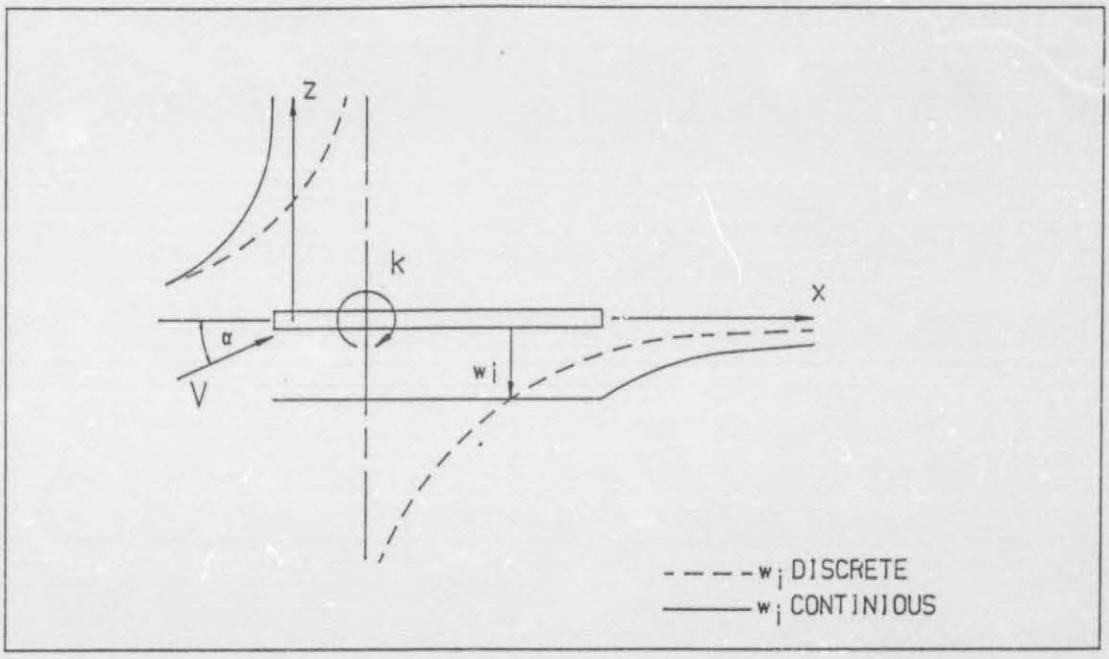

Fig 2.4 Thin airfoil theory discretized model

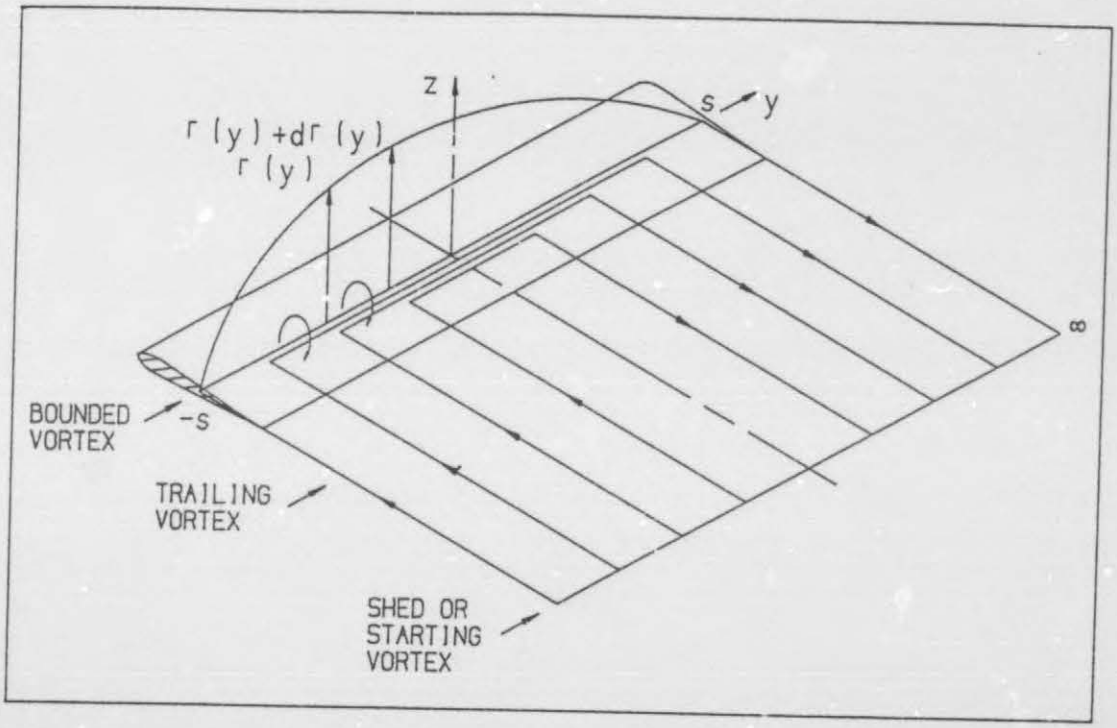

Fig 2.5 Prandtl-Lancaster lifting line model

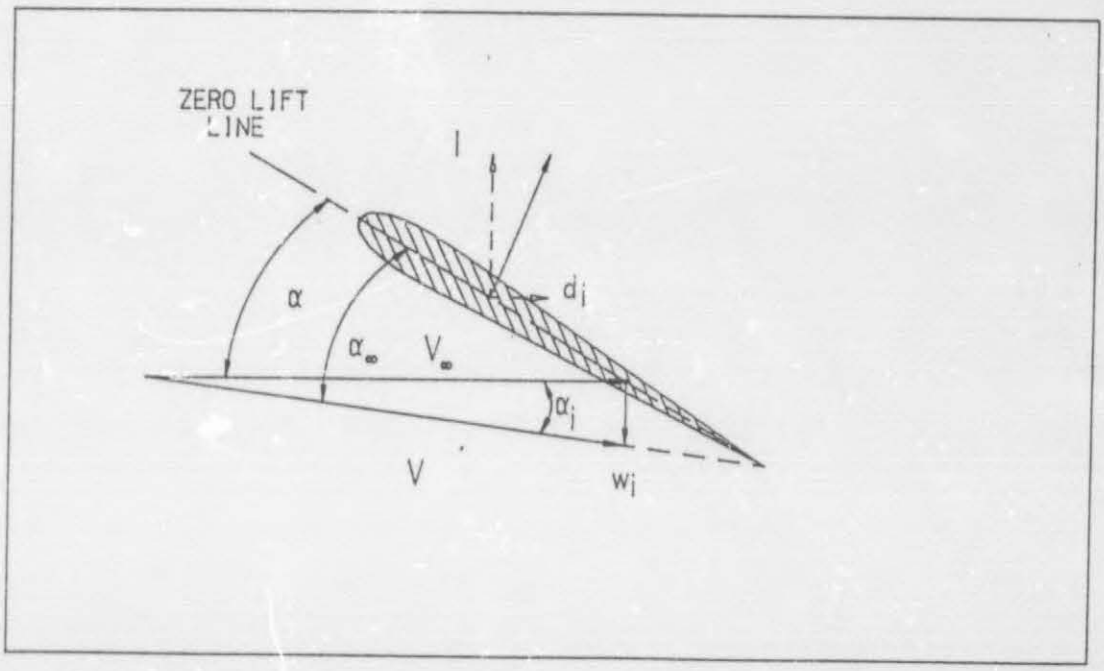

Fig 2.6 Effective flow at section of finite wing

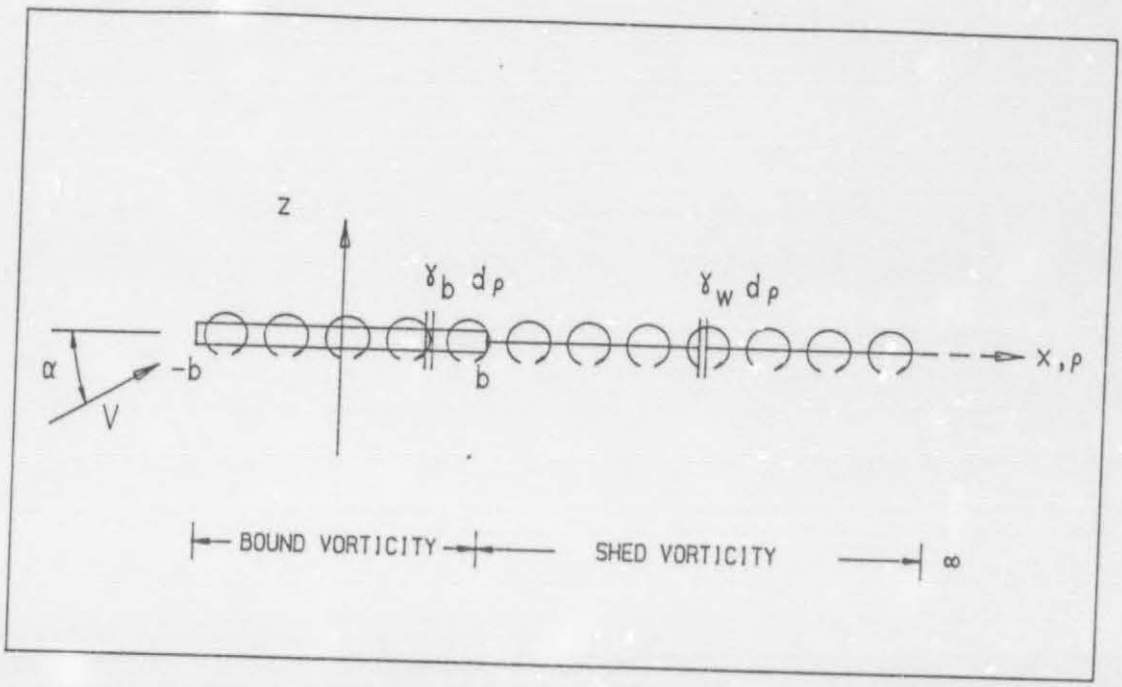

Fig 2.7 Unsteady airfoil model

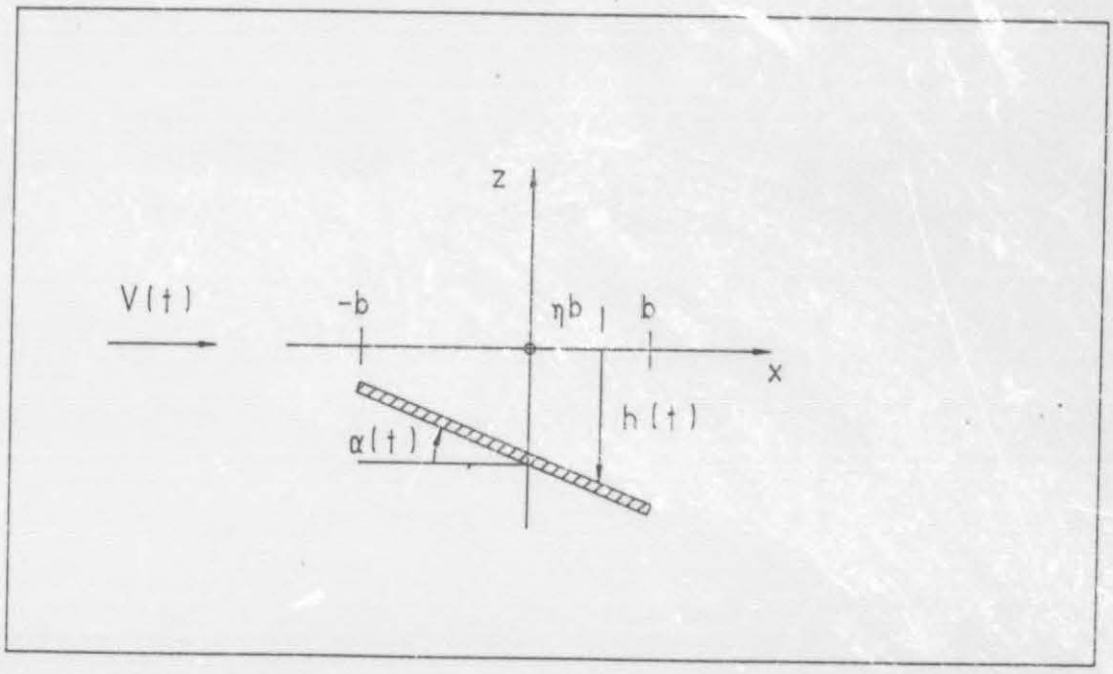

Fig 2.8 Unsteady pitching and heaving motion of airfoil

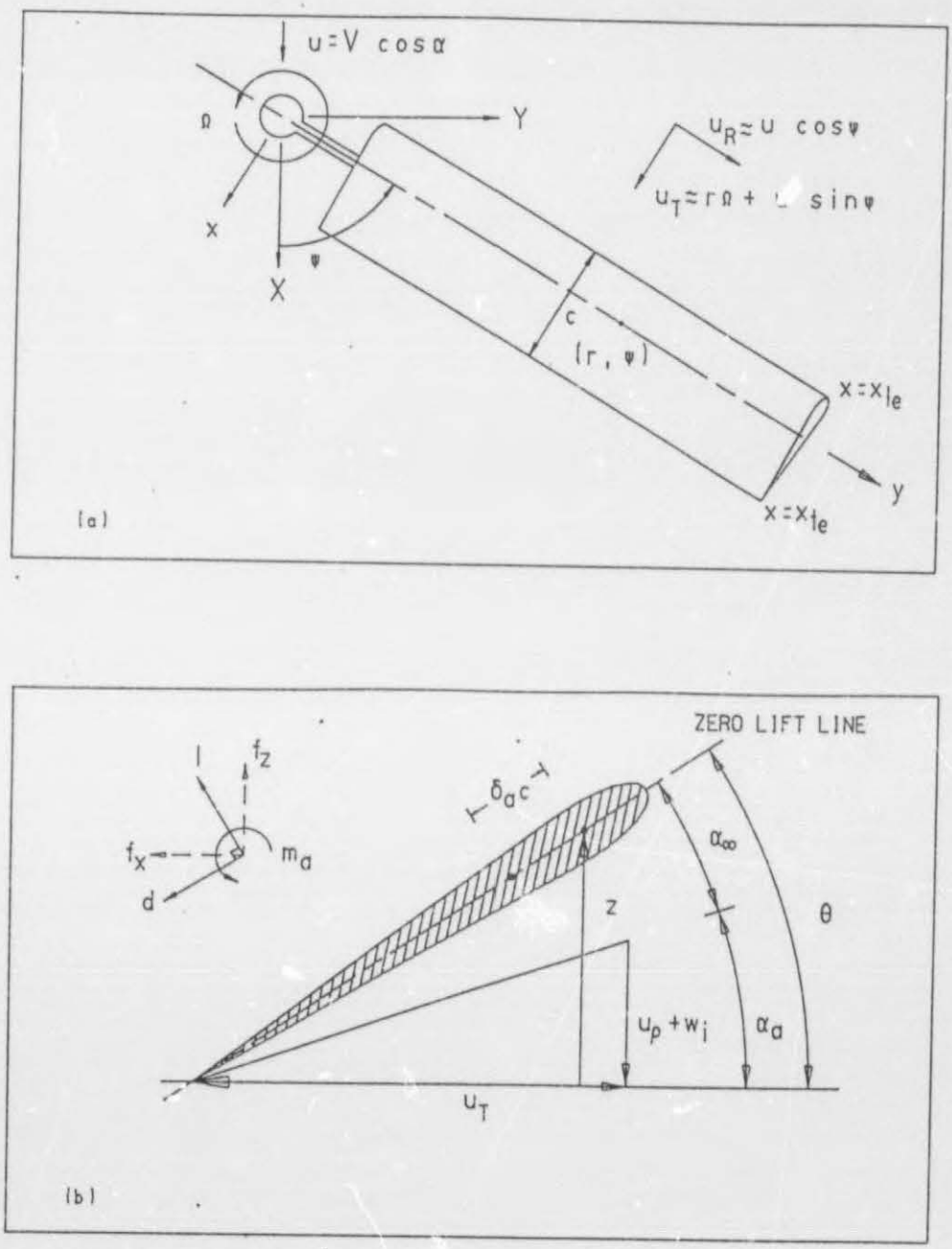

Fig 2.9 (a) Geometry and kinematics for unsteady rotary wing model
(b) Rotor blade section aerodynamics

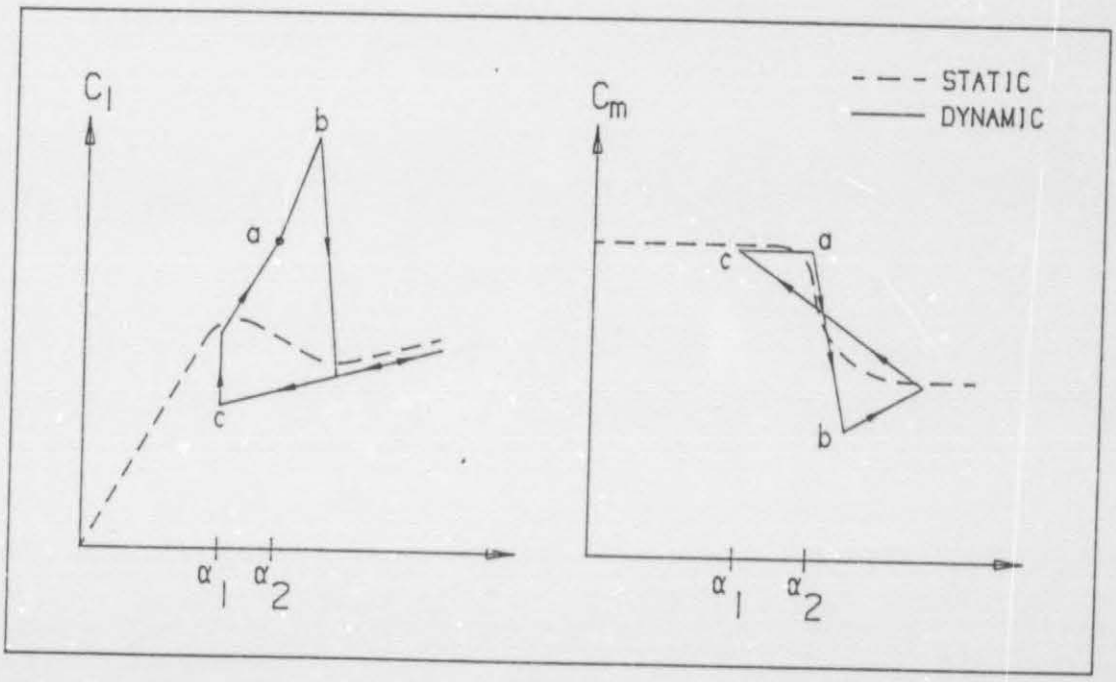

Fig 2.10 Dynamic stall characteristics

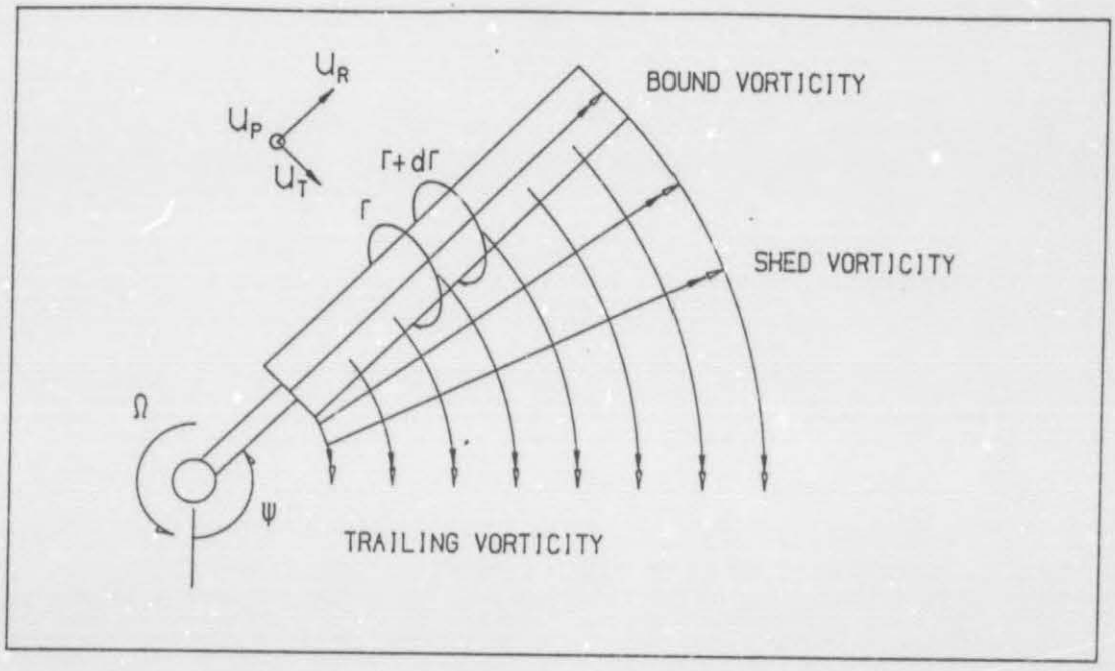

Fig 2.11 Rotating wing vorticity distribution

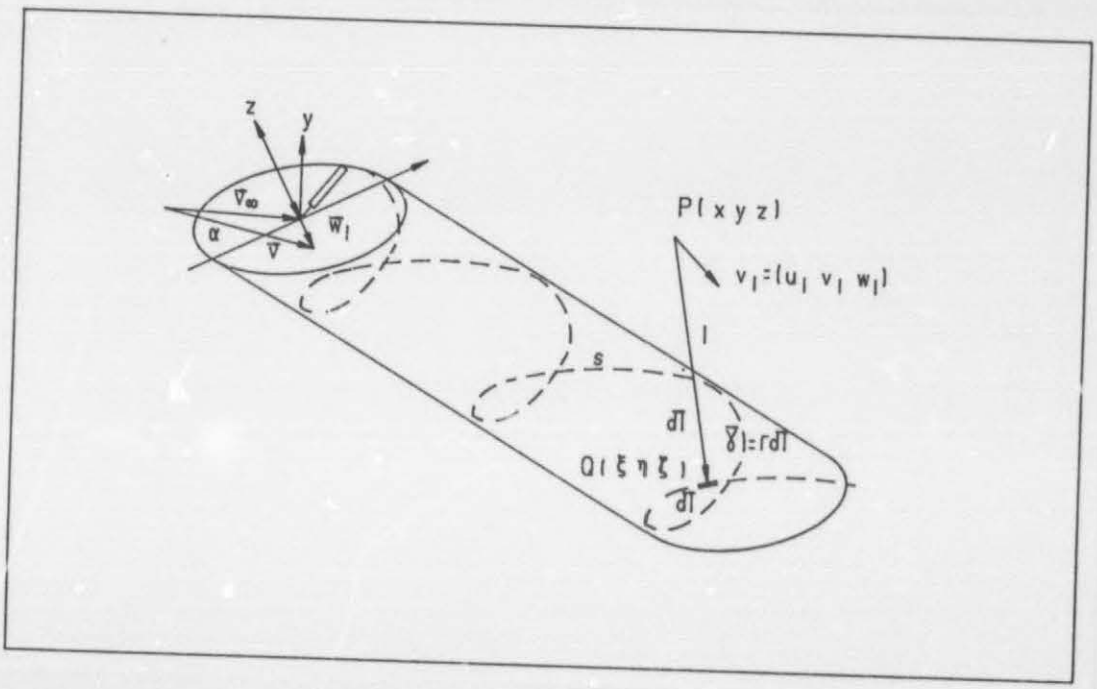

Fig 2.12 Wake structure of advancing rotor

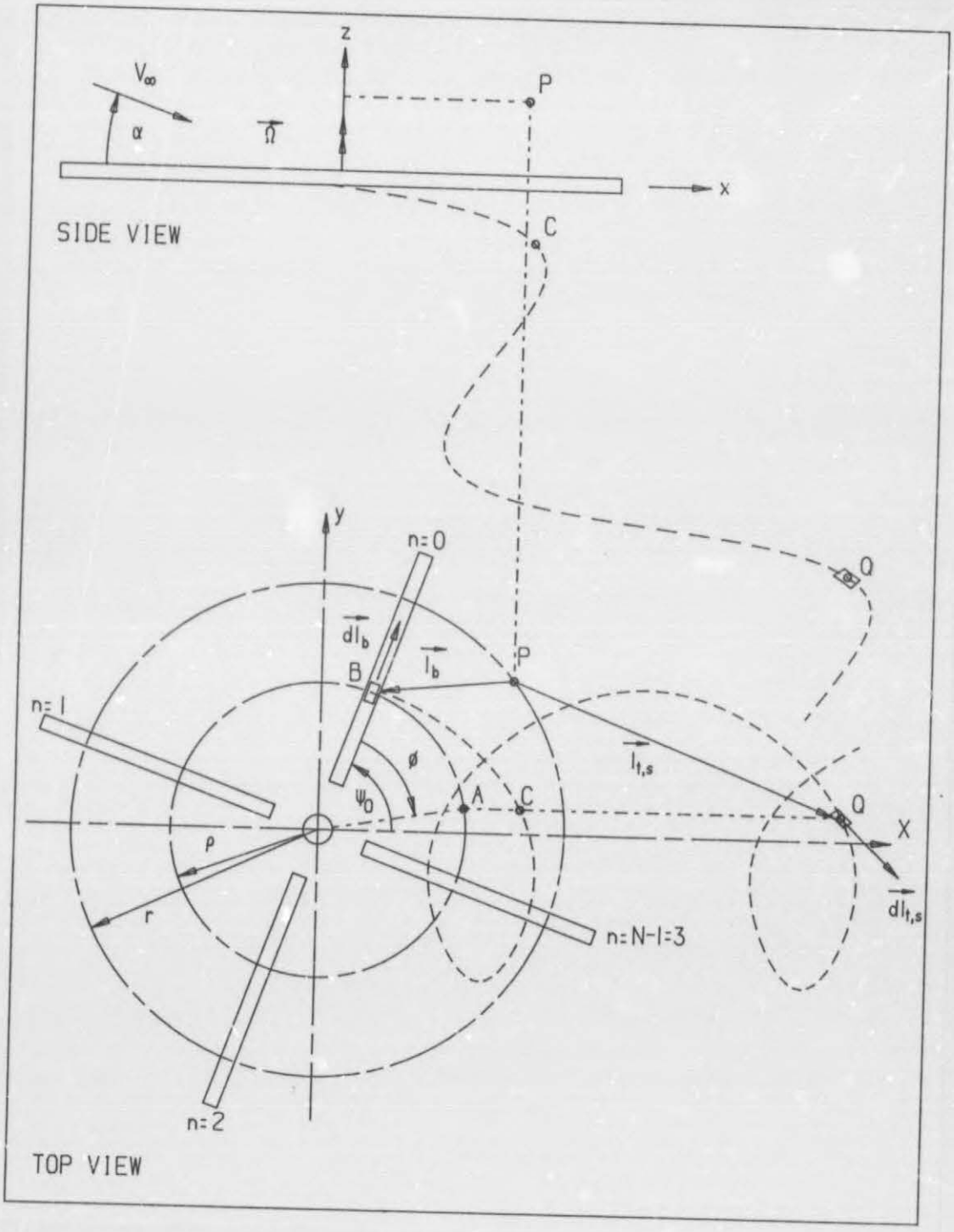

Fig 2.13 Movement of an arbitrary wake element

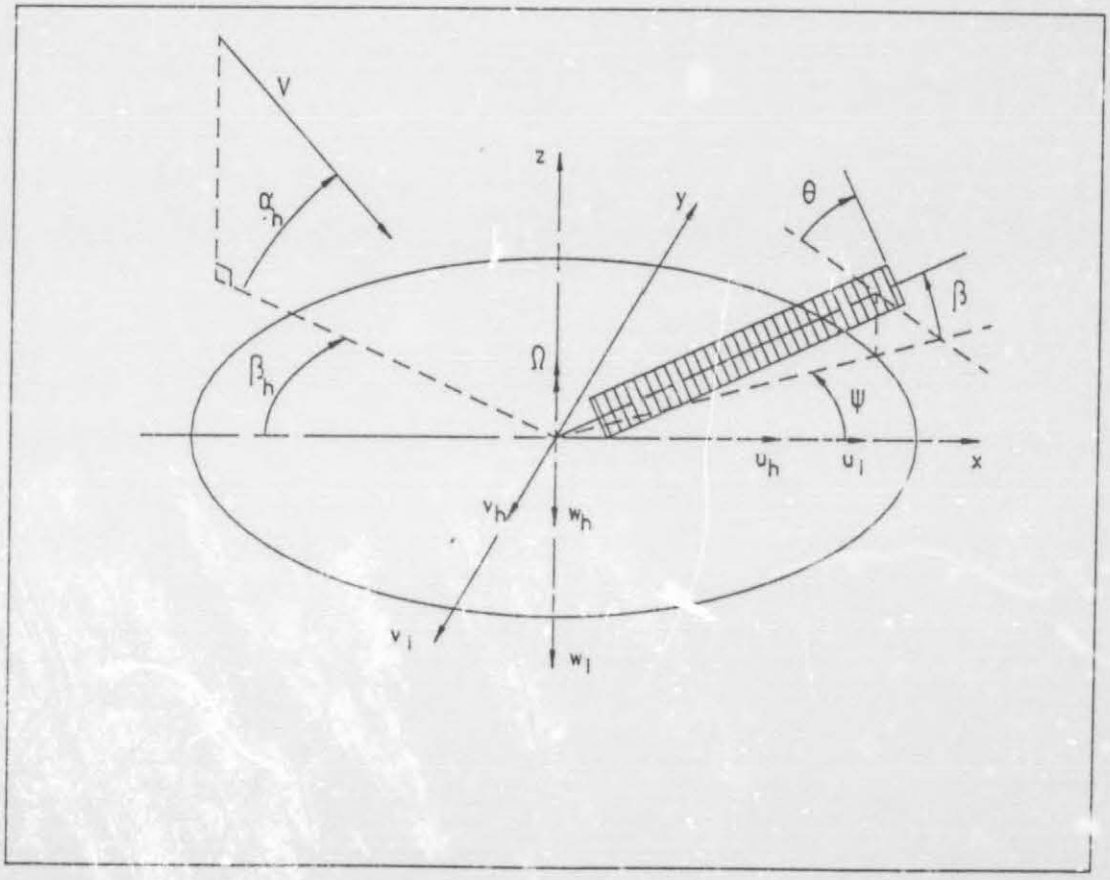

Fig 3.1 Rotor kinematics and flow

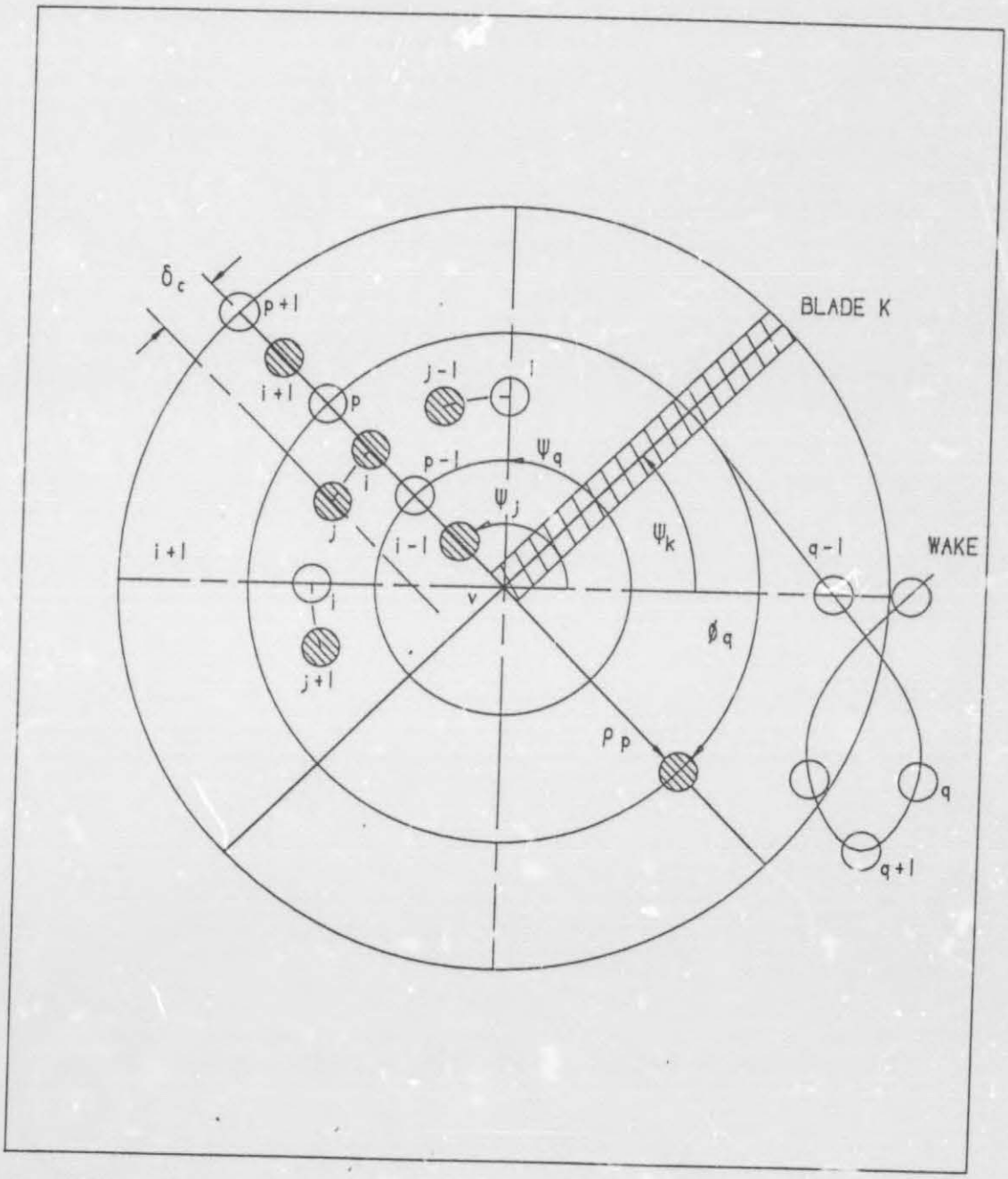

Fig 3.2 Nodes and control points of rotor model

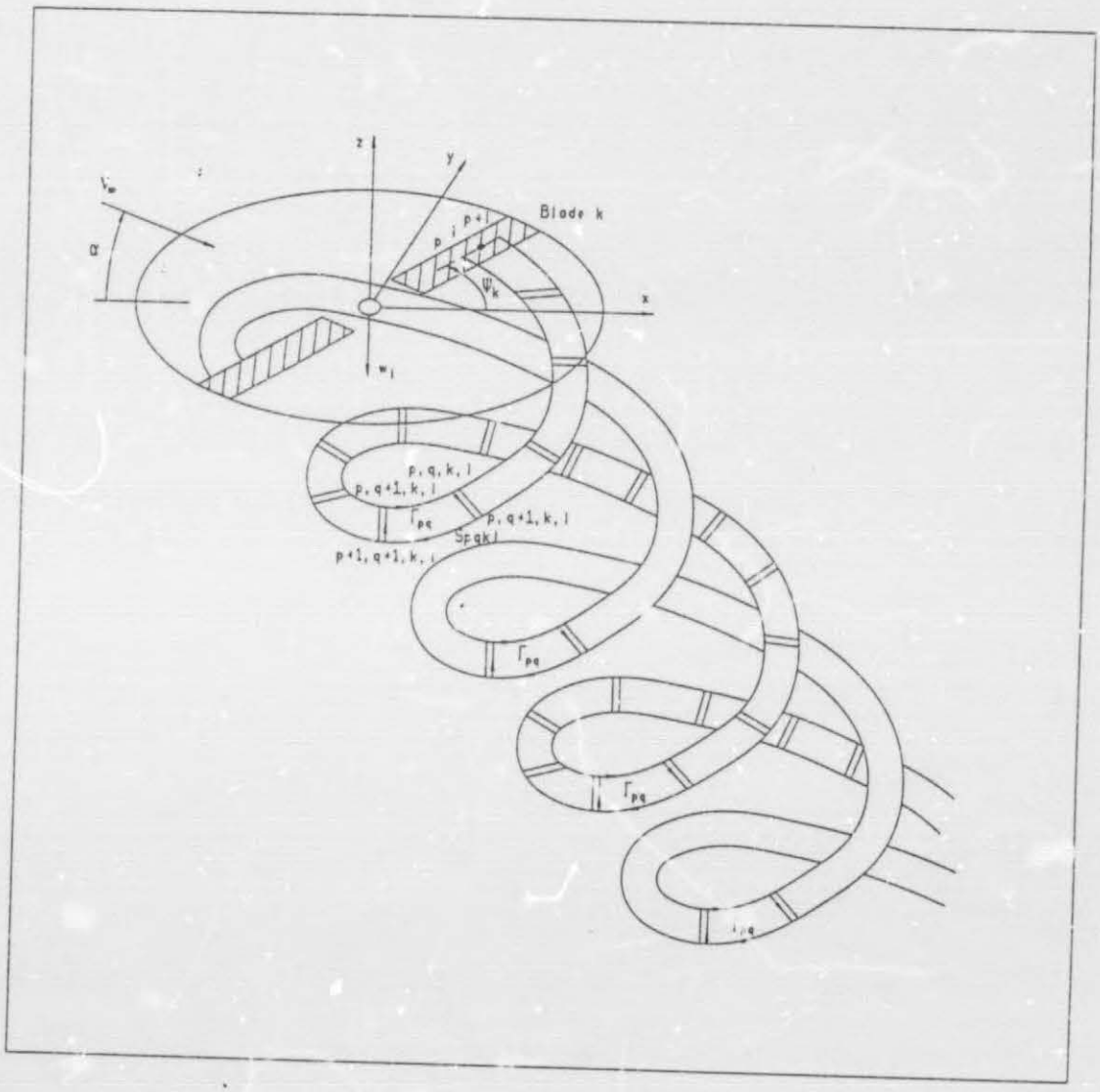

Fig 3.3 Geometry of discretized wake

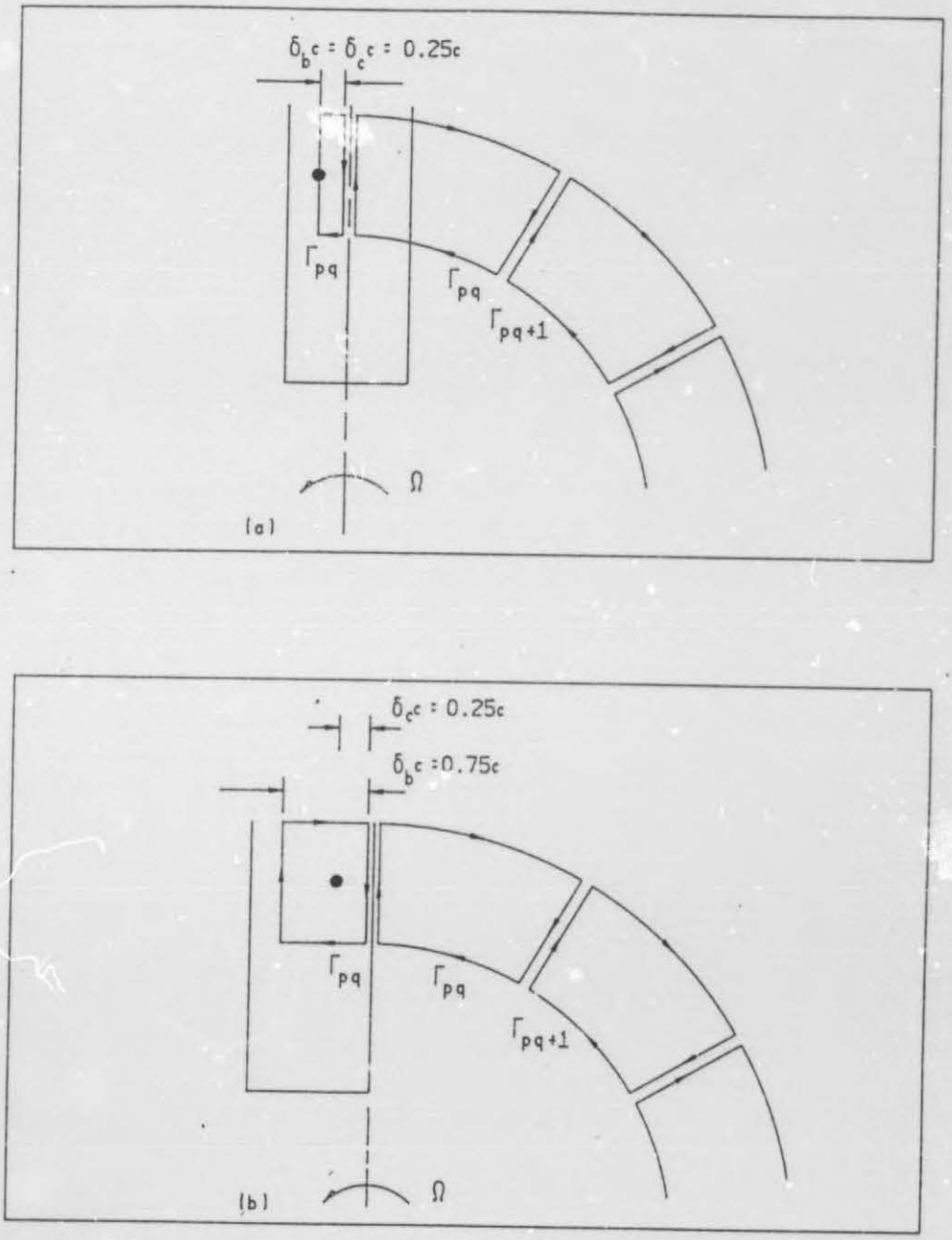

Fig 3.4 (a) Classical lifting line bound vortex cells
(b) Extended lifting line bound vortex cells

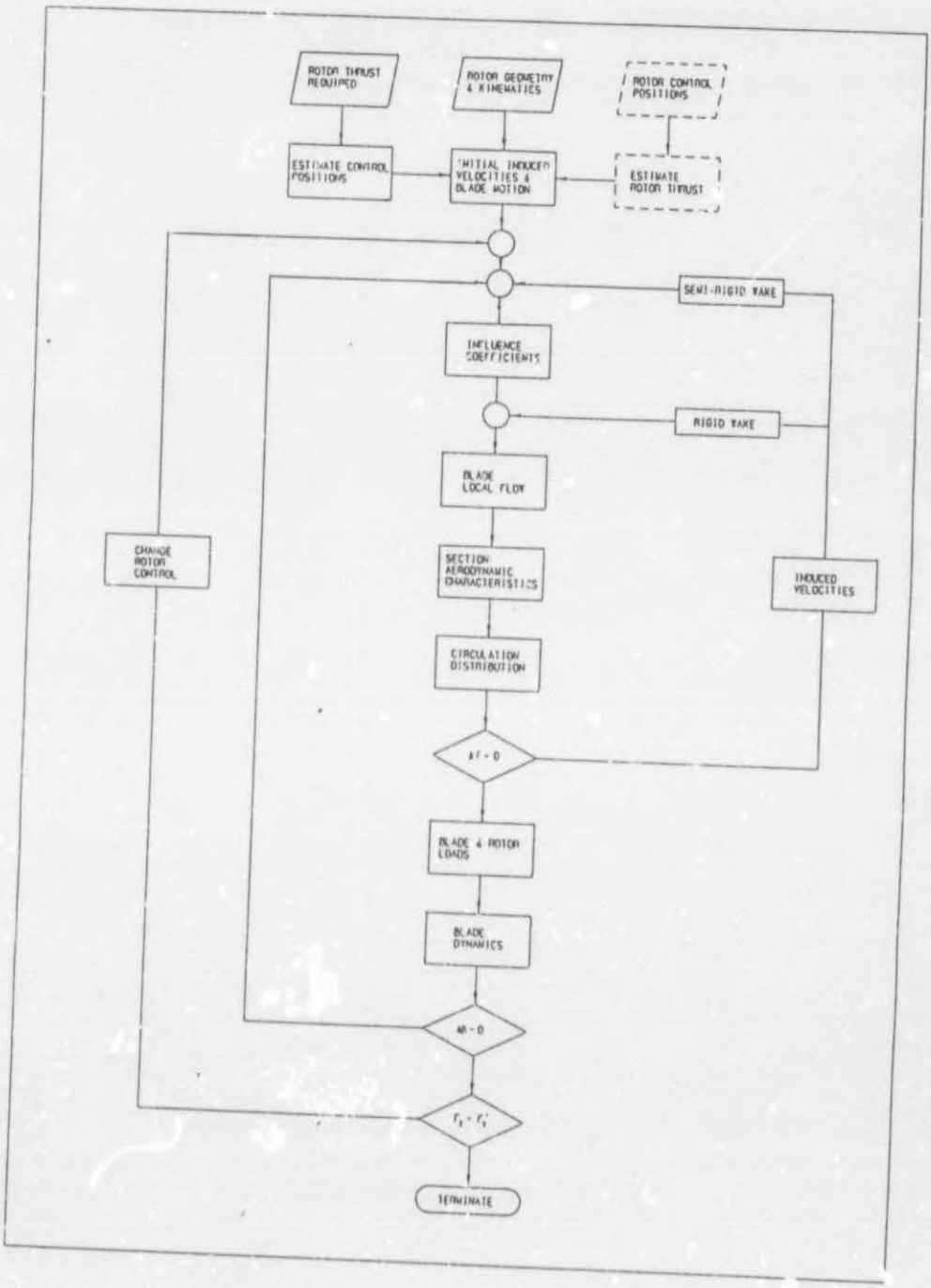

Fig 3.5 Calculation procedure for discretized model

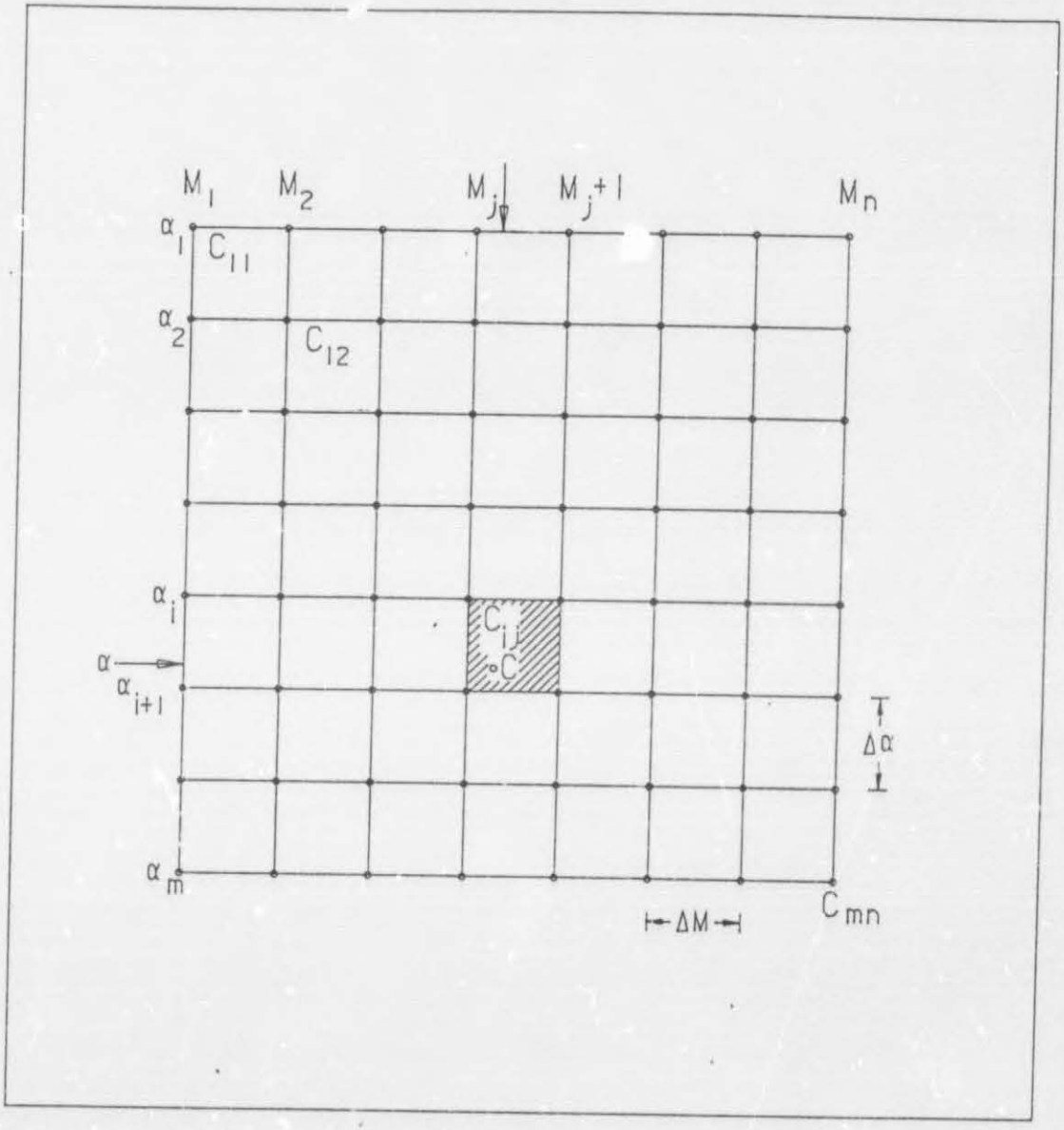

Fig 2.6 Ordering scheme for aerodynamic characteristics

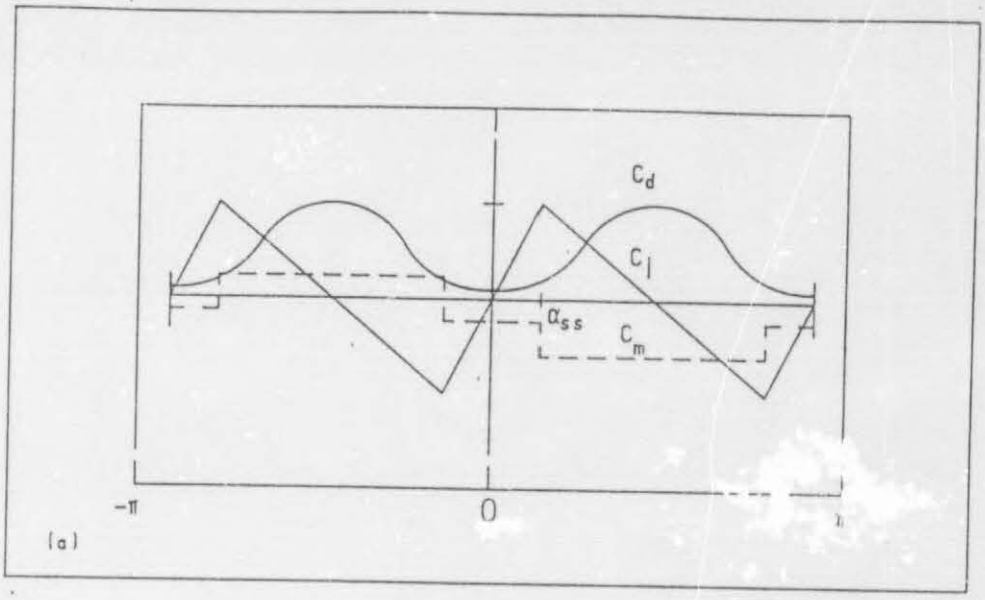

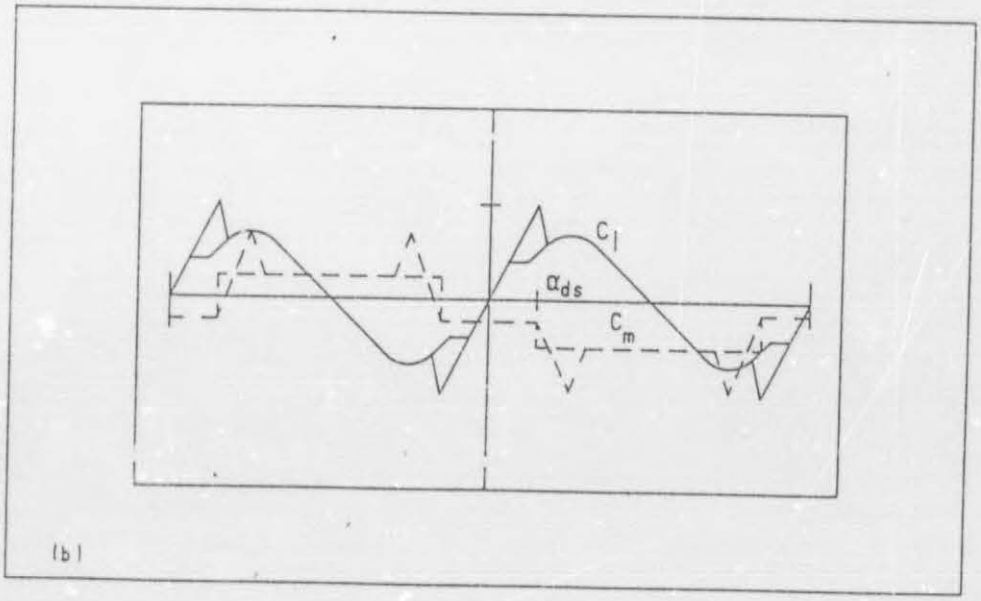

Fig 3.7 (a) Model of static aerodynamic characteristics
(b) Dynamic stall characteristics

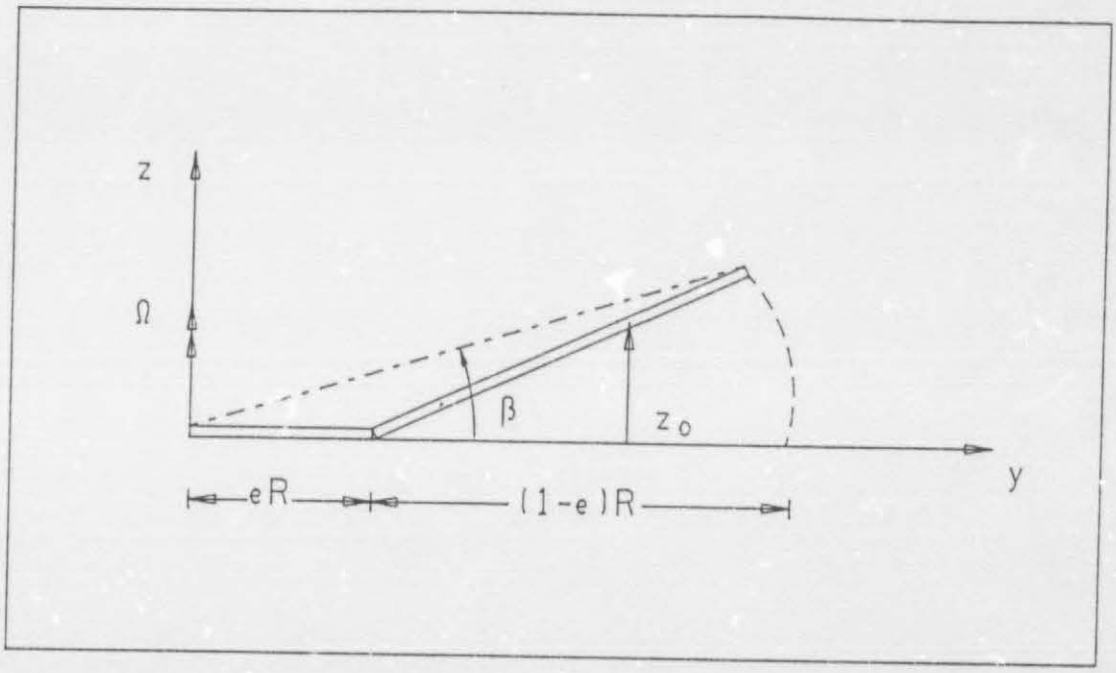

Fig 3.8 Blade geometry and kinematics

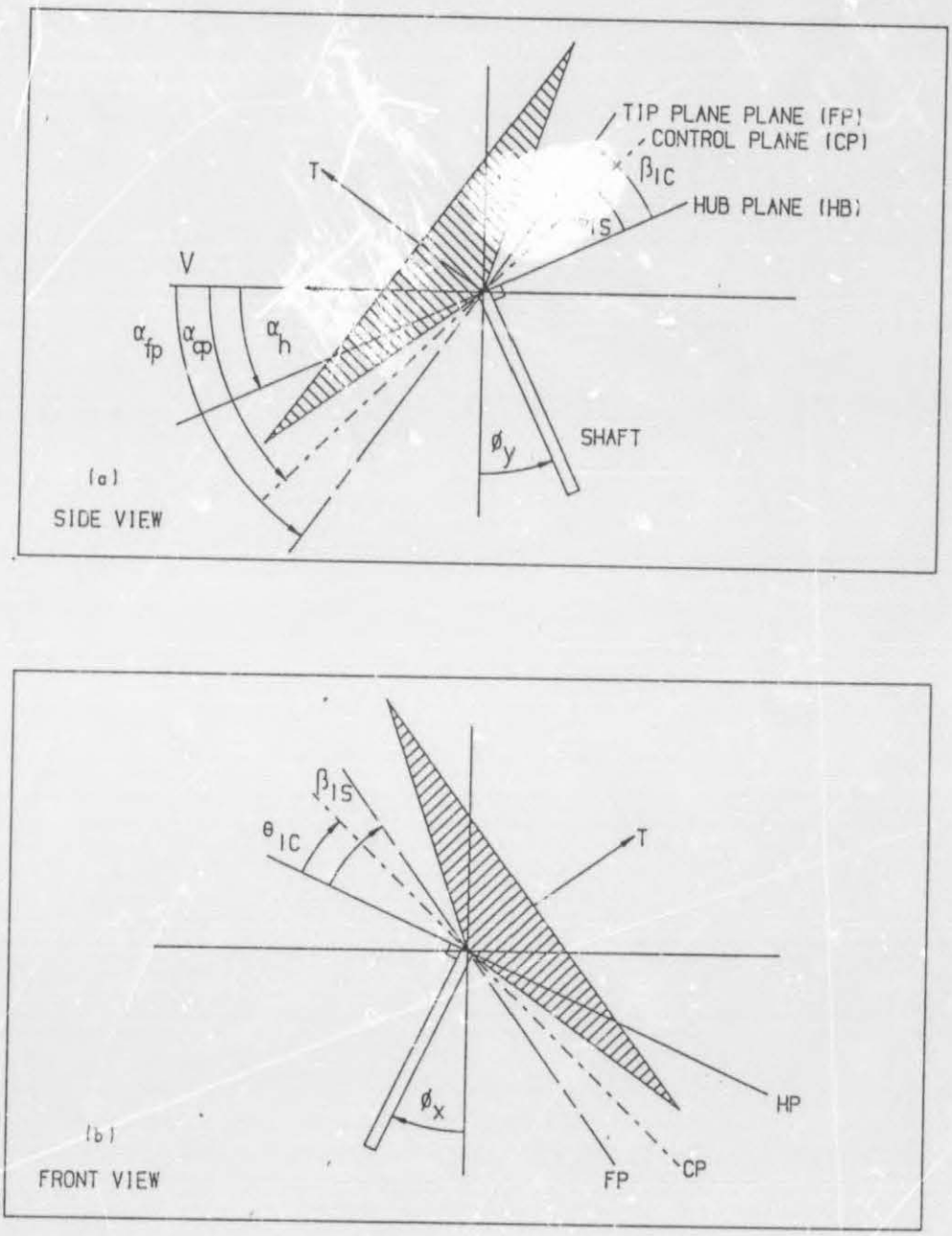

Fig 3.9 (a) Rotor reference planes, side view
(b) Rotor reference planes, front view

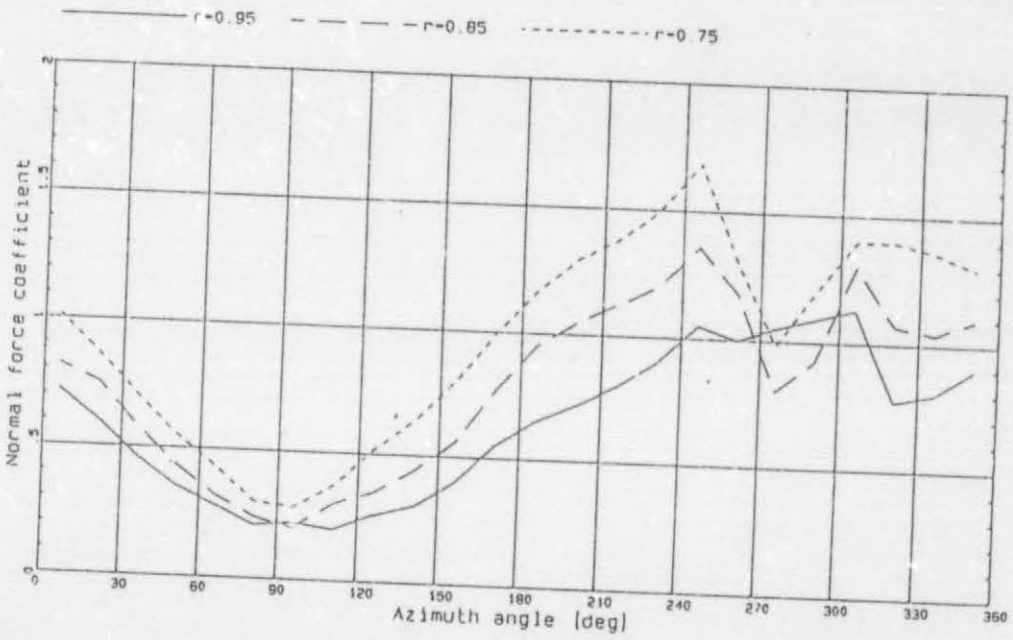

Fig 5.1.0.0 Normal force coefficient from Scheiman & Ludi [1963]

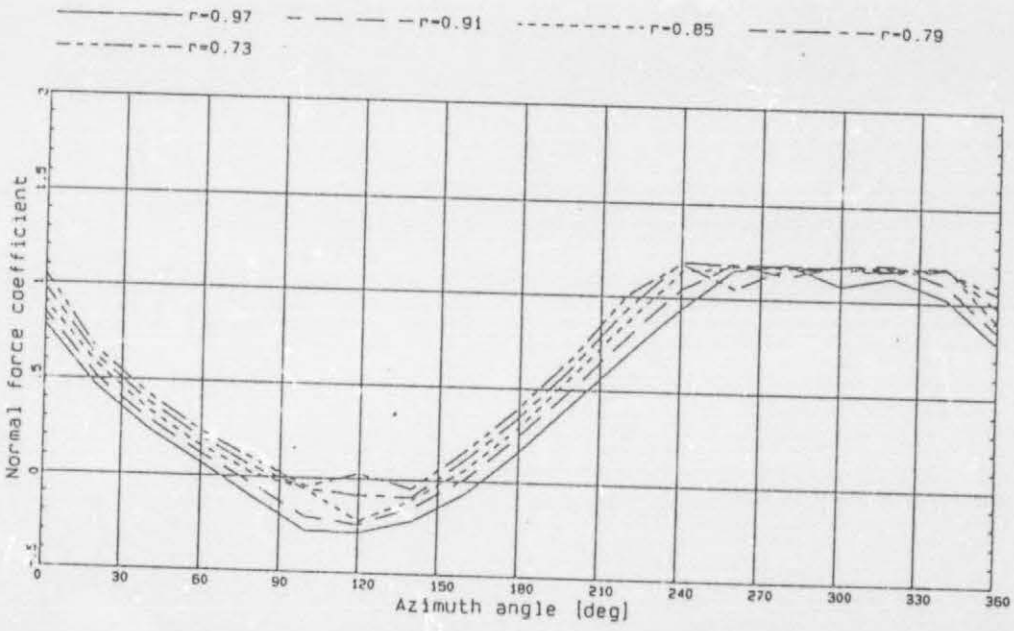

Fig 5.1.1.1 Calculated normal force coefficient, case 111

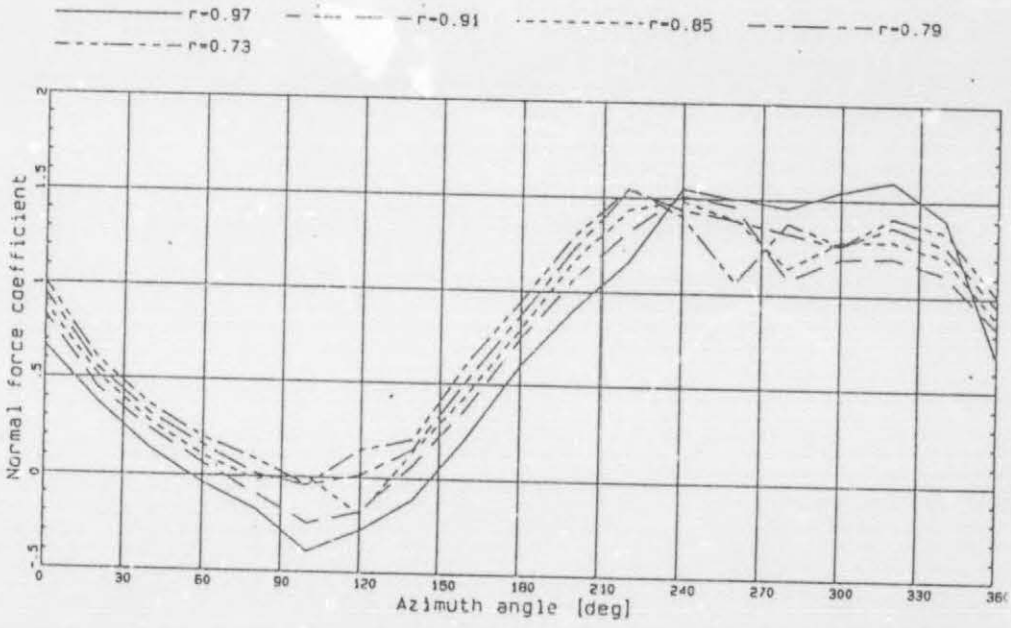

Fig 5.1.1.2 Calculated normal force coefficient, case 112

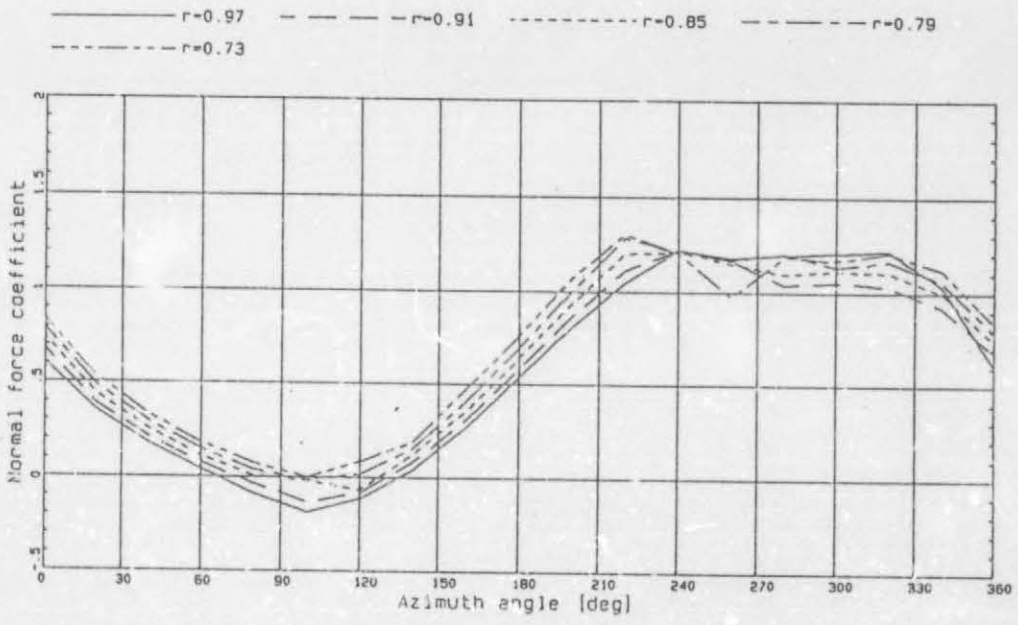

Fig 5.1.1.3 Calculated normal force coefficient, case 11.3

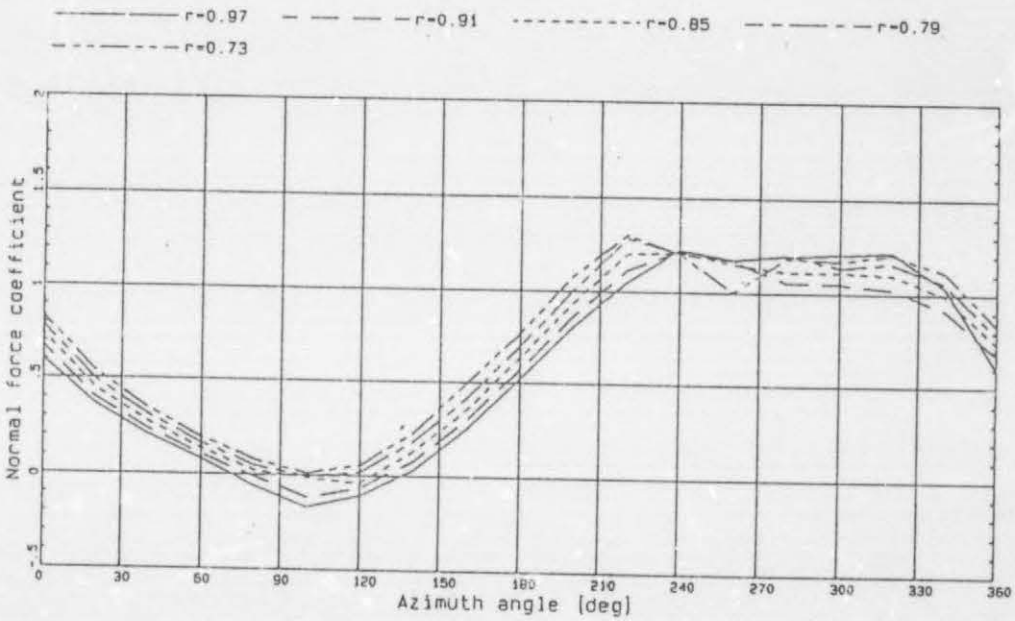

Fig 5.1.1.4 Calculated normal force coefficient, case 114

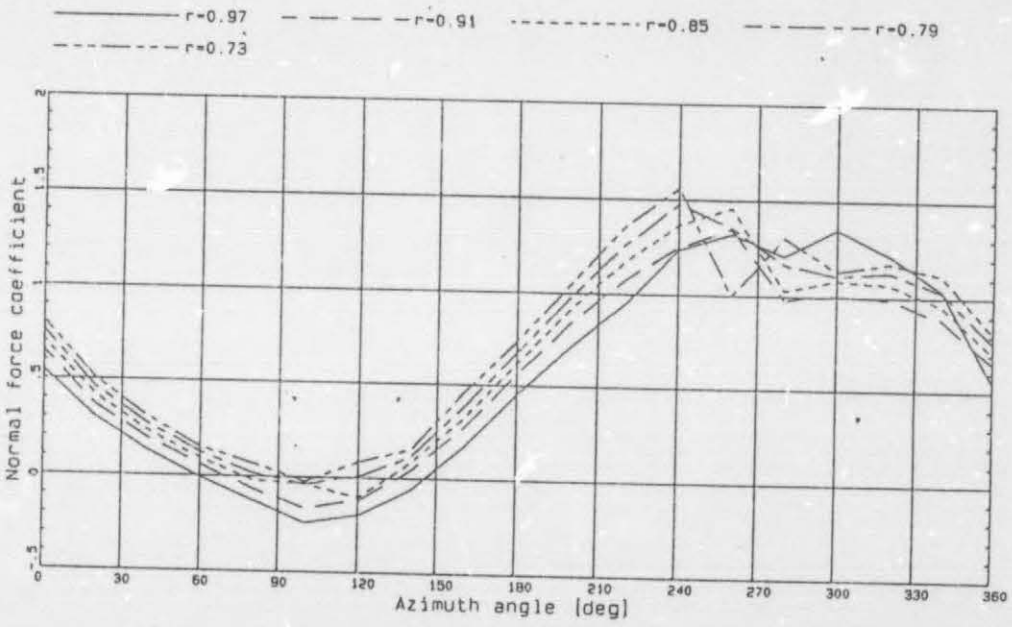

Fig 5.1.1.5 Calculated normal force coefficient, case 115

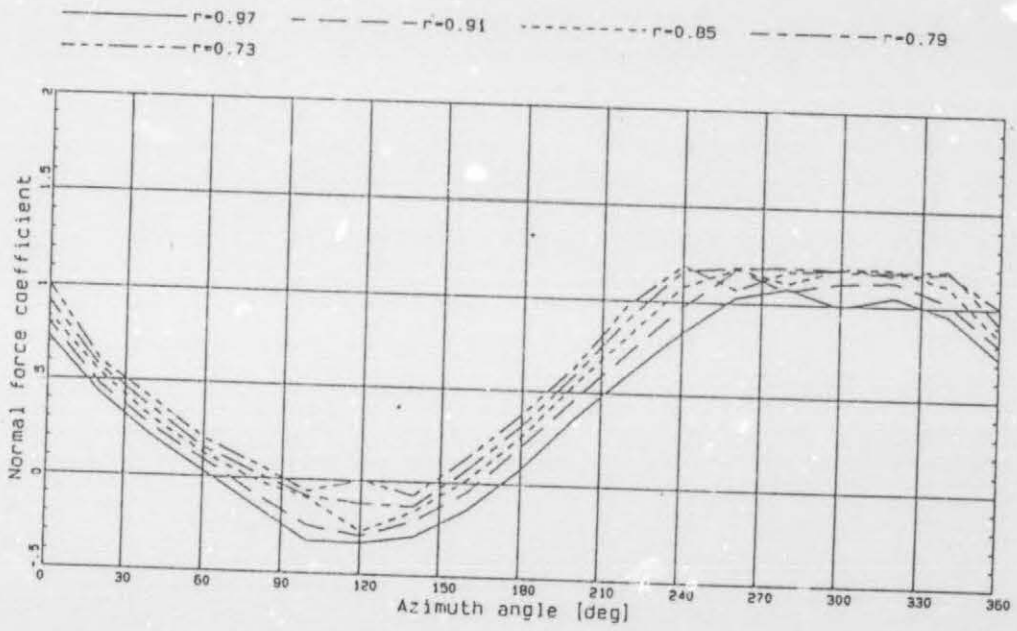

Fig 5.1.2.1 Calculated normal force coefficient, case 121

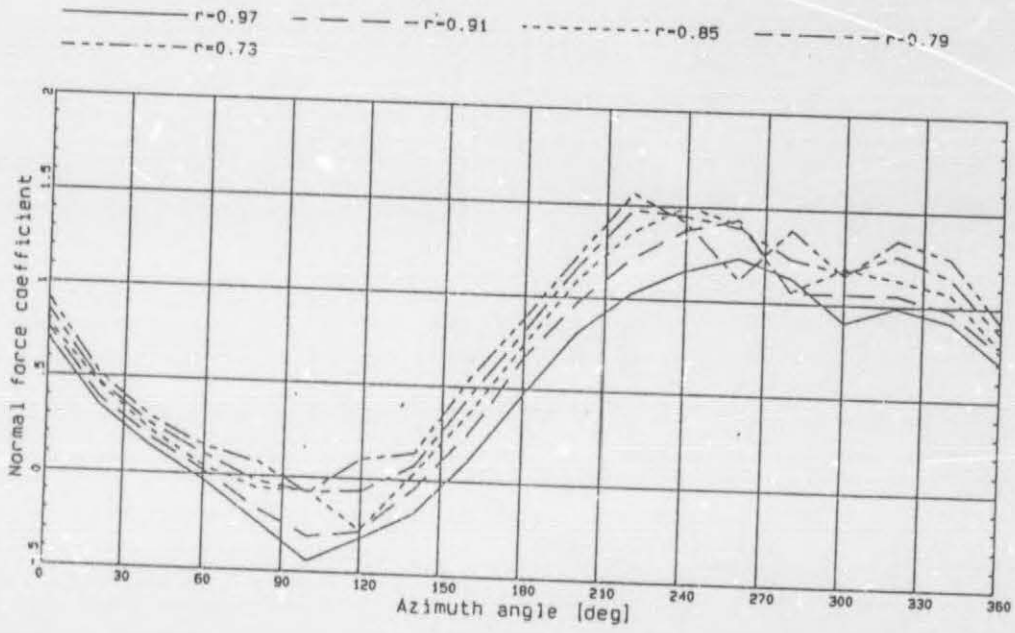

Fig 5.1.2.2 Calculated normal force coefficient, case 122

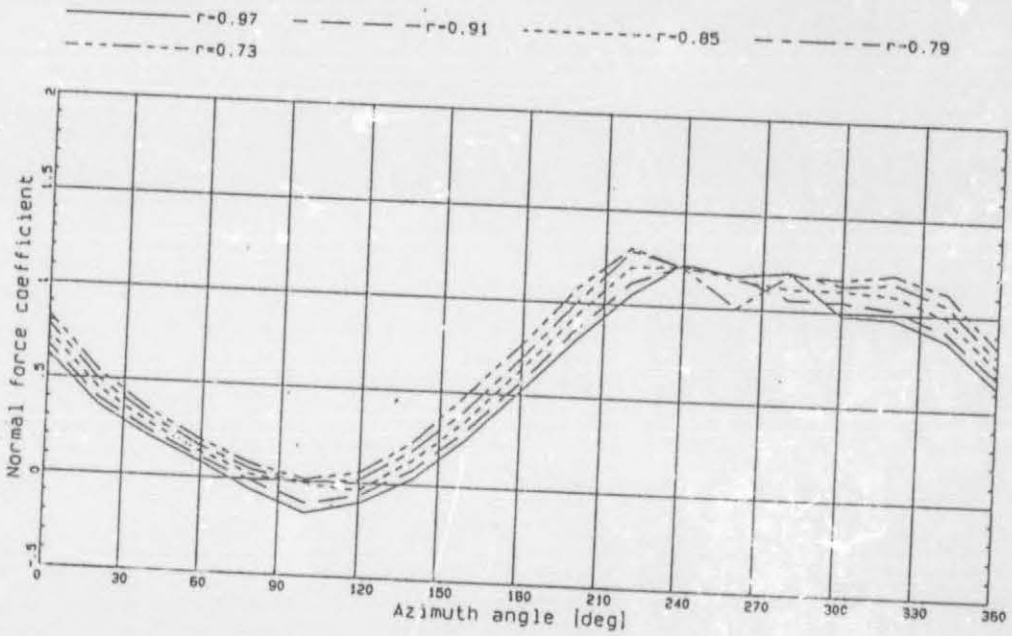

Fig 5.1.2.3 Calculated normal force coefficient, case 123

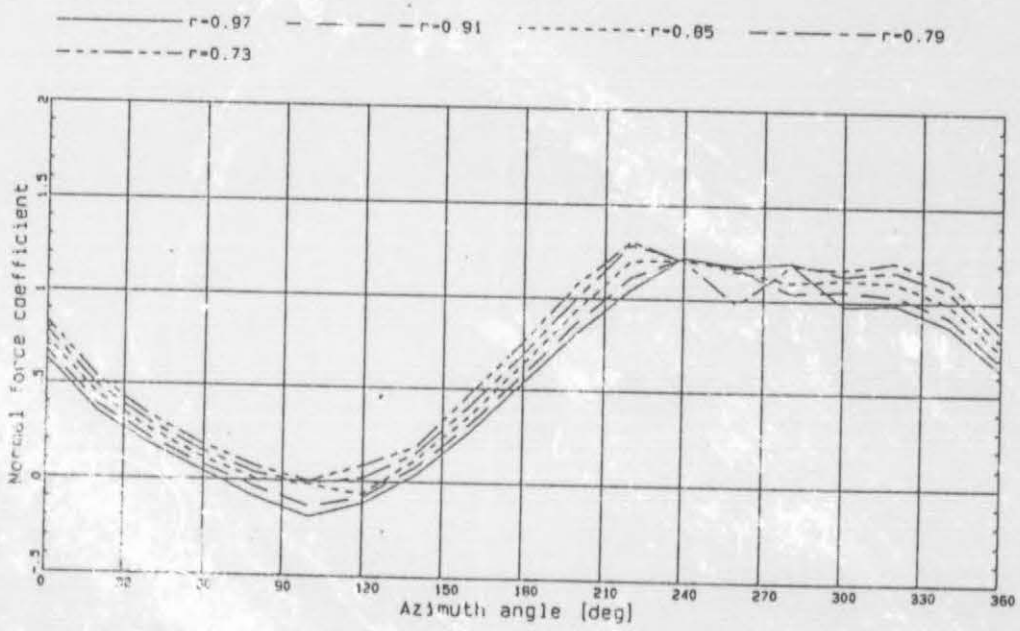

Fig 5.1.2.4 Calculated normal force coefficient, case 124

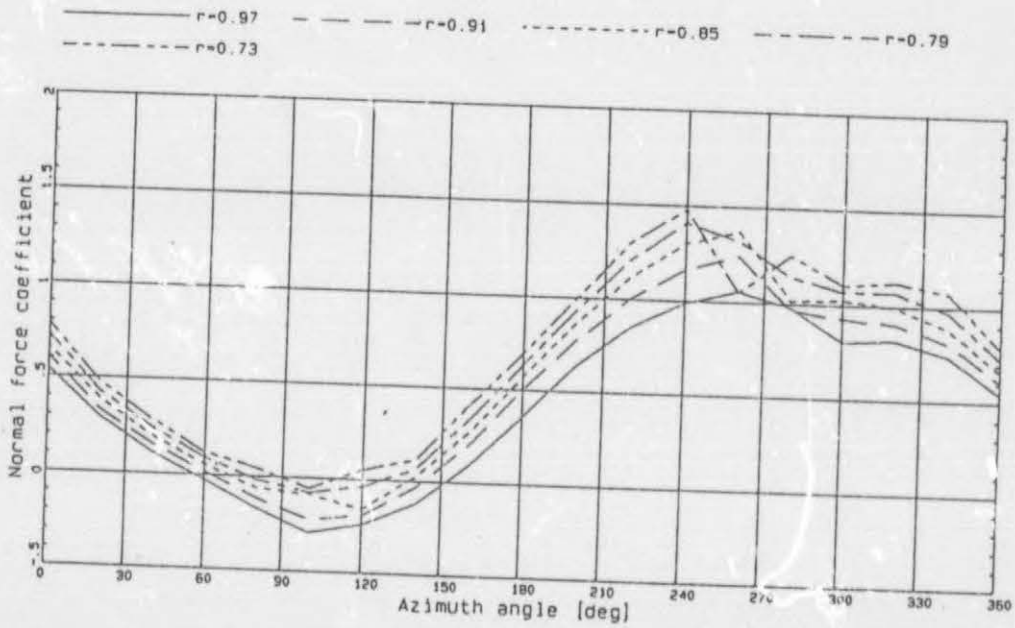

Fig 5.1.2.5 Calculated normal force coefficient, case 125

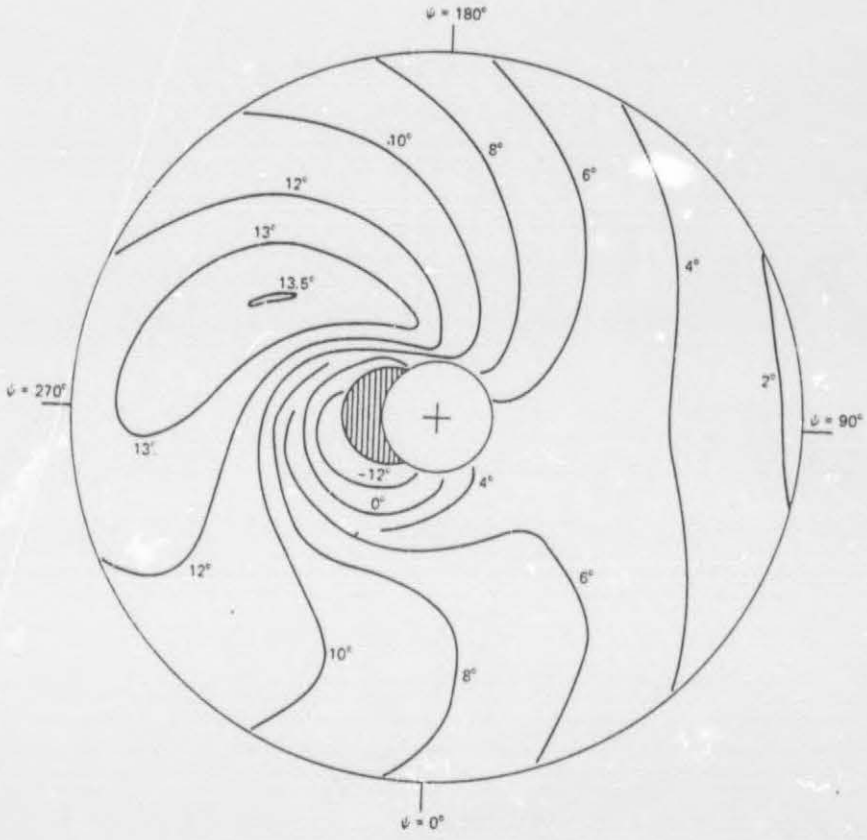

Blade angle-of-attack distribution (in degrees) at $\mu = 0.25$, for $C_T/\sigma = 0.12$, $f/A = 0.015$, and $\theta_{tw} = -8°$ (uniform inflow).

Fig 5.2.0.0 (a) Angle of attack distribution $\alpha(r,\psi)$ from Johnson [1980a]

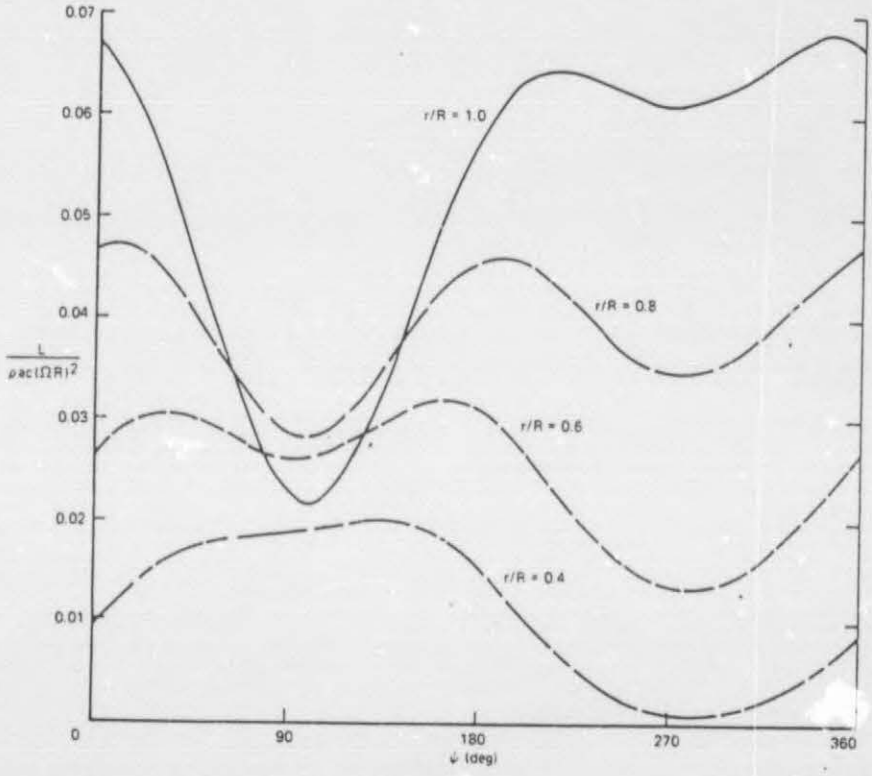

Azimuthal variation of the blade lift $L/\rho ac(\Omega R)^2$ at $\mu = 0.25$, for $C_T/\sigma = 0.12$, $f/A = 0.015$, and $\theta_{tw} = -8°$ (uniform inflow).

Fig 5.2.0.0 (b) Non-dimensional lift distribution $\ell(\psi)$ from Johnson [1980a]

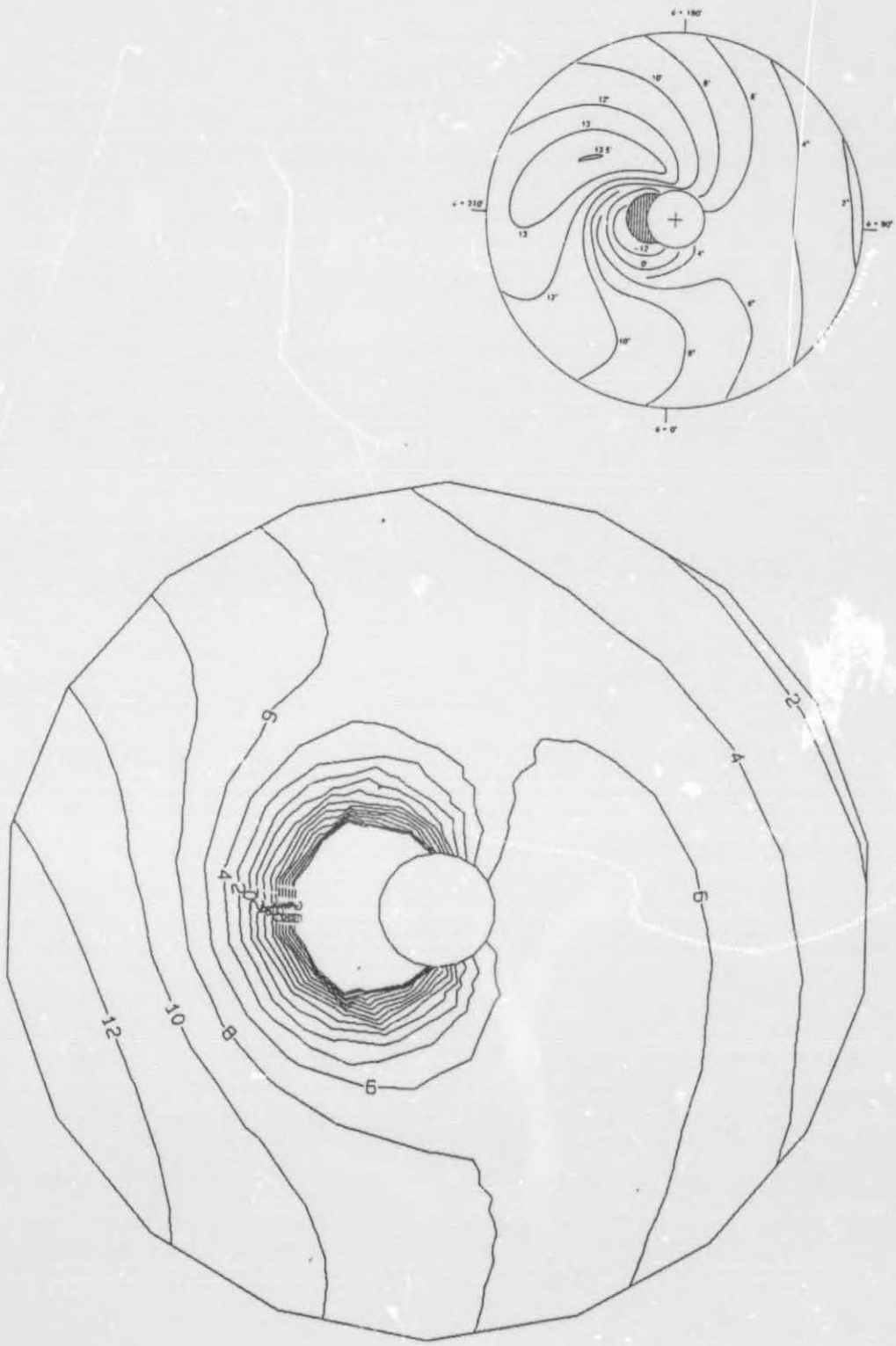

Fig 5.2.1.1(a) Calculated angle of attack distribution $\alpha(r,\psi)$, case 211

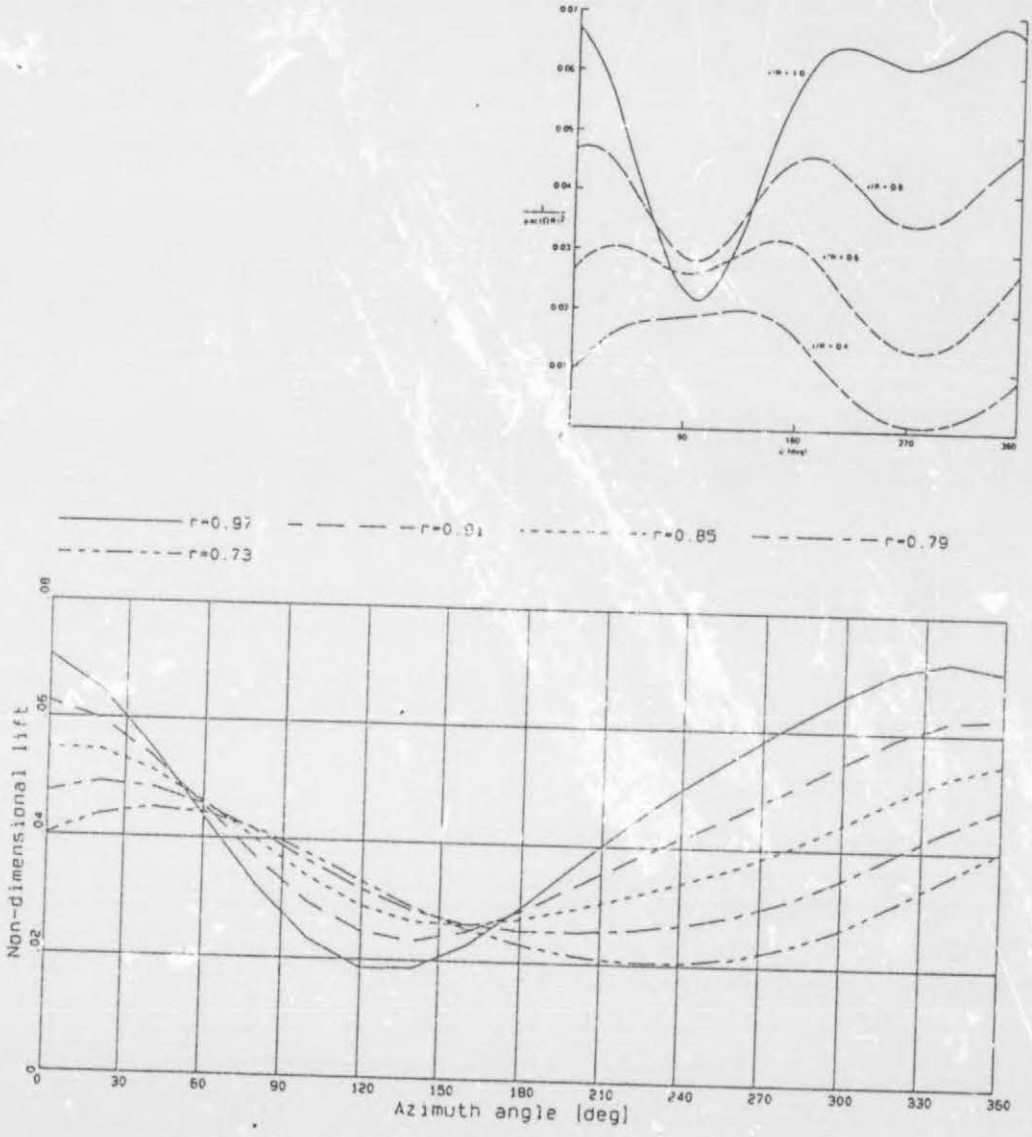

Fig 5.2.1.1(b) Calculated non-dimensional lift distribution $\ell(\psi)$, case 211

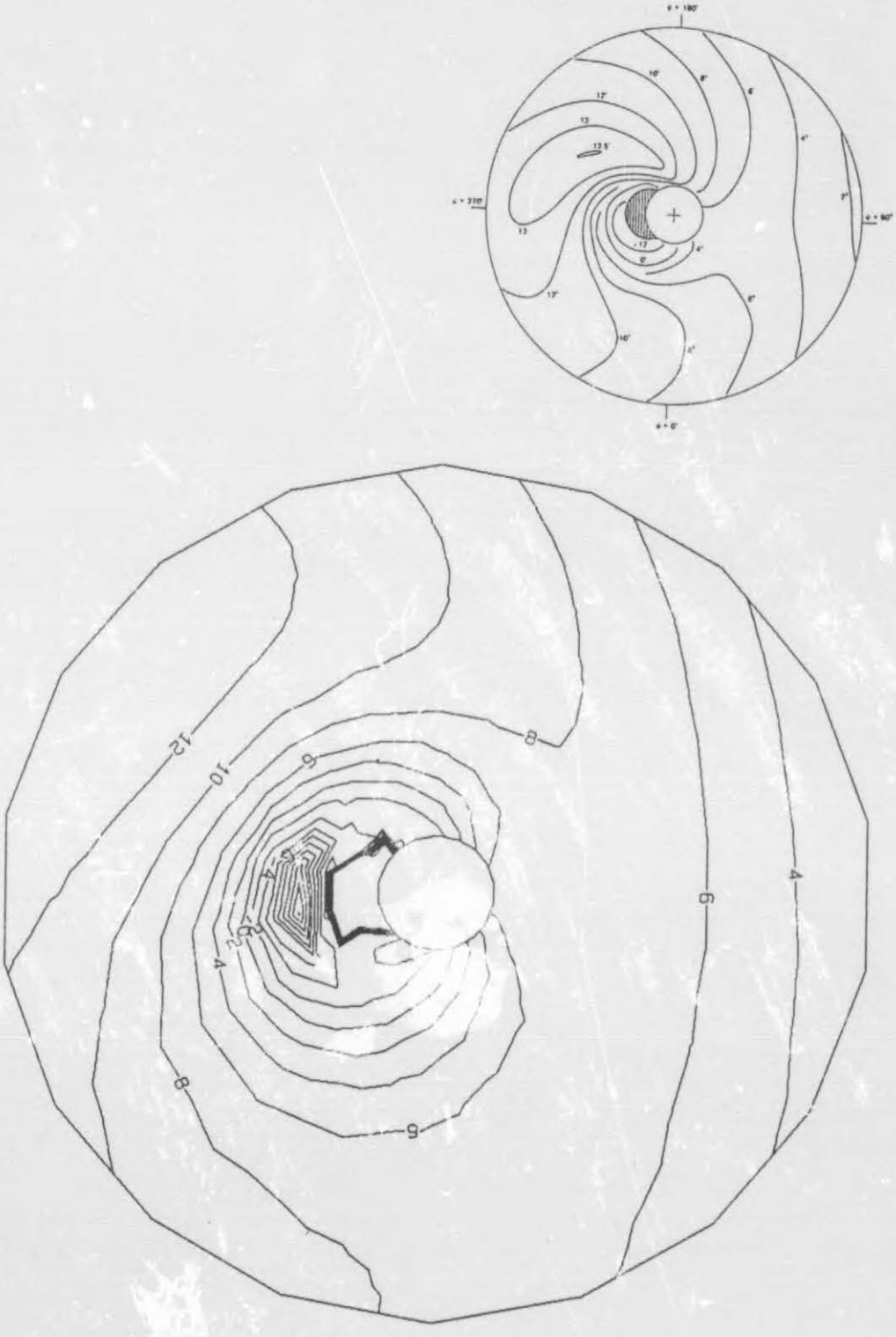

Fig 5.2.1.2(a) Calculated angle of attack distribution $\alpha(r,\psi)$, case 212

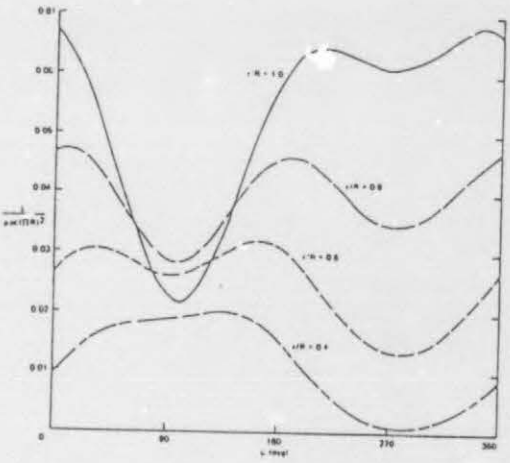

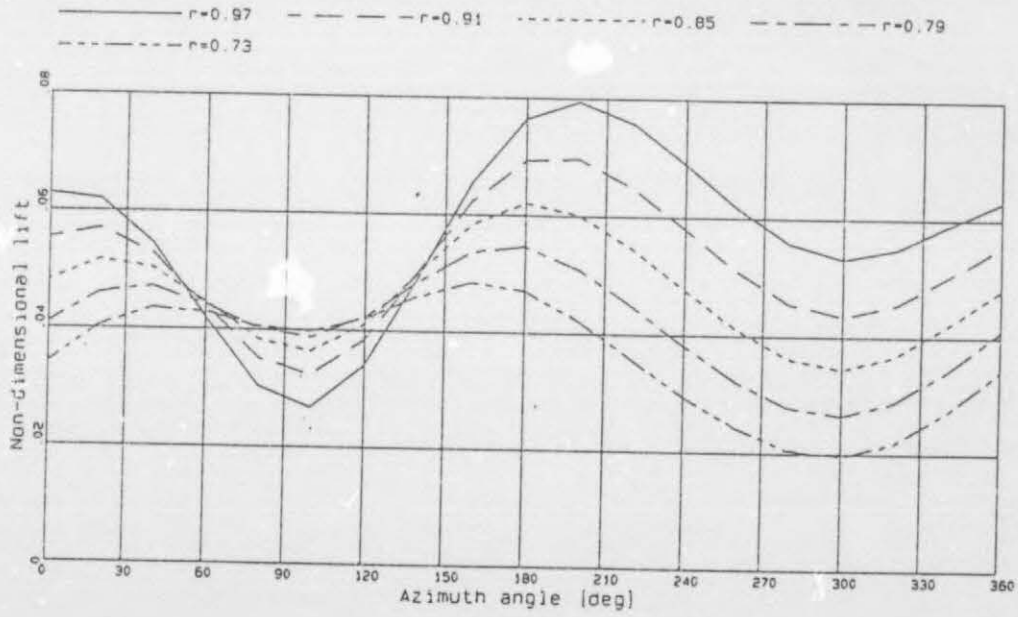

Fig 5.2.1.2(b) Calculated non-dimensional lift distribution $\ell(\psi)$, case 212

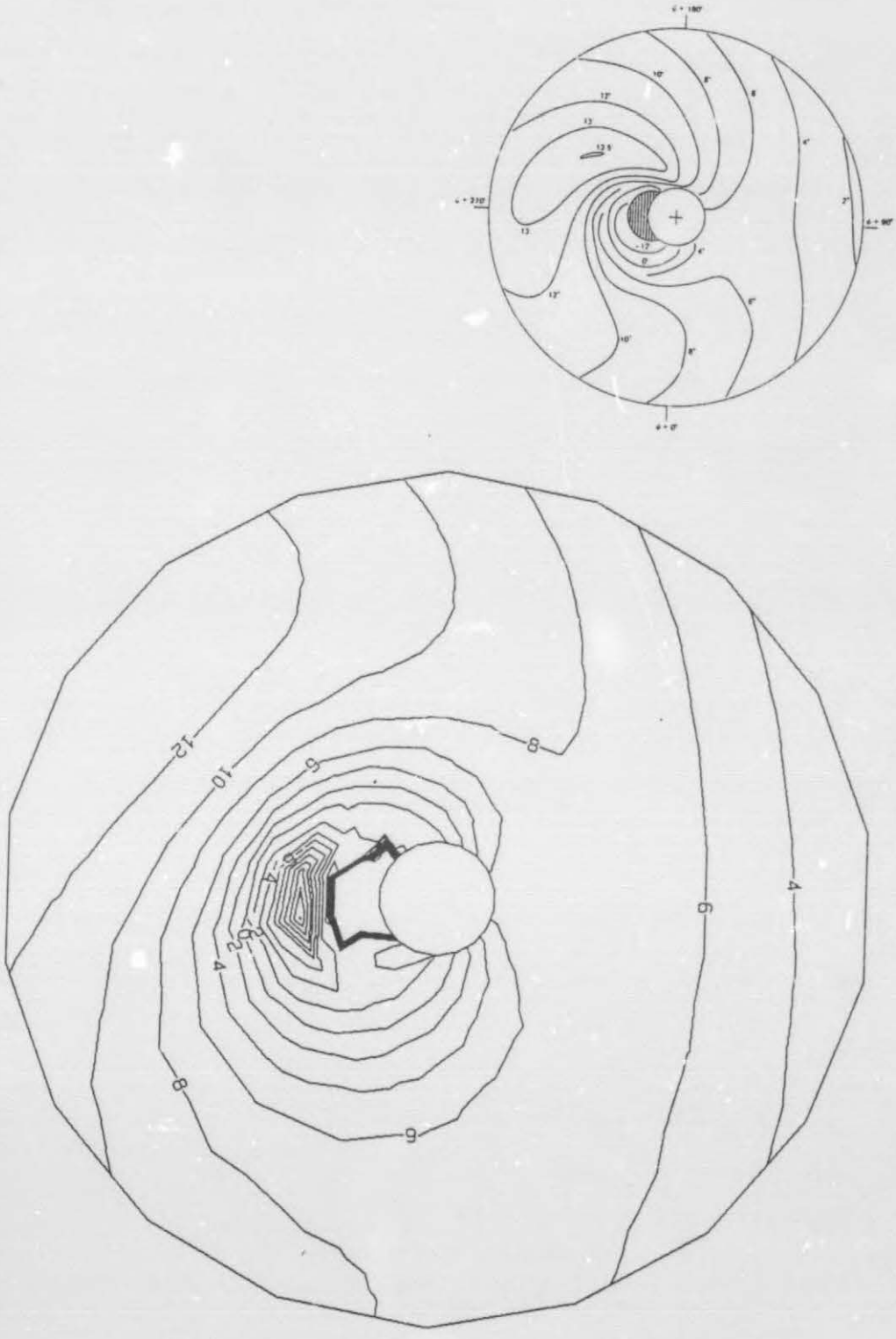

Fig 5.2.1.3(a) Calculated angle of attack distribution $\alpha(r,\psi)$, case 213

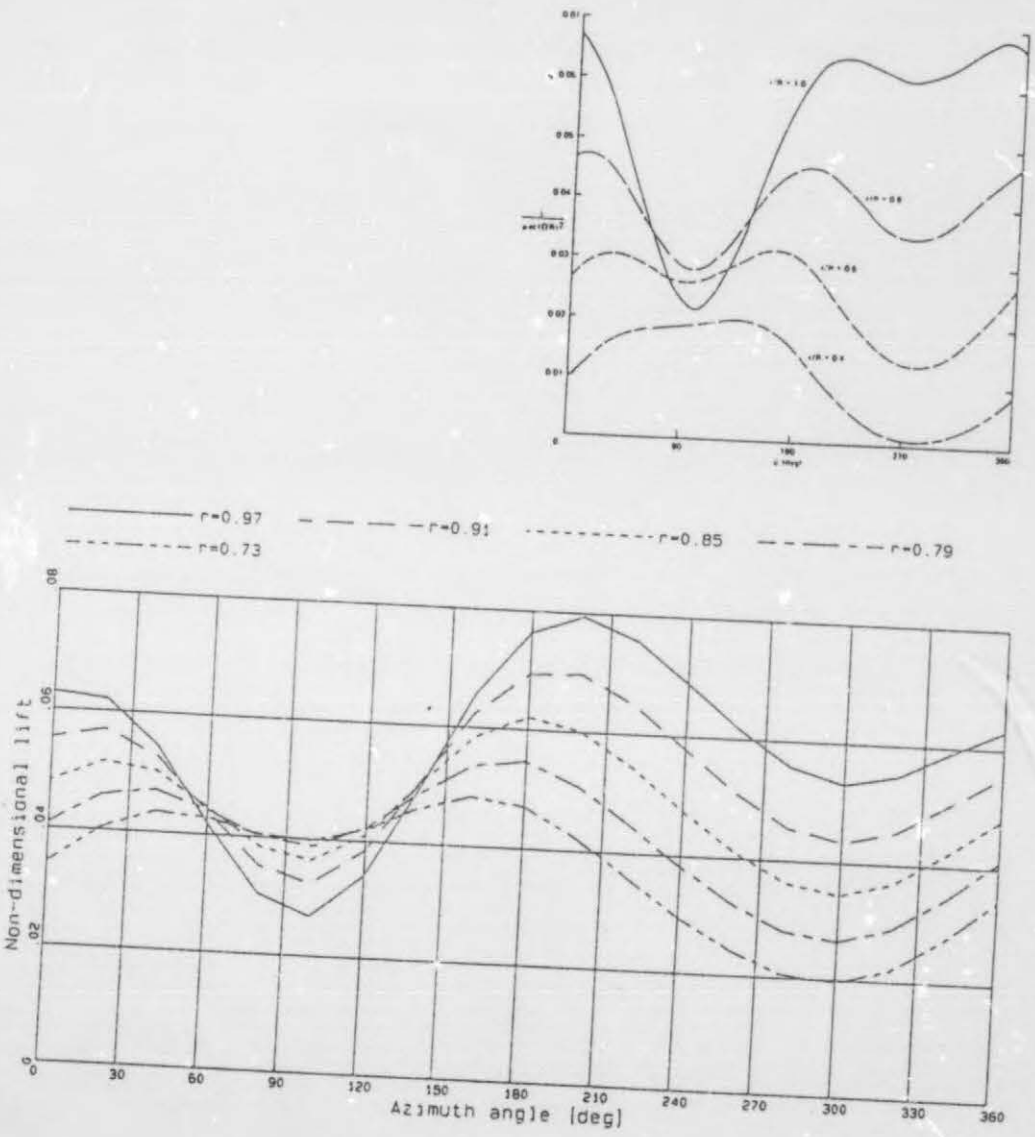

Fig 5.2.1.3(b) Calculated non-dimensional lift distribution $\ell(\psi)$, case 213

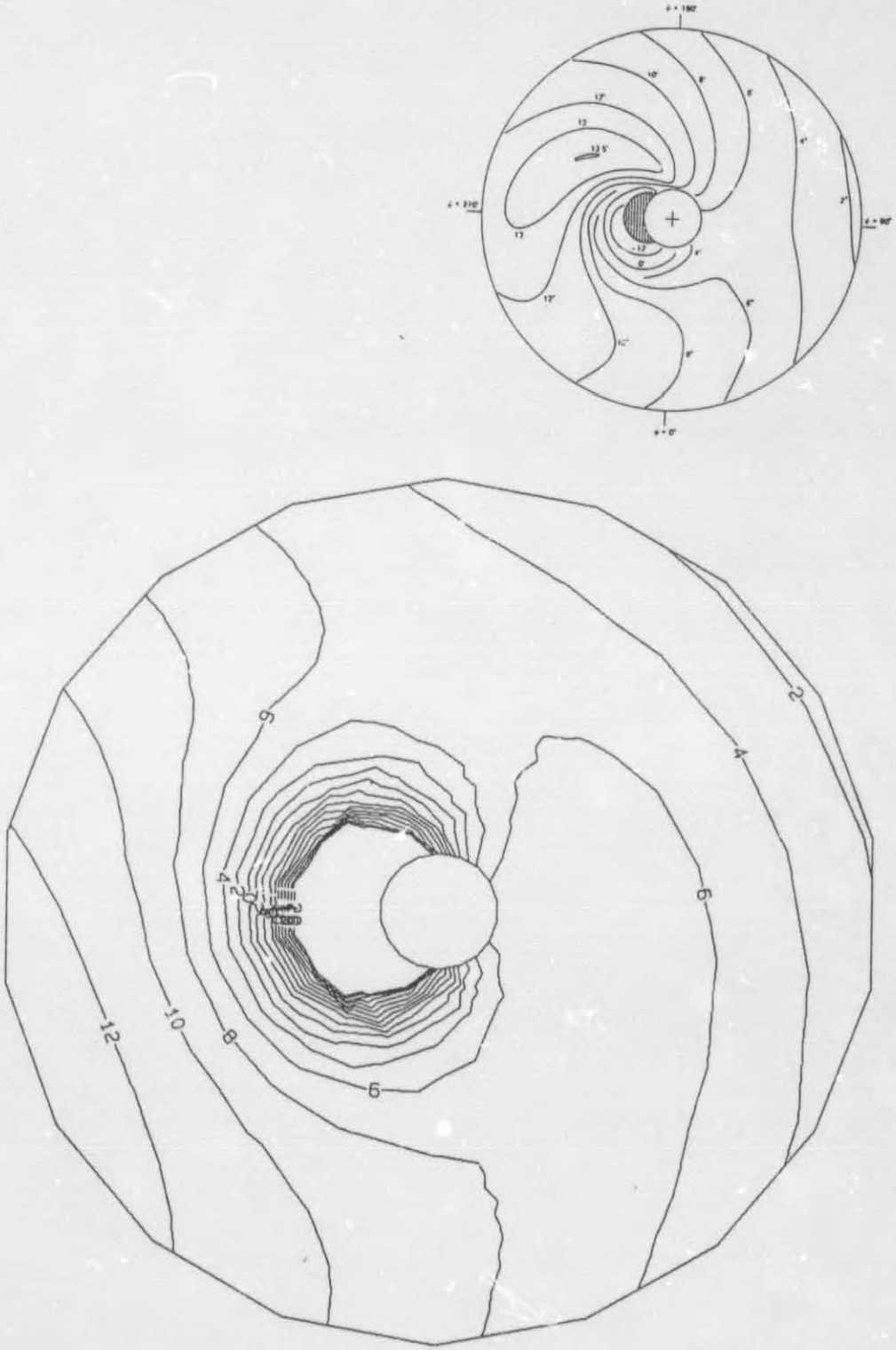

Fig 5.2.1.4(a) Calculated angle of attack distribution $\alpha(r,\psi)$, case 214

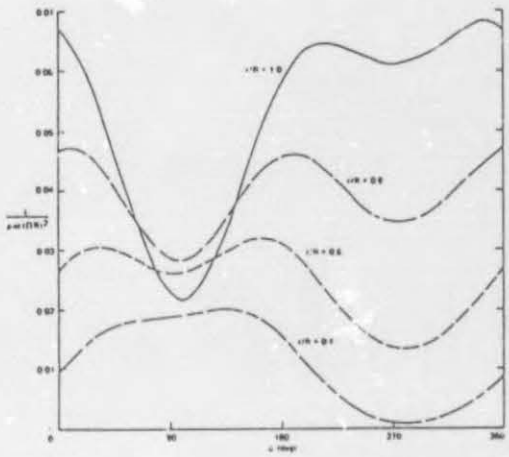

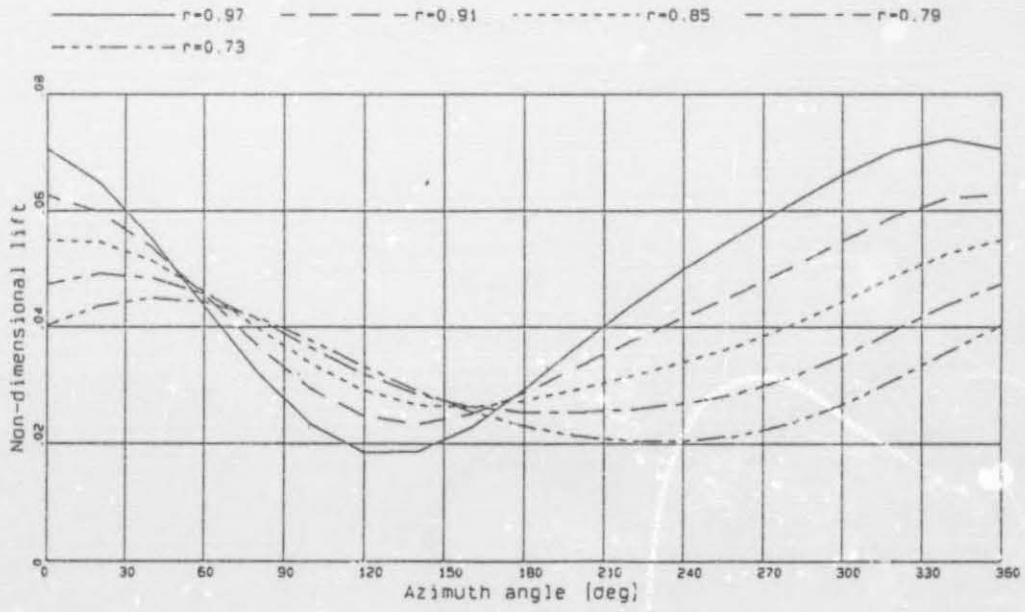

Fig 5.2.1.4(b) Calculated non-dimensional lift distribution $\ell(\psi)$, case 214

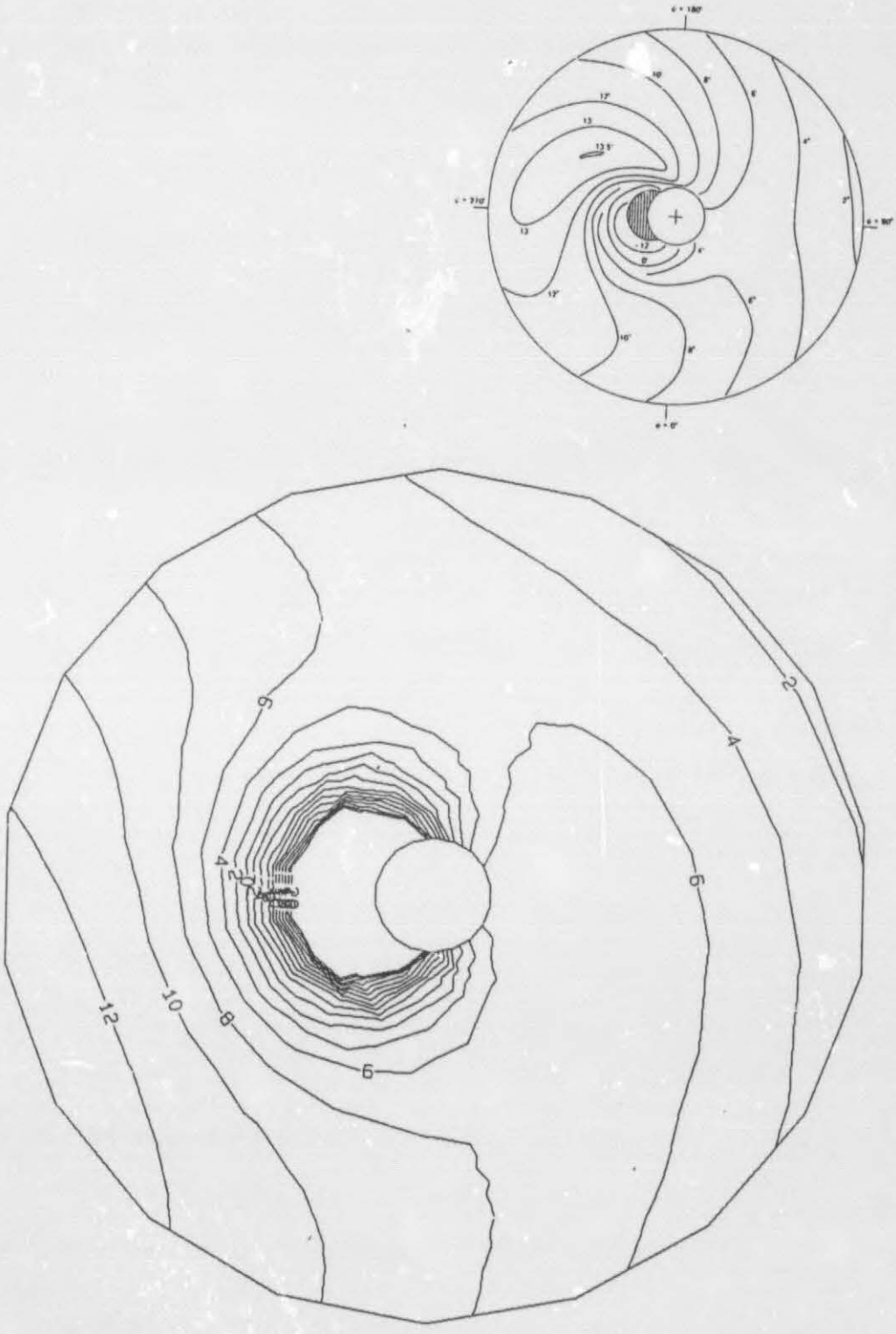

Fig 5.2.1.5(a) Calculated angle of attack distribution $\alpha(r,\psi)$, case 215

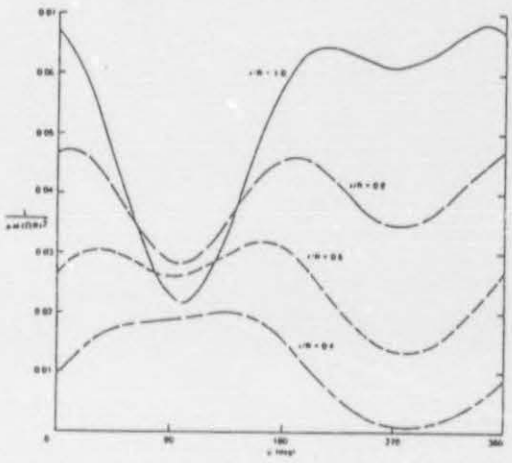

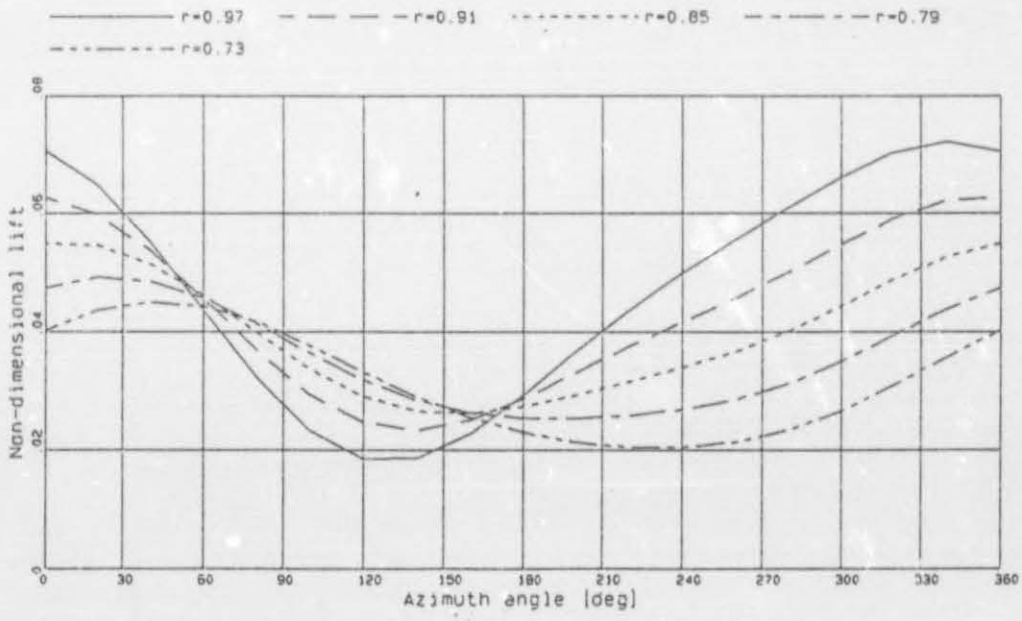

Fig 5.2.1.5(b) Calculated non-dimensional lift distribution $\ell(\psi)$, case 215

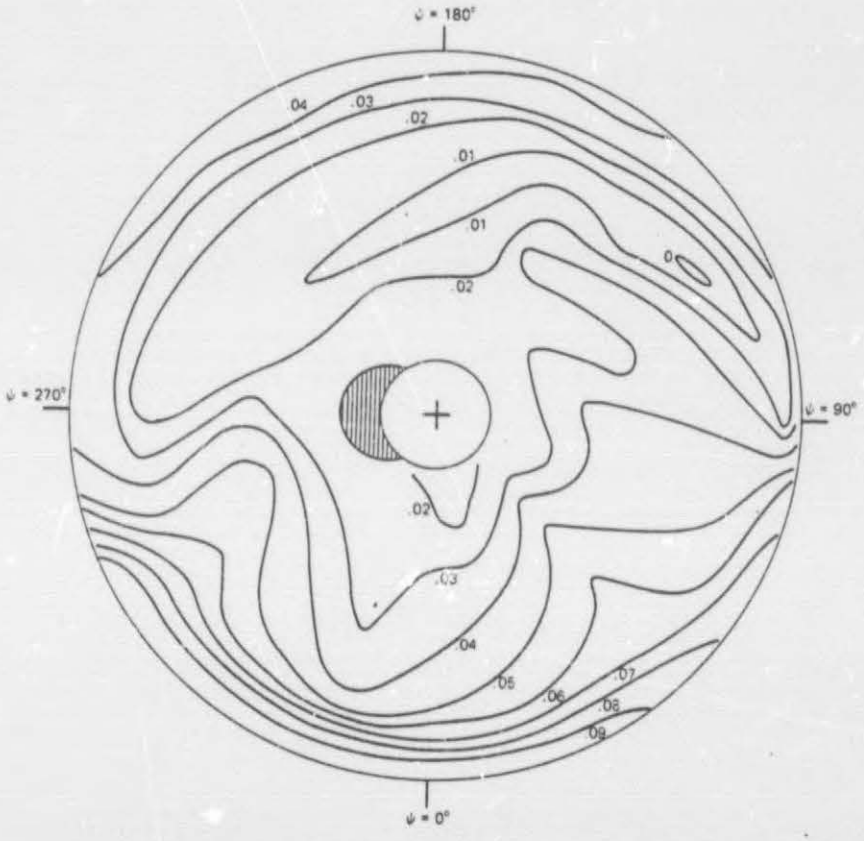

Distribution of the tip-path plane inflow ratio λ_{TPP} over the rotor disk at $\mu = 0.25$, for $C_T/\sigma = 0.12$, $\theta_{tw} = -8°$, and $f/A = 0.015$.

Fig 5.3.0.0 (a) Inflow ratio distribution $\lambda(r,\psi)$ from Johnson [1980a]

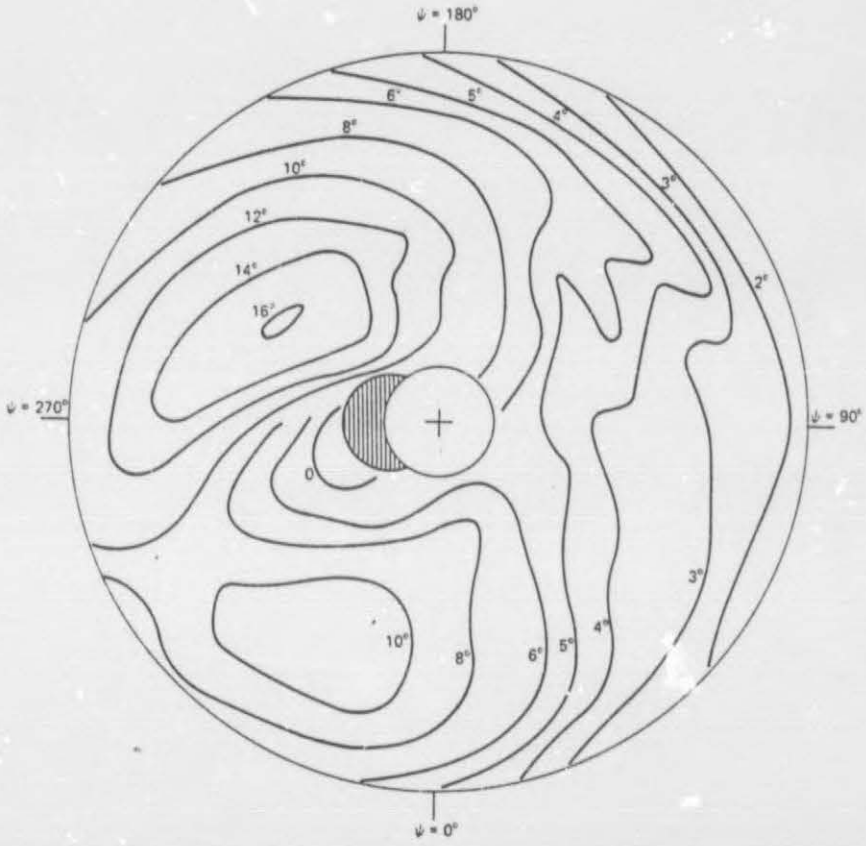

Blade angle-of-attack distribution (in degrees) at $\mu = 0.25$, for $C_T/\sigma = 0.12$, $f/A = 0.015$, and $\theta_{tw} = -8°$ (nonuniform inflow).

Fig 5.3.0.0 (b) Angle of attack distribution $\alpha(r,\psi)$ from Johnson [1980a]

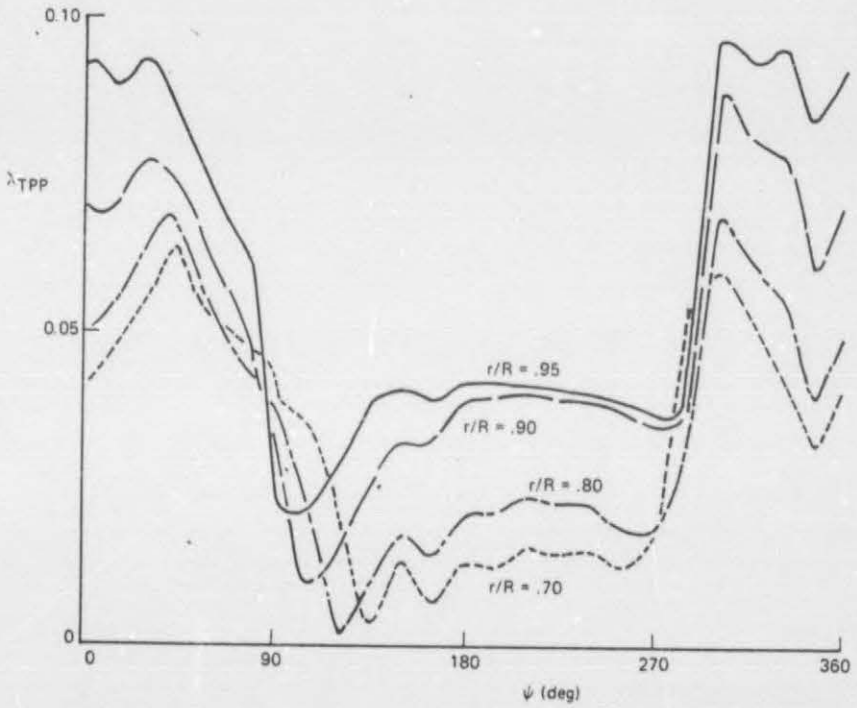

Tip-path plane inflow ratio at several radial stations for $\mu = 0.25$, $C_T/\sigma = 0.12$, $\theta_{tw} = -8°$, and $f/A = 0.015$.

Fig 5.3.0.0 (c) Inflow ratio distribution $\lambda(\psi)$ from Johnson [1980a]

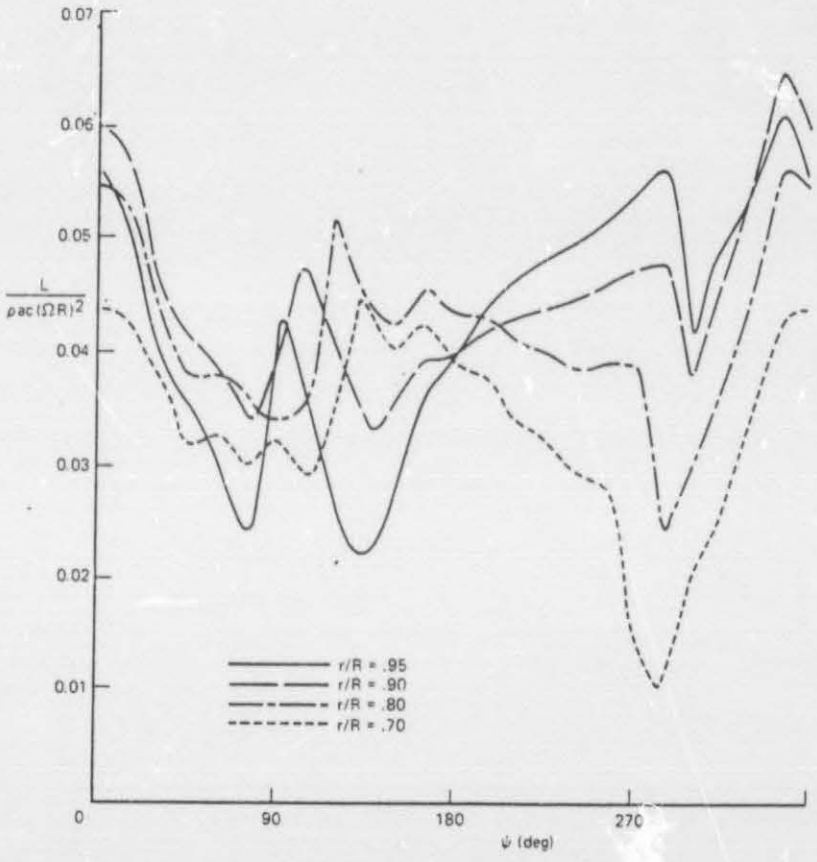

Azimuthal variation of the blade lift $L/\rho ac(\Omega R)^2$ at $\mu = 0.25$, for $C_T/\sigma = 0.12$, $f/A = 0.015$, and $\theta_{tw} = -8°$ (nonuniform inflow).

Fig 5.3.0.0 (d) Non-dimensional lift distribution $\ell(\psi)$ from Johnson [1980a]

Fig 5.3.1.1 (a) Calculated inflow ratio distribution $\lambda(r,\psi)$, case 311

Fig 5.3.1.1 (b) Calculated angle of attack distribution $\alpha(r,\psi)$, case 311

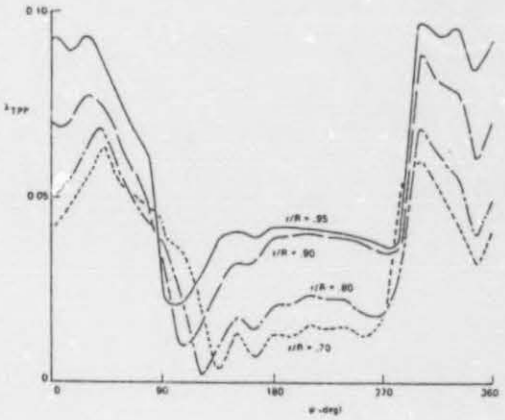

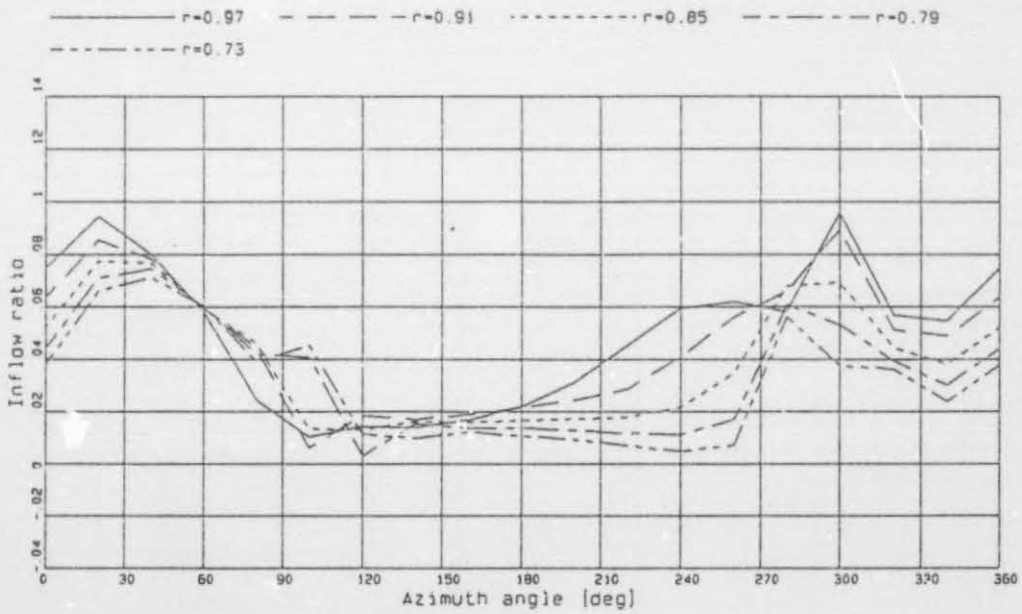

Fig 5.3.1.1 (c) Calculated inflow ratio distribution $\lambda(\psi)$, case 311

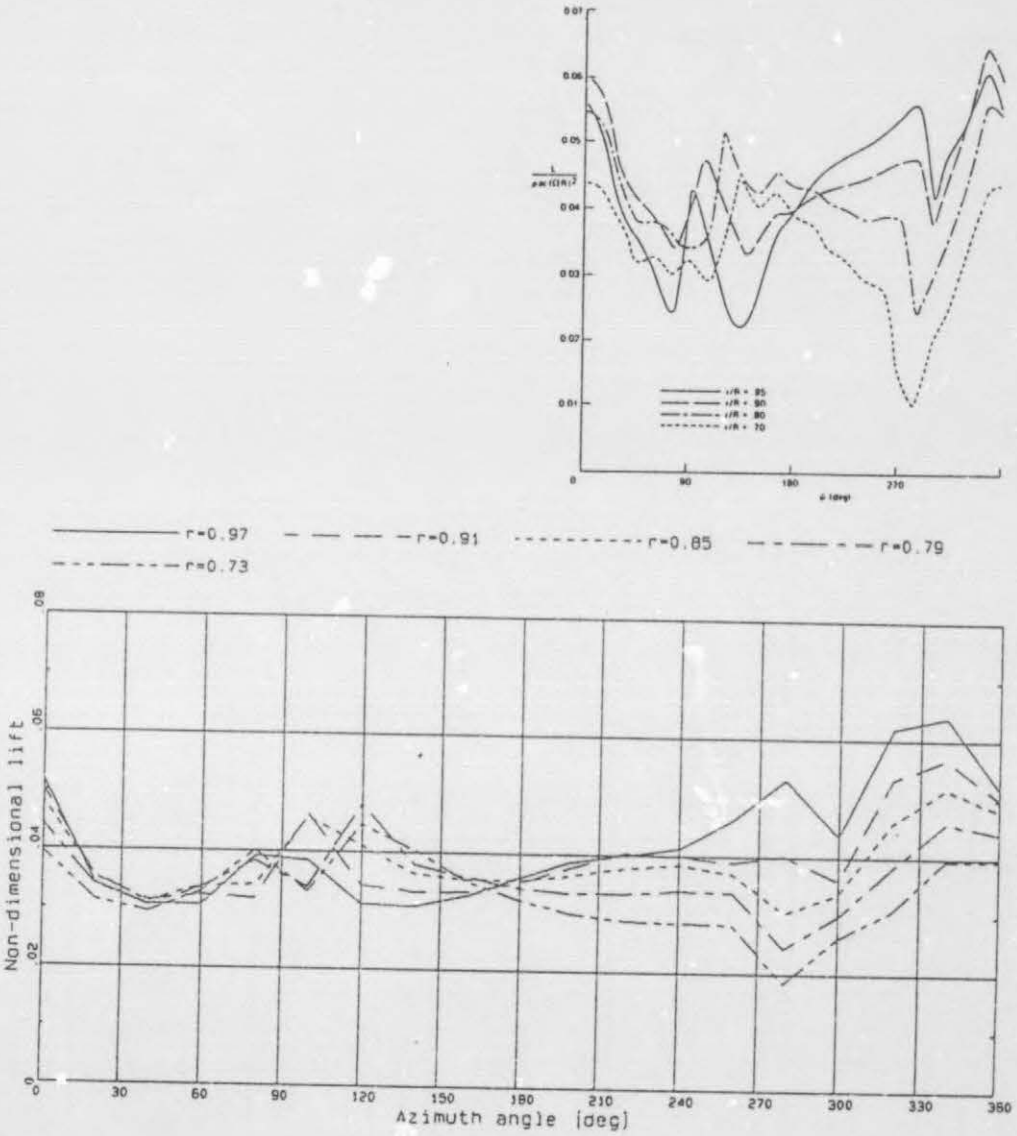

Fig 5.3.1.1 (d) Calculated non-dimensional lift distribution $\ell(\psi)$, case 311

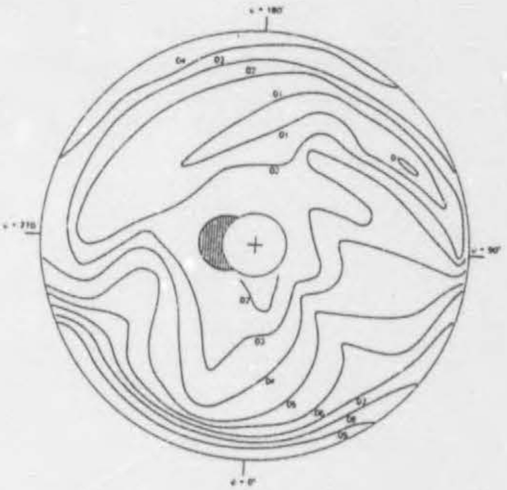

Fig 5.3.1.2 (a) Calculated inflow ratio distribution $\lambda(r,\psi)$, case 312

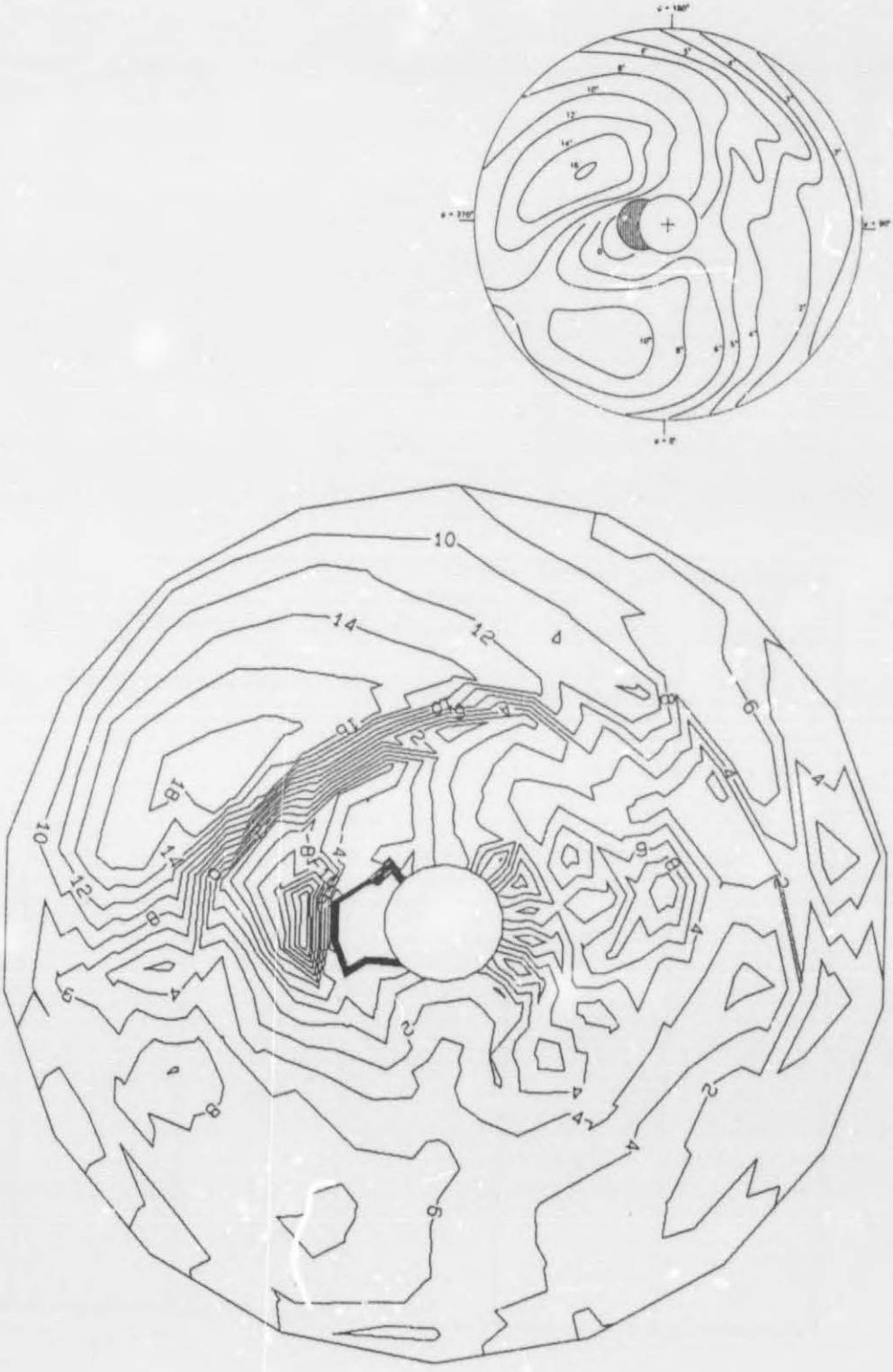

Fig 5.3.1.2 (b) Calculated angle of attack distribution $\alpha(r,\psi)$, case 312

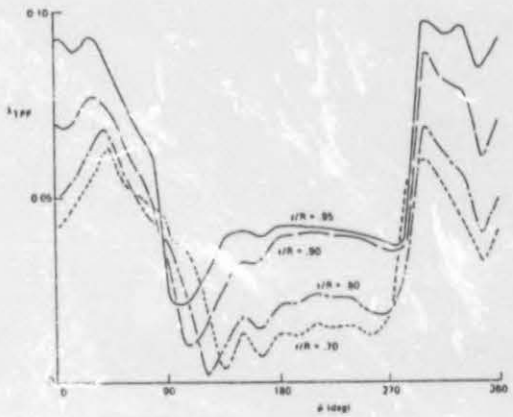

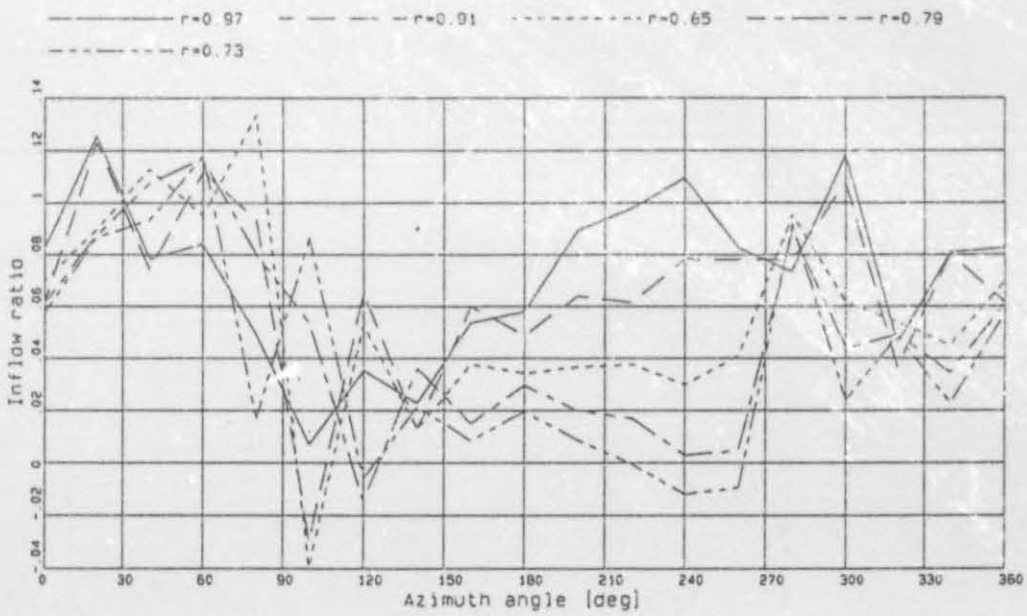

Fig 5.3.1.2 (c) Calculated inflow ratio distribution $\lambda(\psi)$, case 312

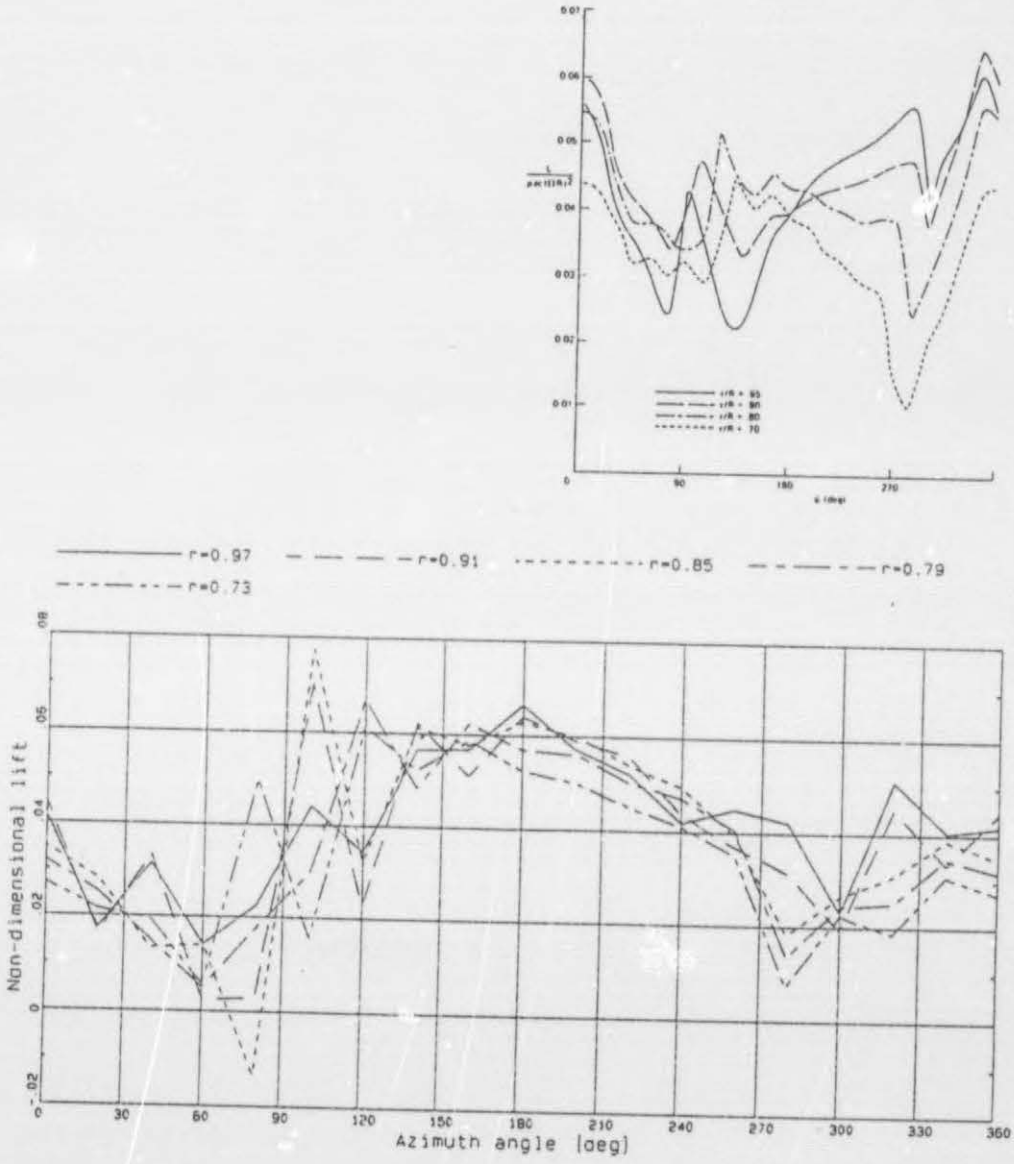

Fig 5.3.1.2 (d) Calculated non-dimensional lift distribution $\ell(\psi)$, case 312

Fig 5.3.1.3 (a) Calculated inflow ratio distribution $\lambda(r,\psi)$, case 313

Fig 5.3.1.3 (b) Calculated angle of attack distribution $\alpha(r,\psi)$, case 313

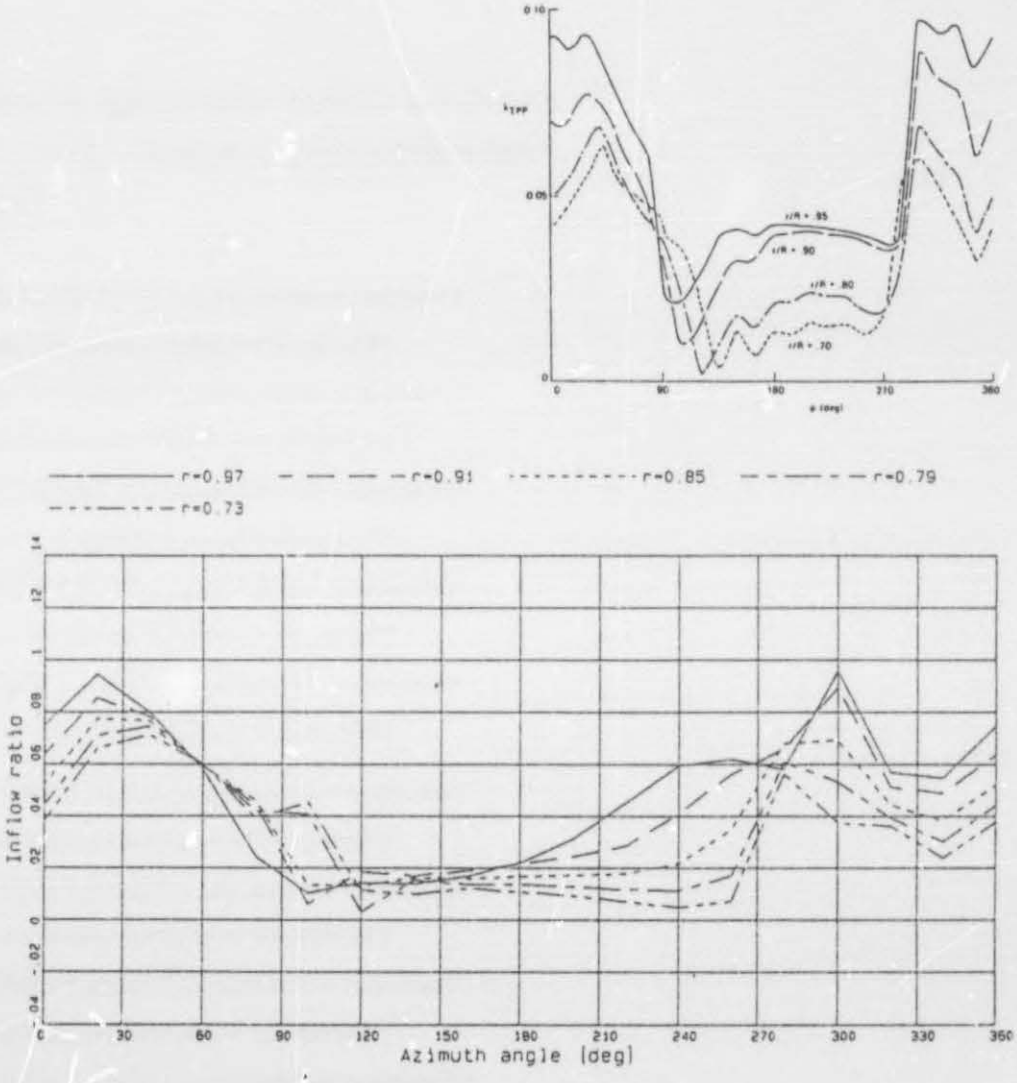

Fig 5.3.1.3 (c) Calculated inflow ratio distribution $\lambda(\psi)$, case 313

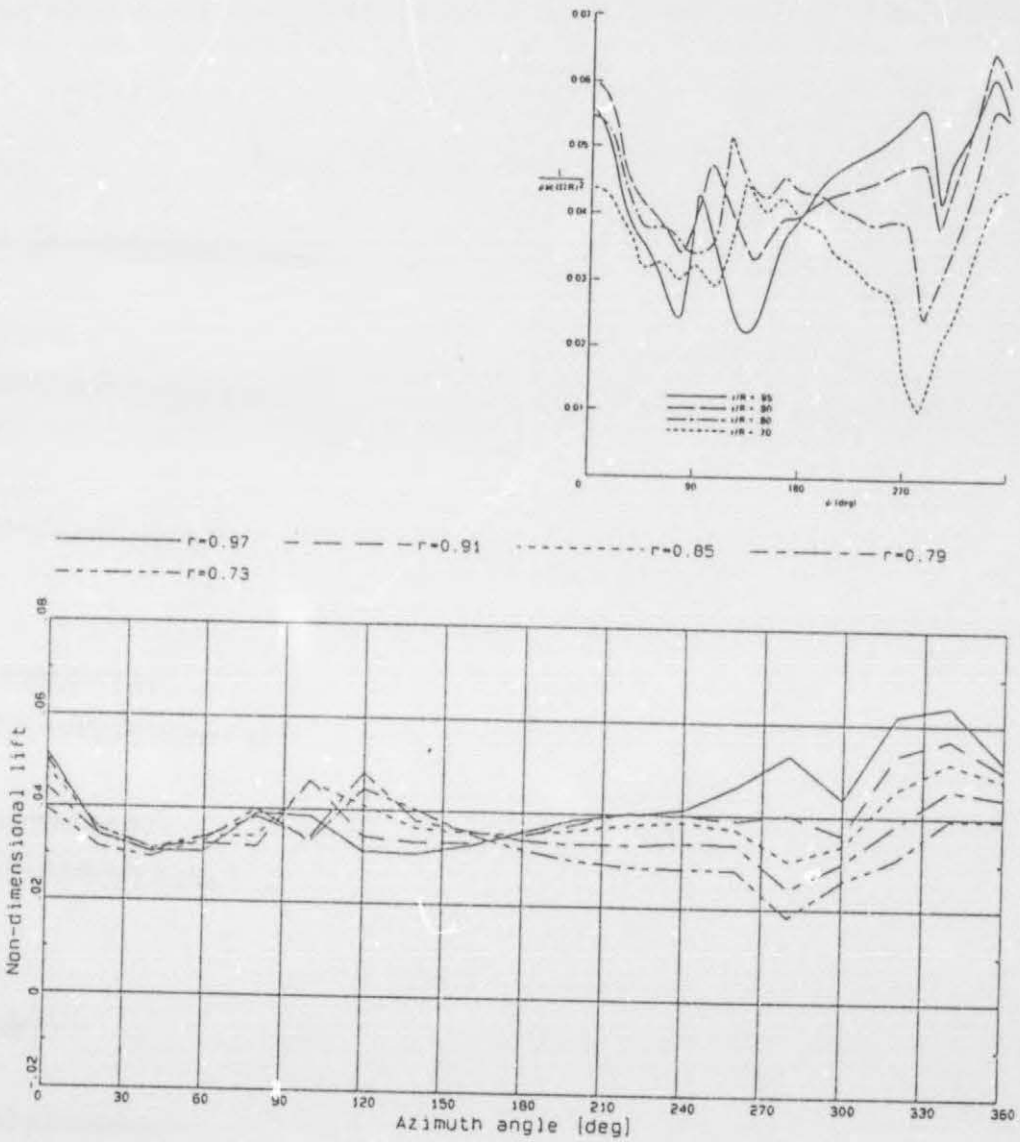

Fig 5.3.1.3 (d) Calculated non-dimensional lift distribution $\ell(\psi)$, case 313

Fig 5.3.1.4 (a) Calculated inflow ratio distribution $\lambda(r,\psi)$, case 314

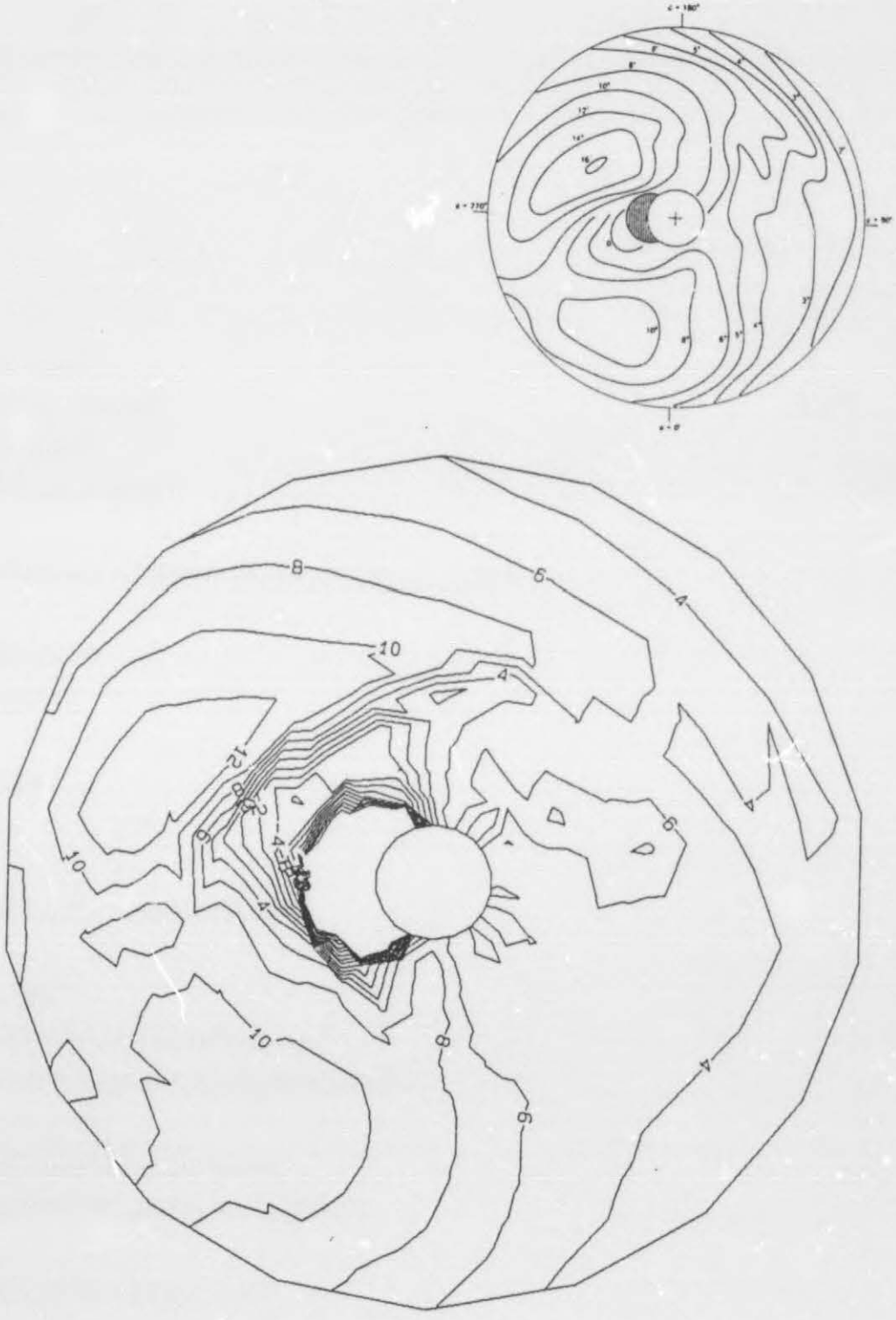

Fig 5.3.1.4 (b) Calculated angle of attack distribution $\alpha(r,\psi)$, case 314

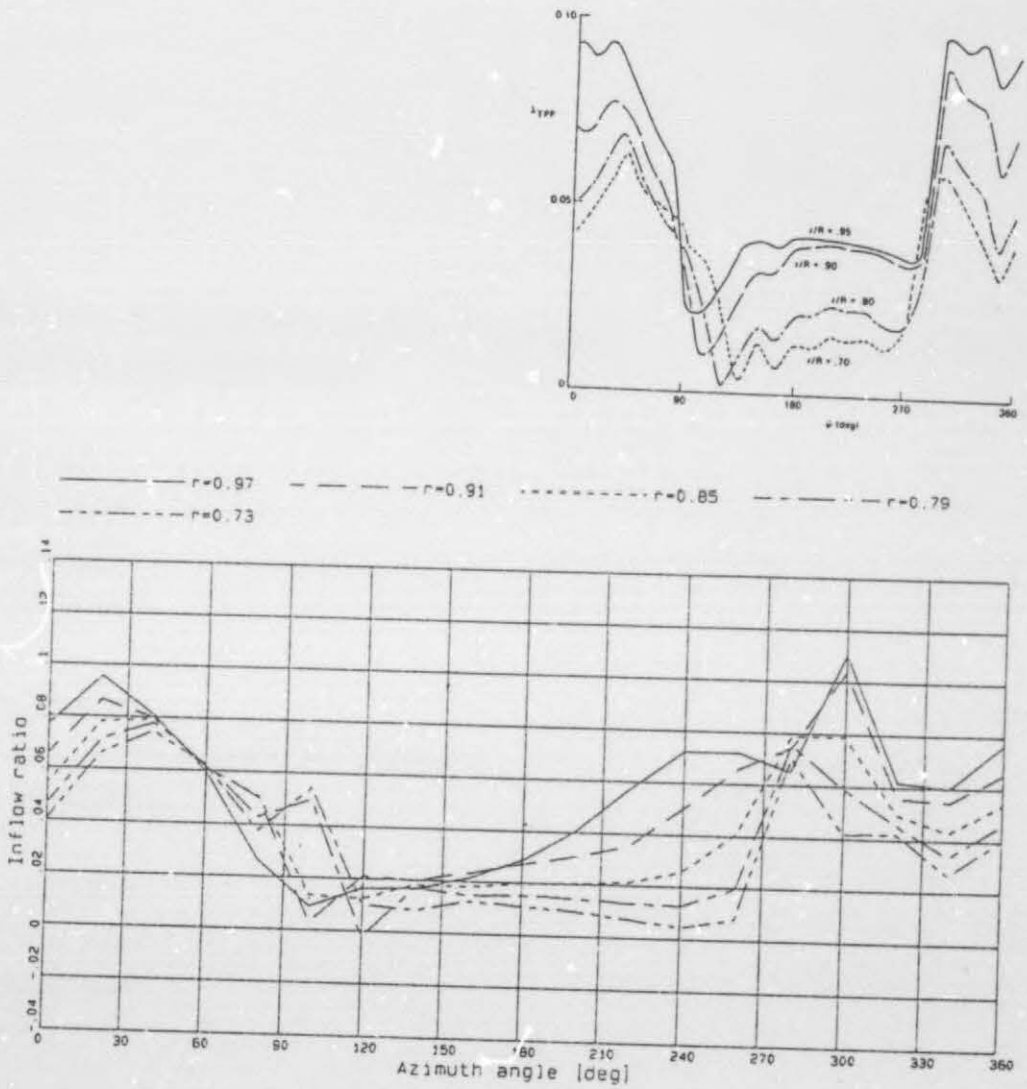

Fig 5.3.1.4 (c) Calculated inflow ratio distribution $\lambda(\psi)$, case 314

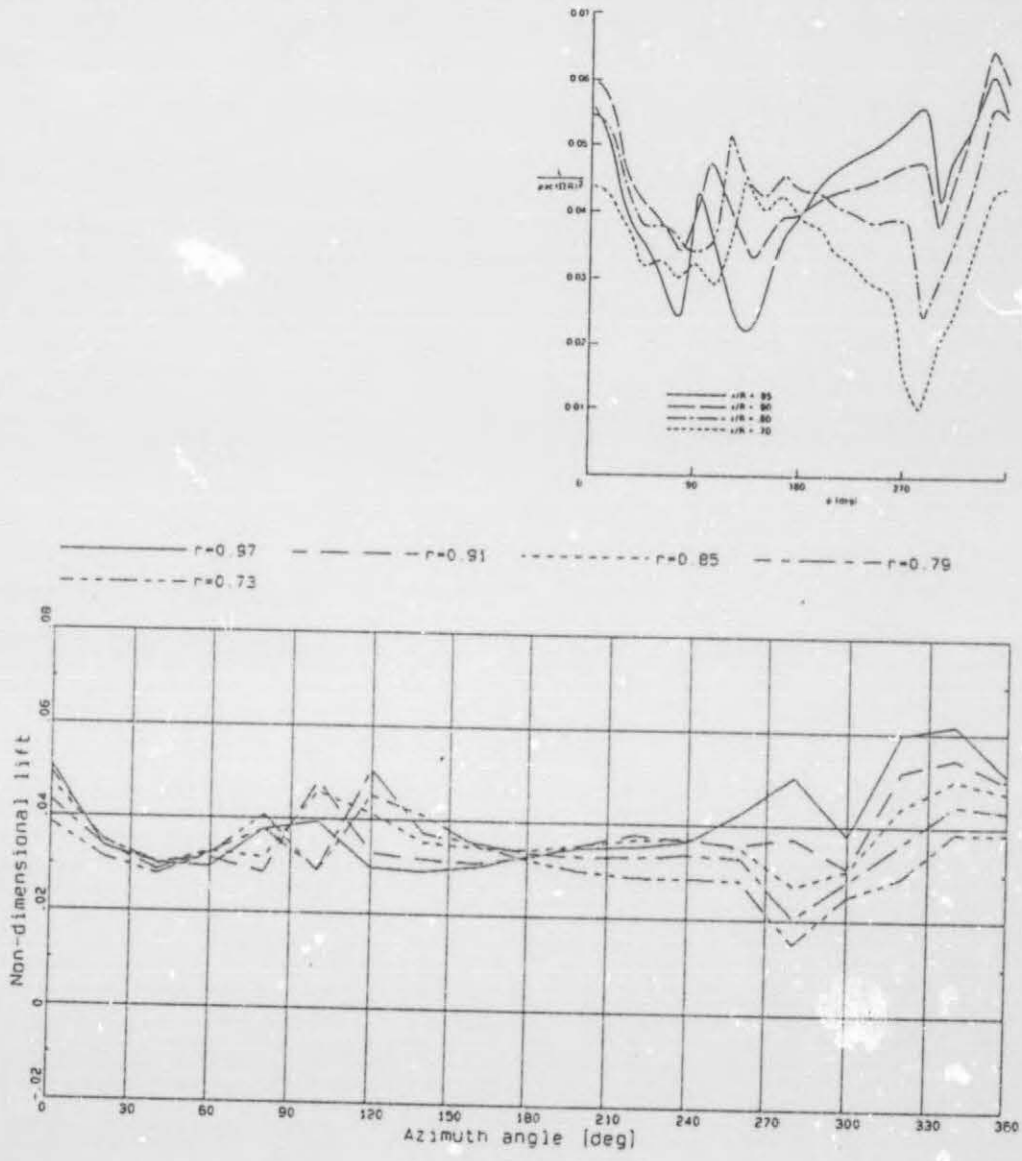

Fig 5.3.1.4 (d) Calculated non-dimensional lift distribution $\ell(\psi)$, case 314

Fig 5.3.1.5 (a) Calculated inflow ratio distribution $\lambda(r,\psi)$, case 315

Fig 5.3.1.5 (b) Calculated angle of attack distribution $\alpha(r,\psi)$, case 315

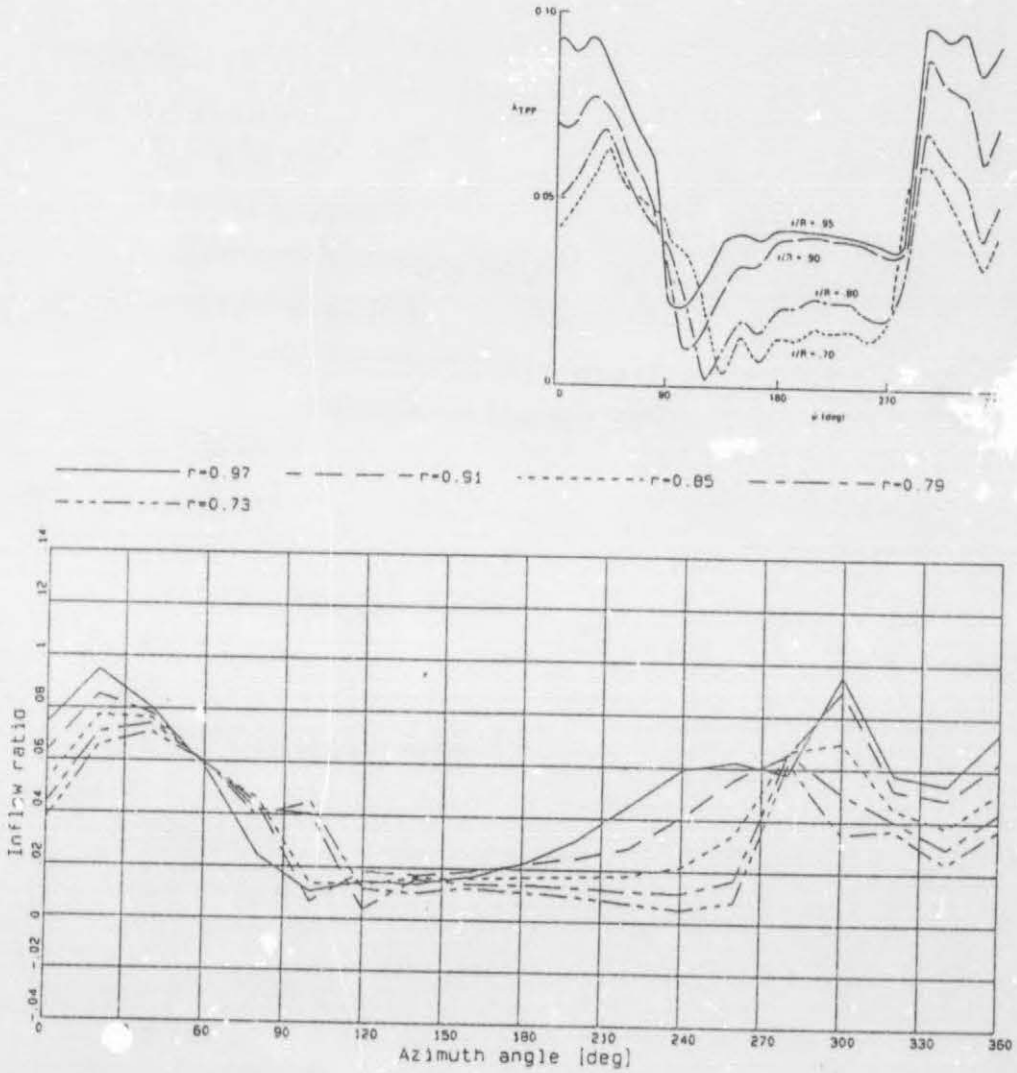

Fig 5.3.1.5 (c) Calculated inflow ratio distribution $\lambda(\psi)$, case 315

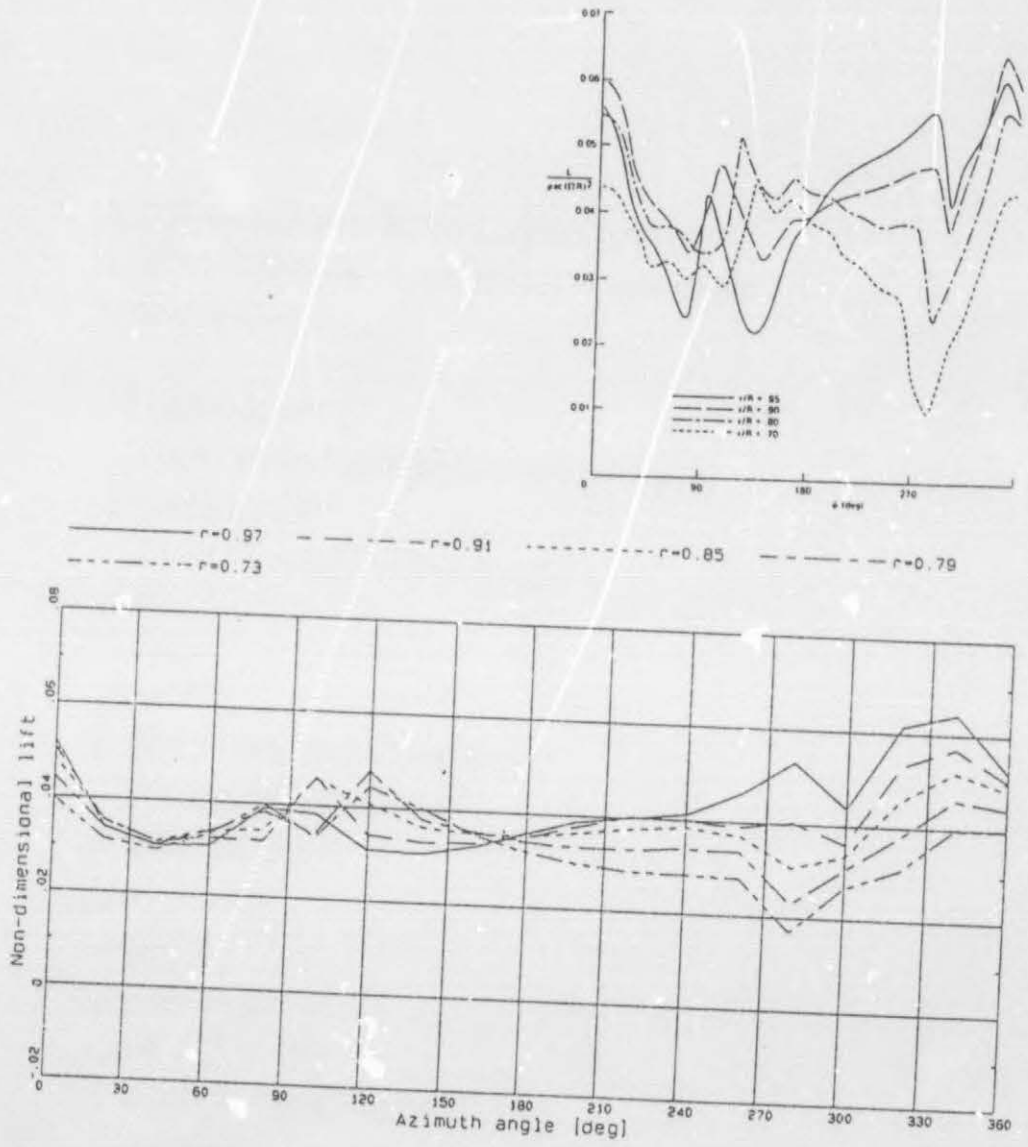

Fig 5.3.1.5 (d) Calculated non-dimensional lift distribution $\ell(\psi)$, case 315

Fig 5.3.2.1 (a) Calculated inflow ratio distribution $\lambda(r,\psi)$, case 321

Fig 5.3.2.1 (b) Calculated angle of attack distribution $\alpha(r,\psi)$, case 321

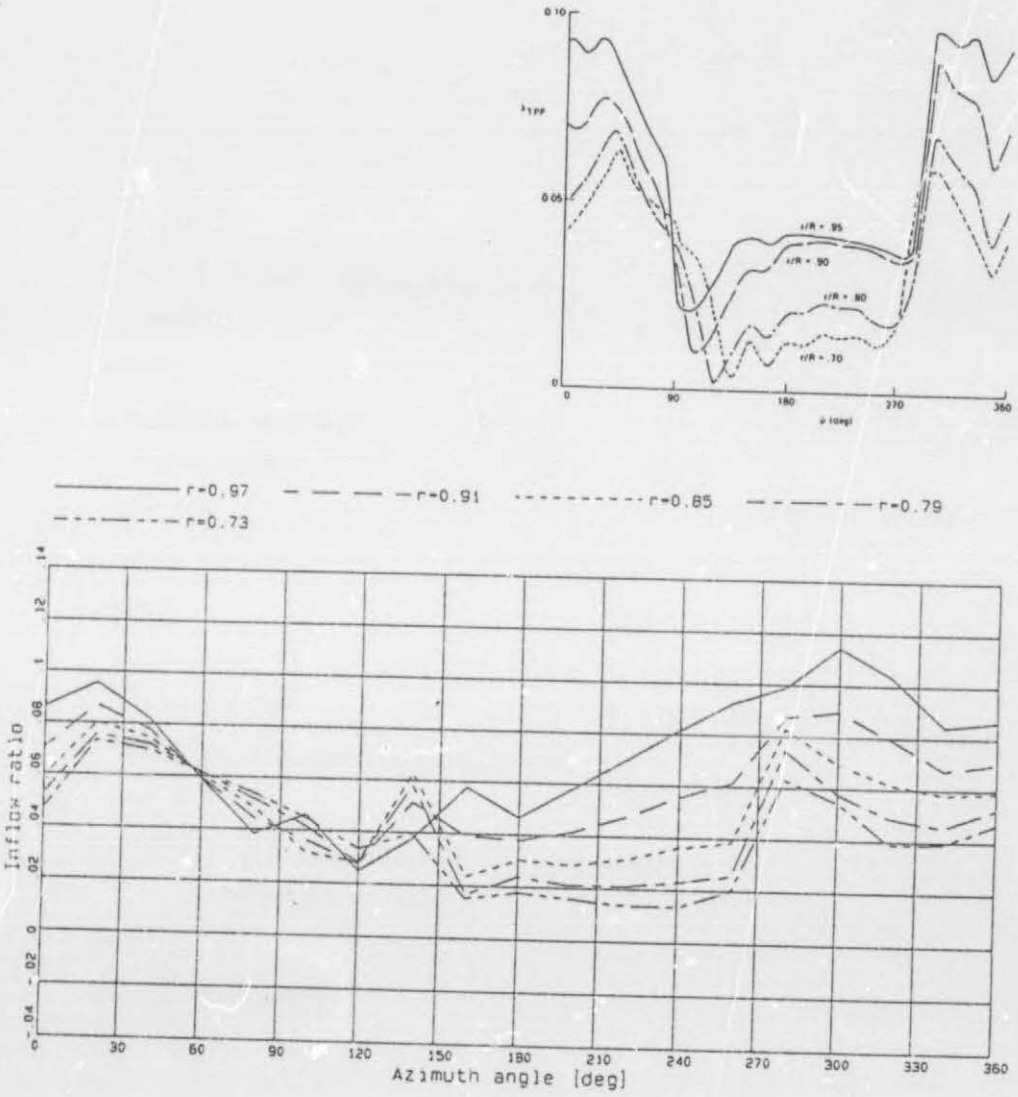

Fig 5.3.2.1 (c) Calculated inflow ratio distribution $\lambda(\psi)$, case 321

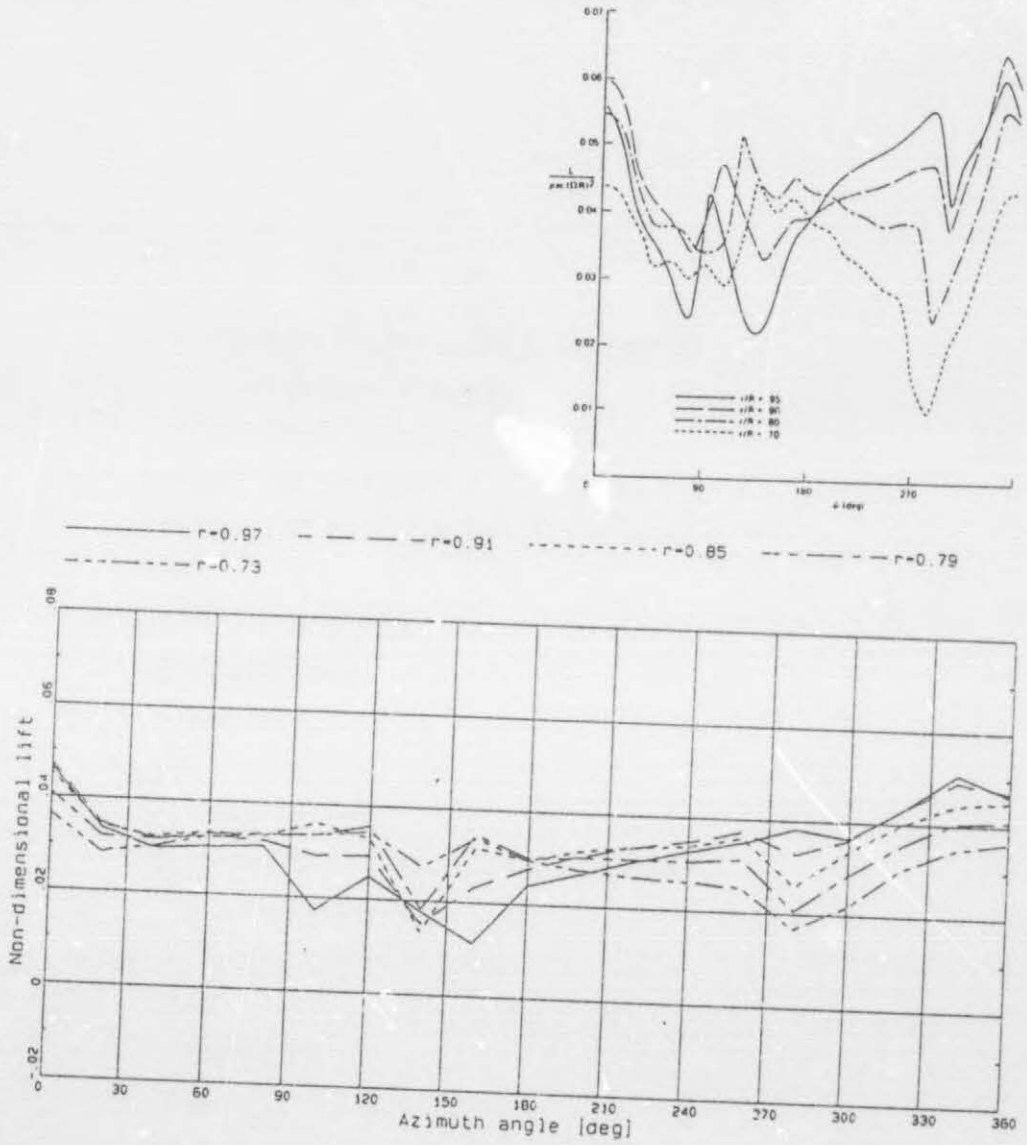

Fig 5.3.2.1 (d) Calculated non-dimensional lift distribution $\ell(\psi)$, case 321

Fig 5.3.2.2 (a) Calculated inflow ratio distribution $\lambda(r,\psi)$, case 322

Fig 5.3.2.2 (b) Calculated angle of attack distribution $\alpha(r,\psi)$, case 322

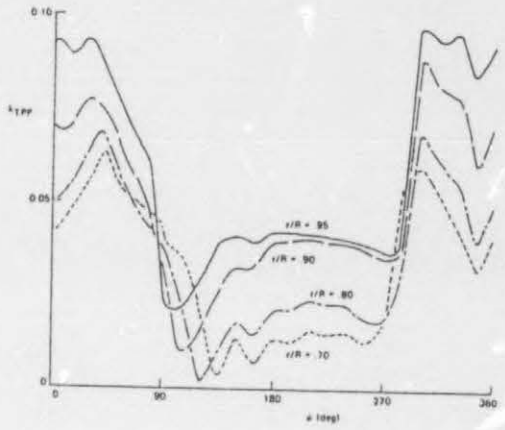

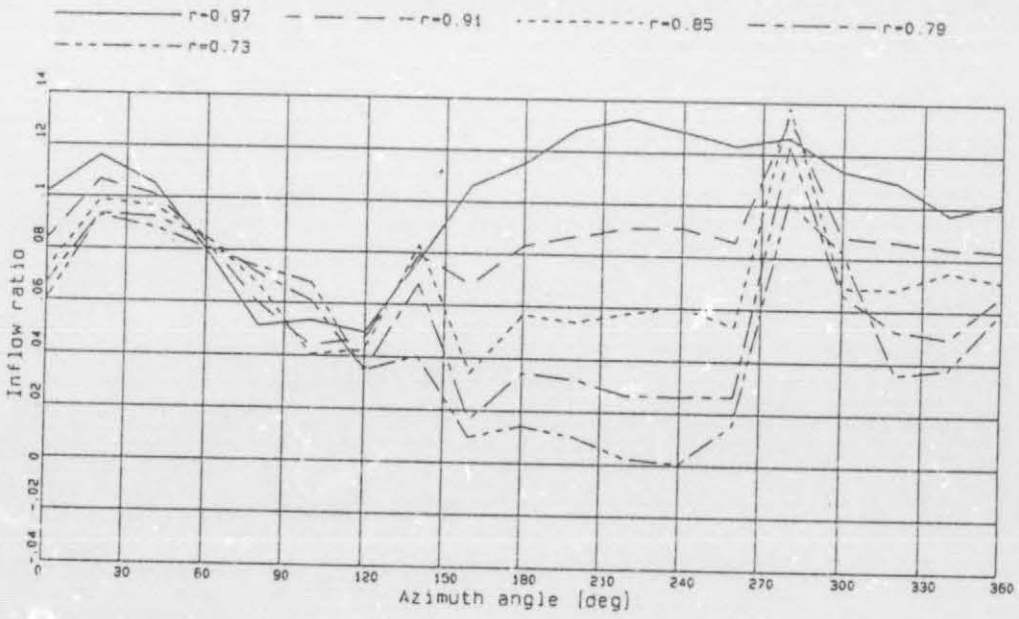

Fig 5.3.2.2 (c) Calculated inflow ratio distribution $\lambda(\psi)$, case 322

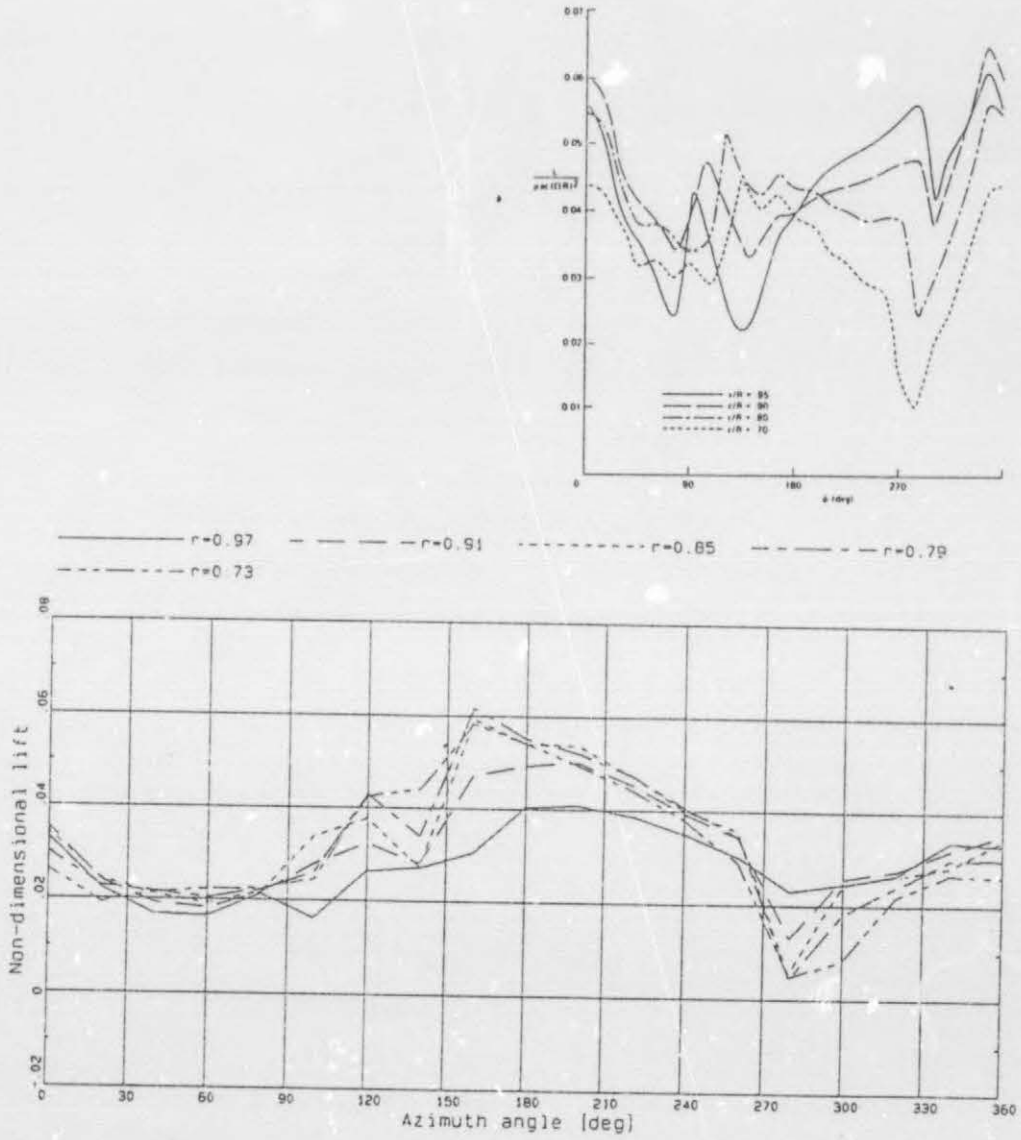

g 5.3.2.2 (d) Calculated non-dimensional lift distribution $\ell(\psi)$, case 322

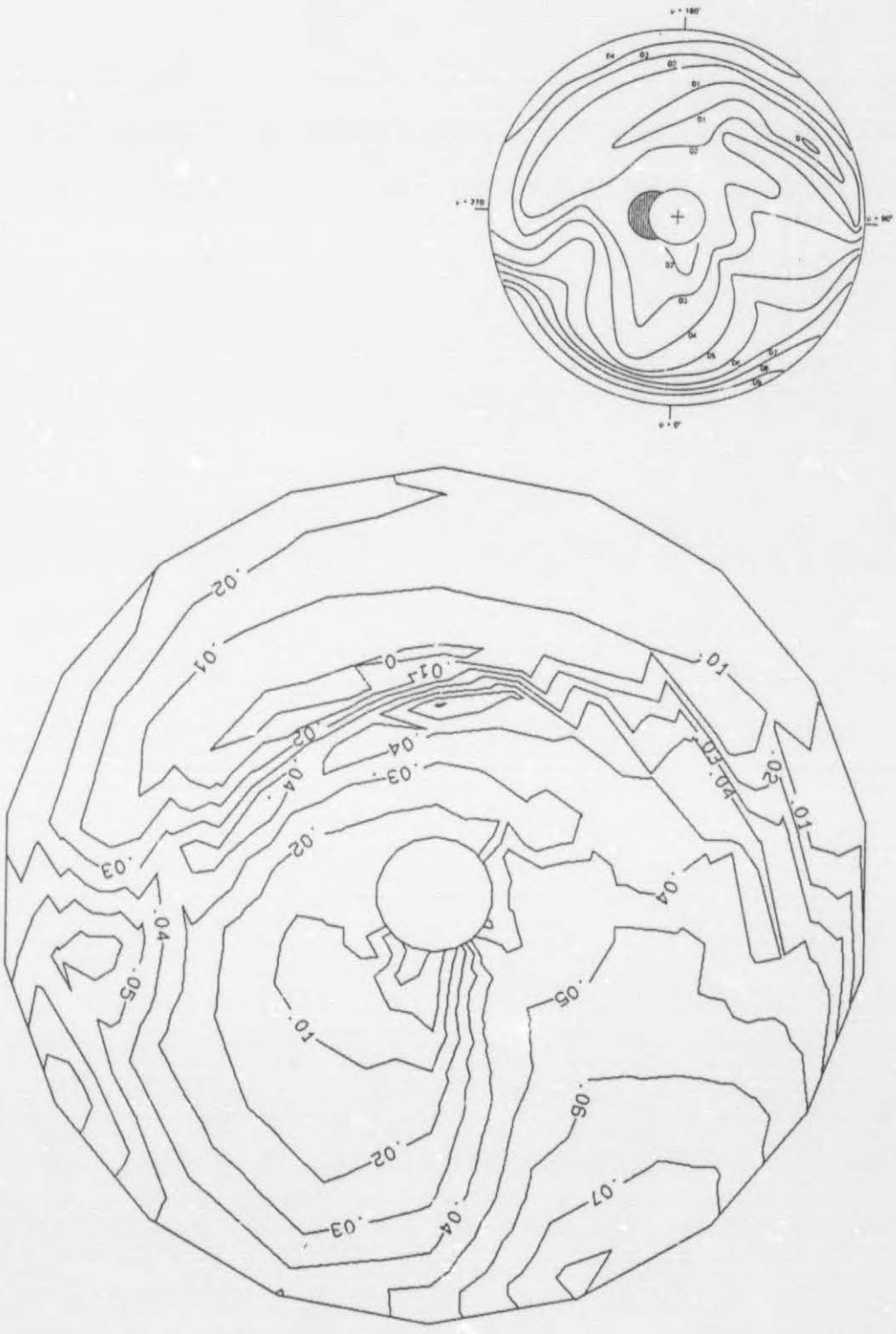

Fig 5.3.2.3 (a) Calculated inflow ratio distribution $\lambda(r,\psi)$, case 323

Fig 5.3.2.3 (b) Calculated angle of attack distribution $\alpha(r,\psi)$, case 323

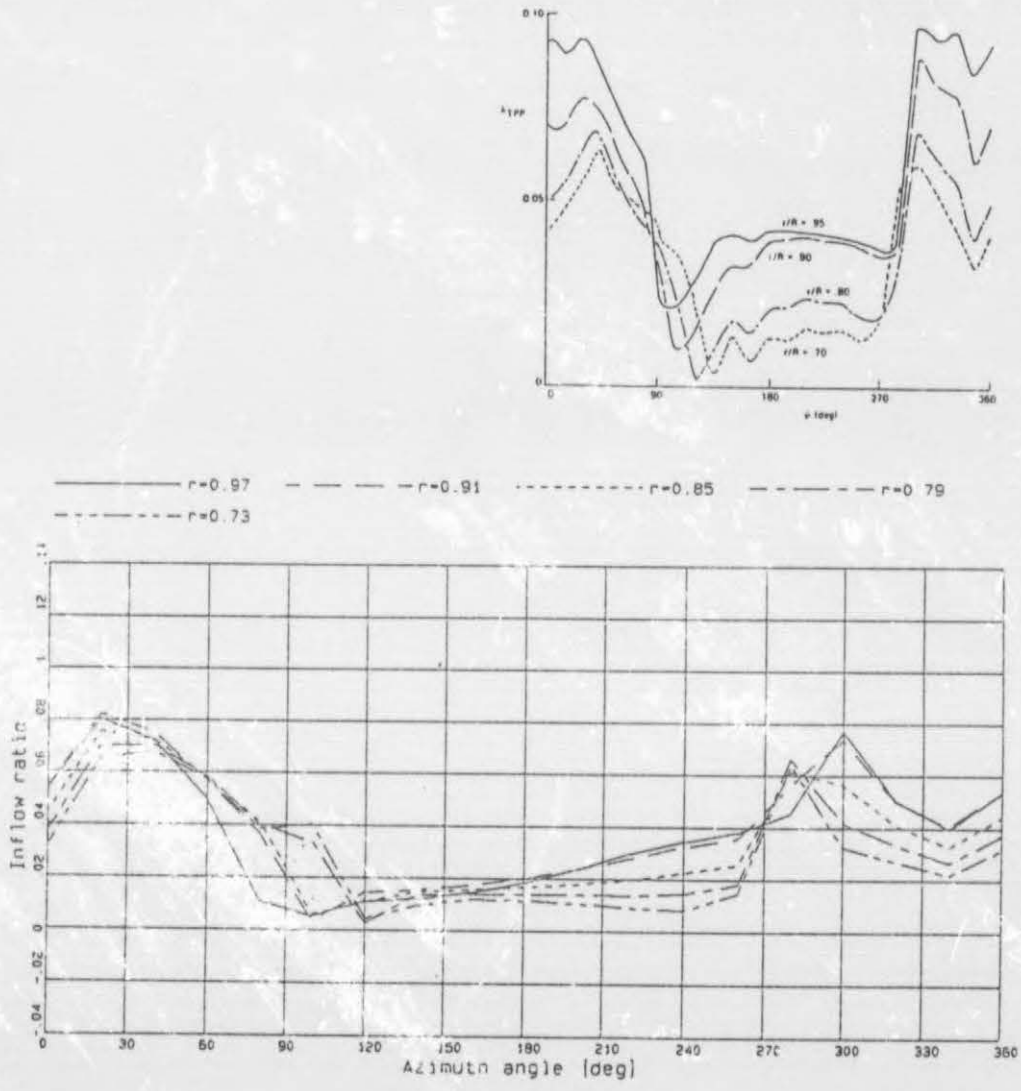

Fig 5.3.2.3 (c) Calculated inflow ratio distribution $\lambda(\psi)$. case 323

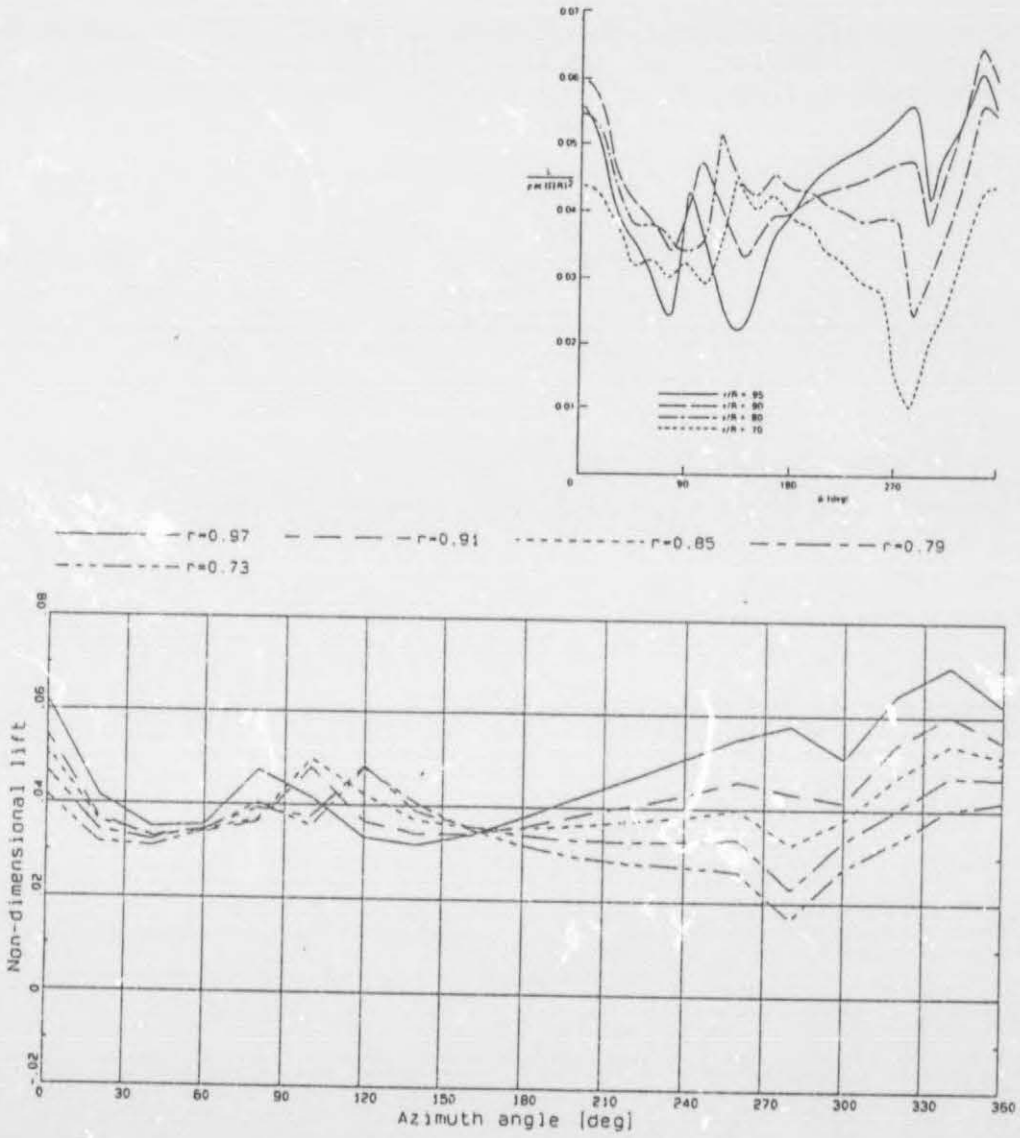

Fig 5.3.2.3 (d) Calculated non-dimensional lift distribution $\ell(\psi)$, case 323

Fig 5.3.2.4 (a) Calculated inflow ratio distribution $\lambda(r,\psi)$, case 324

Fig 5.3.2.4 (b) Calculated angle of attack distribution $\alpha(r,\psi)$, case 324

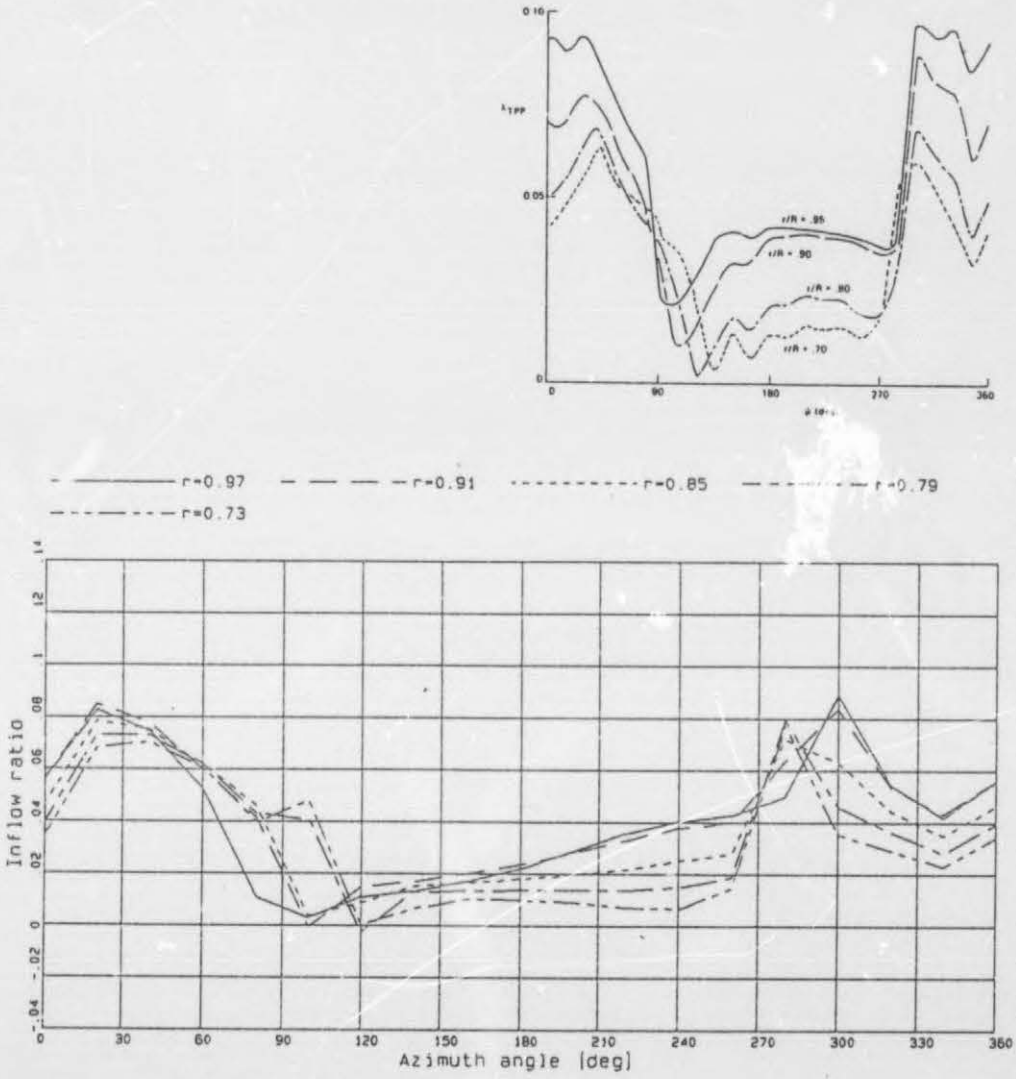

Fig 5.3.2.4 (c) Calculated inflow ratio distribution $\lambda(\psi)$, case 324

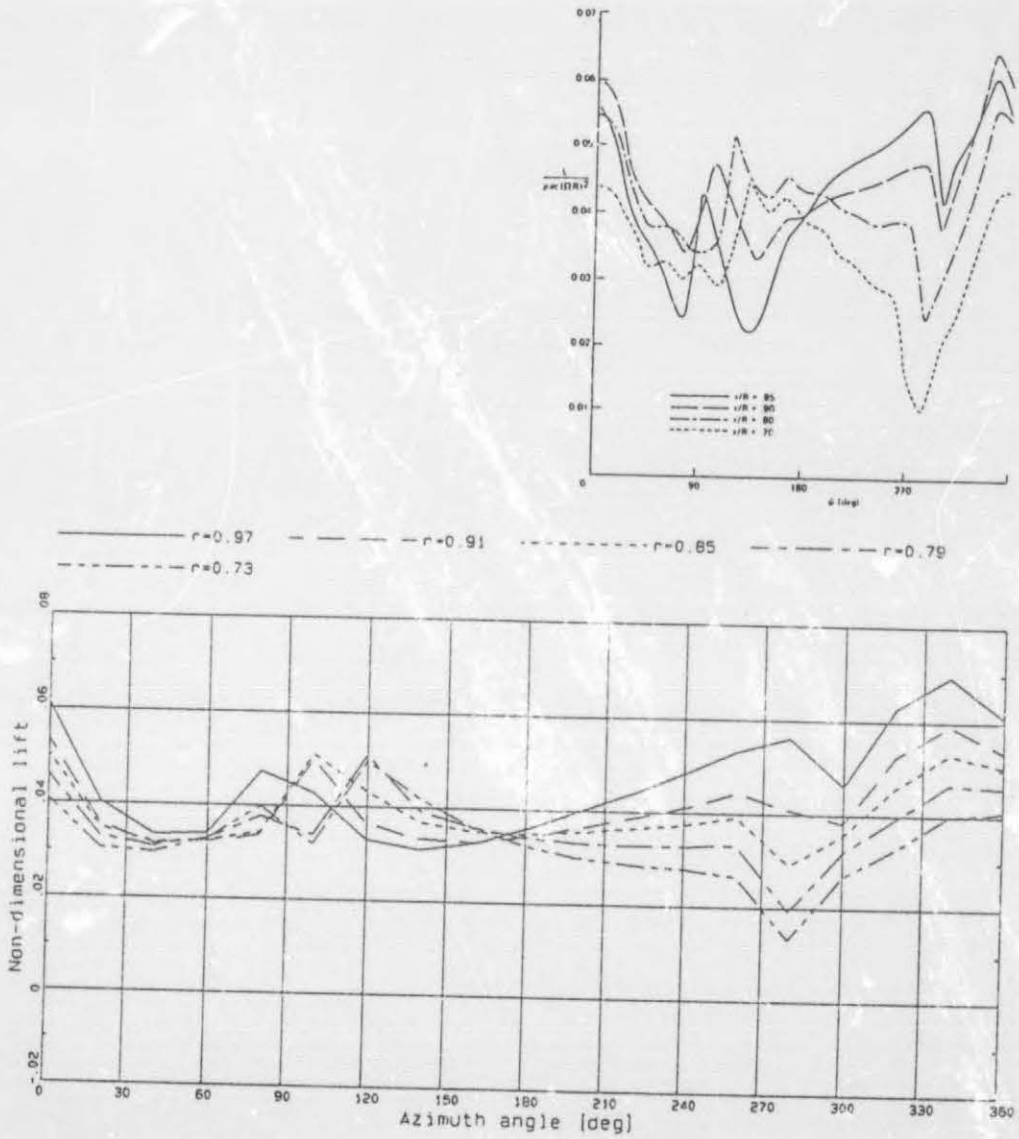

Fig 5.3.2.4 (d) Calculated non-dimensional lift distribution $\ell(\psi)$, case 324

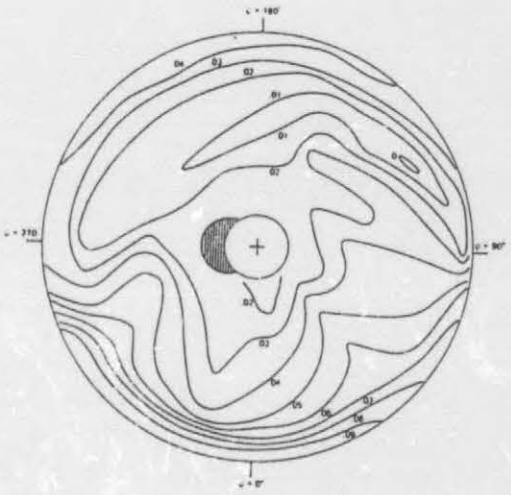

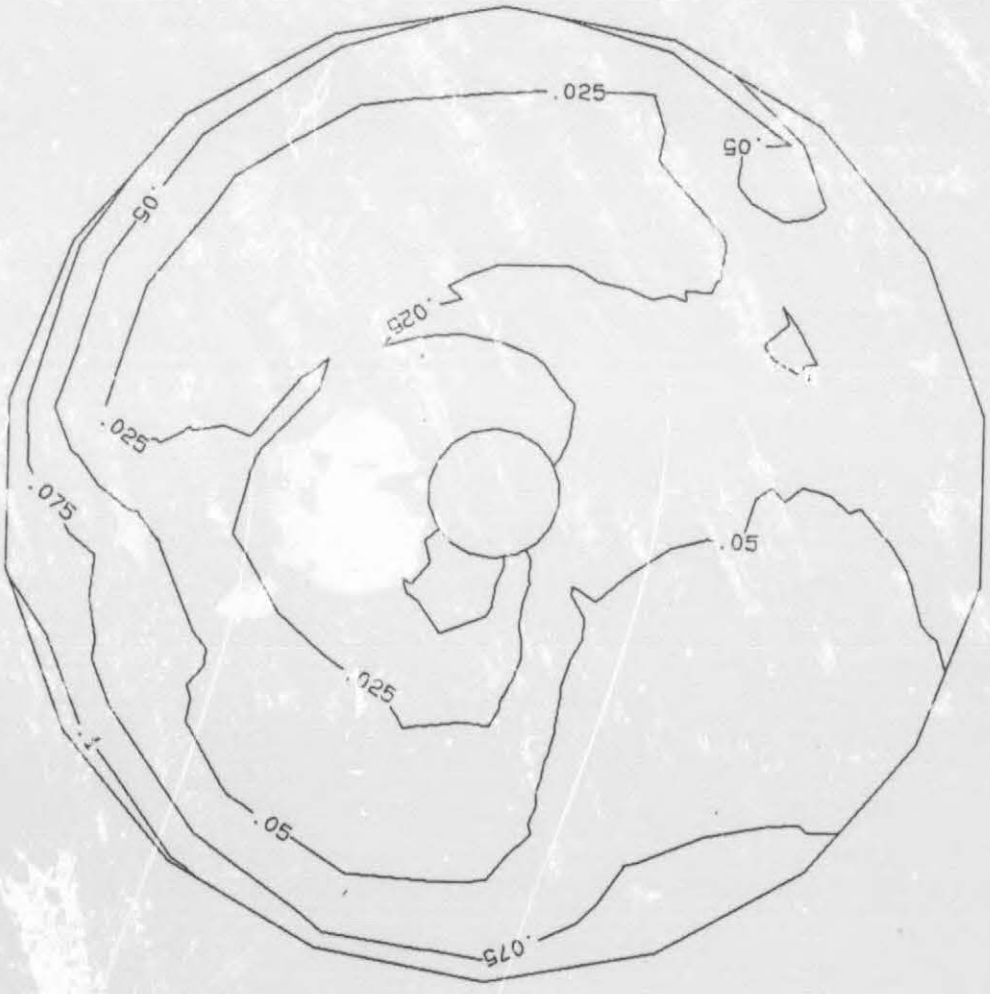

Fig 5.3.2.5 (a) Calculated inflow ratio distribution $\lambda(r,\psi)$, case 325

Fig 5.3.2.5 (b) Calculated angle of attack distribution $\alpha(r,\psi)$, case 325

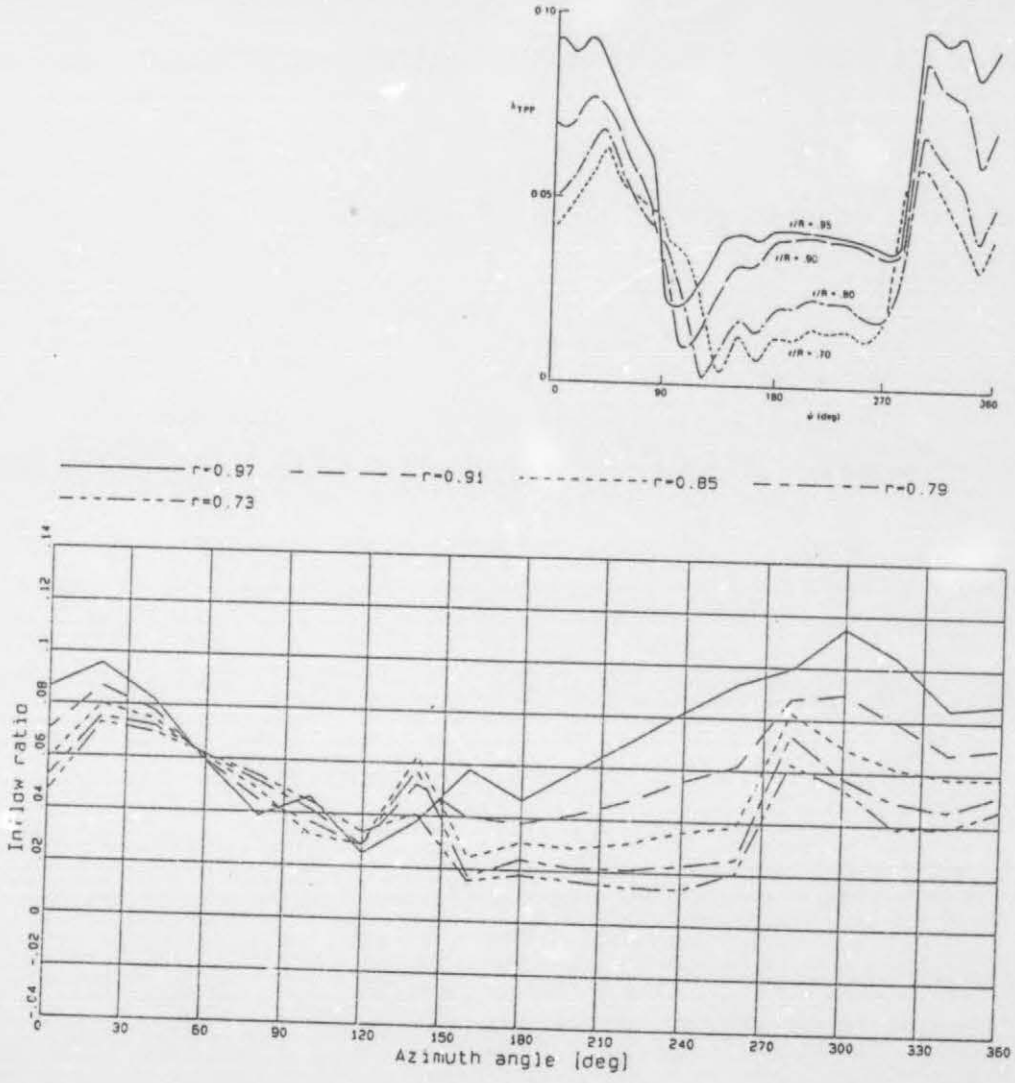

Fig 5.3.2.5 (c) Calculated inflow ratio distribution $\lambda(\psi)$, case 325

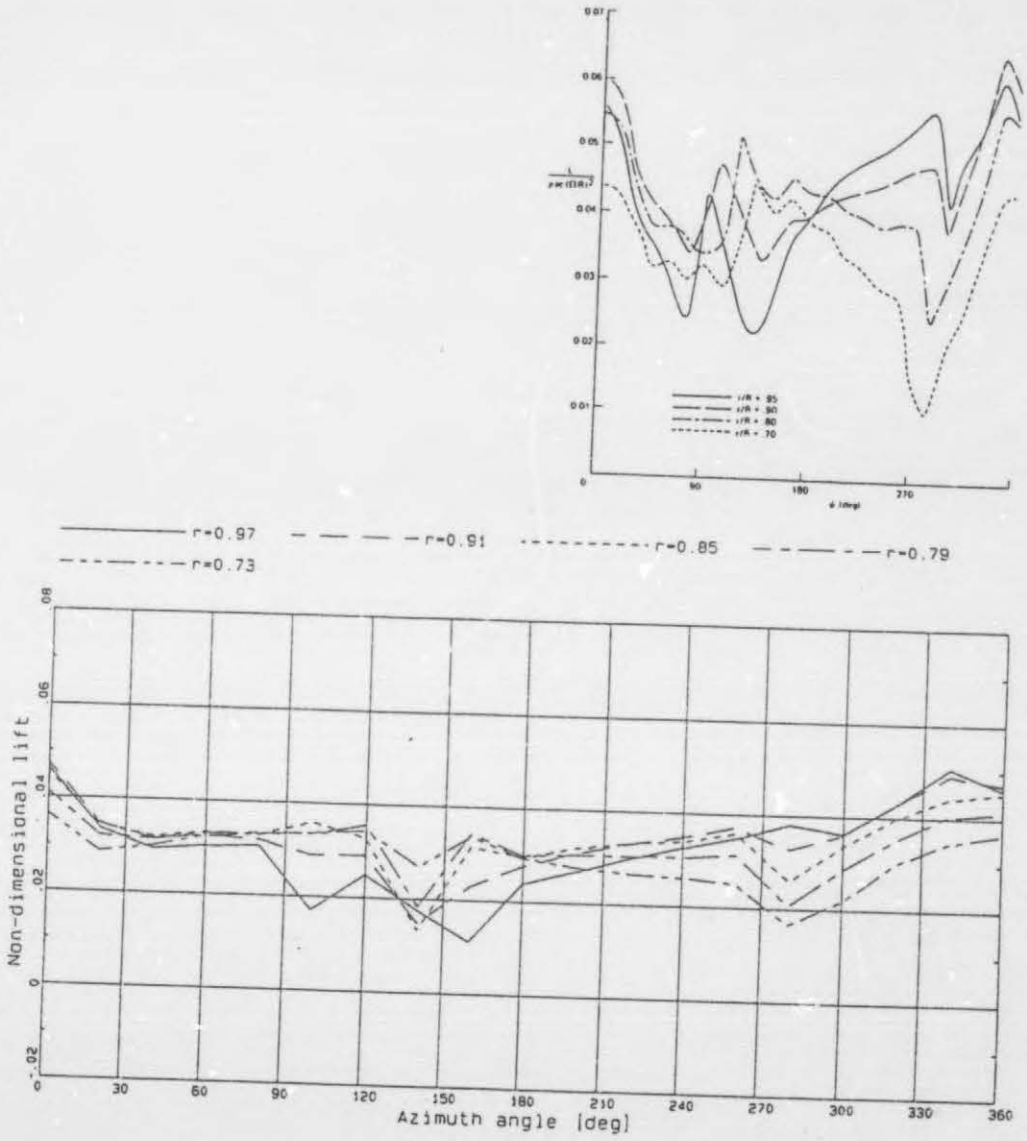

Fig 5.3.2.5 (d) Calculated non-dimensional lift distribution $\ell(\psi)$, case 325

Fig 5.3.3.1 (a) Calculated inflow ratio distribution $\lambda(r,\psi)$, case 331

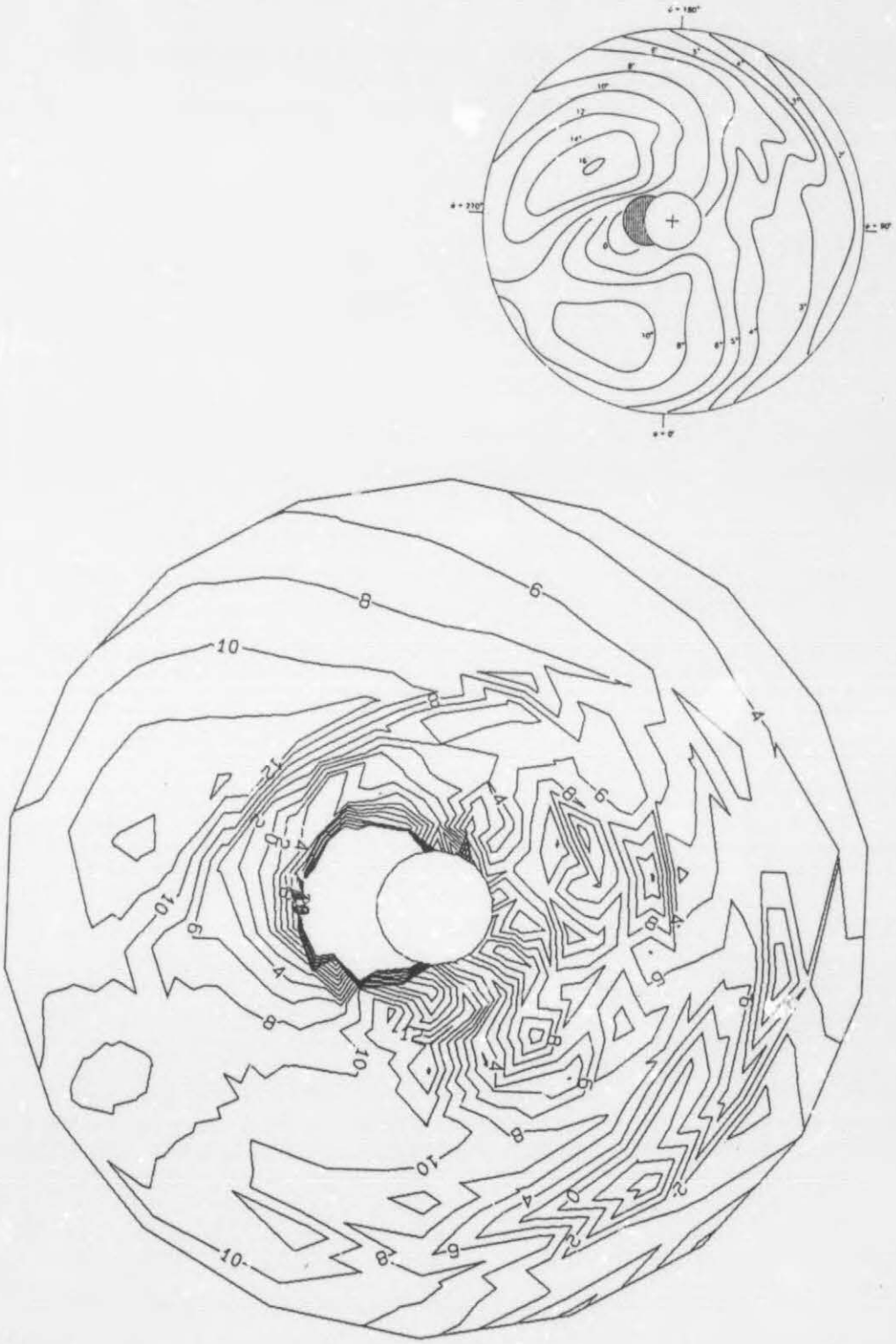

Fig 5.3.3.1 (b) Calculated angle of attack distribution $\alpha(r,\psi)$, case 331

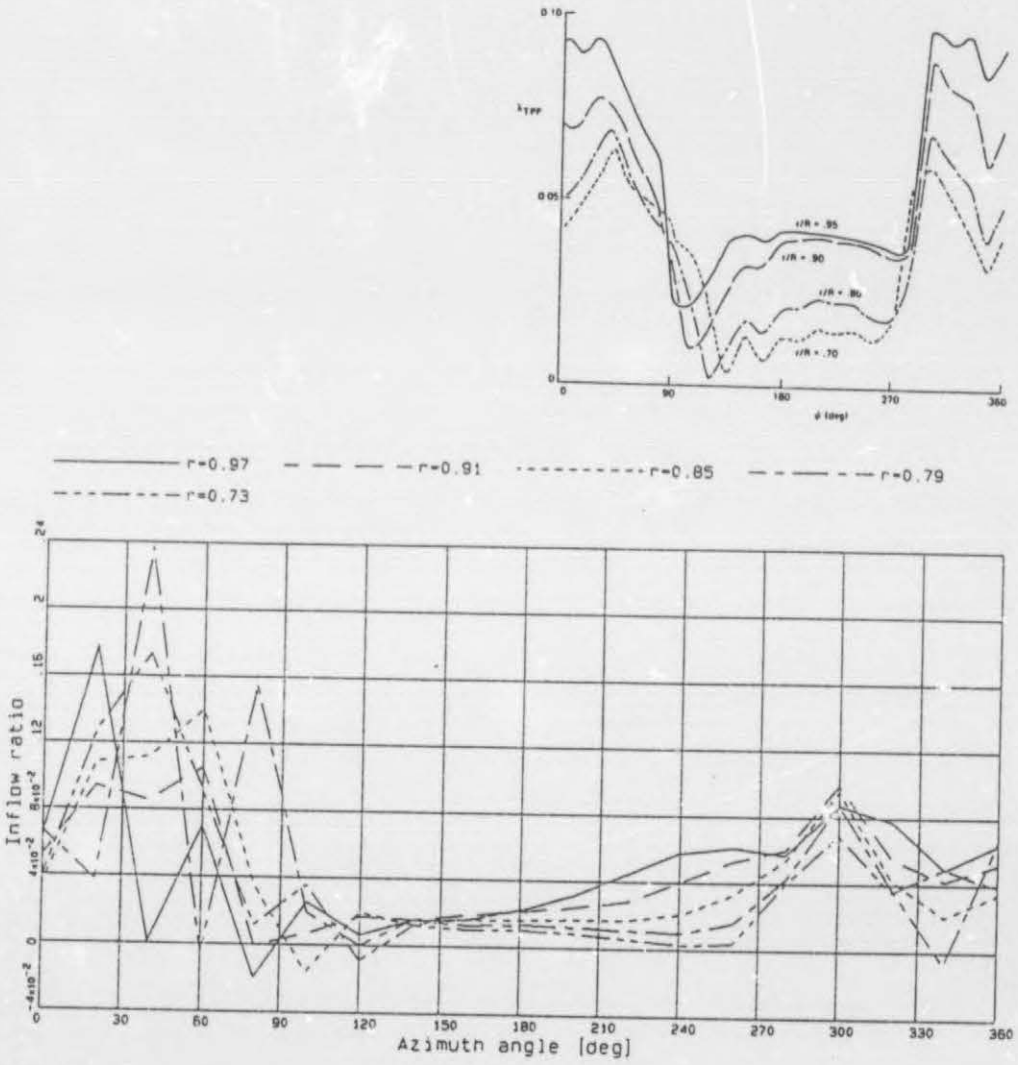

Fig 5.3.3.1 (c) Calculated inflow ratio distribution $\lambda(\psi)$, case 331

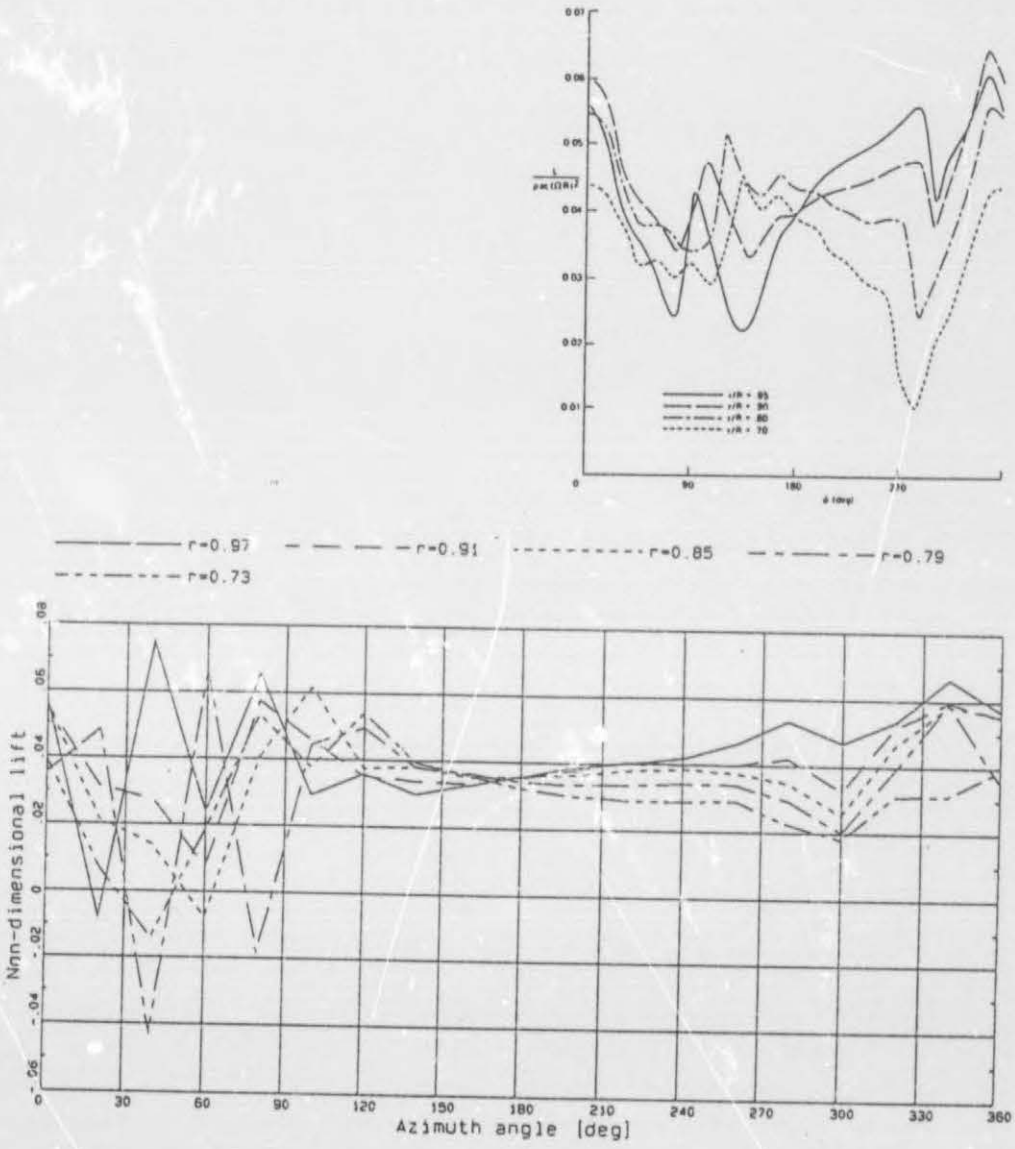

Fig 5.3.3.1 (d) Calculated non-dimensional lift distribution $\ell(\psi)$, case 331

Fig 5.3.4.1 (a) Calculated inflow ratio distribution $\lambda(r,\psi)$, case 341

Fig 5.3.4.1 (b) Calculated angle of attack distribution $\alpha(r,\psi)$, case 341

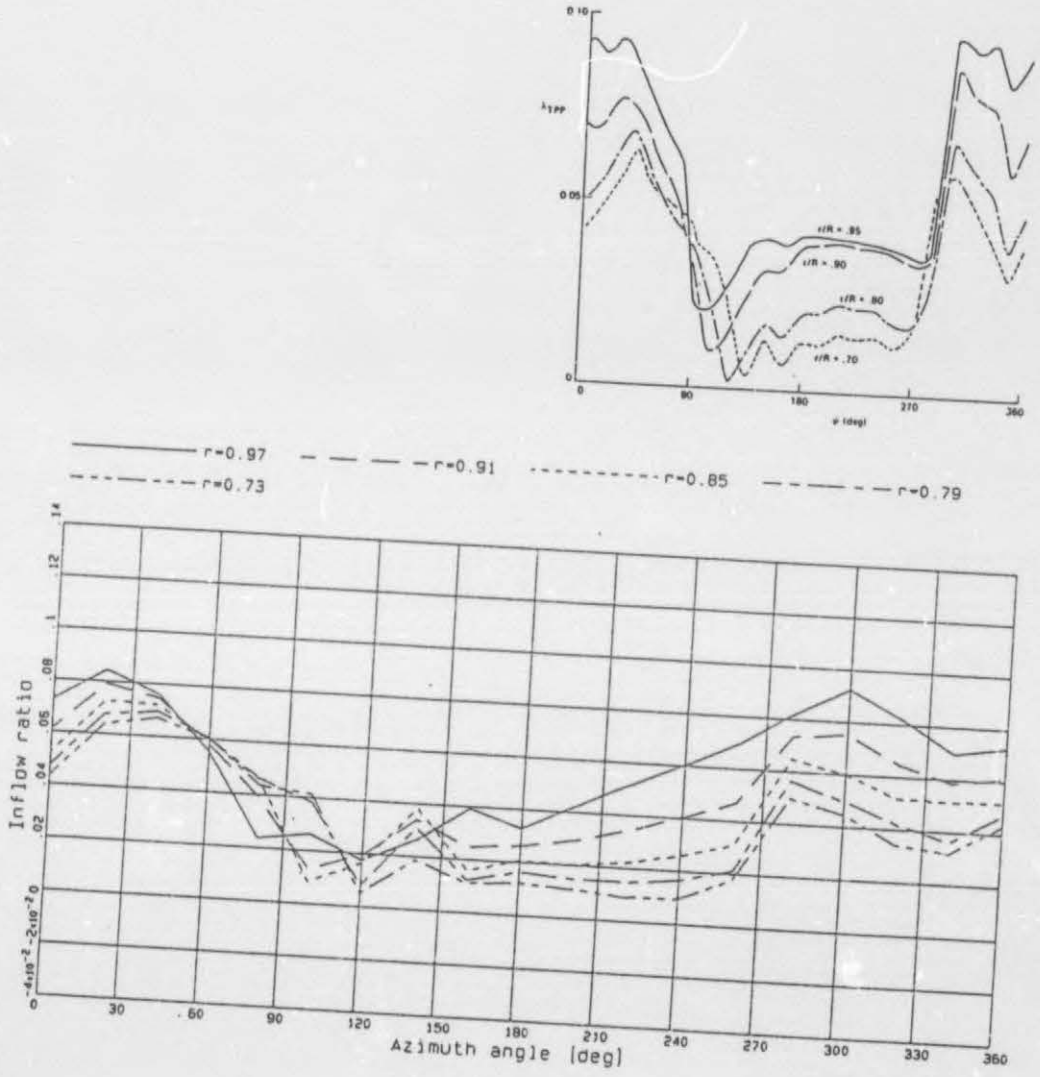

Fig 5.3.4.1 (c) Calculated inflow ratio distribution $\lambda(\psi)$, case 341

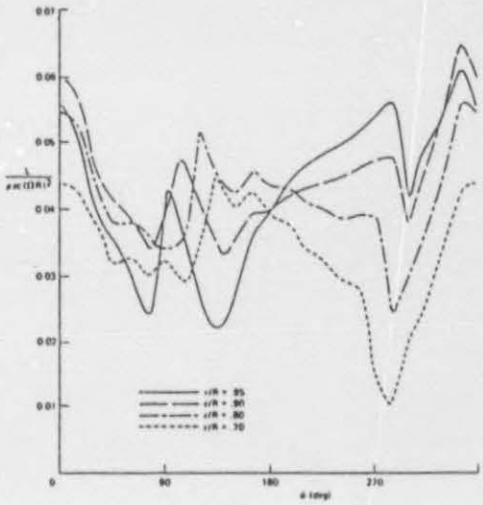

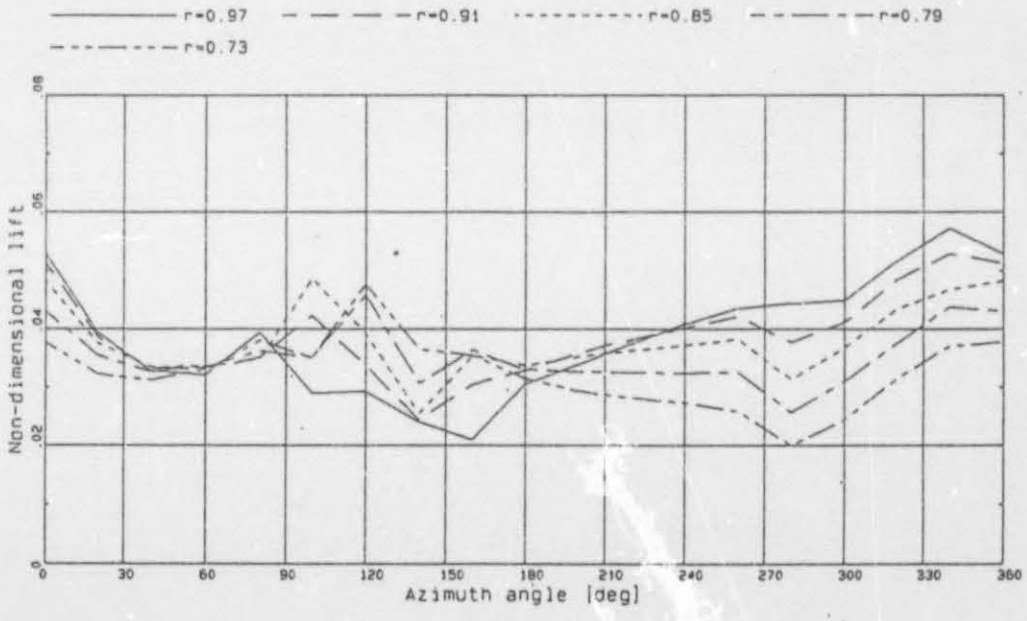

Fig 5.3.4.1 (d) Calculated non-dimensional lift distribution $\ell(\psi)$, case 341

TABLES

	CASE				
OPTION	111	112	113	114	115
nonwke					
rigwke	○	○	○	○	○
semwke					
uniind	○	○	○	○	○
linind					
nonind	○	○	○	○	○
cllmod	○	○	○	○	○
ellmod					
vlmmod					
shdmod	○	○			○
unsmod				○	○
radmod		○	○	○	○
cmpmod		○	○	○	○
dynmod					

Table 5.1 Options selected true for cases 111-115

	CASE				
OPTION	121	122	123	124	125
nonwke					
rigwke	○	○	○	○	○
semwke					
uniind	○	○	○	○	○
linind					
nonind	○	○	○	○	○
cllmod					
ellmod	○	○	○	○	○
vlmmod					
shdmod	○	○			○
unsmod				○	
radmod		○	○	○	○
cmpmod		○	○	○	○
dynmod					○

Table 5.1 (Continued)

	CASE				
OPTION	211	212	213	214	215
nonwke	○	○	○	○	○
rigwke					
semwke					
uniind	○	○	○	○	○
linind					
nonind					
cllmod					
ellmod					
vlmmod					
shdmod					
unsmod				○	
radmod		○	○		
cmpmod			○		
dynmod					○

Table 5.2 Options selected true for cases 211-215

	CASE				
OPTION	311	312	313	314	315
nonwke					
rigwke	○	○	○	○	○
semwke					
uniind	○	○	○	○	○
linind					
nonind	○	○	○	○	○
ellmod	○	○	○	○	○
ellmod					
vlmmod					
shdmod	○	○			○
unsmod				○	
radmod		○			
cmpmod		○			
dynmod					○

Table 5.3 Option selected true for cases 311-315

	CASE				
OPTION	321	322	323	324	325
nonwke					
rigwke	○	○	○	○	○
semwke					
uniind	○	○	○	○	○
linind					
nonind	○	○	○	○	○
cllmod					
ellmod	○	○	○	○	○
vlmmod					
shdmod	○	○			○
unsmod				○	
radmod		○			
cmpmod		○			
dynmod					○

Table 5.3 (Continued)

	CASE				
OPTION	331	341			
nonwke					
rigwke		○			
semwke	○				
uniind					
linind		○			
nonind	○	○			
cllmod	○	○			
ellmod					
vlmmod					
shdmod	○	○			
unsmod					
radmod					
cmpmod					
dynmod					

Table 5.3 (Continued)

APPENDIX A

```
c  ==========================================================
   Program ROTCAL

c  Program for the calculation of rotor aerodynamic loads
c  Developed by J Arnold,  University of Stellenbosch,RSA

c  Hardware requirements:      IBM-PC (186/286/386)
c  Software requirements:      MS FORTRAN  Compilor
c  ==========================================================

$LARGE

c  Insert common block from file
   include 'cmnblk.for'

   logical flag(3)
   integer ss,ds,option(2)
   character*3 case

c  The maximum allowable radial and azimuthal nodes assumed are
c  nri=24 and naj=36 respectively, with nrp=nri+1 and naq=naj+1.
c  Note that the format statements should match  the parameters.

   dimension ri(24),rp(25),psij(36),psiq(37),
  c        wi0(24,36),wi(24,36),tau(24,36),
  c        betaj(36),thetj(36),zij(24,36),tij(24,36),
  c        betaq(37),thetq(37),zpq(25,37),tpq(25,37),
  c        dzdi(24,36),dzdj(24,36),dtdi(24,36),dtdj(24,36),
  c        wpq(25,37),dwdi(24,36),dwdj(24,36),
  c        fij(24,36),bij(24,10),
  c        aoa(24,36),clij(24,36),cdij(24,36),cmij(24,36),
  c        fxh(24,36),fyh(24,36),fzh(24,36),
  c        mxh(24,36),myh(24,36),mzh(24,36),
```

```
c       fxn(24,36),fyn(24,36),fzn(24,36),
c       mxn(24,36),myn(24,36),mzn(24,36),
c       fxj(36),fyj(36),fzj(36),
c       mxj(36),myj(36),mzj(36),
c       upij(24,36),utij(24,36),urij(24,36)

      dimension fac(3),tol(3),relax(5)

c     Scaling, tolerance and relaxation factors

      flag(1)=.true.
      flag(2)=.true.
      flag(3)=.true.
      fac(1)=1000.0
      fac(2)=1.0
      fac(3)=1000.0
      tol(1)=0.1
      tol(2)=0.1
      tol(3)=10
      relax(1)=0.5
      relax(2)=0.25
      relax(3)=0.5
      relax(4)=0.1
      relax(5)=0.0001

      print*,'grid  =[nr,na,nb,nl]'
      read*,nr,na,nb,nz
      print*,'case  =[three character code]'
      read*,case
      print*,'option=[-2],[read inflow and circulation from datfile]'
      print*,'option=[-1],[read influence coefficients from tmpfile]'
      print*,'option=[ 0],[calc influence coefficients ,dv=constant]'
      print*,'option=[+1],[calc influence coefficients ,dv=variable]'
      read*,option(1)
```

```
      print*,'forcit=[ 0],[no  iteration to obtain specified thrust]'
      print*,'      =[ 1],[... iteration to obtain specified thrust]'
      read*,forcit

      open(10,file='for010.'//case,status='unknown',
     c    access='sequential',form='formatted')
      open(20,file='for020.'//case,status='unknown',
     c    access='sequential',form='formatted')
      open(30,file='for030.'//case,status='unknown',
     c    access='sequential',form='formatted')
      open(40,file='for040.'//case,status='unknown',
     c    access='sequential',form='formatted')
      open(50,file='for050.'//case,status='unknown',
     c    access='sequential',form='formatted')
      open(110,file='for110.'//case,status='unknown',
     c    access='sequential',form='formatted')
      open(120,file='for120.'//case,status='unknown',
     c    access='sequential',form='formatted')
      open(130,file='for130.'//case,status='unknown',
     c    access='sequential',form='formatted')
      open(140,file='for140.'//case,status='unknown',
     c    access='sequential',form='formatted')
      open(150,file='for150.'//case,status='unknown',
     c    access='sequential',form='formatted')
      open(100,file='for100.'//case,status='unknown',
     c    access='sequential',form='formatted')

c     Wake lattice parameters

      nri=nint(nr)
      nrp=nint(nr+1.0)
      naj=nint(na)
      naq=nint(na+1.0)
      nbk=nint(nb)
      nzl=nint(nz)

      print*, nri,naj
```

```
c     Calculate radius and azimuth vectors

      do 1001 i=1,nri
        ri(i)=(r-r0)*(real(i)-0.5)/nr+r0
1001  continue
      do 1002 j=1,naj
        psij(j)=2*pi*(real(j)-1.0)/na
1002  continue

      do 1003 p=1,nint(nr+1.0)
        rp(p)=(r-r0)*(real(p)-1.0)/nr+r0
1003  continue
      do 1004 q=1,nint(na+1.0)
        psiq(q)=2*pi*(real(q)-1.0)/na
1004  continue
      dr=ri(2)-ri(1)
      dpsi=psij(2)-psij(1)

c     Calculate model parameters

      vh=sqrt(v(1)*v(1)+v(2)*v(2)+v(3)*v(3))
      if (vh.gt.0.0) then
        aoah=asin(v(3)/vh)
        aosh=atan2(v(2),v(1))
      else
        aoah=0.0
        aosh=0.0
      end if
      mu=vh*cos(aoah)/(om*r)
      lda0hp=mu*aoah
      lda0fp=mu*(aoah+bc(1))
      sig=nb*(c(1)+c(2)*r/2.0)/(pi*r)
      lock=rho*a0(1)*c(1)*(r**4)/ib
      nu=sqrt((1.0+eb*r*yb*mb/ib)*(om**2)+kb/(rottyp*ib*(1.0-eb)))/om
      disc=pi*r**2
```

```
c    Set initial values

     unifwi=0.0
     conpar=0.0
     lda=(v(3)+unifwi)/(om*r)

     do while (option(1).le.4)
     if (option(1).lt.0) then
       if (option(1).lt.-1) then
         dv=dr/sqrt(3)
         flag(1)=.false.
         option(1)=99
         option(2)=0
       else
         dv=dr/sqrt(3)
         flag(1)=.false.
         option(1)=99
         option(2)=1
       end if
     else
       if (option(1).eq.0) then
         dv=dr/sqrt(3)
         flag(1)=.true.
         option(1)=99
         option(2)=1
       else
         dv=dr/sqrt(real(option(1)))
         flag(1)=.true.
         option(1)=option(1)+1
         option(2)=1
       end if
     end if
```

```
      conv(3)=.false.
      do while (.not.conv(3))
      conv(1)=.false.
      do while (.not.conv(1))

c     Determine initial estimate for thrust or collective pitch

      if (ctlinp) then
        call rotthr
      else
       call rotcon
      end if

c     Calculate uniform induced velocity

      unifw0=unifwi
      call inflow(ft0,v(1),v(3),unifwi,first(1))
      unifwi=relax(1)*unifwi+(1.0-relax(1))*unifw0

      lda=(vh*sin(aoah)+unifwi)/(om*r)
      conpar=abs(fac(1)*unifwi-fac(1)*unifw0)

      if (conpar.lt.tol(1)) conv(1)=.true.

      end do
      print*, ft0,unifwi
      chi=atan(mu/lda)
      kc=4.0*(1.0-1.8*mu**2)*tan(chi/2.0)/3.0
      ks=-2.0*mu

c     Calculate approximate blade motion

      if (.not.bldinp) call bldapp
```

```
c    Calculate linear induced velocity matrix and set circulation
c    matrix equal to zero on first iteration

     do 1006 i=1,nri
      do 1005 j=1,naj
       if (uniind) then
         wi0(i,j)=unifwi
       end if
       if (linind) then
         wi0(i,j)=unifwi*(1.0+ri(i)*(kc*cos(psij(j))
c          +ks*sin(psij(j))))/r
       end if
       if (nonind) then
         if (first(3)) then
           wi(i,j)=unifwi
         end if
       else
         wi(i,j)=wi0(i,j)
       end if
       if (first(3)) then
         tau(i,j)=0.0
       end if
1005   continue
1006  continue

c    Calculate bending displacement and pitch angles
c    and their radial and azimuthal derivatives

     do 1009 i=1,nri
      if (ri(i).lt.r0) then
        eta=0.0
      else
      eta=(ri(i)-eb*r)/(r-eb*r)
      end if
```

```
      do 1008 j=1,naj
        bcs=0.0
        tcs=0.0
        do 1007 k=1,5
          bcs=bcs+bc(k)*cos(psij(j))+bs(k)*sin(psij(j))
          tcs=tcs+thc(k)*cos(psij(j))+ths(k)*sin(psij(j))
1007      continue
        betaj(j)=b0+bcs
        thetj(j)=th0(1)+tcs
        zij(i,j)=betaj(j)*eta*r
        tij(i,j)=thetj(j)+th0(2)*ri(i)
1008    continue
1009  continue

    do 1012 p=1,nint(nr+1.0)
      if (rp(p).lt.r0) then
        eta=0.0
      else
        eta=(rp(p)-eb*r)/(r-eb*r)
      end if
      do 1011 q=1,nint(na+1.0)
        bcs=0.0
        tcs=0.0
        do 1010 k=1,5
          bcs=bcs+bc(k)*cos(psij(q))+bs(k)*sin(psij(q))
          tcs=tcs+thc(k)*cos(psij(q))+ths(k)*sin(psij(q))
1010      continue
        betaq(q)=b0+bcs
        thetq(q)=th0(1)+tcs
        zpq(p,q)=betaq(q)*eta*rp(p)
        tpq(p,q)=thetq(q)+th0(2)*rp(p)

1011    continue
1012  continue
```

```
      do 1112 p=1,nint(nr+1.0)
       do 1212 q=1,nint(na+1.0)
        if (q.le.naj) then
          dzdq=(zpq(p,q+1)-zpq(p,q))/(psiq(2)-psiq(1))
          if (q.eq.1)  dzdq0=dzdq
          if (q.eq.na) dzdq1=dzdq
        else
          dzdq=(dzdq0+dzdq1)/2.0
        end if
        ut    =om*ri(p)+v(1)*sin(psij(q))+v(2)*cos(psij(q))
        ur    =v(1)*cos(psij(q))-v(2)*sin(psij(q))
        up    =v(3)+dzdq*om
        wpq(p,q)=ut*sin(psiq(q))-up*cos(psiq(q))
1212    continue
1112  continue

      do 1014 i=1,nri
       do 1013 j=1,naj
        dzdi(i,j)=(zpq(i,j)-zpq(i+1,j))/(rp(i)-rp(i+1))
        dzdj(i,j)=(zpq(i,j)-zpq(i,j+1))/(psiq(j)-psiq(j+1))
        dtdi(i,j)=(tpq(i,j)-tpq(i+1,j))/(rp(i)-rp(i+1))
        dtdj(i,j)=(tpq(i,j)-tpq(i,j+1))/(psiq(j)-psiq(j+1))
        dwdi(i,j)=(wpq(i,j)-wpq(i+1,j))/(rp(i)-rp(i+1))
        dwdj(i,j)=(wpq(i,j)-wpq(i,j+1))/(psiq(j)-psiq(j+1))
1013    continue
1014  continue

c     To record/read influence coefficients of bound and free
c     vortex cells

      open(60,file='bbb.tmp',status='unknown',access='sequential',
     c    form='binary')
      open(70,file='fff.tmp',status='unknown',access='sequential',
     c    form='binary')
```

```
      if (option(2).eq.0) then
        do 2015 i=1,nri
          read(10,2000) (wi(i,j),j=1,naj)
          read(40,2000) (tau(i,j),j=1,naj)
2015    continue
      end if

c     Calculate influence coefficients and non-linear induced
c     velocity matrix using iterative process

      count=0.0
      conv(2)=.false.
      do while (.not.conv(2))
      count=count+1.0

      if (option(2).eq.0) go to 2016

      if (.not.nonwke) then
      if (.not.first(2)) then

      if (.not.flag(1)) then
        rewind (60)
        rewind (70)
      end if

      errsum=0.0
      do 1023 i=1,nri
        print*,i
        ci=c(1)+c(2)*ri(i)
        if (cllmod) then
          db=ci/4.0
          dc=ci/4.0
        else
          db=3.0*ci/4.0
          dc=ci/4.0
        end if
```

```
      do 1022 j=1,naj
       do 1017 p=1,nri
        if (flag(1)) then
         do 1015 k=1,nint(nb)
          q=nint(real(j)+na*real(k-1)/nb)
          if (q.gt.naj) q=q-naj
          call infcfb (ri(i),psij(j),zij(i,j),rp(p),rp(p+1),
     c                 psiq(q),psiq(q+1),zpq(p,q),b)
          bij(p,k)=b
 1015     continue
        if (rigwke) then
         write(60) (bij(p,k),k=1,nbk)
        end if
       else
        read (60) (bij(p,k),k=1,nbk)
       end if
       if (flag(1)) then
        do 1016 q=1,naj
         if (rigwke) then
          wind=wi0(i,j)
         else
          wind=wi(p,q)
         end if
         call infcff (ri(i),psij(j),zij(i,j),rp(p),rp(p+1),
     c                psiq(q),psiq(q+1),zpq(p,q),wind,f)
         fij(p,q)=f
 1016    continue
       if (rigwke) then
        write(70) (fij(p,q),q=1,naj)
       end if
      else
       read(70) (fij(p,q),q=1,naj)
      end if
 1017 continue
```

```
c       First approximation of tau(i,j) using a single panel
c       vortex lattice blade representation and a Gauss-Seidel
c       iterative procedure

        if (vlmmod) then
          ut=om*ri(i)+v(1)*sin(psij(j))+v(2)*cos(psij(j))
          if (radmod) then
            ur=v(1)*cos(psij(j))-v(2)*sin(psij(j))
          else
            ur=0.0
          end if
          up=v(3)+om*dzdj(i,j)+ur*dzdi(i,j)
          aoa(i,j)=(tij(i,j)-atan2(up,ut))
          wi(i,j)=ut*aoa(i,j)
        else
          wif=0.0
          do 1019 p=1,nri
            do 1018 q=1,naj
              wif=wif+tau(p,q)*fij(p,q)
1018          continue
1019        continue
          wib=0.0
          do 1021 p=1,nri
            do 1020 k=1,nint(nb)
              q=nint(real(j)+na*real(k-1)/nb)
              if (q.gt.naj) q=q-naj
              if (shdmod) then
                wib=wib+tau(p,q)*bij(p,k)
              else
                wib=0.0
              end if
1020          continue
1021        continue
```

```
            wi(i,j) = relax(2)*(wif+wib)+(1.0-relax(2))*wi(i,j)
          end if
1022      continue
1023    continue

        if (flag(1).and.(rigwke)) then
          endfile (60)
          endfile (70)
        end if
        if (rigwke) flag(1) = .false.

        end if
        end if

2016    continue

c       Calculate sectional angle of attack, aerodynamic coefficients
c       and circulation distribution

        errsum = 0.0
        do 1026 i = 1,nri
          ds = 0
          ss = 0
          ci = c(1)+c(2)*ri(i)
          ai = a0(1)+a0(2)*ri(i)
          aoa0i = aoa0(1)+aoa0(2)*ri(i)
          aoasi = aoas(1)+aoas(2)*ri(i)
c         Loop 1025 to ensure correct (matured) dynamic stall behaviour
          if (dynmod) then
            m = 2
          else
            m = 1
          end if
```

```
      do 1025 k = 1,m
      do 1024 j = 1,naj
        ut = om*ri(i)+v(1)*sin(psij(j))+v(2)*cos(psij(j))
        if (radmod) then
          ur = v(1)*cos(psij(j))-v(2)*sin(psij(j))
        else
          ur = 0.0
        end if
        up = v(3)+om*dzdj(i,j)+ur*dzdi(i,j)+wi(i,j)
        utij(i,j) = ut
        upij(i,j) = up
        urij(i,j) = ur

        if (radmod) then
          cosswp = ut/sqrt(ut**2+ur**2)
        else
          cosswp = 1.0
        end if

        if (.not.vlmmod) then
        aoa(i,j) = (tij(i,j)-atan2(up,ut))*(cosswp**2)-aoa0i
        end if
        if (first(2)) then
        aoa(i,j) = (tij(i,j)-atan2(up,ut))*(cosswp**2)-aoa0i
        end if
        machnr = sqrt((ut**2+up**2)/(gasrat*gascon*temp))

        if (secinp) then
c         call sectab(ri(i),aoa(i,j),machnr,cl,cd,cm)
        else
          if (dynmod) then
            if(first(2)) then
              call static(ri(i),aoa(i,j),cl,cd,cm)
            else
              call dynmic(ri(i),aoa(i,j),ss,ds,cl,cd,cm)
            end if
```

```
          else
            call static(ri(i),aoa(i,j),cl,cd,cm)
          end if
        end if
        if (cmpmod) then
          ma = machnr
        else
          ma = 0.0
        end if

        if (first(2)) then
          clij(i,j) = (cl/cosswp**2)/sqrt(1.0-ma)
        else
          clij(i,j) = relax(4)*(cl/cosswp**2)/sqrt(1.0-ma)
c               +(1.0-relax(4))*clij(i,j)
        end if
        cdij(i,j) = (cd/cosswp)
        cmij(i,j) = cm

        tauold = tau(i,j)
        if (vlmmod.and.(.not.first(2))) then
          sum1 = 0.0
          do 2019 p = 1,i-1
            do 2018 q = 1,j-1
              sum1 = sum1 + fij(p,q)*tau(p,q)/fij(i,j)
2018        continue
2019        continue
          sum2 = 0.0
          do 3019 p = i+1,nri
            do 3018 q = j+1,naj
              sum2 = sum2 + fij(p,q)*tau(p,q)/fij(i,j)
3018        continue
3019        continue
```

```
          tau(i,j)=relax(5)*(wi(i,j)/fij(i,j)-sum1-sum2)
     c          +(1.0-relax(5))*tauold
          tauerr=(fac(2)*(tau(i,j)-tauold))**2
          errsum=errsum+tauerr
          clij(i,j)=2.0*tau(i,j)/(sqrt(ut**2+up**2)*ci)
        else
          tau0=0.5*ut*ci*clij(i,j)
          if (dynmod) then
            taut=0.0
          else
            if (unsmod) then
              taut=ai*(ci**2)*(om*dtdj(i,j)+om*dzdi(i,j)
     c            +ut*dtdj(i,j)*sin(psij(j)))
     c            *(1.0+2.0*(0.25))/4.0
            else
              taut=0.0
            end if
          end if
          taunew=tau0+taut
          tauerr=(fac(2)*(taunew-tauold))**2
          errsum=errsum+tauerr
          tau(i,j)=taunew
        end if

1024    continue
1025    continue
1026  continue

    if (option(2).eq.0) conv(2)=.true.

    if (errsum.lt.tol(2)) conv(2)=.true.
    write(100,*) count,errsum
    write(*,*) count,errsum,conv(2)
    first(2)=.false.
    end do
```

```
c     Calculate blade section loads

      do 1028 i=1,nri
       ci=c(1)+c(2)*ri(i)
       ai=a0(1)+a0(2)*ri(i)
       cm0i=cm0(1)+cm0(2)*ri(i)
       do 1027 j=1,naj
        ut=om*ri(i)+v(1)*sin(psij(j))+v(2)*cos(psij(j))
        if (radmod) then
          ur=v(1)*cos(psij(j))-v(2)*sin(psij(j))
        else
          ur=0.0
        end if
        up=v(3)+om*dzdj(i,j)+ur*dzdi(i,j)+wi(i,j)
        theta=th0(1)+ri(i)*th0(2)+thetj(j)
        u=sqrt(ut**2+up**2+ur**2)
        u1=ut*cos(tij(i,j))+up*sin(tij(i,j))
        if (u1.ge.0.0) then
          sgn=1.0
        else
          sgn=-1.0
        end if
        dwdx=om*(dtdj(i,j)+dzdi(i,j))+v(1)*dtdi(i,j)*cos(psij(j))

c       Section lift, drag and moment

        lift0=sgn*0.5*rho*(u**2)*ci*clij(i,j)
        if (unsmod) then
          liftt=rho*ci*ai*(ci*ut*dwdx*(1.0+sgn*(1.0-sgn*0.5))/4.0
c              +ci*(om*dwdj(i,j)+ur*dwdi(i,j))/8.0)
        else
          liftt=0.0
        end if
        lift=lift0+liftt
```

```
      drag0=0.5*rho*(u**2)*ci*cdij(i,j)
      dragt=0.0
      drag=drag0+dragt

      mom0=sgn*0.5*rho*(u**2)*(ci**2)*cmij(i,j)
      if (unsmod) then
        momt=rho*ai*(ci**3)*
c           (-sgn*ut*dwdx*(1.0+sgn*(2-sgn*1.0))**2
c           -sgn*(om*dwdj(i,j)+ur*dwdi(i,j))*
c           (1.0+sgn*(2-sgn*1.0)))/32.0
      else
        momt=0.0
      end if
      mom=mom0+momt

c     Section forces relative to blade reference system

      fxb=sgn*(drag*cos(aoa(i,j))-lift*sin(aoa(i,j)))
      fyb=drag*sin(atan2(ur,ut))
      fzb=sgn*(lift*cos(aoa(i,j)))+drag*sin(aoa(i,j))
      mxb=0.0
      myb=mom
      mzb=0.0

      fxn(i,j)=drag
      fyn(i,j)=0.0
      fzn(i,j)=0.5*((ut/(om*r))**2)*aoa(i,j)
c     see Johnson pp199
      mxn(i,j)=mxb
      myn(i,j)=myb
      mzn(i,j)=mzb
```

```
      fxh(i,j) = fxb*cos(theta) + fzb*sin(theta)
      fyh(i,j) = fyb
      fzh(i,j) = fzb*cos(theta)-fxb*sin(theta)
      mxh(i,j) = mxb
      myh(i,j) = myb
      mzh(i,j) = mzb

1027  continue
1028  continue

c     Calculate average rotor forces and torque

      do 1030 j = 1,naj
        fxj(j) = 0.0
        fyj(j) = 0.0
        fzj(j) = 0.0
        mxj(j) = 0.0
        myj(j) = 0.0
        mzj(j) = 0.0
        do 1029 i = 1,nri
          dr = rp(i+1)-rp(i)
          fxj(j) = fxj(j) + fxh(i,j)*dr
          fyj(j) = fyj(j) + (fyh(i,j)-fzh(i,j)*dzdi(i,j))*dr
          fzj(j) = fzj(j) + (fzh(i,j)+fyh(i,j)*dzdi(i,j))*dr
          mxj(j) = mxj(j) + 0.0
          myj(j) = myj(j) + myh(i,j)*dr
          mzj(j) = mzj(j) + 0.0
1029  continue
1030  continue

      xforce = 0.0
      yforce = 0.0
      zforce = 0.0
```

```
      do 1031 j=1,naj
        dpsi  =psiq(j+1)-psiq(j)
        xforce=xforce+(nb/(2*pi))*(fxj(j)*sin(psiq(j))
     c        +fyj(j)*cos(psiq(j)))*dpsi
        yforce=yforce+(nb/(2*pi))*(fyj(j)*sin(psiq(j))
     c        -fxj(j)*cos(psiq(j)))*dpsi
        zforce=zforce+(nb/(2*pi))*(fzj(j))*dpsi
 1031 continue

      torque=0.0
      do 1033 i=1,nri
        fxi=0.0
        do 1032 j=1,naj
          fxi=fxi+(.5*nb/pi)*(fxh(i,j)*sin(psiq(j))
     c        +fyh(i,j)*cos(psiq(j)))*dpsi
 1032   continue
        torque=torque+ri(i)*fxi
 1033 continue
      first(3)=.false.

      write(100,*) zforce,ft0,unifwi
      write(*,*) zforce,ft0,unifwi

      if (forcit.lt.0.5) then
        conpar=0.0
      else
        conpar = ft0-zforce
      end if
      if (abs(conpar).lt.tol(3)) then
        conv(3)=.true.
      else
        if (ctlinp) then
          ft0=relax(3)*zforce+(1-relax(3))*ft0
        else
          th0(1)=th0(1)+0.1*(conpar/ft0)
        end if
      end if
```

```
      close (60,status='keep')
      close (70,status='keep')

      end do

      end do

c     Data output

      do 1034 i=1,nri
       write(10,2000) (wi(i,j),j=1,naj)
       write(20,2000) (aoa(i,j),j=1,naj)
       write(30,2000) (clij(i,j),j=1,naj)
       write(40,2000) (tau(i,j),j=1,naj)
       write(50,2000) (fzn(i,j),j=1,naj)
1034  continue
      do 1036 i=1,nri
       do 1035 j=1,naj
        x=ri(i)*cos(psij(j))
        y=ri(i)*sin(psij(j))
        write(110,*) x,y,lda0fp+wi(i,j)/(om*r)
        write(120,*) x,y,aoa(i,j)*180/pi
        write(130,*) x,y,clij(i,j)
        write(140,*) x,y,tau(i,j)/a0(1)/c(1)/(om*r)
        write(150,*) x,y,fzn(i,j)
1035    continue
1036  continue

      close (10,status='keep')
      close (20,status='keep')
      close (30,status='keep')
      close (40,status='keep')
      close (50,status='keep')
      close (110,status='keep')
```

```
close (120,status='keep')
close (1[illegible]s='keep')
close (140,status='keep')
close (150,status='keep')

open(111,file='for111.'//case,status='unknown',
c    access='sequential',form='formatted')
open(112,file='for112.'//case,status='unknown',
c    access='sequential',form='formatted')
open(113,file='for113.'//case,status='unknown',
c    access='sequential',form='formatted')
open(114,file='for114.'//case,status='unknown',
c    access='sequential',form='formatted')
open(115,file='for115.'//case,status='unknown',
c    access='sequential',form='formatted')
open(151,file='for151.'//case,status='unknown',
c    access='sequential',form='formatted')
open(152,file='for152.'//case,status='unknown',
c    access='sequential',form='formatted')
open(153,file='for153.'//case,status='unknown',
c    access='sequential',form='formatted')
open(154,file='for154.'//case,status='unknown',
c    access='sequential',form='formatted')
open(155,file='for155.'//case,status='unknown',
c    access='sequential',form='formatted')

do 1037 j=1,naj
  az=psij(j)*180/pi
  write(111,*) az,lda0fp+wi(nri-0,j)/(om*r)
  write(112,*) az,lda0fp+wi(nri-1,j)/(om*r)
  write(113,*) az,lda0fp+wi(nri-2,j)/(om*r)
  write(114,*) az,lda0fp+wi(nri-3,j)/(om*r)
  write(115,*) az,lda0fp+wi(nri-4,j)/(om*r)
```

```
      write(151,*) az,clij(nri-0,j)
      write(152,*) az,clij(nri-1,j)
      write(153,*) az,clij(nri-2,j)
      write(154,*) az,clij(nri-3,j)
      write(155,*) az,clij(nri-4,j)
1037  continue
      az=2.0*pi*180/pi
      write(111,*) az,lda0fp+wi(nri-0,1)/(om*r)
      write(112,*) az,lda0fp+wi(nri-1,1)/(om*r)
      write(113,*) az,lda0fp+wi(nri-2,1)/(om*r)
      write(114,*) az,lda0fp+wi(nri-3,1)/(om*r)
      write(115,*) az,lda0fp+wi(nri-4,1)/(om*r)
      write(151,*) az,clij(nri-0,1)
      write(152,*) az,clij(nri-1,1)
      write(153,*) az,clij(nri-2,1)
      write(154,*) az,clij(nri-3,1)
      write(155,*) az,clij(nri-4,1)

2000  format(24(1X,E12.5))

      end

c     ================================================
      Subroutine inflow(t,u,w,wi,flag)

c     Calculates uniform induced velocity using momentum theory
c     and a Newton-Raphson iterative scheme
c     ================================================

      include 'cmnblk.for'
      logical flag
```

```
      ct=t/(2.0*rho*disc)
      if (flag) wi=ct
      cc=u**2+(w+wi)**2
      bb=(w+wi)+(cc**1.5)/ct
      aa=u**2+(w+wi)*wi+(w+wi)**2
      wi=aa/bb
      flag=.false.
        .
      return

      end

c     ================================================
      Subroutine rotthr

c     Calculates rotor thrust for given collective pitch and
c     rotor kinematic state
c     ================================================

      include 'cmnblk.for'

      cq=pi*sig*rho*disc*((om*r)**2)
      ft0=cq*(th0(1)*(1.0+3.0*(mu**2)/2.0)/3.0
     c   +th0(2)*r*(1.0+(mu**2))/4.0-lda/2.0)

      return

      end

c     ================================================
      Subroutine rotcon

c     Calculates collective pitch angle for given thrust
c     and rotor kinematic state
c     ================================================
```

```
      include 'cmnblk.for'

      cq=pi*sig*rho*disc*((om*r)**2)
      th0(1)=((ft0/cq)-th0(2)*r*(1.0+(mu**2))/4.0
     c   +lda/2.0)/((1.0/3.0)+(mu**2)/2.0)

      return

      end

c     ==========================================
      subroutine infcfb (rc,psic,zc,rb1,rb2,psib1,psib2,zb,b)

c     Calculates influence coefficients bij(p,k) of bound vortex cells
c     ==========================================

      include 'cmnblk.for'

      dimension rb(2),psib(2),
     c      xw(2,2,10),yw(2,2,10),zw(2,2,10),
     c      rx(2),ry(2),rz(2)

      rb(1)=rb1
      rb(2)=rb2
      psib(1)=psib1
      psib(2)=psib2

      xc=rc*cos(psic)-dc*sin(psic)
      yc=rc*sin(psic)+dc*cos(psic)
      zc=zc
```

```
      do 1020 k=1,nbk
        psik=psic+2.0*pi*real(k-1)/nb
        if (psik+.001.gt.2.0*pi) psik=psik-2.0*pi
        do 1010 i=1,2
          do 1000 j=1,2
            xw(i,j,k)=rb(i)*cos(psik)-real(j-1)*(db)*sin(psik)
            yw(i,j,k)=rb(i)*sin(psik)+real(j-1)*(db)*cos(psik)
            zw(i,j,k)=zb
1000        continue
1010      continue
1020    continue

        b=0.0
        do 1050 k=1,nbk
          do 1040 i=2,4
            do 1030 j=1,2
              rx(j)=xw(mn(i,j,1),mn(i,j,2),k)-xc
              ry(j)=yw(mn(i,j,1),mn(i,j,2),k)-yc
              rz(j)=zw(mn(i,j,1),mn(i,j,2),k)-zc
1030        continue
            if (k.eq.1) then
              if (i.eq.3) then
                gi=0.0
              else
                call biosav(rx,ry,rz,gi)
              end if
            else
              call biosav(rx,ry,rz,gi)
            end if

            if (shdmod) then
              if ((i.eq.1).or.(i.eq.3)) then
                gi=0.0
              end if
            end if
```

```
        b=b+gi
1040    continue
1050  continue

      return

      end

c     ==========================================
      subroutine infcff (rc,psic,zc,rf1,rf2,psif1,psif2,zf,vi,f)

c     Calculates influence coefficients fij(p,q) of free vortex cells
c     at node (i,j) at location [ri(i),psij(j)]
c     ==========================================

      include 'cmnblk.for'
      dimension rf(2),psif(2),phif(2,10,10),
     c          xw(2,2,10,10),yw(2,2,10,10),zw(2,2,10,10),
     c          rx(2),ry(2),rz(2),rr(2)

      rf(1)=rf1
      rf(2)=rf2

      xc=rc*cos(psic)-dc*sin(psic)
      yc=rc*sin(psic)+dc*cos(psic)
      zc=zc

      do 1040 l=1,nzl
        do 1030 k=1,nbk
          psik=psic+2.0*pi*real(k-1)/nb
          if (psik+.001.gt.2.0*pi) psik=psik-2.0*pi
          if ((psif1+.001).lt.psik) then
            phif(1,k,l)=psik-psif1+2.0*pi*real(l-1)
```

```
          else
            phif(1,k,l) = psik-psif1+2.0*pi*(real(l-1)+1.0)
          end if
          phif(2,k,l) = phif(1,k,l)-abs(psif2-psif1)

          do 1020 i=1,2
            do 1010 j=1,2
              xw(i,j,k,l) = rf(i)*cos(psik-phif(j,k,l))
     c                +phif(j,k,l)*v(1)/om
              yw(i,j,k,l) = rf(i)*sin(psik-phif(j,k,l))
     c                -phif(j,k,l)*v(2)/om
              zw(i,j,k,l) = -phif(j,k,l)*(v(3)+vi)/om+zf
     1010     continue
     1020   continue

     c      Wake geometry with geom.m [Matlab]
     c      write(60,*) xw(1,1,k,l),xw(1,2,k,l),xw(2,2,k,l),
     c  c          xw(2,1,k,l)
     c      write(70,*) yw(1,1,k,l),yw(1,2,k,l),yw(2,2,k,l),
     c  c          yw(2,1,k,l)

     1030   continue
     1040 continue

        f=0.0
        do 1080 l=1,nzl
          do 1070 k=1,nbk
            do 1060 i=1,4
              do 1050 j=1,2
                rx(j)=xw(mn(i,j,1),mn(i,j,2),k,l)-xc
                ry(j)=yw(mn(i,j,1),mn(i,j,2),k,l)-yc
                rz(j)=zw(mn(i,j,1),mn(i,j,2),k,l)-zc
     1050       continue
```

```
            if (phif(1,k,l)-.001.le.0.0) then
              if (i.eq.3) then
                gi=0.0
              else
                call biosav(rx,ry,rz,gi)
              end if
            else
              call biosav(rx,ry,rz,gi)
            end if

            if (shdmod) then
              if ((i.eq.1).or.(i.eq.3)) then
                gi=0.0
              end if
            end if

            f=f+gi

1060      continue
1070    continue
1080    continue

        return

        end

c       ==========================================================
        subroutine biosav(rx,ry,rz,g)

c       Calculates z-component of velocity induced at the origen by
c       an vortex element whos location is given by position vectors
c       r(1) and r(2)
c       ==========================================================
```

```
      include 'cmnblk.for'
      dimension rx(2),ry(2),rz(2)

      r11 = (rx(1)*rx(1)+ry(1)*ry(1)+rz(1)*rz(1))
      r12 = (rx(1)*rx(2)+ry(1)*ry(2)+rz(1)*rz(2))
      r21 = (rx(2)*rx(1)+ry(2)*ry(1)+rz(2)*rz(1))
      r22 = (rx(2)*rx(2)+ry(2)*ry(2)+rz(2)*rz(2))
      r11s= sqrt(r11)
      r22s= sqrt(r22)

      if ((rx(1).eq.rx(2)).and.(ry(1).eq.ry(2)).and.(rz(1).eq.rz(2)))
     c  then
        g= 0.0
      else
        g= (1.0/(4.0*pi))*(((rx(1)*ry(2)-rx(2)*ry(1))*(r11s+r22s)
     c    *(1.0-r12/(r11s*r22s)))
     c    /(r11*r22-r12**2+dv**2*(r11+r22-2.0*r12)))
      end if

      return

      end

c     ==========================================
      subroutine static(rr,aoar,cl,cd,cm)

c     Model of steady-state section aerodynamic characteristics
c     ==========================================

      include 'cmnblk.for'
```

```
aoasr = aoas(1) + aoas(2)*rr
cd0r = cd0(1) + cd0(2)*rr
cm0r = cm0(1) + cm0(2)*rr
cmsr = cms(1) + cms(2)*rr
dcld  = a0(1) + a0(2)*rr
cdsr = cd0r-0.0216*aoasr + 0.400*aoasr**2

d0 = cd0r
d1 = -0.0216
d2 = 0.4000
d3 = (cdsr-sin(aoasr))/(1.0-sin(aoasr))
d4 = (cdsr-1.0)/(1.0-sin(aoasr))

a0r = dclda*aoasr/(aoasr-pi/2.0)

if (aoar.lt.(-pi+aoasr)) then
  cl = dclda*(aoar+pi)
  cd = d0 + d1*(pi+aoar) + d2*(pi+aoar)**2
  cm = cm0r
else
  if (aoar.lt.-aoasr) then
    cl = a0r*(aoar+pi/2.0)
    cd = d3-d4*sin(aoar+pi)
    cm = cm0r-(cmsr-cm0r)
  else
    if (aoar.lt.aoasr) then
      cl = dclda*aoar
      cd = d0 + d1*aoar + d2*aoar**2
      cm = cm0r
    else
      if (aoar.lt.(pi-aoasr)) then
        cl = a0r*(aoar-pi/2.0)
        cd = d3-d4*sin(aoar)
        cm = cm0r + (cmsr-cm0r)
      else
```

```
            cl=dclda*(aoar-pi)
            cd=d0+d1*(pi-aoar)+d2*(pi-aoar)**2
            cm=cm0r
          end if
        end if
      end if
    end if

    return

    end

c   ================================================
    subroutine dynmic(rr,aoar,ss,ds,cl,cd,cm)

c   Dynamic stall model
c   ================================================

    include 'cmnblk.for'
    integer ss,ds
    dimension ff(2)

    call static(rr,aoar,cl,cd,cm)

    aoasr=aoas(1)+aoas(2)*rr
    aoa0r=aoa0(1)+aoa0(2)*rr
    cm0r=cm0(1)+cm0(2)*rr
    cmsr=cms(1)+cms(2)*rr
    dclda=a0(1)+a0(2)*rr
    cl0=dclda*aoa0r
    cls=1.2
    dclm=0.5
    dcmm=-0.65
```

```
ass=aoasr
ads=ass+0.05
a=aoar
dpsis=2.0*dpsi

if (a.lt.-ass) then
  cmsr=cm0r+(cm0r-cmsr)
end if

if (abs(a).gt.pi/2.0) then
  r=-1.0
  if (a.gt.0.0) then
    a=-(pi-a)
  else
    a=pi+a
  end if
else
  r=1.0
end if
if (a.lt.0.0) then
  q=-1.0
else
  q=1.0
end if

ccl=1.1*sin(2.0*a)

if (abs(a).le.ass) then
  ss=0
  ds=0
end if
```

```
 if (ds.eq.0) then
   if (abs(a).lt.ads) then
     g=0.0
   else
     g=1.0
   end if
 else
   g=1.0
 end if

 if (ss.eq.1) then
   cl=ccl
   cm=cmsr
 else
   if ((g-.001).lt.(0.0)) then
     cl=a*(cls-cl0)/ass+cl0
     cm=cm0r
   else
     ds=ds+1
     ff(1)=real(ds)*dpsi/dpsis
     ff(2)=2.0-real(ds)*dpsi/dpsis
     f=min(ff(1),ff(2))
     dcl=f*dclm
     dcm=f*dcmm
     cl=q*(ads*(cls-cl0)/ass+cl0+dcl)
     cm=cm0r+q*r*dcm
     if (abs(ccl).gt.abs(cl)) then
       ci=ccl
       ss=1
     end if
```

```
          if (abs(f-ff(2)).lt.0.001) then
            if (abs(cmsr).gt.abs(cm)) then
              cm = cmsr
              ss = 1
            end if
          end if
        end if
      end if

      return

      end

c     ==========================================
      Block Data Rotor

c     Data initialization for program ROTCAL
c     Source: JOHNSON [1980a]  pp194,720,728
c     ==========================================

      include 'cmnblk.for'

c     ALL UNITS [kg,m,s,K]
c     All linear caracteristics are given as [(*)(r=0),d(*)/dr]

c     Rotor environment [rotenv]
      data rho,temp,gasrat,gascon/1.2256,288.16,1.4,287/

c     Kinematic state of rotor [rotkin]
      data om,(v(n),n=1,3)/220,54.4821,0.0,7.8445/

c     Rotor parameters [rotpar]
      data r,nb/1.0,3.0/
```

```
c     Rotor configuration [rotcnf]
c     [articulated,hingeless=1.0,gimballed(nb>=3)=nb/2,teetering(nb=2)=2.0]
      data rottyp/1.0/

c     Rotor forces [rotfce]
      data ft0,fh0,fy0/2236.0,0.0,0.0/

c     Control input or initialization [rotctl]
      data (th0(n),n=1,2)/0.3054,-0.1396/
      data (thc(n),n=1,5)/0.0,0.0,0.0,0.0,0.0/
      data (ths(n),n=1,5)/0.0,0.0,0.0,0.0,0.0/

c     Blade motion input or initialization [bldkin]
      data b0/0.1204/
      data (bc(n),n=1,5)/-0.1047,0.0,0.0,0.0,0.0/
      data (bs(n),n=1,5)/-0.0681,0.0,0.0,0.0,0.0/

c     Blade geometric and inertia characteristics [bldpar]
      data (c(n),n=1,2)/0.1047,0.0/
      data yb,mb,ib,eb,kb/0.5,0.4,0.0914,0.0,0.0/

c     Blade section aerodynamic characteristics [bldsec]
      data (a0(n),n=1,2)/5.7,0.0/
      data (aoa0(n),n=1,2)/0.0,0.0/
      data (aoas(n),n=1,2)/.21,0.0/
      data (cd0(n),n=1,2)/.006,0.0/
      data (cds(n),n=1,2)/0.02,0/
      data (cm0(n),n=1,2)/0.0,0.0/
      data (cms(n),n=1,2)/-0.4,0.0/
```

```
c   Blade section aerodynamic data table [secdat]
c   [Optional.Should be kown for m angles of attack and n Mach numbers
c    in the attached subcritical flow region]
      data (cldat(1,n),n=1,2)/0.0,0.0/
      data (cldat(2,n),n=1,2)/0.0,0.0/
      data (cldat(3,n),n=1,2)/0.0,0.0/
      data (cldat(4,n),n=1,2)/0.0,0.0/
      data (cddat(1,n),n=1,2)/0.0,0.0/
      data (cddat(2,n),n=1,2)/0.0,0.0/
      data (cddat(3,n),n=1,2)/0.0,0.0/
      data (cddat(4,n),n=1,2)/0.0,0.0/
      data (cmdat(1,n),n=1,2)/0.0,0.0/
      data (cmdat(2,n),n=1,2)/0.0,0.0/
      data (cmdat(3,n),n=1,2)/0.0,0.0/
      data (cmdat(4,n),n=1,2)/0.0,0.0/

c   Numerical modelling parameters [nummod]
c   [Number of azimuthal increments na must be a multiple of
c    the number of blades nb and the minimum  radius r0>=eb]
      data r0,nr,na,nz/.1,15.0,24.0,4.0/
c   [matrix of indices for cyclic calculation of cell influence coeff]
      data mn(1,1,1),mn(1,1,2)/1,1/
      data mn(1,2,1),mn(1,2,2)/2,1/
      data mn(2,1,1),mn(2,1,2)/2,1/
      data mn(2,2,1),mn(2,2,2)/2,2/
      data mn(3,1,1),mn(3,1,2)/2,2/
      data mn(3,2,1),mn(3,2,2)/1,2/
      data mn(4,1,1),mn(4,1,2)/1,2/
      data mn(4,2,1),mn(4,2,2)/1,1/

c   Logical variables for program control [logvar]
      data conv(1),conv(2),conv(3)/.false.,.false.,.false./
      data first(1),first(2),first(3)/.true.,.true.,.true./
```

```
c   Logical variables specifying model options
c   Blade representation
c   [Clasical lifting line model      cllmod=.true.]
c   [Extended lifting line model      ellmod=.true.]
c   [Single panel vortex lattice model vlmmod=.true.]
c   Wake representation
c   [Rigid wake model                 rigwke=.true.]
c   [Semi-rigid wake model            semwke=.true.]
c   [No wake modelling                nonwke=.true.]
c   Induced velocity representation
c   [Uniform induced velocity         uniind=.true.]
c   [Linear induced velocity          linind=.true.]
c   [Non-linear induced velocity      nonind=.true.]
c   Representation of flow phenomena
c   [Unsteady aero model (vorticity)  shdmod=.true.]
c   [Unsteady aero model (deficiency) unsmod=.true.]
c   [Dynamic stall modelling          dynmod=.true.]
c   [Modelling of compressibility     cmpmod=.true.]
c   [Modelling of radial flow         radmod=.true.]
c   [Section data tables given        secinp=.true.]
c   Input representation
c   [Control input given              ctlinp=.true.]
c   [Blade kinematics given           bldinp=.true.]

    data cllmod,ellmod,vlmmod/.true.,.false.,.false./
    data nonwke,rigwke,semwke/.true.,.false.,.false./
    data uniind,linind,nonind/.true.,.false.,.false./
    data shdmod,unsmod/.true.,.false./
    data dynmod,cmpmod,radmod/.true.,.false.,.false./
    data secinp,ctlinp,bldinp/.false.,.true.,.true./
```

```
c   Model parameters [modpar]
c   [Clasical lifting line model:  db=c/4, dc=c/4]   *
c   [Extended lifting line model:  db=3c/4,dc=c/4]   *
c   [Vortex core radius as fraction of chord:  dv]   *
c   * Calculated in main program

c   Numerical values of constants [cnstnt]
    data pi,degrad,raddeg/3.14159265,0.01745328,57.29577951/

    end

c   ==========================================
    Block Data Rotor
c
c   Data initialization for program ROTCAL
c   Source:      SCHEIMAN & LUDI [1963]
c
c   ==========================================

    include 'cmnblk.for'

c   ALL UNITS [kg,m,s,K]
c   All linear caracteristics are given as [(*)(r=0),d(*)/dr]

c   Rotor environment [rotenv]
    data rho,temp,gasrat,gascon/1.1533,288.16,1.4,287/

c   Kinematic state of rotor [rotkin]
    data om,(v(n),n=1,3)/20.21,41.55,0.58,3.1241/

c   Rotor parameters [rotpar]
    data r,nb/8.54,4.0/
```

```
c   Rotor configuration [rotcnf]
c   [articulated,hingeless=1.0,gimballed(nb>=3)=nb/2,teetering(nb=2)=2.0]
    data rottyp/1.0/

c   Rotor forces [rotfce]
    data ft0,fn0,fy0/52466.7,0.0,0.0/

c   Control input or initialization [rotctl]
    data (th0(n),n=1,2)/0.2642,-0.0163/
    data (thc(n),n=1,5)/0.0611,0.0,0.0,0.0,0.0/
    data (ths(n),n=1,5)/-0.1311,0.0,0.0,0.0,0.0/

c   Blade motion input or initialization [bldkin]
    data b0/0.0735/
    data (bc(n),n=1,5)/-0.0148,0.0,0.0,0.0,0.0/
    data (bs(n),n=1,5)/-0.0138,0.0,0.0,0.0,0.0/

c   Blade geometric and inertia characteristics [bldpar]
    data (c(n),n=1,2)/0.4168,0.0/
    data yb,mb,ib,eb,kb/4.27,80.0,3300.0,0.44,0.0/

c   Blade section aerodynamic characteristics [bldsec]
    data (a0(n),n=1,2)/5.7,0.0/
    data (aoa0(n),n=1,2)/0.0,0.0/
    data (aoas(n),n=1,2)/.21,0.0/
    data (cd0(n),n=1,2)/.006,0.0/
    data (cds(n),n=1,2)/0.02,0/
    data (cm0(n),n=1,2)/0.0,0.0/
    data (cms(n),n=1,2)/-0.4,0.0/
```

```
c     Blade section aerodynamic data table [secdat]
c     [Optional.Should be kown for m angles of attack and n Mach numbers
c      in the attached subcritical flow region]
      data (cldat(1,n),n=1,2)/0.0,0.0/
      data (cldat(2,n),n=1,2)/0.0,0.0/
      data (cldat(3,n),n=1,2)/0.0,0.0/
      data (cldat(4,n),n=1,2)/0.0,0.0/
      data (cddat(1,n),n=1,2)/0.0,0.0/
      data (cddat(2,n),n=1,2)/0.0,0.0/
      data (cddat(3,n),n=1,2)/0.0,0.0/
      data (cddat(4,n),n=1,2)/0.0,0.0/
      data (cmdat(1,n),n=1,2)/0.0,0.0/
      data (cmdat(2,n),n=1,2)/0.0,0.0/
      data (cmdat(3,n),n=1,2)/0.0,0.0/
      data (cmdat(4,n),n=1,2)/0.0,0.0/

c     Numerical modelling parameters [nummod]
c     [Number of azimuthal increments na must be a multiple of
c      the number of blades nb and the minimum  radius r0>=eb]
      data r0,nr,na,nz/.8540,15.0,24.0,4.0/
c     [matrix of indices for cyclic calculation of cell influence coeff]
      data mn(1,1,1),mn(1,1,2)/1,1/
      data mn(1,2,1),mn(1,2,2)/2,1/
      data mn(2,1,1),mn(2,1,2)/2,1/
      data mn(2,2,1),mn(2,2,2)/2,2/
      data mn(3,1,1),mn(3,1,2)/2,2/
      data mn(3,2,1),mn(3,2,2)/1,2/
      data mn(4,1,1),mn(4,1,2)/1,2/
      data mn(4,2,1),mn(4,2,2)/1,1/

c     Logical variables for program control [logvar]
      data conv(1),conv(2),conv(3)/.false.,.false.,.false./
      data first(1),first(2),first(3)/.true.,.true.,.true./
```

```
c   Logical variables specifying model options
c   Blade representation
c   [Clasical lifting line model      cllmod=.true.]
c   [Extended lifting line model      ellmod=.true.]
c   [Single panel vortex lattice model vlmmod=.true.]
c   Wake representation
c   [Rigid wake model                 rigwke=.true.]
c   [Semi-rigid wake model            semwke=.true.]
c   [No wake modelling                nonwke=.true.]
c   Induced velocity representation
c   [Uniform induced velocity         uniind=.true.]
c   [Linear induced velocity          linind=.true.]
c   [Non-linear induced velocity      nonind=.true.]
c   Representation of flow phenomena
c   [Unsteady aero model (vorticity)  shdmod=.true.]
c   [Unsteady aero model (deficiency) unsmod=.true.]
c   [Dynamic stall modelling          dynmod=.true.]
c   [Modelling of compressibility     cmpmod=.true.]
c   [Modelling of radial flow         radmod=.true.]
c   [Section data tables given        secinp=.true.]
c   Input representation
c   [Control input given              ctlinp=.true.]
c   [Blade kinematics given           bldinp=.true.]

      data cllmod,ellmod,vimmod/.true.,.false.,.false./
      data nonwke,rigwke,semwke/.false.,.true.,.false./
      data uniind,linind,nonind/.true.,.false.,.true./
      data shdmod,unsmod/.true.,.false./
      data dynmod,cmpmod,radmod/.false.,.false.,.false./
      data secinp,ctlinp,bldinp/.false.,.true.,.true./

c   Model parameters [modpar]
c   [Clasical lifting line model: db=c/4, dc=c/4]   *
c   [Extended lifting line model: db=3c/4,dc=c/4]   *
```

```
c   [Vortex core radius as fraction of chord:  dv]   *
c   * Calculated in main program

c   Numerical values of constants [cnstnt]
    data pi,degrad,raddeg/3.14159265,0.01745328,57.29577951/

    end

c   Common block and declaration of variables

    implicit real(a-z)
    integer i,j,k,l,m,n,o,p,q,mn,nri,nrp,naj,naq,nbk,nzl
    logical conv,first,
   c      cllmod,ellmod,vlmmod,nonwke,rigwke,semwke,
   c      uniind,linind,nonind,shdmod,unsmod,dynmod,cmpmod,radmod,
   c      ctlinp,bldinp,secinp
    common/rotenv/rho,temp,gasrat,gascon
   c    /rotkin/om,v(3),vh,aoah,aosh
   c    /rotpar/r,r0,disc,nb,mu,lda,sig,lock,nu,kc,ks
   c    /rotcnf/rottyp
   c    /rotfce/ft0,fh0,fy0
   c    /rotctl/th0(2),thc(5),ths(5)
   c    /bldkin/b0,bc(5),bs(5)
   c    /bldpar/c(2),yb,mb,ib,eb,kb
   c    /bldsec/a0(2),aoa0(2),aoas(2),cd0(2),cds(2),cm0(2),cms(2)
   c    /secdat/daoa,dma,aoadat(4),madat(2),
   c          cldat(4,2),cddat(4,2),cmdat(4,2)
   c    /nummod/nr,nri,nrp,na,naj,nap,nz,nzl,nbk,mn(4,2,2),dr,dpsi
   c    /modtyp/cllmod,ellmod,vlmmod,shdmod,unsmod,dynmod,
   c          nonwke,rigwke,semwke,uniind,linind,nonind,
   c          cmpmod,radmod,secinp,ctlinp,bldinp
   c    /modpar/db,dc,dv
   c    /cnstnt/pi,degrad,raddeg
   c    /logvar/conv(3),first(3),sstall,dstall

c   End of common block
```

REFERENCES

ABBOTT H, VON DOENHOFF A E, "Theory of Wing Sections", Dover Publications, 1949

ARIELI R, TAUBER M E, SANDERS D A, CAUGHEY, "Computation of Transonic flow about Helicopter Rotor Blades", AIAA Journal, Vol 24, No. 5, 1986

ARNOLD J, DE WAARD P G, "Explicit Rotor Equations using a Symbolic Manupulation Code: Derivation and Exposition", Aeronautica Meridiana, Vol 8, No 2, 1990

BASKIN V E, VIL'DGRUBE L S, VOZHDAYEV Y S, MAVKAPAR G I, "Theory of the Lifting Airscrew", NASA TT F-823, 1976

BAUCHAU O A, HONG C H, "Finite Element Approach to Rotor Blade Modelling", Journal of the American Helicopter Society, Vol 32, 1987

BEDDOES T S, "A Synthesis of Unsteady Aerodynamic Effects Including Stall Hysteresis", Vertica, Vol 1, No 1, 1976

BEDDOES T S, "Representation of Airfoil Behaviour", Vertica, Vol 7, No 2, 1983

BEDDOES T S, "Practical Computation of Unsteady Lift", Vertica, Vol 8, No 1, 1984

BELOTSERKOVSKII S M, "The theory of thin wings in Subsonic flow", Plenum Press, 1967

BERTIN J J, SMITH M L, "Aerodynamics for Engineers", Prentice Hall, 1979

BISPLINGHOFF R L, ASHLEY H, HALFMAN R L, "Aeroelasticity", Addisson-Wesley Publishing Company Inc, 1955

BOUSMAN W G, GILBERT N, JOHNSON W, RILEY M J, TOULMAY F, YOUNG C, "Correlation of Puma Airloads - Lifting Line and Wake Calculation", Fifteenth European Rotorcraft Forum, 1989

BRAMWELL A R S, "Helicopter Dynamics", Edward Arnold, 1976

CANTALAUBE B, HUBERSON S, "A New Approach using Vortex Point Method for Prediction of Rotor Performance in Hover & Forward Flight", Vertica, Vol 10, No 2, 1986

CARR L W, "Progress in Analysis and Prediction of Dynamic Stall", Journal of Aircraft, Vol 25, No 1, 1988

CHEESEMAN I D, HADDOW C, "An Experimental Investigation of the Downwash beneath a Lifting Rotor at low Advance Ratios", Vertica, Vol 13, No 4, 1989

CHEESEMAN I C, "Developments in Rotary Wing Aircraft Aerodynamics", Vertica, Vol 6, No 2, 1982

CHEN R T N, "A Survey of Non-uniform Inflow models for Rotorcraft Flight Dynamics and Control Applications", Fifteenth European Rotorcract Forum, 1989

CLARK D R, LEIPER A C, "The Free Wake Analysis", Journal of the American Helicopter Society, Vol 15, No 1, 1970

DAVIS S S, CHANG I, "The Critical Role of Computational Fluid Dynamics in Rotory Wing Aerodynamics", Vertica, Vol 11, No 1/2, 1987

DESOPPER A, LAFON P, CéRONI P, PHILIPPE J J, "Ten Years of Rotor flow studies at ONERA", Journal of the American Helicopter Society, Jan 1989

FAVIER D, NSI-MBA M, BARBI C, MARESCA C, "A Free Wake Analysis for Hovering Rotors and Advancing Propellors", Vertica, Vol 11, No 3, 1987

FRIEDMAN P P, "Recent Trends in Rotory-Wing Aeroelasticity", Vertica, Vol 11, No 1/2, 1987

FRIEDMAN P P, "Arbitrary Motion Unsteady Aerodynamics and its Application to Rotary Wing Aeroelasticity", Journal of Fluid and Structures, 1987

HEYSON H H, KATZOFF S, "Induced Velocities Near a Lifting Rotor with Nonuniform Disc Loading", NACA Report 1319, 1957

HOOPER W E, "The Vibratory Airloading of Helicopter Rotors", Vertica, Vol 8, No 2, 1984

JENNY D S, OLSON J R, LANDGREBE A J, "A Reassesment of Rotor Hovering Performanve Prediction Methods", Journal of the American Helicopter Society, Vol 13, No 2, 1968

JOHNSON W, "Helicopter Theory", Princeton University Press, 1980a

JOHNSON W, "A Comprehensive Analytical Model of Rotorcraft Aerodynamics and Dynamics", NASA TM 81182, 1980b

JOHNSON W, "Development of a Comprehensive Analysis for Rotorcraft", Vertica, Vol 5, 1981

JOHNSON W, "Recent Development in Rotary-Wing Aerodynamic Theory", AIAA Journal, Vol 24, No 8, 1986

JOHNSON W, "Time Domain Unsteady Aerodynamics of Rotors with Complex Wake Configurations", Vertica, Vol 12, No 1/2, 1988

JOHNSON W, "Airloads and Wake Models for a Comprehensive Helicopter analysis", Vertica, Vol 14, No 3, 1990

KUETHE A M, CHOW C, "Foundations of Aerodynamics: Basis of Aerodynamic Design", John Wiley & Sons, 1976

LANDGREBE A J, MOFFIT R C, CLARK D R, "Aerodynamic Technology for Advanced Rotorcraft, Vol I & II", Journal of the American Helicopter Society, Vol 22, No 1 & 2, 1977

LANDGREBE A J, "An Analytical Method of Predicting Rotor Wake Geometry", Journal of the American Helicopter Society, Oct 1969

LOEWY R G, "A Two-Dimensional Approximation to the Unsteady Aerodynamics of Rotory Wings", Journal of the Aeronautical Sciences, Vol 24, No 2, 1957

McCORMICK B W, "Aerodynamics of V/STOL Flight", Academic Press, 1967

McCORMICK B W, "Aerodynamics, Aeronautics and Flight Mechanics", John Wiley & Sons, 1979

MILLER R H, "Factors Influencing Rotor Aerodynamics in Hover and Forward Flight", Vertica, Vol 9, No 2, 1985

MILLER R H, "Rotor Blade Harmonic Air Loading", AIAA Journal, Vol 2, No 7, 1964

MIL' M L, NEKRASOV A V, BRAVERMAN A S, GRODKO L N, "Helicopters: Calculation and Design", NASA TT F-494, 1966

MORAN J, "An Introduction to Theoretical and Computational Aerodynamics", John Wiley & Sons, 1984

PIZIALI R A, "Method for the Solution of the Aeroelastic Response Problem for Rotating Wings", Journal of Sound and Vibration, Vol 4, No 3, 1966

PELEAU B, DIDIER P, "Aeroelastic Prediction of Rotor Loads in Forward Flight", Vertica, Vol 13, No 2, 1989

RAND O, ROSEN A, "Prediction of the Aerodynamic Loads on Helicopter Blades in Hovering and Axial Flight using Lifting Line Theory", Israel Journal of Technology, Vol 20, 1982

ROSEN A, RAND O, "A Model of a Curved Helicopter Blade in Forward Flight", Vertica, Vol 11, No 1/2, 1987

ROSEN A, GRABER A, "Free Wake Model of Hovering Rotors Having Straight or Curved Blades", Journal of the American Helicopter Society, July 1988

SADLER S G, "Development and Application of a Method for Predicting Rotor Free Wake Positions and Resulting Rotor Blade Air Loads", NASA CR-1911, 1971

SCHEIMAN J, LUDI L H, "Qualitative Evaluation of Effect of Helicopter Rotor Blade Tip Vortex on Blade Airloads", NASA TN D-1637, 1963

SCHLICHTING H, TRUCKENBRODT E, "Aerodynamics of the Airplane", McGraw-Hill Book Company, 1979

SCULLY M P, "Computation of Helicopter rotor wake geometry and its influence on Rotor Harmonic airloads", MIT Ph.D. Thesis, 1975

STEPNIEWSKI W Z, KEYS C N, "Rotary Wing Aerodynamics", Dover Publications, 1984

TOROK M S, CHOPRA I, "A Coupled Rotor Aeroelastic Analysis Utilizing Non-linear Aerodynamics and Refined Wake Modelling", Vertica, Vol 13, No 2, 1989

TRAN C T, FALCHERO D, "Application of the ONERA Dynamic Stall Model to a Helicopter Blade in Forward Flight", Vertica, Vol 6, 1982

TRAN C T, DESOPPER A, "An Iteration technique coupling 3-D Transonic Small Perturbation Aerodynamic Theory and Rotor Dynamics in Forward Flight", Vertica, Vol 13, No 4, 1989

VAN HOLTEN T, "On the Validity of Lifting Line Concepts in Rotor Analysis", Vertica, Vol 1, 1977

VAN HOLTEN T, "Some notes on Unsteady Lifting Line Theory", Journal of Fluid Mechanics, Vol 77, Part 3, 1976

VON KáRMáN T, "Aerodynamics", Cornell University Press, 1954

WAKE B E SANKAR N L, "Solutions of Navier Stokes Equations for the Flow about a Rotor Blade", Journal of the American Helicopter Society, April 1989

WAKE B E M, SANKAR N L, LEKOUDIS S G, "Computation of Rotor Blade flows using Euler Equations", Journal of Aircraft, Vol 23 No 7, July 1986

YIH C, "Fluid Mechanics", West River Press, 1977